第54回 フラーレン・ナノチューブ・グラフェン 総合シンポジウム講演要旨集

平成30年3月9日～12日

FNTG Research Society

第 54 回
フラーレン・ナノチューブ・グラフェン
総合シンポジウム

The 54th Fullerenes-Nanotubes-Graphene General Symposium

講演要旨集
Abstracts

2018 年 3 月 9 日(金) ～ 12 日(月)
東京大学　伊藤国際学術研究センター
The University of Tokyo, ITO INTERNATIONAL RESEARCH CENTER

主催　フラーレン・ナノチューブ・グラフェン学会
The Fullerenes, Nanotubes and Graphene Research Society

共催・後援
日本化学会　The Chemical Society of Japan
東京大学大学院工学系研究科　School of Engineering, The University of Tokyo
東京大学 CIAiS　Consortium for Innovation of Advanced Integrated Science (UTokyo)
東京大学 GMSI　Graduate Program for Mechanical Systems Innovation (UTokyo)

協賛
日本物理学会　The Physical Society of Japan
応用物理学会　The Japan Society of Applied Physics
高分子学会　The Society of Polymer Science, Japan
電気化学会　The Electrochemical Society of Japan

Princeton Instruments

高感度
高ダイナミックレンジ
高繰り返し

高感度近赤外線2次元InGaAsカメラ

NIRvana™:640

- 低暗電流ノイズ（電子冷却：-80℃、液体窒素：-190℃）
- 110fps（ビデオレート以上）
- 標準GigEインターフェースで50mまで延長可
- 空冷ファンと水冷を切替可能

アプリケーション例

・フォトニック結晶PLイメージング及びスペクトル
・一重項酸素イメージング及びスペクトル
・太陽電池PLイメージング及びスペクトル
・天体観測微弱光イメージング
・食品断面イメージング
・In-Vivoイメージング　など

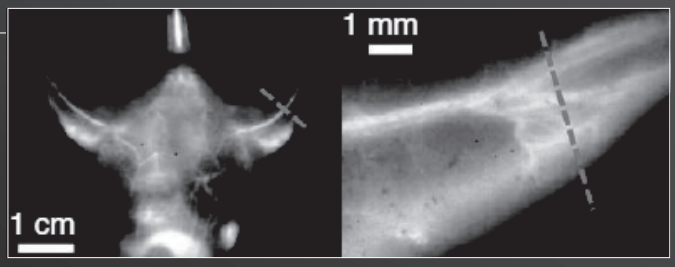

仕様

モデル	NIRvana:640ST	NIRvana:640	NIRvana:640LN
センサー	640 x 512 x InGaAs		
素子サイズ	20μm x 20μm		
波長範囲	0.9 ～ 1.7 μm		
冷却温度	-60℃	-80℃	-190℃
ダークチャージ	1500 e-/p/sec	300 e-/p/sec	<8 e-/p/sec
読み出しノイズ	<120 e-rms		15 e-rms
ダイナミックレンジ	16 Bit (>15Bit@1 素子)		
フレームレート	110 fps@10MHz		2.77 fps@250KHz
インターフェース	Gig E		
ソフトウェア	LightField, SITK-LabVIEW, WinX32		

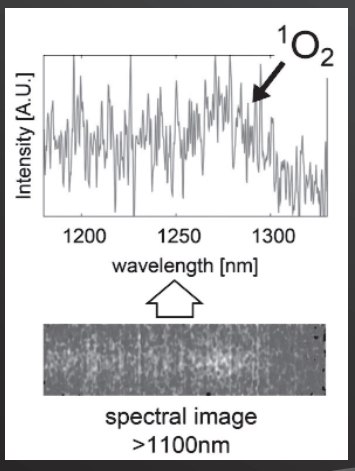

www.pi-j.jp

株式会社 日本ローパー　P I 事業部
〒135-0033 東京都江東区深川2 - 8 - 19 サクライビル3F
電話 03-5639-2741　FAX 03-5639-2775

NIPPON ROPER

Abstract of
The 54th Fullerenes-Nanotubes-Graphene General Symposium

Sponsored by : The Fullerenes, Nanotubes and Graphene Research Society

Co-Sponsored by : The Chemical Society of Japan
School of Engineering, The University of Tokyo
Consortium for Innovation of Advanced Integrated Science(UTokyo)
Graduate Program for Mechanical Systems Innovation(UTokyo)

Supported by : The Physical Society of Japan
The Japan Society of Applied Physics
The Society of Polymer Science, Japan
The Electrochemical Society of Japan

Date : March 9th (Fri.) – March 12th (Mon.), 2018

Place : The University of Tokyo, ITO INTERNATIONAL RESEARCH CENTER
7-3-1 Hongo, Bunkyo-ku, Tokyo 113-8656

Presentation Time : Special Lecture (25 min presentation + 5min discussion)
Invited Lecture (10 min presentation + 5min discussion)
General Lecture (10 min presentation + 5min discussion)
Poster Preview (1 min presentation without discussion)

第 54 回フラーレン・ナノチューブ・グラフェン総合シンポジウム
講演要旨集

主催 : フラーレン・ナノチューブ・グラフェン学会

共催・後援 : 日本化学会
東京大学大学院工学系研究科
東京大学 CIAiS
東京大学 GMSI

協賛 : 日本物理学会、応用物理学会、高分子学会、電気化学会

日時 : 平成 30 年 3 月 9 日(金)～3 月 12 日(月)

場所 : 東京大学　伊藤国際学術研究センター　伊藤謝恩ホール
〒113-8656　東京都文京区本郷 7-3-1

発表時間 : 特別講演　（発表　25 分 + 質疑応答　5 分）
招待講演　（発表　10 分 + 質疑応答　5 分）
一般講演　（発表　10 分 + 質疑応答　5 分）
ポスタープレビュー（発表 1 分・質疑応答　なし）

展示団体御芳名 （五十音順、 敬称略）

（株）島津製作所

（株）シンキー

（株）セントラル科学貿易

ナノフォトン（株）

日本シノプシス(同）

（株）日本ローパー

（株）堀場製作所

（株）名城ナノカーボン

DKSHジャパン（株）

WITec （株）

広告掲載団体御芳名 （五十音順、 敬称略）

アイクストロン(株）

（株）コロナ社

（株）セントラル科学貿易

ソーラボジャパン（株）

日本電子（株）

（株）日本ローパー

（株）堀場製作所

Contents

目次

プログラム早見表

3月10日 （土）

	受付開始 8:30～ 講演開始 9:45～
9:45	特別講演（Esko I. Kauppinen） 9:45–10:15
10:15	特別講演（Yan Li） 10:15–10:45
10:45	休憩 10:45–11:00
11:00	一般講演 4件 （ナノチューブの生成と精製・ナノチューブの応用） 11:00–12:00
12:00	昼食 （幹事会） 12:00–13:15
13:15	特別講演（河野 淳一郎） 13:15–13:45
13:45	招待講演(Qiang Zhang)13:45–14:00
14:00	一般講演 4件 （ナノチューブの応用） 14:00–15:00
15:00	ポスタープレビュー （ 1P–1 ～ 1P–38 ） 15:00–16:00
16:00	ポスターセッション （多目的スペース） 16:00–17:45
17:45	休憩 17:45–18:00
18:00	チュートリアル 講師： 松尾 豊 東京大学 （伊藤謝恩ホール） 18:00–19:30
19:30	

3月9日 （金）

第10回ﾅﾉｶｰﾎﾞﾝ実用化推進研究会
（伊藤謝恩ホール）
10:00–16:45

3月11日 （日）

	受付開始 8:30～ 講演開始 9:00～
9:00	特別講演（大島 久純） 9:00–9:30
9:30	一般講演 4件 （ナノチューブの物性・ナノ環境と安全評価・ナノチューブの生成と精製・内包ナノチューブ） 9:30–10:30
10:30	休憩 10:30–10:45
10:45	招待講演（Erik Einarsson）10:45–11:00
11:00	一般講演 4件 （グラフェンの物性・フラーレン・その他・ナノ炭素粒子） 11:00–12:00
12:00	昼食 12:00–13:15
13:15	授賞式 13:15–14:00
14:00	ポスタープレビュー （ 2P–1 ～ 2P–39 ） 14:00–15:00
15:00	ポスターセッション （ 多目的スペース ） 15:00–16:45
16:45	特別講演 （齋藤 弥八） 16:45–17:15
17:15	特別講演 （町田 友樹） 17:15–17:45
17:45	一般講演 5件 （グラフェンの応用・原子層・その他） 17:45–19:00
19:00	懇親会 （多目的スペース） 19:00–20:45
20:45	

3月12日 （月）

	受付開始 8:30～ 講演開始 9:00～
9:00	特別講演（伊丹 健一郎） 9:00–9:30
9:30	一般講演 4件 （フラーレンの化学・金属内包フラーレン・フラーレンの応用） 9:30–10:30
10:30	休憩 10:30–10:45
10:45	特別講演（有江 隆之） 10:45–11:15
11:15	一般講演 3件 （グラフェンの物性・原子層） 11:15–12:00
12:00	昼食 12:00–13:15
13:15	ポスタープレビュー （ 3P–1 ～ 3P–39 ） 13:15–14:15
14:15	ポスターセッション （多目的スペース） 14:15–16:00
16:00	特別講演 （柳 和宏） 16:00–16:30
16:30	一般講演 4件 （グラフェンの物性・ナノチューブの物性・ナノチューブの応用） 16:30–17:30
17:30	

講演会場 伊藤謝恩ホール

特別講演 発表25分・質疑5分
招待講演 発表10分・質疑5分
一般講演 発表10分・質疑5分
ﾎﾟｽﾀｰﾌﾟﾚﾋﾞｭｰ 発表1分・質疑なし

Time table

March 10 (Sat.)	
	Registration begins at 8:30 Lectures begin at 9:45
9:45	Special Lecture (Esko I. Kauppinen) 9:45–10:15
10:15	Special Lecture (Yan Li) 10:15–10:45
10:45	Coffee Break 10:45–11:00
11:00	General Lectures [4] (Formation and purification of nanotubes・Applications of nanotubes) 11:00–12:00
12:00	Lunch (Administrative meeting) 12:00–13:15
13:15	Special Lecture (Junichiro Kono)13:15–13:45
13:45	Invited Lecture(Qiang Zhang)13:45–14:00
14:00	General Lectures [4] (Applications of nanotubes) 14:00–15:00
15:00	Poster Preview (1P–1 through 1P–38) 15:00–16:00
16:00	Poster Session (Event Space) 16:00–17:45
17:45	Coffee Break 17:45–18:00
18:00	Tutorial Lecturer : Yutaka Matsuo The University of Tokyo (Ito Hall) 18:00–19:30
19:30	

March 9 (Fri.)
The 10th NanoCarbon Application Forum (Ito Hall) 10:00–16:45

March 11 (Sun.)	
	Registration begins at 8:30 Lectures begin at 9:00
9:00	Special Lecture (Hisayoshi Oshima) 9:00–9:30
9:30	General Lectures [4] (Properties of nanotubes・Environmental/Safety characterization of nanomaterials・ Formation and purification of nanotubes・Endohedral nanotubes) 9:30–10:30
10:30	Coffee Break 10:30–10:45
10:45	Invited Lecture (Erik Einarsson)10:45–11:00
11:00	General Lectures [4] (Properties of graphene・ Fullerenes・Other topics・ Carbon nanoparticles) 11:00–12:00
12:00	Lunch 12:00–13:15
13:15	Award Ceremony 13:15–14:00
14:00	Poster Preview (2P–1 through 2P–39) 14:00–15:00
15:00	Poster Session (Event Space) 15:00–16:45
16:45	Special Lecture (Yahachi Saito) 16:45–17:15
17:15	Special Lecture (Tomoki Machida) 17:15–17:45
17:45	General Lectures [5] (Applications of graphene・ Atomic Layers・Other topics) 17:45–19:00
19:00	Banquet (Event Space) 19:00–20:45
20:45	

March 12 (Mon.)	
	Registration begins at 8:30 Lectures begin at 9:00
9:00	Special Lecture (Kenichiro Itami) 9:00–9:30
9:30	General Lectures [4] (Chemistry of fullerenes・ Endohedral metallofullerenes・ Applications of fullerenes) 9:30–10:30
10:30	Coffee Break 10:30–10:45
10:45	Special Lecture (Takayuki Arie) 10:45–11:15
11:15	General Lectures [3] (Properties of graphene・ Atomic Layers) 11:15–12:00
12:00	Lunch 12:00–13:15
13:15	Poster Preview (3P–1 through 3P–39) 13:15–14:15
14:15	Poster Session (Event Space) 14:15–16:00
16:00	Special Lecture (Kazuhiro Yanagi) 16:00–16:30
16:30	General Lectures [4] (Properties of graphene・ Properties of nanotubes・Applications of nanotubes) 16:30–17:30
17:30	

Place : Ito Hall
Special Lecture : 25 min (Presentation) + 5 min (Discussion)
Invited Lecture : 10 min (Presentation) + 5 min (Discussion)
General Lecture : 10 min (Presentation) + 5 min (Discussion)
Poster Preview : 1 min (Presentation)

座長一覧 (Chairpersons)

3月10日（土） （敬称略）

セッション	時　　間	座　　長
特別講演(Esko I. Kauppinen)	9:45 ~10:15	丸山 茂夫
特別講演(Yan Li)	10:15 ~10:45	丸山 茂夫
一般講演	11:00 ~ 12:00	千足 昇平
特別講演(河野 淳一郎)	13:15~ 13:45	齋藤 理一郎
招待講演(Qiang Zhang)	13:45 ~ 14:00	項 榮
一般講演	14:00 ~ 15:00	項 榮
ポスタープレビュー	15:00 ~ 16:00	杉目 恒志 井ノ上 泰輝
チュートリアル(松尾 豊)	18:00 ~ 19:30	丸山 茂夫

3月11日（日）

セッション	時　　間	座　　長
特別講演(大島 久純)	9:00 ~ 9:30	野田 優
一般講演	9:30 ~10:30	野田 優
招待講演(Erik Einarsson)	10:45 ~11:00	山本 貴博
一般講演	11:00 ~ 12:00	山本 貴博
ポスタープレビュー	14:00 ~ 15:00	大町 遼 蓬田 陽平
特別講演(齋藤 弥八)	16:45 ~ 17:15	篠原 久典
特別講演(町田 友樹)	17:15 ~ 17:45	高井 和之
一般講演	17:45 ~ 19:00	北浦 良

3月12日（月）

セッション	時　　間	座　　長
特別講演(伊丹 健一郎)	9:00 ~ 9:30	松尾 豊
一般講演	9:30 ~ 10:30	村田 靖次郎
特別講演(有江 隆之)	10:45 ~ 11:15	長汐 晃輔
一般講演	11:15 ~ 12:00	長汐 晃輔
ポスタープレビュー	13:15 ~ 14:15	廣谷 潤 上野 裕
特別講演(柳 和宏)	16:00 ~ 16:30	竹延 大志
一般講演	16:30 ~ 17:30	加藤 雄一郎

3月10日（土）

特別講演　　発表 25分 ・ 質疑応答 5分
招待講演　　発表 10分 ・ 質疑応答 5分
一般講演　　発表 10分 ・ 質疑応答 5分
ポスタープレビュー　　発表 1分 ・ 質疑応答 なし

特別講演（ 9:45-10:15 ）

特別講演（ 10:15-10:45 ）

＞＞＞＞＞＞＞ 休憩（ 10:45-11:00 ）＜＜＜＜＜＜＜

一般講演（ 11:00-12:00 ）
ナノチューブの生成と精製 ・ ナノチューブの応用

＞＞＞＞＞＞＞ 昼食（ 12:00-13:15 ）＜＜＜＜＜＜＜

特別講演（ 13:15-13:45 ）

招待講演（ 13:45-14:00 ）

3月10日（土）

一般講演（ 14:00-15:00 ）
ナノチューブの応用

ポスタープレビュー（ 15:00-16:00 ）
ポスターセッション（ 16:00-17:45 ）　　（☆） 若手奨励賞候補
フラーレンの化学

金属内包フラーレン

フラーレン

3月10日（土）

ナノチューブの物性

ナノチューブの応用

ナノチューブの生成と精製

3月10日（土）

グラフェン生成

グラフェンの応用

グラフェンの物性

原子層

3月10日（土）

バイオ

＞＞＞＞＞＞ 休憩（ 17:45-18:00 ）＜＜＜＜＜＜

チュートリアル（ 18:00-19:30 ）

有機太陽電池の基礎とナノカーボン材料を積極的に活用した太陽電池
＊松尾 豊

3月11日（日）

特別講演　　発表 25分 ・ 質疑応答 5分
招待講演　　発表 10分 ・ 質疑応答 5分
一般講演　　発表 10分 ・ 質疑応答 5分
ポスタープレビュー　　発表 1分 ・ 質疑応答 なし

特別講演（ 9:00-9:30 ）

一般講演（ 9:30-10:30 ）
ナノチューブの物性 ・ ナノ環境と安全評価 ・ ナノチューブの生成と精製 ・ 内包ナノチューブ

>>>>>>> 休憩（ 10:30-10:45 ）<<<<<<<

招待講演（ 10:45-11:00 ）

一般講演（ 11:00-12:00 ）
グラフェンの物性 ・ フラーレン ・ その他 ・ ナノ炭素粒子

3月11日（日）

>>>>>>> 昼食（ 12:00-13:15 ）<<<<<<<

大澤賞・飯島賞・若手奨励賞の授賞式（ 13:15-14:00 ）

ポスタープレビュー（ 14:00-15:00 ）
ポスターセッション（ 15:00-16:45 ）　　（☆） 若手奨励賞候補
フラーレンの応用

金属内包フラーレン

ナノチューブの物性

ナノチューブの応用

3月11日（日）

ナノチューブの生成と精製

内包ナノチューブ

グラフェン生成

グラフェンの応用

グラフェンの物性

3月11日（日）

3月11日（日）

その他

特別講演（16:45-17:15）

特別講演（17:15-17:45）

一般講演（17:45-19:00）
グラフェンの応用 ・ 原子層 ・ その他

懇親会（19:00-20:45）

3月12日（月）

特別講演　　発表 25分 ・ 質疑応答 5分
一般講演　　発表 10分 ・ 質疑応答 5分
ポスタープレビュー　　発表 1分 ・ 質疑応答 なし

特別講演（ 9:00–9:30 ）

一般講演（ 9:30–10:30 ）
フラーレンの化学 ・ 金属内包フラーレン ・ フラーレンの応用

>>>>>>> 休憩（ 10:30–10:45 ）<<<<<<<

特別講演（ 10:45–11:15 ）

一般講演（ 11:15–12:00 ）
グラフェンの物性 ・ 原子層

>>>>>>> 昼食（ 12:00–13:15 ）<<<<<<<

3月12日（月）

ポスタープレビュー（ 13:15–14:15 ）
ポスターセッション（ 14:15–16:00 ）　　（☆） 若手奨励賞候補
金属内包フラーレン

ナノチューブの物性

ナノチューブの応用

3月12日（月）

グラフェンの物性

原子層

ナノ炭素粒子

その他

特別講演（ 16:00-16:30 ）

一般講演（ 16:30-17:30 ）
グラフェンの物性 ・ ナノチューブの物性 ・ ナノチューブの応用

March 10th, Sat.

Special Lecture: 25min (Presentation) + 5min (Discussion)
Invited Lecture: 10min (Presentation) + 5min (Discussion)
General Lecture: 10min (Presentation) + 5min (Discussion)
Poster Preview: 1min (Presentation)

Special Lecture （ 9:45–10:15 ）

Special Lecture （ 10:15–10:45 ）

>>>>>>> Coffee Break （ 10:45–11:00 ）<<<<<<<

General Lecture （ 11:00–12:00 ）

Formation and purification of nanotubes ・ Applications of nanotubes

>>>>>>> Lunch Time （ 12:00–13:15 ）<<<<<<<

Special Lecture （ 13:15–13:45 ）

March 10th, Sat.

Invited Lecture （ 13:45–14:00 ）

General Lecture （ 14:00–15:00 ）

Applications of nanotubes

Poster Preview （ 15:00–16:00 ）

Poster Session （ 16:00–17:45 ）（☆）Candidates for the Young Scientist Poster Award

Chemistry of fullerenes

Endohedral metallofullerenes

Fullerenes

Properties of nanotubes

Applications of nanotubes

>>>>>>> Coffee Break（17:45-18:00）<<<<<<<

Tutorial（18:00-19:30）

Basics of Organic Solar Cells and Nano-carbon Materials-utilized Solar Cells
** Yutaka Matsuo*

March 11th, Sun.

Special Lecture: 25min (Presentation) + 5min (Discussion)
Invited Lecture: 10min (Presentation) + 5min (Discussion)
General Lecture: 10min (Presentation) + 5min (Discussion)
Poster Preview: 1min (Presentation)

Special Lecture （ 9:00–9:30 ）

General Lecture （ 9:30–10:30 ）
Properties of nanotubes ・ Environmental/Safety characterization of nanomaterials
Formation and purification of nanotubes ・ Endohedral nanotubes

>>>>>>> Coffee Break （ 10:30–10:45 ）<<<<<<<

Invited Lecture （ 10:45–11:00 ）

General Lecture （ 11:00–12:00 ）
Properties of graphene ・ Fullerenes ・ Other topics ・ Carbon nanoparticles

>>>>>>> Lunch Time （ 12:00-13:15 ）<<<<<<<

Awards Ceremony （ 13:15-14:00 ）

Poster Preview （ 14:00-15:00 ）
Poster Session （ 15:00-16:45 ）（☆）Candidates for the Young Scientist Poster Award
Applications of fullerenes

Endohedral metallofullerenes

Properties of nanotubes

Atomic Layers

Carbon nanoparticles

Bio

Other topics

Special Lecture （ 16:45-17:15 ）

Special Lecture （ 17:15-17:45 ）

General Lecture （ 17:45-19:00 ）

Applications of graphene ・ Atomic Layers ・ Other topics

Banquet （ 19:00-20:45 ）

March 12th, Mon.

Special Lecture: 25min (Presentation) + 5min (Discussion)
General Lecture: 10min (Presentation) + 5min (Discussion)
Poster Preview: 1min (Presentation)

Special Lecture （ 9:00–9:30 ）

General Lecture （ 9:30–10:30 ）
Chemistry of fullerenes ・ Endohedral metallofullerenes ・ Applications of fullerenes

>>>>>>> Coffee Break （ 10:30–10:45 ）<<<<<<<

Special Lecture （ 10:45–11:15 ）

General Lecture （ 11:15–12:00 ）
Properties of graphene ・ Atomic Layers

>>>>>>> Lunch Time （ 12:00-13:15 ）<<<<<<<

Poster Preview （ 13:15-14:15 ）
Poster Session （ 14:15-16:00 ）（☆）Candidates for the Young Scientist Poster Award
Endohedral metallofullerenes

Properties of nanotubes

Applications of nanotubes

Formation and purification of nanotubes

Atomic Layers

Carbon nanoparticles

Other topics

Special Lecture （ 16:00-16:30 ）

General Lecture （ 16:30-17:30 ）

Properties of graphene ・ Properties of nanotubes ・ Applications of nanotubes

特別講演
Special Lecture

1S – 1 ～ 1S – 3
2S – 4 ～ 2S – 6
3S – 7 ～ 3S – 9

Fast characterization of FC-CVD nanotubes using an array of transistors

○Nan Wei[1], Patrik Laiho[1], Saeed Ahmed[1], Aqeel Hussain[1], Qiang Zhang[1], Taher Khan[1], Yongping Liao[1],Ying Tian[1,3], Er-Xiong Ding[1], Yutaka Ohno [2], Esko I. Kauppinen[1]

[1] Department of Applied Physics, Aalto University School of Science, Puumiehenkuja 2, 00076 Aalto, Finland

[2]Institute of Materials and Systems for Sustainability, Nagoya University, Furo-cho, Chikusa-ku, Nagoya 464-8603, Japan

[3] Department of Physics, Dalian Maritime University, Dalian, Liaoning 116026, China

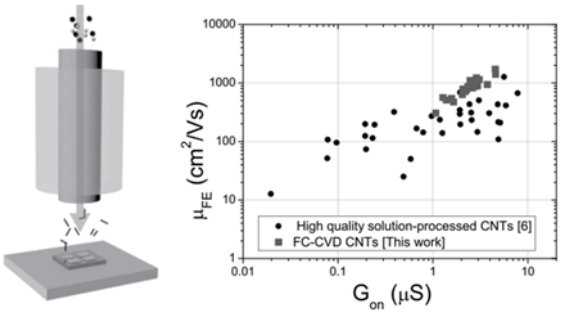

Fig.1 Fabrication method and resulting mobility.

Carbon nanotubes (CNTs) grown by the floating-catalyst chemical vapor deposition (FC-CVD) are known to make fast thin-film transistors [1,2], however, the electronic quality of individual FC-CVD SWNTs has not been directly investigated. As the limitations of other types of electronic grade SWNTs become relatively obvious [3-5], if this type of SWNTs have indeed superior performance, it may work around those limitations by a new route of SWNT processing. We introduce a new method (Fig. 1) for fabricating a statistically significant number of ultraclean field-effect transistors using FC-CVD SWNTs, revealing the superior quality of these tubes with a mean field-effect mobility 3.3 times higher than that of high-quality solution-processed SWNTs [6] and on-off current ratios higher than $10^{7.5}$. This method enables a fast, reliable and fine-grained inspection of FC-CVD SWNT population, and provides a strong direct evidence about their electronic quality. The resulting method can contribute to development of further processing techniques, and the obtained large number of ultraclean SWNT transistors provide new possibilities to study the properties of pristine tubes.

[1] D. Sun *et al. Nat. Nanotechnol.* 6, 156 (2011).
[2] D.-M. Sun *et al. Nat. Commun.* 4,2302 (2013).
[3] A. E. Islam, J. A. Rogers, and M. A. Alam *Adv. Mater.* 27, 7908 (2015).
[4] Q. Cao, S. Han, G. S. Tulevski, A. D. Franklin, and W. Haensch *ACS Nano* 6, 6471 (2012).
[5] E. A. Laird *et al. Rev. Mod. Phys.* 87, 703 (2015).
[6] P. Stokes and S. I. Khondaker *Appl. Phys. Lett.*96, 83110 (2010).

Corresponding Author: E. Kauppinen
Tel: +358-40-509-8064, Fax: +358-9-2451-3517,
E-mail: esko.kauppinen@aalto.fi

Manipulating Crystallization and Assembly of Nanomaterials via Fluidic Engineering

Yitan Li[1,2], Yuguang Chen[1], Hao Wang[3], ○Yan Li[1,2]

[1]*College of Chemistry and Molecular Engineering, Peking University, Beijing 100871, China*
[2]*Academy for Advanced Interdisciplinary Studies, Peking University, Beijing 100871, China*
[3]*College of Engineering, Peking University, Beijing 100871, China*

Solution-based approaches have been intensively employed to prepare, pattern, and assemble nanomaterials. In such processes, the spontaneous fluid flow caused by evaporation, heating, and composition gradient is inevitable. Actually, such fluid flow can be utilized to manipulate the mass transfer and the crystallization and assembly of nanomaterials. By controlling the pattern of the Marangoni flow, which is resulted from the surface tension variation, we are able to control the morphology of nanocrystals formed and the patterns of assembled nanomaterials. The examples include the preparation of thin films of carbon nanotubes or organic semiconductors on water surface, the morphology control of $CH_3NH_3PbBr_3$ crystals, the patterning of ordered functional materials (such as perovskite and carbon nanotubes) on substrates.

Corresponding Author: Yan. Li
Tel & Fax: +86-10-6275-6773
E-mail: yanli@pku.edu.cn

Science and Applications of Wafer-Scale Aligned Carbon Nanotube Films

○W. Gao,[1] N. Komatsu,[1] F. Katsutani,[1] X. Li,[1] K. Yanagi,[2] and J. Kono[1]

[1]*Department of Electrical and Computer Engineering, Rice University, Houston, Texas, USA*
[2]*Department of Physics, Tokyo Metropolitan University, Hachioji, Tokyo, Japan*

We have recently developed a slow vacuum filtration technique (Fig. 1a) to fabricate wafer-scale films (1 inch [1] and 2 inches [2] in diameter, as shown in Figs. 1b and 1c, respectively) of aligned and packed SWCNTs; see Figs. 1d-1g. We can further build unique architectures and devices through stacking and doping (Fig. 1c). In this talk, we summarize some of our recent accomplishments using these unique samples.

We have made the first observation of intersubband plasmons (ISBPs) in gated aligned films. For parallel polarization (Fig. 1h), the S_{11}, S_{22}, and M_{11} transitions disappear as carriers are injected; for perpendicular polarization (Fig. 1i), a new peak due to ISBP appears and grows as the carrier density increases. We have also made the first direct observation of the E_{12}/E_{21} peak in the optical absorption of an aligned (6,5) film (Fig. 1j), which allowed us to quantitatively determine the oscillator strength of this transition. We further built an exciton-polariton architecture by incorporating such films inside a Fabry-Pérot microcavity. This system displayed a continuous transition from the strong-coupling to the weak-coupling regime through facile polarization control (Figs. 1k-1m). The obtained dispersion surfaces revealed the existence of exceptional points and two equienergy arcs (Fig. 1n). Furthermore, the vacuum Rabi splitting exhibited cooperative enhancement (Fig. 1o).

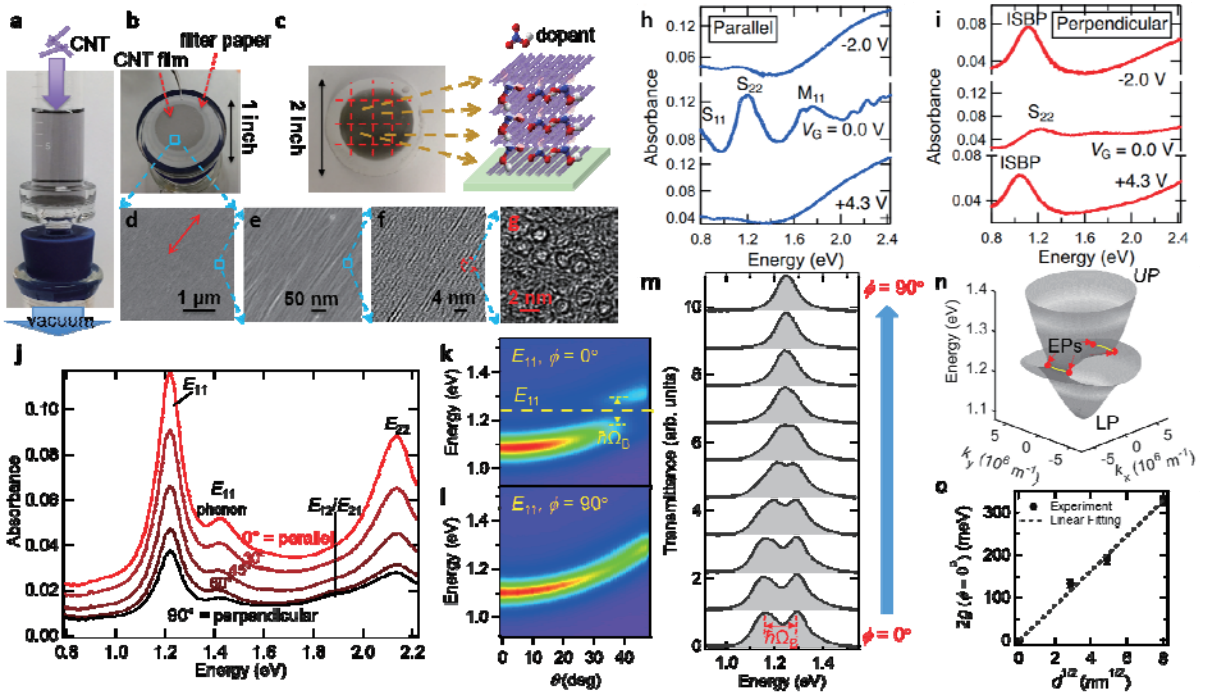

Fig. 1 (a) Vacuum filtration system to produce (b) 1-inch films, (c) 2-inch films and 3D achitectures of aligned and packed SWCNTs, as shown in images of (d, e) scanning electron microscopy and (f, g) transmision electron microscopy. (h) Parallel- and (i) perpendicular-polarization optical absorption spectra for gated films of aligned SWCNTs. (j) Polarization-dependent absorption spectra for an aligned (6,5) SWCNT film. Transmittance spectra of an exciton-polariton device with an 8-nm-thick aligned (6,5) SWCNT film for (k) ϕ = 0° and (l) ϕ = 90°. (m) Transmittance spectra at zero detuning for varying ϕ. (f) Dispersion surfaces for the device. (g) Vacuum Rabi splitting at ϕ = 0° versus the square root of the film thickness.

[1] He, X., *et al*., Nat. Nanotech. **11**, 633 (2016). [2] Komatsu, N., *et al*., Adv. Func. Mater. **27**, 1606022 (2017).
Corresponding Author: Junichiro Kono, Tel: +1-713-348-2209, Fax: +1-713-348-3091, E-mail: kono@rice.edu

Potential applications of CNT in automotive industries

○Hisayoshi Oshima

Advanced Research and Innovation Center, DENSO CORPORATION, Nisshin, Aichi 470-0111, Japan

Role and function of the automotive will be changed drastically in the near future. Key words are Connected, Autonomous, Shared, and Electric (CASE). Automotive industries think about they should change their business domains from manufacturing to value creation. However, I believe that “Those who control materials control technology” pointed by Eiji Kobayashi, Panasonic.

Carbon nanotube (CNT) have great potential in various fields including automotive applications, such as, heater, electrical wire, electrode of energy storage devices, reinforced filler, conductive filler, and so on. However it is very difficult to create killer products at the present time.

DESNO has been studying nano-carbon materials synthesis included CNT[1-3] and those applications[4,5] since 1999. In this symposium, I would like to introduce some of our activities related CNTs and discuss important points to achieve practical applications.

[1] H. Oshima *et al*. Jpn. J. Appl. Phys. **47**, 1982 (2008).
[2] H. Oshima *et al*. J. Phys. Chem C **113**, 18523(2009)
[3] R. Ohta *et al*. Chem. Com. **47**, 3873(2011)
[4] T. Iijima *et al*. Mat. Exp. **2**, 357(2012)
[5] H. Oshima *et al*. *The 24th Fullerene Nanotubes General Symposium, 72(2003)*

Corresponding Author: H. Oshima
Tel: +81-561-75-1827, Fax: +81-561-75-1185,
E-mail: HISAYOSHI_OOSHIMA@denso.co.jp

Field Emission from Carbon Nanotube and Graphene: Unique Characteristics and Related Phenomena

Yahachi Saito

Department of Applied Physics, Nagoya University, Nagoya 464-8603, Japan

Carbon nanotube (CNT) possesses various benefits as a field electron emitter, e.g., needle shape with a sharp tip, high chemical stability, mechanical strength and electrical conductivity. The sharp tip enables not only low voltage operation but also realization of high brightness and a small virtual source size which are advantageous for forming a finely focused electron beam with a simple lens system. Chemical inertness and stability of a CNT surface make an electron emission stable even under moderate ultrahigh vacuum, which alleviates the need for a massive vacuum pumping system. By employing CNT as an electron source, therefore, a field emission scanning electron microscope (FE-SEM) can be miniaturized whilst keeping high performance. Recently, a CNT-based FE-SEM hosting a projection type X-ray microscope (XRM) is developed [1].

Carbon forms a variety of allotropes: e.g., diamond, graphite, fullerene, and CNT. Besides the established allotropes, carbyne, an infinite carbon chain, has attracted much interest with significant controversy since the late 1960's. In 2003 and 2016, linear carbon-chains (LCCs) encapsulated inside CNTs were discovered in multiwall CNTs produced by arc discharge [2] and in double-wall CNTs (DWCNTs) annealed at high-temperature [3], respectively. Recently, we found unexpectedly LCCs inside SWCNTs, as shown in Fig. 1, after an electric discharge of the SWCNT films which were used as a cathode of field emission [4]. This method of LCC synthesis is a new route toward a bulk production of LCCs.

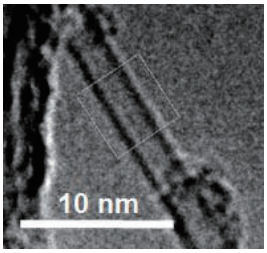

Fig. 1 LCC inside SWCNT

Graphene with a finite size has edges by itself, and electronic states at the edges exhibit peculiar properties, e.g., spin polarization (ferromagnetic order) at zigzag edges (Fig. 2). Field emission microscopy (FEM) study on electron emission from graphene edges [5] has revealed that FEM patterns from an open graphene edge show a symmetry of π orbitals at a graphene edge. In addition to FEM studies, field ion microcopy (FIM) images exhibiting unoccupied π* orbitals at graphene edges are observed. Recently, spin-polarization of electrons field-emitted from graphene edges was measured using an FE appratus with Mott detectors, showing the magnitude of spin polarization of about 25 % [6].

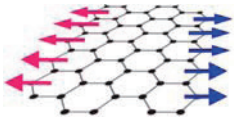

Fig. 2 Spin polarization at zigzag edges

[1] M. Irita, S. Yamazaki, H. Nakahara, Y. Saito, Presented at ALC'17 (Dec. 3-8, 2017, Kauai, Hawaii).

[2] X. Zhao Y. Ando, Y. Liu, M. Jinno, T. Suzuki, Phys. Rev. Lett. **90** (2003) 187401.

[3] L. Shi et al., Nature Mater. **15** (2016) 634.

[4] S. Toma, K. Asaka, M. Irita Y. Saito, Presented at ALC'17 (Dec. 3-8, 2017, Kauai, Hawaii).

[5] N. Yokoyama, K. Nakakubo, K. Iwata, K. Asaka, H. Nakahara, Y. Saito, Surf. Interface Anal. **48** (2016) 1217.

[6] S. Nagai, H. Ikemizu, K. Kunoh, K. Hata, Y. Watanabe, T. Hoshino, M. Irita, H. Nakahara and Y. Saito, Presented at ALC'17 (Dec. 3-8, 2017, Kauai, Hawaii).

Tel: +81-52-789-4459, Fax: +81-52-789-3703, E-mail: ysaito@nagoya-u.jp

Quantum transport in van der Waals junctions of 2D materials

Tomoki Machida[1,2]

[1] *Institute of Industrial Science, University of Tokyo, Tokyo 153-8505, Japan*
[2] *CREST, Japan Science and Technology Agency, Japan*

Recent advances in transfer techniques of atomic layers have enabled one to fabricate van der Waals junctions of various two-dimensional (2D) materials, which include graphene, hexagonal boron nitride (h-BN), transition-metal dichalcogenides (TMDs), layered ferromagnetic metal, and layered superconductors. Unique characteristics of the van der Waals junctions have been opening up new possibilities in fundamental science and device applications: the stacking of various atomic layers with different material properties without their lattice matching at the interface, the controllability of twist angle between atomic layers to modulate the band structure, and the ideal digital-like interfaces without diffusion and segregation.

Here, we present development of the fabrication techniques and quantum transport experiments in van der Waals junctions: (i) Dirac fermion reflector in ballistic graphene/h-BN [1], (ii) mechanical exfoliation of magnetic-atom-intercalated transition metal dichalcogenides, $Cr_{1/3}TaS_2$ and $Fe_{1/4}TaS_2$, and their van der Waals assembly to exhibit tunnel magnetoresistance effect [2], (iii) p-type and n-type carrier injection into WSe_2 using $NbSe_2$ and graphite, respectively [3], (iv) suppression of the exciton-exciton annihilation rate in hBN/WS_2/hBN studied by time-resolved photoluminescence spectroscopy [4], (v) inter-subband Landau level couplings induced by in-plane magnetic fields in trilayer graphene [5], (vi) cyclotron resonance absorption in monolayer, bilayer, twisted bilayer, and trilayer graphene, (vii) the influence of the C-doped domains in h-BN on electrical transport and optical properties of 2D materials above, and (viii) robotic searching and assembly of van der Waals superlattices.

[1] S. Morikawa, Q. Wilmart S. Masubuchi, K. Watanabe, T. Taniguchi, B. Placais, and T. Machida, Semicond. Sci. and Technol. **32**, 045010 (2017).
[2] Y. Yamasaki, R. Moriya, M. Arai, S. Masubuchi, S. Pyon, T. Tamegai, K. Ueno, and T. Machida, 2D Materials **4**, 041007 (2017).
[3] Y. Sata, R. Moriya, S. Masubuchi, K. Watanabe, T. Taniguchi, and T. Machida, Jpn. J. Appl. Phys. **56**, 04CK09 (2017).
[4] Y. Hoshi T. Kuroda, M. Okada, R. Moriya, S. Masubuchi, K. Watanabe, T. Taniguchi, R. Kitaura, and T. Machida, Phys. Rev. B **95**, 241403 (2017).
[5] Y. Asakawa, S. Masubuchi, N. Inoue, S. Morikawa, K. Watanabe, T. Taniguchi, and T. Machida, Phys. Rev. Lett. **119**, 186802 (2017).
[6] Y. Ota, R. Moriya, N. Yabuki, M. Arai, M. Kakuda, S. Iwamoto, T. Machida, and Y. Arakawa, Appl. Phys. Lett. **110**, 223105 (2017).
[7] Y. Sata, R. Moriya, N. Yabuki, S. Masubuchi, and T. Machida (submitted).
[8] S. Masubuchi, M. Morimoto, M. Onodera, S. Morikawa, K. Watanabe, T. Taniguchi, and T. Machida (submitted).

Corresponding Author: T. Machida
Tel: +81-3-5452-6742, Fax: +81-3-5452-6743
E-mail: tmachida@iis.u-tokyo.ac.jp

Exploring Molecular Nanocarbon Science

Kenichiro Itami [1,2,3]

[1] *Institute of Transformative Bio-Molecules (WPI-ITbM), Nagoya University, Chikusa, Nagoya 464-8602, Japan*
[2] *Department of Chemistry, Nagoya University, Chikusa, Nagoya 464-8602, Japan*
[3] *JST-ERATO, Itami Molecular Nanocarbon Project, Chikusa, Nagoya 464-8602, Japan*

Toward addressing the grand challenge in nanocarbon science, we are trying to synthesize structurally uniform nanocarbons and a new form of carbons.[1] To achieve this goal, the development of new reactions and catalysts has been the key. For example, our powerful palladium catalyst can promote the regioselective aromatic π-extension (APEX)[2] of polycyclic aromatic hydrocarbons (PAHs). This C-H activation methodology can be applied to various planar and geodesic PAHs to generate graphene nanoribbons[3-5] and three-dimensional warped nanographenes.[6] In addition to the above-mentioned chemistry of nanoribbons and saddles, our synthetic campaign toward carbon nanotubes[7] and carbon nanobelts[8] will also be described.

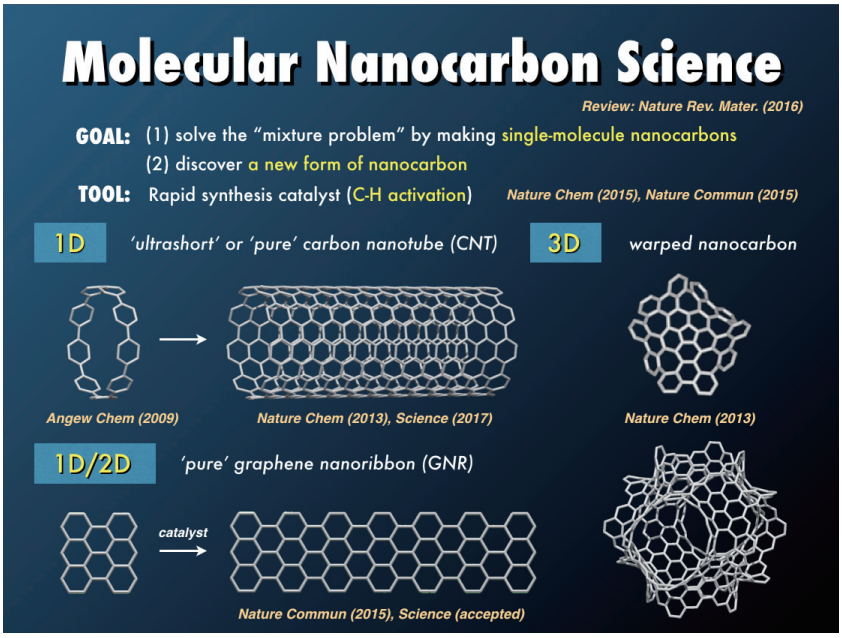

[1] Y. Segawa *et al.* Nature Rev. Mater. **1**, 15002 (2016).
[2] H. Ito *et al.* Angew. Chem. Int. Ed. **56**, 11144 (2017).
[3] K. Ozaki *et al.* Nature Commun. **6**, 6251 (2015).
[4] Y. Yano *et al.* In preparation.
[5] Y. Koga *et al.* Science, in press (2018).
[6] K. Kawasumi *et al.* Nature Chem. **5**, 739 (2013).
[7] H. Omachi *et al.* Nature Chem. **5**, 572 (2013).
[8] G. Povie *et al. Science* **356**, 172 (2017).

Corresponding Author: K. Itami
Tel: +81-52-788-6098, Fax: +81-52-788-6098, E-mail: itami@chem.nagoya-u.ac.jp

Phonon engineering of graphene for thermal management

○Takayuki Arie

Department of Physics and Electronics, Osaka Prefecture University, Osaka 599-8531, Japan

Graphene is expected as a candidate for next-generation electronic devices due to its extremely high carrier mobility, flexibility, and thermal conductivity. Since the main heat carrier in graphene is phonon, the structural modification alters the thermal transport properties in graphene. For example, isotopically modified graphene shows 50% reduction in thermal conductivity by introducing 50% ^{13}C into carbon networks [1]. Further reduction is possible by creating isotopic heterojunctions, by which the thermal conductance of graphene is reduced by approximately 90% without changing its electrical properties [2,3]. These techniques to reduce the thermal conductivity can be applied for enhancing the thermoelectric device performance.

In this talk, the thermal conductivity reduction of graphene by another structural modification, defects, is mainly introduced. The graphene used in this study was synthesized by chemical vapor deposition with Cu foils as a catalyst. After transferred onto the substrates, controlled amount of defects was introduced by O_2 plasma. As the defect density increases, the defect stage changes from sp^3-type to vacancy-type, which was identified by Raman spectroscopy and X-ray photoelectron spectroscopy. Consequently, the electrical and thermoelectric properties of graphene decrease with the defect development. The thermal conductivity of graphene with defects, on the other hand, shows tremendous reduction, one order of magnitude lower than that of pristine graphene. At the vacancy-type defect stage, the thermoelectric performance of graphene predominantly relies on its thermal conductivity, resulting in threefold increase in thermoelectric figure of merit of graphene devices [4].

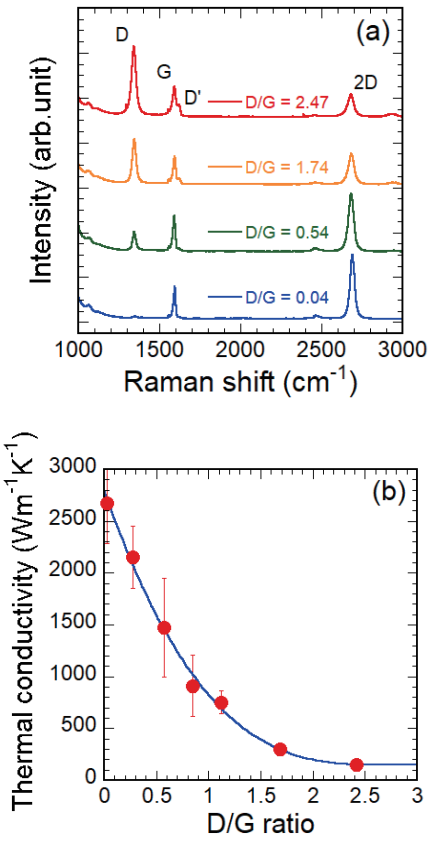

Fig.1 (a) Raman spectra and (b) thermal conductivity of graphene with various defect densities.

[1] S. Chen et al., Nat. Mater. 11, 203 (2012).
[2] Y. Anno, K. Takei, S. Akita, and T. Arie, Phys. Status Solidi RRL 8, 692 (2014).
[3] Y. Anno, K. Takei, S. Akita, and T. Arie, Adv. Electron. Mater. 1, 1500175 (2015).
[4] Y. Anno, Y. Imakita, K. Takei, S. Akita, and T. Arie, 2D Mater. 4, 025019 (2017).

Corresponding Author: T. Arie
Tel/Fax: +81-72-254-9265
E-mail: arie@pe.osakafu-u.ac.jp

Thermoelectric Properties of Fermi Level Tuned and Aligned Single Wall Carbon Nanotube Thin Films

Kazuhiro Yanagi

Department of Physics, Tokyo Metropolitan University, Tokyo 192-0397, Japan

Single wall carbon nanotubes (SWCNTs) are one-dimensional materials with sharp van Hove singularities. Preparation of SWCNTs with a selected electronic structure, fabrication of their aligned thin films,[1] and tuning of their Fermi level allow us to reveal unique phenomena, which cannot be observed or correctly understood in conventional SWCNT random networks. For example, we observed anomalously large optical absorption for perpendicular polarization to the tube axis in highly doped aligned SWCNTs, which is related to intersubband transition plasmon phenomena in SWCNTs.[2] This topic may be discussed by Prof. Kono in this symposium, thus here I discuss thermoelectric properties of Fermi level tuned and aligned SWCNT thin films.

In our society, a large amount of heat at relatively low temperature, which is emitted from factories, houses, human bodies, and so on, is left unused. Development of high-performance flexible thermoelectric devices is crucial to efficiently convert such unused waste heat into electric power. Understanding of relationships between electrical conductivity σ, Seebeck coefficient S, and thermal conductivity κ in thin films of flexible materials and tuning of these parameters is of great importance to improve the performance. SWCNTs are a model of low dimensional flexible materials, and will play important roles for realization of high-performance flexible thermoelectric devices. Since the seminal study by Hicks and Dresselhaus,[3] the thermoelectric properties of low dimensional materials have been intensively studied, but it still has been of great importance to experimentally clarify how the low dimensionality of a material influences and enhances its thermoelectric properties. For flexible thermoelectric applications, we must evaluate the thermoelectric properties in a thin film situation of the materials. Although the thermoelectric properties in a single rope situation of the materials are well understood, thermoelectric properties in the form of thin films are still under discussion. For example, in conventional solid metallic materials, there is a trade off between S and σ, such as increase of S leads to decrease of σ, however, in the case of SWCNTs sometimes we can observe the breaking of the trade-off (Fig. 1).[4] There is a universal trend in S versus σ, $S \propto \sigma^{-1/4}$, but we do not have a good theoretical model to explain the trend.[5] Moreover, it is not clear whether the Wiedemann-Franz law is applicable in thin films. Femi level tuned and aligned SWCNTs allow us to investigate the details of the background because we can systematically change the electronic structure, location of Fermi level, and conditions of contacts between the tubes. In this talk, I will present recent our results about thermoelectric properties of Fermi-level tuned and aligned SWCNTs and discuss how electronic structure, location of Fermi level, current, and thermal flow directions with respect to the tube axis influence on the S, σ and κ of SWCNT thin films.

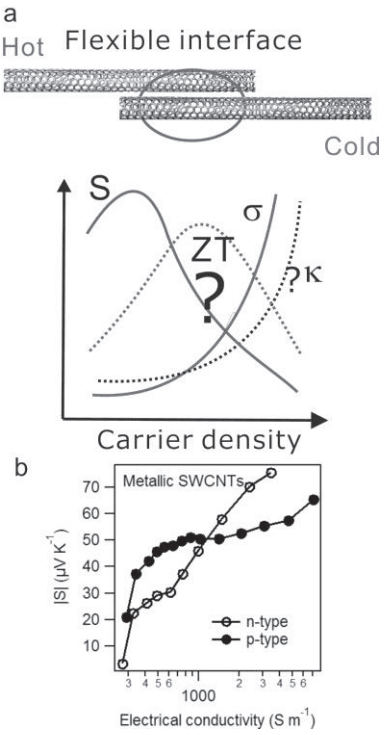

Fig. 1 (a) Relationships between S, σ, and κ at flexible interfaces as a function of carrier density are not well understood. For example, (b) the trade off between S and σ is broken in metallic SWCNTs

References: [1] He et al., Nat. Nanotechnol. 11, 1 (2016), [2] Yanagi, Kono et al., submitted., [3] Hicks & Dresselhaus, PRB 47, 16631 (1993) [4] Yanagi et al., Nano Lett. 14, 6437 (2014) [5] Kang & Snyder, Nature Mater. 16, 252 (2017). Corresponding Author: K. Yanagi, Tel: +81-42-677-2493, E-mail: yanagi-kazuhiro@tmu.ac.jp

招待講演
Invited Lecture

1 I – 1
2 I – 2

Advanced Carbon Based Energy Materials for Lithium-Sulfur Batteries

Qiang Zhang [1]

[1] *Department of Chemical Engineering, Tsinghua University, Beijing 100084, China*

Among various promising candidates with high energy densities, lithium-sulfur (Li-S) batteries with a high theoretical capacity and energy density are highly attractive;[1-2] while the commercial application of Li-S batteries still faces some persistent obstacles, such as the low electrical conductivity of sulfur and lithium sulfide and the dissolution of polysulfides. The introduction of nanocarbon into the field of Li-S batteries sheds a light on the efficient utilization of sulfur by improving the conductivity of the composites and restraining the shuttle of polysulfides. In this presentation, the concept for the rational design of nanocarbon for energy storage is explained. The advances in the use of advanced energy materials in the cathode, separator, and anode is explained.[3-14] New insights on the relationship between the nanostructure and the electrochemical performance are presented.

References

1) Peng HJ, Cheng XB, Huang JQ, Zhang Q. *Adv Energy Mater* 2017, 7, 1700260.
2) Cheng XB, Zhang R, Zhao CZ, Zhang Q. *Chem Rev* 2017, 117, 10403
3) Zhao MQ, Zhang Q, et al. *Nature Commun* 2014, 5, 3410.
4) Tang C, Zhang Q, et al. *Adv Mater* 2014. 26, 6100.
5) Peng HJ, Zhang Q. *Angew Chem Int Ed* 2015, 54, 11018.
6) Peng HJ, Zhang G, Chen X, Zhang ZW, Xu WT, Huang JQ, Zhang Q. *Angew Chem Int Ed* 2016, 55, 12990
7) Peng HJ, Zhang ZW, Huang JQ, Zhang G, Xie J, Xu WT, Shi JL, Chen X, Cheng XB, Zhang Q. *Adv. Mater.* 2016, 28, 9551
8) Cheng XB, Yan C, Chen X, Guan C, Huang JQ, Peng HJ, Zhang R, Yang ST, Zhang Q. *Chem* 2017, 2, 258.
9) Zhang XQ, Cheng XB, Chen X, Yan C, Zhang Q. *Adv Funct Mater* 2017, 27, 1605989.
10) Peng HJ, Huang JQ, Liu XY, Cheng XB, Xu WT, Zhao CZ, Wei F, Zhang Q. *J Am Chem Soc* 2017, 139, 8458.
11) Hou TZ, Xu WT, Chen X, Peng HJ , Huang JQ, Zhang Q. *Angew Chem Int Ed* 2017, 56, 8178
12) Zhang R, Chen XR, Chen X, Cheng XB, Zhang XQ, Yan C, Zhang Q. *Angew Chem Int Ed* 2017, 56, 7764.
13) Zhang XQ, Xu R, Chen X, Cheng XB, Zhang R, Chen XR, Zhang Q. *Angew Chem Int Ed* 2017, 56, 14207.
14) Sun YZ, Huang JQ, Zhao CZ, Zhang Q. Sci China Chem 2017, 60, 1508.

….

Corresponding Author: T. Tokyo
Tel: +86-10-6278-9041, Fax: +86-10-6277-2051.
E-mail: zhang-qiang@mails.tsinghua.edu.cn

Photoexcited states in transition metal dichalcogenide heterostructures

Fei Lu[1] and ○Erik Einarsson[1,2]

[1]*Department of Electrical Engineering, University at Buffalo, Buffalo, NY USA*
[2]*Department of Materials Design and Innovation, University at Buffalo, Buffalo, NY USA*

Two-dimensional transition metal dichalcogenides (TMDCs), such as MoS_2 and WS_2, have been researched extensively for their unique electrical and optical properties. TMDCs are also excellent material systems for studying the underlying physics of photoexcited states, namely excitons and trions. It is known that the photoluminescence (PL) intensity I and the excitation laser power L are related by the power law $I = L^k$.[1] The value of the exponent k depends on the type of excited state, with $k = 1$ for excitons and $k = 3/2$ for trions.[2] Based on this relation, many researchers have studied various exciton states in monolayer (1L) MoS_2 and 1L WS_2. Values of k ranging from approximately 0.9 to 1.3 have been reported, and were attributed to bound excitons, [2–5] but there are no reports to date of free trions in TMDCs indicated by $k = 1.5$.

Here we report power-dependent PL measurements of CVD-grown TMDC heterostructures consisting of 1L WS_2 atop 1L MoS_2. Our data show power law relations with $k = 1.43$ in the WS_2 layer and k = 1.51 in the MoS_2 layer, providing the first evidence of free trions in TMDC heterostructures.

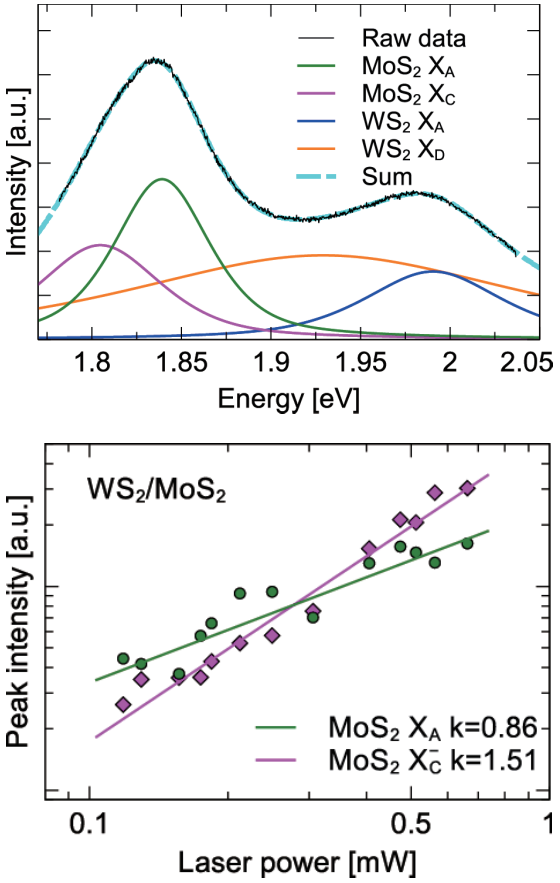

Fig. 1 (Top) Decomposed PL spectrum from WS_2/MoS_2 heterostructure and (bottom) MoS_2 PL peak intensity vs. excitation laser power.

[1] T. Schmidt, K. Lischka, W. Zulehner. *Phys Rev B* **45** (1992) 8989.

[2] D. Kaplan, Y. Gong, K. Mills, V. Swaminathan, P. M. Ajayan, S. Shirodkar, E. Kaxiras. *2D Mater* **3** (2016) 015005.

[3] Z. He, W. Xu, Y. Zhou, X. Wang, Y. Sheng, Y. Rong, S. Guo, J. Zhang, J. M. Smith, J. H. Warner. *ACS Nano* **10** (2016) 2176.

[4] V. Carozo, Y. Wang, K. Fujisawa, B. R. Carvalho, A. McCreary, S. Feng, Z. Lin, C. Zhou, N. Perea-López, A. L. Elías, B. Kabius, V. H. Crespi, M. Terrones. *Sci Adv* **3** (2017) e1602813.

[5] J. Shang, X. Shen, C. Cong, N. Peimyoo, B. Cao, M. Eginligil, T. Yu. *ACS Nano* **9** (2015) 647.

Corresponding Author: E. Einarsson
Tel: +1-716-645-5089,
E-mail: erikeina@buffalo.edu

一般講演
General Lecture

1 – 1 ～ 1 – 8
2 – 1 ～ 2 – 13
3 – 1 ～ 3 – 11

Tracing growth processes of individual single-walled carbon nanotubes by digital isotope coding

○Keigo Otsuka[1], Shun Yamamoto[1], Taiki Inoue[1], Rong Xiang[1], Shohei Chiashi[1], Shigeo Maruyama[1,2]

[1] *Department of Mechanical Engineering, The University of Tokyo, Tokyo 113-8656, Japan*
[2] *Energy NanoEngineering Laboratory, National Institute of Advanced Industrial Science and Technology (AIST), Tsukuba 305-8564, Japan*

Single-walled carbon nanotubes (SWNTs) attract attentions as a perfect alternative of silicon for high-performance electronics if those exclusively with semiconducting properties are prepared in a dense array structure. Despite significant progresses in controlled synthesis of SWNTs [1], the growth process remains a mystery due to their size, variety and system complexity. Although thermodynamic and kinetic control is important for the chirality controlled-synthesis, it is controversial, for example, whether the growth rate of SWNTs depends on their chirality [2-4]. Previous *in situ* and *ex situ* measurements often missed a variation of SWNTs and the presence of incubation/lifetime of the growth, respectively. Here we present a method to analyze the growth behavior, *e.g.* growth rate, incubation and lifetime, of individual SWNTs with length of 10–250 μm by embedding digital isotope labels.

SWNTs were grown from iron nanoparticles patterned in stripes on r-cut quartz substrates [4]. Binary-like codes were incorporated in SWNTs by periodically introducing the pulse of ^{13}C ethanol with three different ratios (Figure 1a), and then detected by *ex situ* Raman mapping. A Raman intensity map along an SWNT (Figure 1b) clearly shows G-band downshifts in three different levels. We found that after various lengths of incubation, SWNTs elongated at constant rates until abrupt termination (Figure 1c). This indicates the catalytic activity of nanoparticles does not change with time. In a rare event, the chirality changed along SWNTs, resulting in sudden modulation of the growth rate (Figure 1d). Such junctions could provide unique insights on intrinsic chirality-dependences. Similar analyses for the growth with a variety of catalysts and conditions, in combination with other characterization methods, would lead to a quantum leap in the control of chirality, length and density.

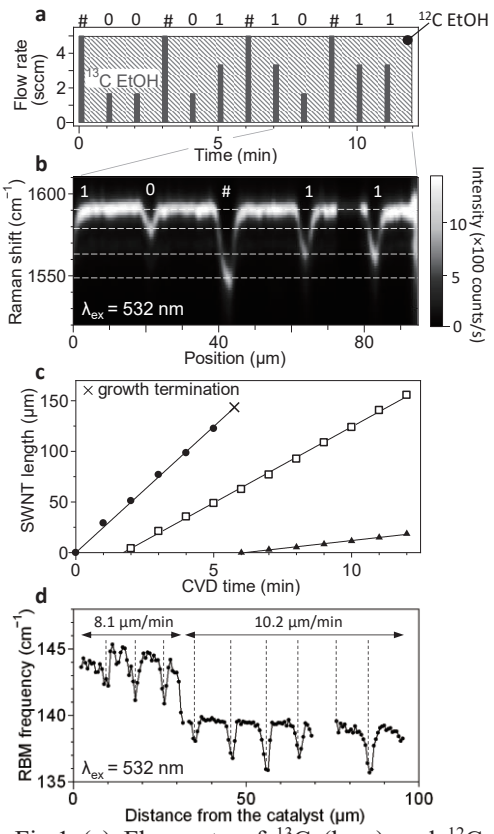

Fig.1 (a) Flow rate of ^{13}C (bars) and ^{12}C (shaded) ethanol for 2-bit isotope coding. (b) G-band spectra along an SWNT. (c) Typical time evolution of SWNT lengths. (d) Transition of RBM frequency along the SWNT with an intramolecular junction.

[1] S. Zhang *et al*., Nature **543**, 234 (2017).
[2] R. Rao *et al*., Nat. Mater. **11**, 213 (2012).
[3] M. He *et al*., Carbon **113**, 231 (2017).
[4] T. Inoue *et al*., J. Mater. Chem. A **3,** 15119 (2015).

Corresponding Author: S. Maruyama
Tel: +81-3-5841-6421, Fax: +81-3-5841-6983,
E-mail: maruyama@photon.t.u-tokyo.ac.jp

Effects of Pre-forming the different density layers on ELF method for the separation of metallic and semiconducting SWCNTs

○Yuki Kuwahara[1,3], Fusako Sasaki[3], Fumiyuki Nihey[2], Takeshi Saito[1,3]

[1] *National Institute of Advanced Industrial Science and Technology, Tsukuba 305-8565, Japan*
[2] *IoT Devices Research Laboratories, NEC Corporation, Tsukuba 305-8501, Japan*
[3] *Technology Research Association for Single Wall Carbon Nanotubes, Tsukuba 305-8565, Japan*

Single wall carbon nanotubes (SWCNTs) have received much attention as ink materials having both excellent electronic properties and chemical stability, especially in printed electronics. In particular, the separation of metallic/semiconducting SWCNTs is very important for the use of semiconducting properties. Among various separation methods, we have investigated the electric-field-induced layer formation (ELF) method.[1)] By applying an electric field in the longitudinal direction to SWCNT dispersion, separating metallic and semiconducting SWCNTs into upper and lower layer, respectively. Though the separation mechanism was unclarified, the difference in specific weight of the solution in the separation cell has been confirmed in previous work. In this study, we have focused on the density gradient in the separation cells on the separation of SWCNTs by ELF method and investigated the effect of introducing layers with different densities pre-formed in advance on separating SWCNTs. The analysis showed that the highly pure and concentrated layers of metallic and semiconducting SWCNT dispersion were formed by the ELF method with pre-formed layers. It is considered that pre-formed layers play an important role in producing effective density gradient for the separation of metallic and semiconducting SWCNTs. In this presentation, we will show the detailed results including the separation behavior of SWCNTs performed under various separation conditions.

References

[1] K. Ihara *et al.*, J. Phys. Chem. C **115**, 22827 (2011).

[2] T. Saito *et al.*, J. Nanosci. Nanotechnol. **8**, 6153 (2008).

Corresponding Author: T. Saito,

Tel: +81-29-861-4863, Fax: +81-29-861-4413,

E-mail: takeshi-saito@aist.go.jp

Influence of Dissolved Oxygen on Introduction of Defects into SWCNTs during Ultrasonic Dispersion Process

○Hiromichi Kataura, Tomoko Sugita, Mariko Kubota, Takeshi Tanaka

Nanomaterials Research Institute, AIST, Tsukuba, Ibaraki, 305-8565, Japan

Ultrasonic dispersion is very important process to get individually dispersed single-wall carbon nanotubes (SWCNTs), which is especially crucial for the metal/semiconductor separation and electronic device applications. However, it is well known that the ultrasonic dispersion process inevitably induces defects in SWCNT walls. It was suggested that in the dispersion process, dissolved oxygen gives influence to the defects introduction. Since there have been no systematic research on the effect of dissolved oxygen on the defects introduction on the SWCNTs, we tried to clarify it in this work.

For the assessment of defect introduction, we used a G/D intensity ratio of Raman spectrum. SWCNTs produced by electric arc discharge (AP grade, Carbon solutions INC, USA) was used as starting material. Sodium cholate 0.5 wt% aqueous solution was used as solvent. To avoid the effect of dissolved oxygen, all equipment was installed in a grove box filled with highly purified N_2 gas. As a control, the same experiments were done in air. After the dispersion process, samples were ultracentrifuged for 30 min and upper 80% supernatant was collected. Then we measured Raman spectra of all samples using 488, 532, 633, and 785 nm lasers. Since mean diameter of AP SWCNT is around 1.4 nm, resonance of semiconducting SWCNTs were observed for 488 and 532 excitations. We have analyzed G/D ratios for them. Interestingly, G/D ratio of SWCNTs dispersed in pure N_2 was lower than that in air. Because saturated N_2 concentration in water is smaller than that of air (N_2+O_2), a cavitation effect was lower in pure N_2 condition. Therefore, ultrasonic power was applied to SWCNT more effectively in pure N_2 condition, which causes quicker dispersion but more defects. To see the true effect of dissolved oxygen, therefore, we have to analyze a relationship between the dispersion efficiency and defect introduction. Figure 1 shows a relation between G/D ratio and the dispersion efficiency. In pure N_2 condition, G/D ratio was higher for the same dispersion efficiency. This result suggests that the ultrasonic dispersion process in pure N_2 is effective to get lower defective SWCNT dispersion.

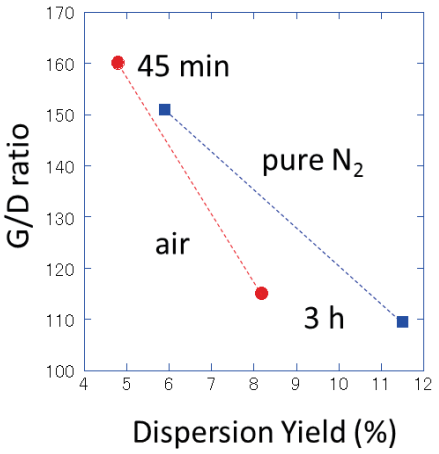

Figure 1. G/D ratio and dispersion yield

This work was supported by JST CREST Grant Number JPMJCR16Q2, Japan.

Corresponding Author: H. Kataura
Tel: +81-29-861-2551, Fax: +81-29-861-2786,
E-mail: h-kataura@aist.go.jp

Determination of association constants in complexation of nanotweezers and nanocalipers with SWNTs

○ Alejandro López-Moreno, Naoki Komatsu

Graduate School of Human and Environmental Studies, Kyoto University, 606-8501 Kyoto

In contrast to soluble host–guest system, the insolubility of SWNTs makes impossible the determination of the molar concentration of SWNTs in solution, which limits understanding of the supramolecular association of SWNTs. However, a new and simple procedure for the quantitative determination of association constants between soluble molecules and insoluble CNT samples has recently been reported [1]. In this paper, we applied this method to determine the association constants of pyrene **1**, pyrene-based nanotweezers **2**, and pyrene-nanocalipers **3** with SWNTs. The structures of the host moelcules **1** - **3** are shown in Figure 1 [2].

The procedure is as follows: SWNTs (65-CoMoCAT) were suspended in a solution of known concentration of the host, stirred for two hours and filtered. After thermogravimetric analysis of the solid, the association constant was calculated by plotting the degree of functionalization against the concentration of the free host. The association constants (K_a) determined in DMF are shown in Table 1. The nanotweezers **2** and nanocalipers **3** exhibit higher association constants than pyrene **1** by two and three orders of magnitude, respectively. This trend is proportional qualitatively to the number of interactions between the host molecules with SWNT surface to stabilize the complexes. We will also determine the association constants of porphyrin and porphyrin-based nanotweezers and nanocalipers, and will compare with those of the pyrene analogues.

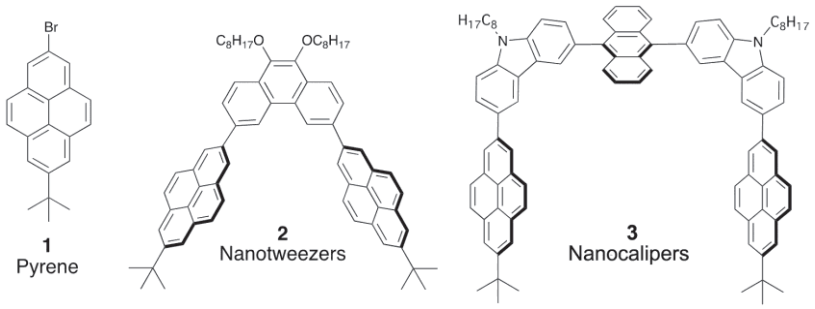

Figure 1 Structures of pyrene **1**, pyrene-based nanotweezers **2**, and pyrene-based nanocalipers **3**.

Table 1 Association constants of **1 – 3** with SWNTs in DMF

	Pyrene **1**	Nanotweezers **2**	Nanocalipers **3**
Association constant K_a (M^{-1})	12.6 ± 0.6	(4 ± 2) x 10^3	(5 ± 2) x 10^4

[1] A. de Juan, A. López-Moreno, J. Calbo, E. Ortí, E. M. Pérez, Chem. Sci. **6**, 7008 (2015); J. Calbo, A. López-Moreno, A. de Juan, J. Comer, E. Ortí, E. M. Pérez, Chem. Eur. J. **23**, 12909 (2017)

[2] G. Liu, A. F. M. M. Rahman, S. Chaunchaiyakul, T. Kimura, Y. Kuwahara, N. Komatsu, Chem. Eur. J. **19**, 16221 (2013); G. Liu, F. Wang, S. Chaunchaiyakul, Y. Saito, A. K. Bauri, T. Kimura, Y. Kuwahara, N. Komatsu, J. Am. Chem. Soc. **135**, 4805 (2013); F. Wang, K. Matsuda, A. F. M. M. Rahman, X. Peng, T. Kimura, N. Komatsu, J. Am. Chem. Soc., **132**, 10876 (2010); G. Liu, Y. Miyake, N. Komatsu, Org. Chem. Front. **4**, 911 (2017)

Corresponding Author: A. López-Moreno
Tel: +75-753-7871, E-mail: lopez.alejandro.74a@st.kyoto-u.ac.jp

Record-high Efficiency in Carbon Nanotube Electrode-used Perovskite Solar Cells via employing Formamidinium Lead Iodide ($FAPbI_3$) and Trifluoromethanesulfonic Acid Vapor Doping

○Il Jeon [1], Jin-Wook Lee [2], Anton Anissimov [3,4], Esko. I. Kauppinen [4], Yang Yang [2], Shigeo Maruyama [1,5], Yutaka Matsuo [1,6]

[1] *Department of Mechanical Engineering, The University of Tokyo, Tokyo 113-8656, Japan*
[2] *Department of Materials Science and Engineering and California Nano Systems Institute, University of California Los Angeles (UCLA), Los Angeles, CA 90095, USA*
[3] *Canatu Ltd., FI-00390 Helsinki, Finland*
[4] *Department of Applied Physics, Aalto University School of Science, Aalto FI-00076, Finland*
[5] *Research Institute for Energy Conservation, National Institute of Advanced Industrial Science and Technology (AIST), Tsukuba 305-8565, Japan*
[6] *Hefei National Laboratory for Physical Sciences at Microscale, University of Science and Technology of China (USTC), Hefei, Anhui 230026, China*

Perovskite solar cells (PSCs) with their reported power conversion efficiencies (PCEs) over 20% have emerged as next-generation solar cells. However, stability and high fabrication cost are limitations to further advancement. Since the first application by Li et al.,[1] researchers around the world have started to incorporate single-walled carbon nanotubes (SWNTs) in PSCs to increase the stability and to bring down the fabrication cost. Snaith and his colleagues have reported significant improvement in stability by inserting SWNTs under metal electrode.[2] Aitola et al. reported high thermal and air stability by replacing expensive metal electrode with SWNTs.[3] In addition, we employed fullerenes and polymer-wrapped SWNTs at the same time to achieve hysteresis-free and 1000 hour-long stable PSCs.[4] However, the reported top SWNT electrode-based PSCs have exhibited lower PCEs than the metal electrode-based PSCs, due mainly to 1) SWNT-based PSCs not being able to exploit reflection of sunlight unlike metals and 2) SWNTs possessing lower conductivity than metals.

In metal-electrode PSCs, the long-wavelengths of sunlight, which do not get fully absorbed by the perovskite layer, are reflected by the metal electrode for further absorption. As SWNT electrode are not reflective, the long-wavelengths of incoming sunlight are wasted in SWNT top electrode-based PSCs. Therefore, maximising the light absorption by using low-band gap perovskites, such as $FAPbI_3$, is crucial for the SWNT-used PSCs. Recently, Prof. Yang Yang of UCLA achieved stable fully $FAPbI_3$ PSCs (submitted). Applying this technology, we achieved a high short-circuit current density (J_{SC}) of 24.2 mA cm^{-2}. To enhance the device performance even further, we doped the SWNTs with trifluoromethanesulfonic acid (TFMS), which is extremely effective and durable. We used vapour doping on SWNTs before the lamination, because applying dopant directly onto SWNTs damages underneath layers and this is why doped SWNT top electrode has not been reported in PSCs, thus far. TFMS vapour-doped SWNT PSCs resulted in an increased fill factor (FF), producing a record-high PCE of 17.6% among the reported SWNT PSCs.

[1] Li *et al*. ACS Nano **8**, 6797 (2014). [2] Habisreutinger *et al.* Nano Lett. **14**, 5561 (2014)., Habisreutinger *et al.* ACS Energy Lett. **2**, 622 (2017). [3] Aitola *et al.* Energy Environ. Sci. **7**, 3690 (2014)., Aitola *et al.* Adv. Mater. **29**, 1606398 (2017). [4] Ahn *et al.* J. Mater. Chem. A in print.

Corresponding Author: Y. Matsuo
Tel: +81-3-5814-0978
E-mail: matsuo@photon.t.u-tokyo.ac.jp

Carbon-nanotube differential amplifier on flexible substrate

Tomoki Matsuura[1], Taiga Kashima[1], Jun Hirotani[1], Shigeru Kishimoto[1], and ○Yutaka Ohno[1,2]

[1]*Department of Electronics, Nagoya University, Nagoya 464-8603, Japan*
[2]*Institute of Material and Systems for Sustainability, Nagoya University, Nagoya 464-8603, Japan*

A differential amplifier is a fundamental analog amplification circuit used for various sensor devices. For wearable sensors, mechanically-flexible amplifiers are desirable. Carbon nanotube thin-film transistors (CNT TFTs) are considered as a possible active component of flexible devices because of their high mobility [1] and flexibility. In recent years, high-yield and reproducible fabrication of CNT TFTs became possible by using purified semiconducting CNTs, leading extensive study on circuit applications. In this work, we are focusing on the analog circuit application of CNT TFTs. To design CNT-based analog circuits, circuit simulations have been performed by using a precise device model which has been built on the basis of electrical characterizations of CNT TFTs. We have realized differential amplifiers on a flexible and transparent plastic film. CNT-based differential amplifiers were fabricated on a polyethylene naphthalate film as shown in Fig. 1. Bottom-gate CNT TFTs with purified semiconducting CNTs were used as the active device. A differential output was obtained with respect to a differential input. Maximum voltage gain of 16.3 (24.3 dB) was achieved for a sinusoidal wave input of 100 mV_{pp} at 100 Hz with a power source of -12 V. Figure 2 shows the gain as a function of frequency, exhibiting -20 dB/ decay. The unity gain frequency was 2.1 kHz.

Acknowledgments: The semiconducting CNTs were provided by TASC. This work was partially supported by JST/CREST.

[1] D.-M. Sun, et al., Nature Nanotechnol. 6, 156 (2011).

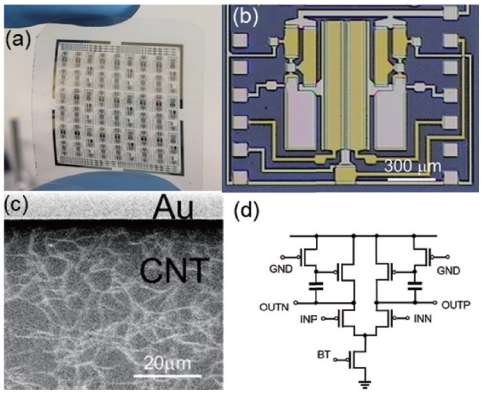

Fig. 1 CNT differential amplifier on plastic film. (a) Photograph of chip, (b) photograph of circuit, (c) SEM image of CNT thin film.

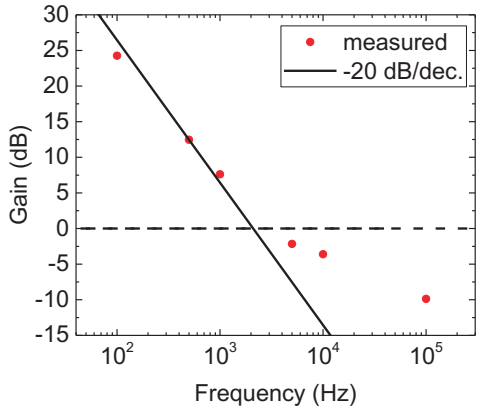

Fig. 2 Frequency dependence of voltage gain.

Corresponding Author: Yutaka Ohno, Phone & Fax: +81-52-789-5387, E-mail: yohno@nagoya-u.jp

Carbon Nanotubes versus Graphene as Flexible Transparent Electrodes in Inverted Perovskite Solar Cells

Jungjin Yoon [1], Il Jeon [2], Namyoung Ahn [1], Mohamed Atwa [2], Clement Delacou [2], Anton Anisimov [3], Esko I. Kauppinen [4], Shigeo Maruyama [2], and Yutaka Matsuo [2], and Mansoo Choi [1]

[1]*Global Frontier Center for Multiscale Energy Systems, Seoul National University, Seoul 08826, South Korea*
[2]*Department of Mechanical Engineering, School of Engineering, The University of Tokyo, Tokyo 113-8656, Japan*
[3]*Canatu Ltd. Konalankuja 5, FI-00390 Helsinki, Finland*
[4]*Department of Applied Physics, Aalto University School of Science, FI-00076 Aalto, Finland*

Due to the compatibility of fabrication at low temperature, perovskite solar cells (PSCs) have attracted much anticipation from scientists and engineers with flexible applications as well as their high power conversion efficiency (PCE) over 20%. However, the commonly-used transparent electrode material in flexible solar cells, indium tin oxide (ITO) hinders a realization of cheap, flexible and highly efficient portable energy devices because of its cost-issue by limited reserves in nature and inflexibility by its brittleness [1]. This being so, a cost-effective transparent electrode with high flexibility is needed to realize the flexible PSCs. Among various candidates as the alternative, carbon-based nanomaterials such as graphene and carbon nanotubes (CNTs) satisfy both aspect of cost and flexibility and each of them was utilized as a transparent electrode of solar cells in previous reports. Still, there has not been a direct comparison of two carbon-based electrode materials as flexible transparent electrodes in PSCs.

In this work, we conducted a comparative study of graphene and CNTs as a flexible transparent electrode in PSCs in terms of reliability and a device performance including PCE and flexibility [2]. Two commonly used doping method to increase electrical conductance of the carbon-based materials were tried and compared. The CNTs- and graphene- based devices showed PCEs of 12.8% and 14.2%, respectively. The difference of CNTs and graphene in the photovoltaic performance was due to the difference in surface roughness and optical transmittance. Raman spectroscopy and four-probe measurement after stretching samples showed that graphene is more susceptible to degradation by stretching (bending) than CNTs due to wrinkles and fissures formed on the graphene during its transfer process. Bending test of the flexible PSCs also showed higher flexural robustness of CNT-based devices compared with graphene-based ones, though the difference was marginal. Overall, graphene seems to be a better option than CNTs as flexible transparent electrodes in PSCs because the smoother roughness and transparency, if the transfer process of graphene guarantees the reproducibility and quality of graphene.

[1] B. J. Kim *et al*. Energy Environ. Sci., **8**, 916 (2015).
[2] I. Jeon *et al*. J. Phys. Chem. Lett., **8**, 21 (2017).
Corresponding Author: Professor Mansoo Choi
Tel: +81-2-887-8626, Fax: +82-2-887-8762,
E-mail: mchoi@snu.ac.kr

Interdigitated electrode with high mass density carbon nanotube forests for electrochemical biosensors

○Hisashi Sugime[1], Takuya Ushiyama[2], Keita Nishimura[2], Yutaka Ohno[2], Suguru Noda[3]

[1] *Waseda Institute for Advanced Study, Waseda University, Tokyo 169-8050, Japan*
[2] *Institute of Materials and Systems for Sustainability, Nagoya University, Nagoya 464-8603, Japan*
[3] *Department of Applied Chemistry, Waseda University, Tokyo 169-8555, Japan*

Electrochemical label-free sensing using redox reactions is one of the powerful and feasible methods to detect biomolecules with high sensitivity. Among several geometries of electrodes, interdigitated electrode (IDE) has an advantage for high sensitivity because the current by redox reactions is amplified by shuttling of analytes if the distance of the electrodes is smaller than the diffusion length of analytes. As a candidate material for the electrodes in IDE, carbon materials are widely studied due to their fast electron transfer kinetics and wide potential windows.[1] Among others, carbon nanotubes (CNTs) have several advantages such as high aspect ratio with large surface area and high electrical conductivity. Direct growth of CNTs on substrates by chemical vapor deposition is especially a suitable way to integrate the CNTs into the IDE.

In this report, we applied the dense CNT forests on conductive supports[2,3] to the IDE by combining the UV lithography and the CVD process (Fig. 1a and 1b). By optimizing the geometry of the electrodes (width and gap) and the morphology of the CNT forests (height and density), the performance of the IDE was significantly improved. The cyclic voltammetry (CV) measurements of $K_4[Fe(CN)_6]$ (100 µM) in KCl (100 mM) showed that the redox current of IDE with CNTs (CNTF-IDE) reached to the diffusion-limited current much more rapidly compared to that of conventional Au-IDE (Fig. 1c and 1d). By the redox cycling, the redox current was amplified by a factor of ~18 with the CNTF-IDE which is ~3 times higher than that with the Au-IDE. As a model case of the biomolecules, dopamine (DA) which is one of the main neurotransmitters was measured under coexistence of L-ascorbic acid (100 µM). The selective detection of DA was achieved with the linear range of 100 nM – 100 µM and the limit of detection (LOD, S/N=3) of ~40 nM with the optimized electrode structure.

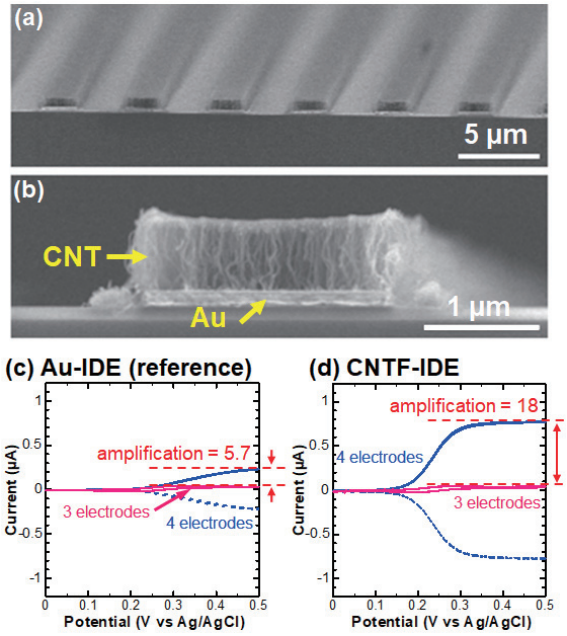

Fig. 1: (a) Oblique-view and (b) side-view SEM images of the CNT forests on Au electrodes. CV results of (c) Au-IDE (reference) and (d) CNTF-IDE with the $K_4[Fe(CN)_6]$ (100 µM) in KCl (100 mM) at the scan rate of 10 mV/s.

[1] Niwa et al., Anal. Chem. 66, 285 (1994).
[2] Sugime et al., Appl. Phys. Lett. 103, 073116 (2013).
[3] Sugime et al., ACS Appl. Mater. Interfaces 6, 15440 (2014).

Corresponding Author: H. Sugime
Tel: +81-3-5286-2769
E-mail: sugime@aoni.waseda.jp

Systematic studies on structures and properties of commercialized CNT fibers

○Takayuki Watanabe[1], Satoshi Yamashita[2], Takahiro Morimoto[1], Kazufumi Kobashi[1] and Toshiya Okazaki[1]

[1] CNT Application Research Center, National Institute of Advanced Industrial Science and Technology (AIST), Tsukuba, 305-8565, Japan
[2] Research Association of High-Throughput Design and Development for Advanced Functional Materials (ADMAT), Tsukuba, 305-8565, Japan

Fiber structure is one of the commonly used forms when carbon nanotubes (CNTs) are processed for application. They have potential abilities as electric wires and high strength materials because of CNT's high conductivity and superior mechanical properties. However, in most reports, homemade CNT fibers were used and systematic study of various CNT fibers have so far been limited. In this presentation, several types of commercially available CNT fibers are investigated and compared.

Figure 1 shows macro scale structure of CNT fibers studied in this presentation. They are categorized into 3 types, *i.e.*, A) fiber spun from multi-wall CNT (MWCNT) forest grown by the CVD method, which is most common type in CNT fiber, B) wet spun fiber and C) others. Nanocomp Miralon is type C), Meijo eDIPS EC-Y is type B) and other fibers belong to type A). It is clearly seen that same type CNT fibers show similarities in structural shapes such as homogeneity and fiber roundness. This result implies that structural quality of A type is high while the other types still have room for improvement.

In the presentation, further information of fiber structure (e.g. micro scale structure), basic property of CNT fiber (conductivity, mechanical strength and so on) and the relationship between them will be reported.

This presentation is based on results obtained from a project (P16010) commissioned by the New Energy and Industrial Technology Development Organization (NEDO).

Corresponding Author: T. Okazaki
E-mail: toshi.okazaki@aist.go. jp

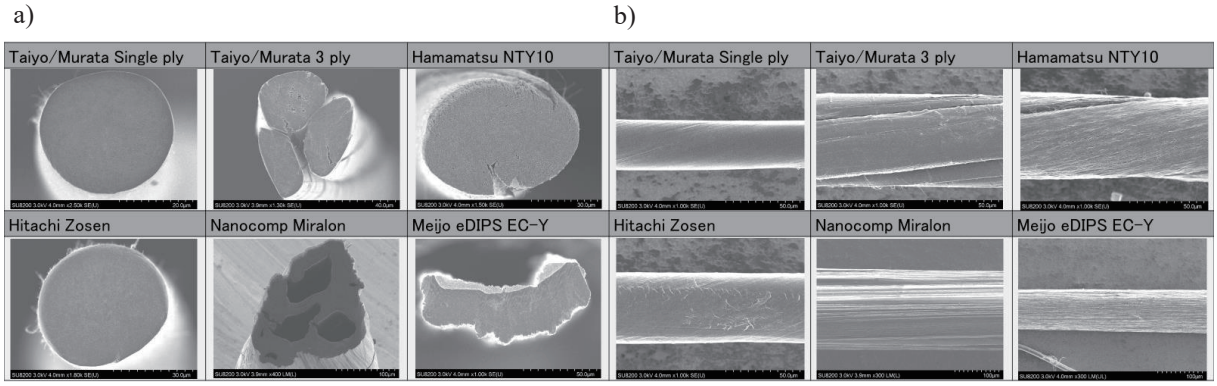

Fig.1 SEM images of commercially available CNT fibers. a) cross section, and b) side.

Biodegradation Rate of Carbon Nanotube Depending on Diameters

○M. Zhang[1], Y. Deng[1], M. Yang[1], H. Nakajima[1], M. Yudasaka[1, 2], S. Iijima[2], T. Okazaki1[1]

[1] *National Institute of Advanced Science and Technology (AIST)*
[2] *Faculty of Science & Technology, Meijo University*

The widespread applications of carbon nanotubes (CNTs) raise the possibility to get into the environment. Although studies have shown that most types of CNTs had low toxicity in vitro and in vivo, the inhalation exposure of a few types of CNTs induced malignant mesothelioma in animal studies, suggesting that CNTs may pose hazards similar to asbestos [1]. In order to protect environment and mitigate health problem caused by CNTs, we need to fully understand the fate of various types of CNTs after entering environment or human body. The previous studies have shown that CNTs are possible to be degraded by enzymatic oxidation in neutrophil or macrophages [2-3], however, biodegradation characteristics for different types of CNTs are still not clear. Because the biodegradation mechanism of CNTs was confirmed to be the oxidation of CNTs with hypochlorous acid, which was generated by enzymatic reaction [4], in this study, we have used sodium hypochlorite directly as oxidant to treat CNTs. Our purpose is to clarify the relationships between the structural characteristics and the degradation capacity of several types of CNTs.

7-types of CNTs including single- and multi-walled CNTs were dispersed homogenously in BSA aqueous solution by ultrasonic homogenizer for 5 h. The dispersions of CNTs were added into 5% sodium hypochlorite solution and kept at 37^{o}C for 24 h. The quantity-change of CNTs after treatment with sodium hypochlorite solution for 0-24 h was estimated from the absorbance at 700 nm. The results showed that the degradation of CNTs by sodium hypochlorite is greatly dependent on their types and diameters. Single-wall CNTs (SWNTs) and smaller diameter of multi-wall CNTs (MWNTs) were completely degraded by 24 h treatment, but the decrease of larger diameter MWNTs amount was only ~30%. The degradation rates of CNTs were SWNTs > MWNTs with small diameter > MWNTs with larger diameter. In addition, we have found that the graphene oxide was an intermediate product during the degradation of SWNTs, suggesting that the oxidative degradation of CNTs might proceed via unzipping process. The results obtained in this study will be significant for clarifying the factors that influence the degradation characteristics of CNTs and, therefore, be helpful to predict the toxicity of CNTs from their physical and chemical properties.

[1] A. Takagi, et al. J. Toxicol. Sci. 33, 105–116 (2008).
[2] V. E. Kagan et al. Nature Nanotech. 5, 354–359 (2010).
[3] M. Zhang et al. Nanoscale, 7, 2834-2840 (2015).
[4] I. I. Vlasova, et al. Russian Journal of Bioorganic Chemistry, 37, 453–463 (2011).

Corresponding Author: M. Zhang
Tel: +81-29-861-6758
E-mail: m-zhang@aist.go.jp

Growth of Horizontally Aligned Chirality-Specific SWNTs using Intermetallic W_6Co_7 Catalysts

○ Feng Yang, Yan Li*
College of Chemistry and Molecular Engineering, Peking University, Beijing 100871 China

High-performance and integrated circuits essentially require SWNT samples with well-aligned arrays of pure chirality. We have developed a new family of catalysts, tungsten-based intermetallic compounds, which have unique crystal structure and desired atomic arrangements and therefore can act as the structural templates for chirality specific growth of SWNTs, relying on the high selectivity in geometry match between catalysts and SWNTs [1-4]. The characterization of catalyst structure is very important to reveal the growth mechanism of SWNTs. The W_6Co_7 catalyst structure during and after the CVD process was clearly revealed by X-ray absorption spectroscopy (XAS) and transmission electron microscopy (TEM). The size correlation of SWNTs and catalyst seeds including tangential and perpendicular modes observed from TEM are compared between solid W_6Co_7 catalysts and low-melting point metals (*e.g.*, Co and Cu).

Recently, we have developed an approach for the growth of horizontally aligned chirality-specific SWNT arrays by using uniform and well-dispersed W_6Co_7 nanocrystals on the sapphire surface. The chiral structure and chirality abundance were characterized by the comprehensive methods including Raman, polarized optical absorption, scalable Rayleigh imaging as well as electron diffraction.

[1] F. Yang, Y. Li *et al*. Nature **510**, 522 (2014).
[2] F. Yang, Y. Li *et al*. Acc. Chem. Res. **49**, 606 (2016).
[3] F. Yang, Y. Li *et al*. J. Am. Chem. Soc. **137**, 8688 (2015).
[4] F. Yang, Y. Li *et al*. ACS Nano, **11**, 186 (2017).

Corresponding Author: Yan Li
Tel: +86-10-6275-6773
E-mail: yanli@pku.edu.cn

Direct Microscopic Analysis of Individual [60]Fullerene Dimerization Events: Kinetics and Mechanisms

○Koji Harano, Satoshi Okada, Satori Kowashi, Luca Schweighauser, Kaoru Yamanouchi, Eiichi Nakamura

Department of Chemistry, The University of Tokyo, Tokyo, 113-0033, Japan

Observation of the motions and reactions of molecules, being quantum mechanical entities, has long been an impossible dream. Through advances in transmission electron microscopy (TEM) and methods to anchor molecules on a carbon nanotube (CNT, Fig. 1a), we can visually study the structural changes of molecules in situ using single-molecule atomic-resolution real-time TEM (SMART-TEM) imaging [1]. To go one step further to study reaction kinetics, we need statistical information over time and temperature—information that is so far inaccessible by many of the single-molecule analytical methods. Here, a long-standing interest in this context is to know if the behavior of individual molecules conforms to the basic assumption of the quantum mechanical theory that isolated molecules behave as if all their accessible states were occupied in random order.

To address this question, we chose to study [2 + 2] electrocyclic conversion of a van der Waals (vdW) complex of C_{60} **1** in a CNT to an adduct **2** (step 1, Fig 1b and c)—a well-known reaction without mechanistic information [2, 3]. Through counting reaction events one by one, we could identify four concurrent reactions. One observed at 393–493 K (step 1_H), where the CNT maintained its structural integrity, involves a singlet excited state [2 + 2] cycloaddition reaction with an activation energy of 33.5 ± 6.8 kJ/mol. Here the pristine CNT acts as a sensitizer of the cycloaddition. Another pathway found at 103–203 K (step 1_L) to occur after CNT was heavily damaged by the electron beam. This reaction takes place with an activation energy of only 1.9 ± 0.7 kJ/mol. Here an ionized form of the damaged CNT is considered to act as an oxidant to generate a reactive radical cation of C_{60}. The third is the further conversion of **2** to a fused dimer **3** (step 2), and the fourth is a purely thermal retro [2 + 2] reaction frequently occurring above 493 K. Overall we found that the rate profile of the [2 + 2] dimerization of the vdW complex **1** under the 1D constraints depends heavily on the reaction temperature, the quality of the CNT, and the competing thermal cycloreversion reaction.

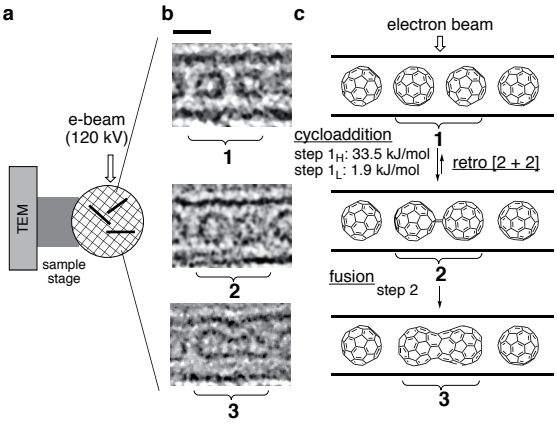

Fig.1 SMART-TEM imaging of the dimerization of C_{60}@CNT. (a) A schematic illustration of the experiments using C_{60}@CNTs on a temperature-controlled microgrid. (b) TEM images of intermediates in a 1.4-nm CNT. The scale bar is 1 nm. (c) Four types of reactions observed using TEM.

[1] E. Nakamura, Acc. Chem. Res. **50**, 1281 (2017).

[2] M. Koshino *et al*. Nat. Chem. **2**, 117 (2010).

[3] S. Okada *et al.* J. Am. Chem. Soc. **139**, 18281 (2017)

Corresponding Authors: K. Harano & E. Nakamura

Tel: +81-3-5841-4369, Fax: +81-3-5841-4369

E-mail: harano@chem.s.u-tokyo.ac.jp, nakamura@chem.s.u-tokyo.ac.jp

Energetics and electronic structure of nitrogen-doped graphene with pyridinic structure

○Mina Maruyama, Susumu Okada

Graduate School of Pure and Applied Sciences, University of Tsukuba, Tsukuba 305-8571, Japan

Graphene with structural imperfections, such as atomic vacancies, topological defects, and substitutional dopants, has been attracting much attention in terms of their peculiar electronic structures which are absent in pristine graphene. Substitutional doping of N atoms in graphene causes versatile electronic structures in the resultant graphene hybrids, depending on the geometric structure and mutual arrangement of doped N atoms. The π state of pyridinic nitrogen (two-fold coordinated N atom in hexagonal network) effectively imitate that of C atom and can terminates π network of graphene without formation of dangling bond states at the Fermi level. Therefore, we can design the graphitic π electron network by implanting pyridinic N atoms. In this work, to explore the energetics and electronic structure of graphene with monovacancies and three pyridinic N atoms in terms of their mutual arrangement and densities, based on the density functional theory (Fig. 1).

The formation energy of N-doped graphene with monovacancies and pyridinic N atoms is inversely proportional to the defect spacing (Fig. 2). Furthermore, the formation energy also depends on the mutual arrangement of defect whether or not the graphitic network possesses Clar structure (full benzenoid structure) as in the case of B_3N_3-doped graphene [1]. Electronic structures also depend on the mutual arrangement of defects whether the graphene network possess Clar structure or not. Owing to the sublattice imbalance in the network, N-doped graphene with monovacancy possess less dispersive π state near the Fermi level exhibiting nonbonding state nature throughout the Brillouin zone. Bandwidth of the non-bonding π state also depend on the graphene network whether they satisfy Clar structure or not.

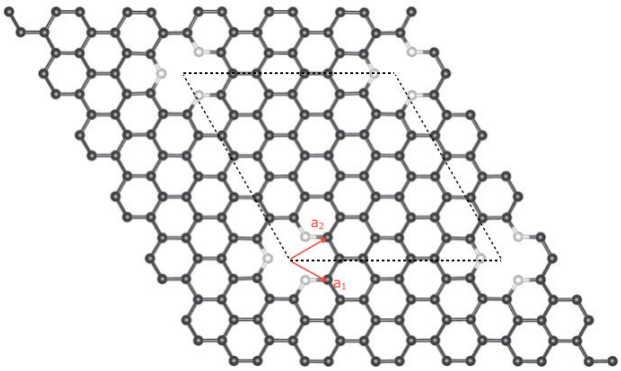

Fig.1 Optimized structure of N-doped graphene with monovacancies and pyridinic N atoms.

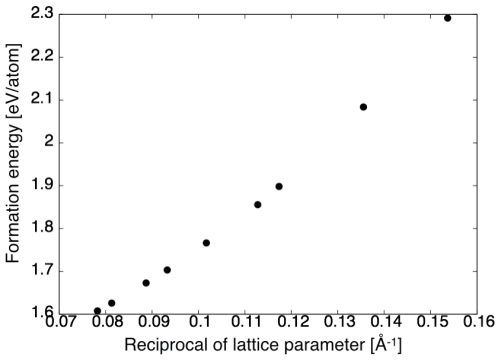

Fig.2 Formation energy per atom of N-doped graphene as a function of the inverse of the lattice parameter.

[1] H. Sawahata *et al*. ChemPhysChem DOI: 10.1002/cphc.201700972.

Corresponding Author: M. Maruyama
Email: mmaruyama@comas.frsc.tsukuba.ac.jp

Bilayer fullerenes (carbon nano-onions) studied by ion mobility mass spectrometry

○Motoyoshi Nakano[1,2], Ryoichi Moriyama[2], Jenna W. J. Wu[2], Keijiro Ohshimo[2], Fuminori Misaizu[2,3]

[1] *Institute for Excellence in Higher Education, Tohoku University, Sendai 980-8576, Japan*
[2] *Department of Chemistry, Grad. School of Sci., Tohoku University, Sendai, 980-8578, Japan*
[3] *New Industry Creation Hatchery Center, Tohoku University, Sendai 980-8579, Japan*

Carbon cluster ions, $C_n^{\pm}$, grow and increase in size (n < 100) from linear to two-dimensional cyclic, and then to cage-like structures. In contrast, nanometer-scale carbon materials form various structures. After the discovery of carbon nano-onions [1], they were investigated intensively by electron microscopy and by theoretical calculations, where information about separated multi-shell fullerenes was obtained. However, only few bilayer structures were reported among the structures, and the actual numbers of constituent carbon atoms are uncertain with electron microscopic images. Structural isomers of carbon cluster cations in the intermediate size range (C_n^{z+}, n = 100 – 800) have been investigated in this study by ion mobility mass spectrometry to discuss the growth process of the carbon clusters.

In the experiments, pulsed carbon cluster ions generated by laser vaporization and supersonic expansion were injected into an ion-drift cell filled with 2.0-Torr He buffer gas. The ions reached a constant drift velocity with a balance of acceleration with an applied electrostatic field and deceleration by collisions with He in the ion-drift cell. Thus, the ions exited the cell with different "arrival times" depending on their charge and collision cross section (CCS). Finally, the ions were analyzed by the reflectron type time-of-flight mass spectrometer.

As a result, bilayer fullerene ion series were observed as continuous distributions for n = 260-700. Figure shows the experimental CCSs as a function of the number of carbon atoms, n, in the cluster. Both CCSs of monolayer and bilayer fullerenes increase monotonically, however, the slope of the bilayer series CCSs was smaller than that of the monolayer series. This difference in slope indicated that the inner layer fullerene does not maintain specific structure such as C_{60}, instead, it grows as the outer layer grows. The ratio of the slopes, bilayer/monolayer = 1.4, suggested that as carbon atoms in the outer layer of bilayer fullerenes increased by 22, the number of atoms in their inner layer increased by 8. According to this relationship, the inner and outer fullerene layer structure for n = 260 was $[C_{30}@C_{230}]^+$, 300 was $[C_{40}@C_{260}]^+$, 600 was $[C_{120}@C_{480}]^+$, and so on. The smallest nano-onion size at $n \approx 260$ was reasonable from the fact that the inner layer of C_{30} was the smallest fullerene observed in this study and in a previous one [2].

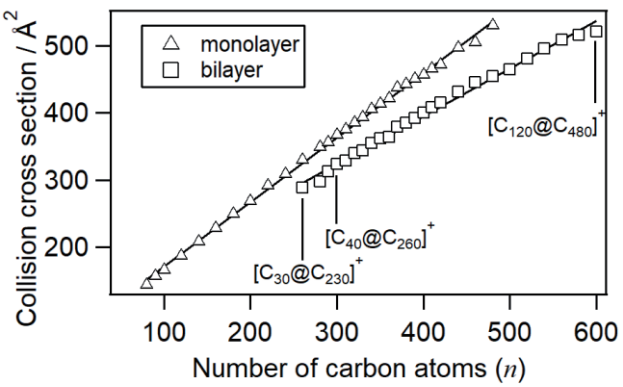

Figure: Plots of collision cross sections of monolayer and bilayer fullerene ions.

[1] S. Iijima, J. Cryst. Growth, **50**, 675 (1980).
[2] N. G. Gotts *et al*. Int. J. Mass Spectrom. **149/150**, 217 (1995).

Corresponding Author: F. Misaizu
Tel: +81-22-795-6577, Fax: +81-22-795-6580
E-mail: misaizu@m.tohoku.ac.jp

Development of Ion Trap Ion Mobility Measurement System and Observation of Observation of Nanomaterials

○Toshiki Sugai , Yudai Hoshino, Hiroki Morita, Reona Miyamoto, Yuta Hamano, Kazumasa Somei, and Ryota Jinnouchi

Department of Chemistry, Toho University, Miyama 2-2-1 Funabashi, 274-8510, Japan

Ion mobility spectrometry (IMS) has been utilized to reveal novel information on nano materials[1]. However, no long-term successive measurement has been performed with IMS usually because of the lack of trap functions, which limits the resolution and the varieties of information. Recently ion trap ion mobility system has been developed to enhance the resolution but the trap time is restricted to less than 2 seconds and no other measurement such as optical spectroscopy is combined[2]. Here we present long-term successive IMS measurements with optical measurements on nano materials such as graphene quantum dots (GQD) and metal clusters as single molecules.

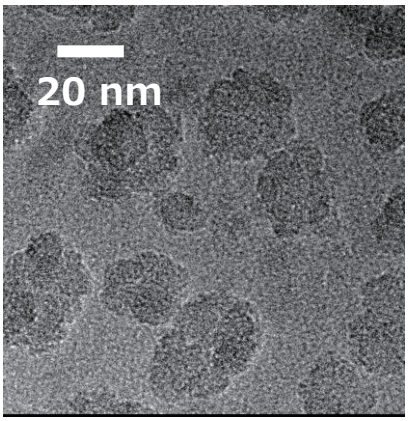

Fig. 1 TEM images of GQD

Fig. 1 shows TEM images of GQD with average diameter around 20 nm. Fig. 2 shows the long-term time dependence of the observed velocities of each GQD molecule with various charges. Single GQD molecules can be observed and the structures and charge states are conserved for up to 7 hours. The diameter evaluated to be 20 nm from the velocity and the estimated charge state, which is in good agreement with that from the TEM observation. We have also succeeded to observe noble metal clusters. Optical spectroscopy on each molecule are also in progress by utilizing thus realized long-term trap functions.

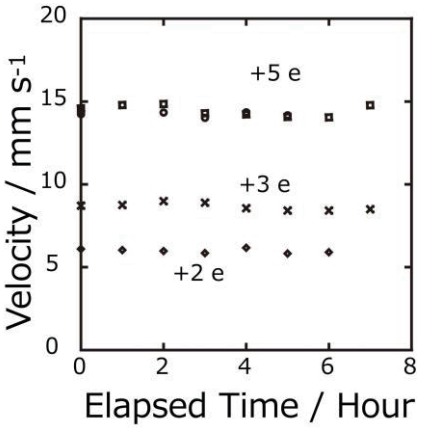

Fig. 2 Observed velocity of GQD with various charges

[1] T. Sugai *et al.*, *J. Am. Chem. Soc.* ***123,*** 6427 (2001).

[2] F. Fernandez-Lima *et al.*, *J. Ion Mobil. Spec.* ***14***, 93 (2011)

TEL: +81-47-472-4406, E-mail: sugai@chem.sci.toho-u.ac.jp

Self-Assembly of Detonation Nanodiamonds from their Colloidal Solutions

○Toshihiko Tanaka[1,3], Yasuhiro F. Miura[2], Tetsuya Aoyama[3], Makoto Takahashi[4], Takumi Sato[1], Eiji Osawa[4]

[1] Department of Chemistry and Biochemistry, National Institute of Technology, Fukushima College, 30 Aza-nagao, Tairakamiarakawa, Iwaki, Fukushima, 970-8034, Japan
[2]Hamamatsu University School of Medicine, 1-20-1 Handayama, Higashi-ku, Hamamatsu city, Shizuoka, 431-3192, Japan
[3]Elements Chemistry Laboratory, RIKEN, 2-1 Hirosawa, Wako, Saitama, 351-0198, Japan
[4]Nano Carbon Research Institute Ltd., Asama Research Extension Center, Shinshu University, 3-15-1 Tokida, Ueda, Nagano, 386-8567 Japan

We demonstrate herein the recent results on the self-assembly of detonation nanodiamonds (DND) from their aqueous colloidal solutions. The self-assembly is significant with respect to their research and applications because it has suggested the existence of elementary particles of detonation nanodiamonds (EPDND), which might be the first novel nanocarbon species containing sp^3 carbons. Furthermore, its early stage probably includes a part of the process where a successful drug delivery[1] takes place. Their whiskers were first reported through slow drying from the solutions by the last author in 2007[2] and similar ones[3] or microsheets[4] were also assembled from acid treated DND solutions. A Langmuir monolayer from arachidic acid also induced precipitates of ultrathin rectangular nanosheets on the water surface.[5]

Recent careful observations have revealed that the whiskers has the fine geometry of rectangular shapes ($18 \times 106 \times > 300$: μ m) as well as uniaxial uniform optical anisotropy, thus showing that they are kinds of colloidal crystals. A laser microscopy image exhibits the surprisingly fine shape and crossed nicol polarized images demonstrate the uniaxial birefringence of Δn=0.0013~0.0027[**Fig.1a**]. A substantial part of the DND must be similar both in size and shape and otherwise the shape with the optical anisotropy cannot be explained well. Perhaps such similar species are EPDND or their dimers. The nanosheets [**Fig.1b**] also have the fine uniformity in thickness of 26 nm shown by AFM. We will discuss the significance of the self-assembly with respect to the purity of the whiskers or nanosheets.

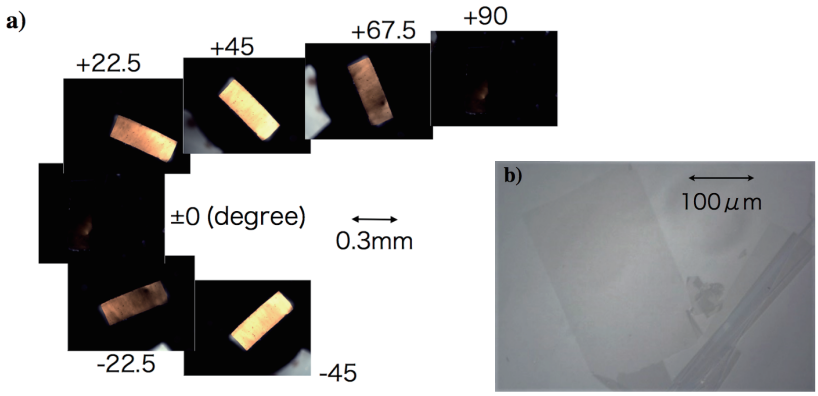

Fig.1 Microscopic images: a) a rectangular DND whisker by a crossed nicol polarization with various in-plane angular positions; b) a rectangular ultrathin nanosheet (~26 nm thick) precipitated on the water surface with a Langmuir monolayer of arachidic acid.

[1] E. K. Chow,X-Q. Zhang, M. Chen, R. Lam, E. Robinson, H. Huang, D. Schaffer, E. Osawa, A. Goga, D. Ho; *Sci. Trans. Med*. 3(73ra21), 1-11(2011). [2] E. Osawa; *Diamond & Related Materials.* 16, 2018–2022(2007).
[3] H. Huang, L. Dai, D. H. Wang, L-S. Tanc, E. Osawa; *J. Mater. Chem.*, 18, 1347–1352 (2008,).
[4] T. Petit, H. A. Girard, A. Trouve´, I. Batonneau-Gener, P. Bergonzoa, J.-C. Arnault; *Nanoscale*, 5(19), 8958-62 (2013). [5] T.Tanaka, Y.F. Miura, T. Sato, E. Osawa; *Abstract of the 53th FNTG Symposium*, 66(2017).
Corresponding Author: Eiji Osawa / Tel: +81--268-75-8381 / E-mail: osawa@nano-carbon.jp

Graphene-Silicon Schottky Junction for Optoelectronic Devices

○Xinming Li [1,2], Hongwei Zhu [2], Renzhi Ma [1], Takayoshi Sasaki [1]

[1] *International Center for Materials Nanoarchitectonics (WPI-MANA), National Institute for Materials Science (NIMS), 1-1 Namiki, Tsukuba, Ibaraki 305-0044, Japan*
[2] *School of Materials Science and Engineering, Tsinghua University, Beijing 100084, China*

In the last few decades, the advances and breakthroughs in carbon materials and two-dimensional (2D) materials have been witnessed both scientific fundamentals and potential applications.[1] Graphene's unique electronic and optical properties have made it an attractive material for developing optoelectronic devices.[1-2]

The graphene-silicon Schottky junction solar cell was firstly reported in 2010 by the co-author of the present work (Fig.1(a)).[3-4] This solar cell is considered to be a promising demonstration and the power conversion efficiency is raised to 15.6% with electrical and optical improvement, such as chemical doping, interface engineering, and optical anti-reflection.[4-8] Furthermore, this graphene-silicon Schottky junction can be utilized for the development of high-performance photodetectors.[9-10] After employing the vertical built-in field and plasmonic effects, graphene-silicon Schottky junction can be used as the short-wave infrared (SWIR) photodetectors which can overcome the low optical absorption of graphene, as well as the ultrashort lifetime of photoinduced carriers (Fig.1(b)).[11]

This device design concept addresses key challenges for high-performance graphene-silicon Schottky junction optoelectronic devices and is promising for the development of graphene-based optoelectronic applications.

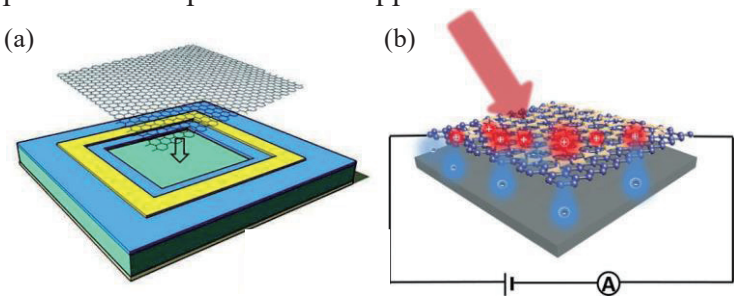

Fig.1 Schematic diagram of the graphene-Si Schottky junction for solar cell (a) and SWIR photodetector (b).

[1] X.M. Li *et al*. ***Applied Physics Reviews*** **4**, 021306 (2017).
[2] X.M. Li *et al*. ***Physics Today*** **69(9)**, 46-51 (2016).
[3] X.M. Li *et al*. ***Adv. Mater.*** **22**, 2743-2748 (2010).
[4] X.M. Li *et al*. ***Adv. Mater.*** **27**, 6549–6574 (2015).
[5] Y. Song, X.M. Li *et.al.* ***Nano Lett.*** **15**, 2104-2110 (2015).
[6] X.M. Li *et al*. ***Adv. Energy Mater.*** **3**, 1029-1034 (2013).
[7] X.M. Li *et al*. ***Nanoscale*** 5, 1945-1948 (2013).
[8] Y.X. Lin, X.M. Li(Co-first author) *et al*. ***Energy Environ. Sci.*** **6**, 108-115 (2013).
[9] X.M. Li *et al*. ***Small*** **12**, 595-601 (2016).
[10] L. Tao, Z.F. Chen, X.M. Li* et al. ***npj 2D Materials and Applications*** **1**, 19 (2017).
[11] Z.F. Chen, X.M. Li* *et al*. ***ACS Nano*** **11**, 430-437 (2017).

Corresponding Author: Xinming Li
E-mail: xmli1015@gmail.com

Schottky barrier control between indium tin oxide and WSe_2 for fabrication of transition metal dichalcogenide-based transparent solar cell

○Y. Yamaguchi[1], W. Okita[1], C. Li[1], T. Kaneko[1], and T. Kato[1,2]

[1]*Department of Electronic Engineering, Tohoku University, Sendai 980-8579, Japan*
[2] *JST-PRESTO*

Layered transition metal dichalcogenide (TMD) is known as a true 2D material with excellent semiconducting properties. TMD is one of the most attractive materials for future transparent and flexible optoelectrical devices due to their atomically thin structure, band gap in visible light range, and high optical transparency. Although the solar cell of TMD has been widely investigated by many groups, those are based on the pn junction type solar cell. Since complicated structures are required to form pn junction structures in TMD such as dual gate electrodes or position selective doping, the device size of pn junction solar cell with TMD is limited within very small region (few μm). In spite of the outstanding advantages of TMD, those merits of TMD have not been applied for transparent and flexible solar cell, which is attracted intense attention as a next-generation energy harvesting technology.

Recently, we have developed a new fabrication process of TMD-based solar cell [1]. In our process, Schottky type device configuration is utilized, which can be simply formed by asymmetrically contacting electrodes and TMD (Fig.1). The power conversion efficiency clearly depended on the work function difference between two electrodes (ΔWF), and a higher efficiency could be obtained with higher ΔWF (Pd-Ni), which is consistent with our concept, where Ni and Pd can form large and small Schottky barriers to operate as power-generation and carrier-collect regions, respectively. Based on the optimizations of electrodes and distance, the power conversion efficiency can be reached up to 0.7 %, which is the highest value for solar cell with similar TMD thickness [1].

In our previous study, we used conventional metals such as Ni and Pd to tune the Schottky barrier height between electrode and TMD. To improve the transparency of whole device, however, it is required to use transparent electrodes. In this study, we use indium tin oxide (ITO) as an electrode and form transparent and flexible solar cell. Since controlling ΔWF is a key to improve the power conversion efficiency in our device, the surface of ITO was functionalized by various plasma treatments with hydrogen, nitrogen and oxygen as reactive species. It is found that the work function of ITO can be controlled by changing plasma species and treatment time. After controlling the ΔWF of ITO electrodes with plasma treatments, clear power generation can be observed with TMD/ITO based transparent solar cell. Since our simple fabrication process includes high potential for large scale fabrication, this achievement is very important for realizing the industrial application of TMD as a transparent and flexible solar cell.

Fig. 1. Optical image of a transparent and flexible solar cell fabricated with TMD.

[1] T. Akama, W. Okita, R. Nagai, C. Li, T. Kaneko, and T. Kato, Sci. Reports **7**, 11967 (2017).

Corresponding Author: Y. Yamaguchi

Tel: +81-22-795-7046, Fax: +81-22-263-9225, E-mail: yoshiki.yamaguchi.t5@dc.tohoku.ac.jp

Angular momentum conservation in helicity-dependent Raman and Rayleigh scattering

○Yuki Tatsumi, Tomoaki Kaneko, and Riichiro Saito

Department of Physics, Tohoku University, Sendai 980-8578, Japan

Left- (σ_+) and right-handed (σ_-) circularly-polarized light have angular momentum $+\hbar$ and $-\hbar$, respectively [1]. In recent study, many researchers try to use circularly-polarized light in Raman spectroscopy (helicity-dependent Raman spectroscopy). Chen *et al.* reported that in-plane vibrating modes of transition metal dichalcogenides (IMC modes) change helicity of the light from σ_- (σ_+) incident light to σ_+ (σ_-) scattered light in Raman scattering [2]. Furthermore, Drapcho *et al.* reported that well-known G band in graphene is also the mode changing the helicity of light in Raman scattering [3]. When the helicity of light changes in scattering process, angular momentum of photon exchanges to the material. In such a case, we have to consider the discrete rotational symmetry of crystal to derive the angular momentum conservation law. Conservation law of angular momentum in discrete rotational symmetry is discussed for nonlinear optics from a long time ago [4-7], and also for impulsive stimulated Raman scattering [8]. However, helicity-dependent Raman spectroscopy is reported in recent studies and conservation law of angular momentum in scattering phenomena is unclear yet. In this study, we formulate the angular momentum conservation law of Raman and Rayleigh scattering and discuss the dependence of rotational symmetry in a material.

In order to discuss the conservation law of angular momentum in helicity-dependent Raman and Rayleigh scattering, we combine the conservation law of angular momentum for electron-photon and electron-phonon interaction in discrete rotational symmetry. For Rayleigh scattering, we found that helicity-changing scattering is observed only in the material with less than 3-fold rotational symmetry. In Fig. 1, we show the calculated helicity-dependent Rayleigh spectra of monolayer (1L) (a) MoS_2 and (b) black phosphorus which have 3- and 2-fold rotational symmetry, respectively. Weak helicity-changing peak appears only in 1L black phosphorus. In the presentation, we also discuss the detail of symmetry dependence for Raman scattering.

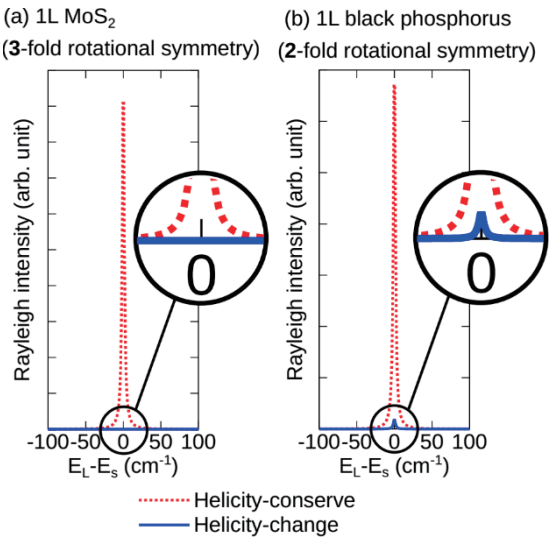

Fig. 1 Helicity-dependent Rayleigh spectra for 1L (a) MoS_2 and (b) black phosphorus, calculated by first-principles method. Dotted (Solid) line indicates the helicity-conserving (changing) scattering. The E_L and E_s are, respectively, the energy of incident laser and scattered light.

[1] K.Y. Bliokh *et al.*, Phys. Rep. **592**, 1 (2015)
[2] S.-Y. Chen *et al.*, Nano Lett. **15**, 2526 (2015)
[3] S.G. Drapcho *et al.*, Phys. Rev. B **95**, 165417 (2017)
[4] H.J. Simon *et al.*, Phys. Rev. **171**, 1104 (1968)
[5] N. Bloembergen, J. Opt. Soc. Am. **70**, 1429, (1980)
[6] J. Visser *et al.*, Phys. Rev. A **66**, 033814 (2002)
[7] T. Higuchi *et al*, Phys. Rev. Lett. **106**, 047401 (2011)
[8] T. Higuchi *et al*, Phys. Rev. A **87**, 013808 (2013)

Corresponding Author: Yuki Tatsumi
Tel: +81-22-795-6442, Fax: +81-22-795-6447,
E-mail: tatsumi@flex.phys.tohoku.ac.jp

Carrier dynamics in 3-layer ReS_2 studied by ultrafast spectroscopy

○Xiaofan Wang, Keisuke Shinokita, Hong En Lim, Nur Baizura Mohamed,
Yuhei Miyauchi, Kazunari Matsuda
Institute of Advanced Energy, Kyoto University, Uji, Kyoto 611-0011, Japan

Atomically-thin layered materials including graphene and transition metal dichalcogenides possess intriguing physical properties originating from the two dimensional honeycomb structure. ReS_2 is a new class of the layered material with reduced symmetry because of the distorted *1T* structure, which imparts highly anisotropic one dimensionarity to optical and electronic properties [1]. The early study reported that ReS_2 remains direct bandgap semiconductor from bulk to monolayer [2], while the other reported that the band structure depends on the layer number [3]. The understandings of electronic and optical properties including the optically excited carrier dynamics are still controversial, and are not fully understood. Here we described the ultrafast spectroscopy of 3-layer ReS_2 using ultrafast spectroscopy to obtain the insight of band structure and carrier dynamics.

The sample was prepared by mechanically exfoliation onto a quartz substrate using a polydimethylsiloxane (PDMS). The ReS_2 flakes were preferentially broke along b-axis parallel to Re-Re bonds, and shows the elongated shapes. Figure 1(a) shows the reflectance contrast of 3-layer ReS_2 at 5 K, where the polarization angles of light with respect to the b-axis are shown. The spectra show polarization dependence of two exciton absorption peaks at 1.58 and 1.62 eV, reflecting an anisotropic feature of ReS_2. Figure 1(b) shows pump-probe differential reflectivity probed at two-different configuration. The transient differential reflectivity shows almost no polarization dependence with decay times of around 100 ps. In contrast, time-resolved photoluminescence (PL) spectroscopy shows much faster decay signals with less than 10 ps. The different time scale in the transient reflectivity and PL measurement suggests the electron and hole relax to the different momentum space in the indirect band structure of 3-layer ReS_2. The detail carrier dynamics and band structure of atomically thin ReS_2 will be discussed.

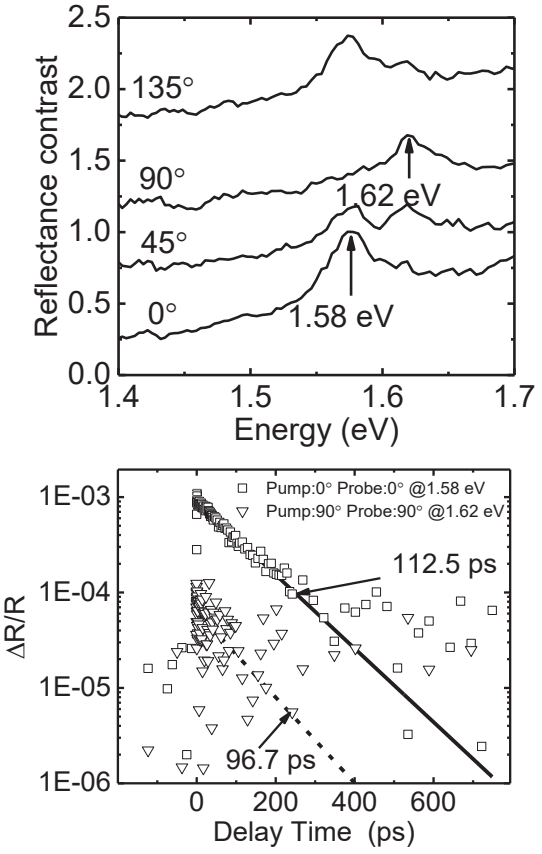

Fig.1 (a) Polarization-resolved reflectance contrast of 3-layer ReS_2 with respect to b-axis. (b) Polarization-resolved transient differential reflectivity.

[1] O. B. Aslan *et.al.,* ACS Photonics **3**, 96 (2015).
[2] S. Tongay *et.al.,* Nat. Commun. **5**, 3252 (2013).
[3] M. Gehlmann *et.al.,* Nano Lett. **17**, 5187 (2017).

Corresponding Author: Kazunari Matsuda
Tel: +81-774-38-3460,
E-mail: matsuda@iae.kyoto-u.ac.jp

In situ transmission electron microscopy of the formation and annihilation of charge density waves in 1*T*-$TaSe_2$

○Keita Kobayashi[1], Hidehiro Yasuda [1,2]

[1] *Research Center for Ultra-High Voltage Electron Microscopy, Osaka University, 7-1, Mihogaoka, Ibaraki, Osaka 567-0047, Japan*
[2] *Division of Materials and Manufacturing Science, Graduate School of Engineering, Osaka University, 2-1, Yamadaoka, Suita, Osaka 565-0871, Japan*

Some transition metal dichalcogenides (TMDCs) exhibit charge density waves (CDWs) due to their unique two-dimensional electron systems [1]. The CDW phase in TMDCs is generally a stable low-temperature phase, and the formation or annihilation of the CDW is dipendent on the specimen temperature.

In this study, to clarify the dynamics of the formation and annihilation of CDWs in TMDCs, we observed the behavior of the long-periodic structure (LPS) attributed to the formation of CDWs in 1*T*-$TaSe_2$ at elevated temperature by *in-situ* transmission electron microscopy (TEM).

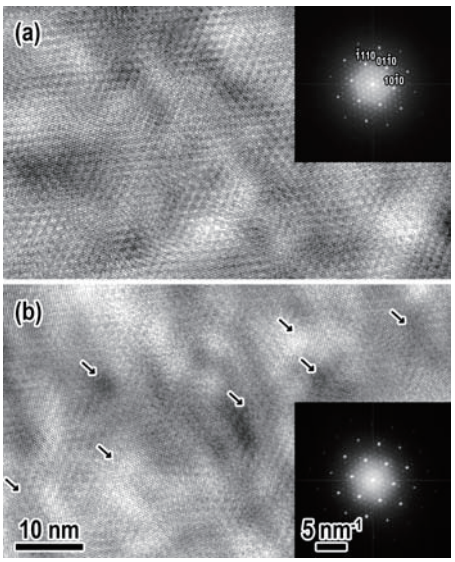

Fig.1: TEM images and corresponding FFT patterns of 1*T*-$TaSe_2$ acquired at (a) 298 and (b) 478 K.

Figures 1(a) and (b) show the TEM images of 1*T*-$TaSe_2$ acquired at 298 and 478 K, respectively, and the corresponding fast Fourier transform (FFT) patterns. In the TEM image acquired at 298 K, a periodic contrast attributable to the LPS can be clearly observed. The FFT pattern also exhibits ordered reflection due to the LPS. In contrast, although the periodic contrast and ordered reflection attributable to LPS remain in the TEM image acquired at 478 K and the corresponding FFT pattern, respectively, the TEM image also contains domains lacking the periodic contrast as indicated by the arrowheads. The area of these domains increases over time at 478 K. Eventually, the periodic contrast in the TEM image and the ordered reflection in the corresponding FFT pattern completely disappear. This result indicates that the annihilation of the CDW originates from localized structural fluctuations and progressively expands throughout the 1*T*-$TaSe_2$. Furthermore, based on the *in situ* TEM observations, we consider that CDW formation also occurs via a similar process.

K. K. thanks Gatan, Inc. for lending the CCD camera and the double-tilt Heating *in-situ* holder.

[1] J. A. Wilson, F. J. Di Salvo, S. Mahajan, Adv. Phys. **24**, 117 (1975).

Corresponding Author: K. Kobayashi
Tel: +81-6-6879-7941, Fax: +81-6-6879-7942,
E-mail: kobayashi-z@uhvem.osaka-u.ac.jp

Functionalization of [60]Fullerene Through Fullerene Cation Intermediates

○Yutaka Matsuo[1,2]

[1]*Hefei National Laboratory for Physical Sciences at the Microscale, University of Science and Technology of China, Hefei, Anhui 230026, China*
[2]*Department of Mechanical Engineering, School of Engineering, The University of Tokyo, Bunkyo-ku, Tokyo 113-8656, Japan*

Fullerene cations, namely, [60]fullerene radical cation ($C_{60}^{\bullet+}$) and organo[60]fullerenyl cation (RC_{60}^{+}), were less investigated as an intermediates in synthetic fullerene chemistry, because of the intrinsic electro-negativity of C_{60}. However, these two intermediates mediated reactions provided fullerenes with versatile unexpected derivatives. This presentation mainly describes the $C_{60}^{\bullet+}$ and RC_{60}^{+} intermediates from generation of these cationic species to their application in fullerene modification reaction, including Friedel–Crafts hydroarylations, nucleophilic additions, dimerization, intramolecular rearrangement reactions, intramolecular cyclization reactions, as well as organic solar cells application research. Importantly, this presentation deeply discusses the mechanism for the formation of unique [60]fullerene derivatives involved with [60]fullerene radical cation and organo[60]fullerenyl cation intermediates containing newly generated lowest unoccupied molecular orbital (LUMO) after removal of two electrons. These new LUMO are the key for unexpected and important products useful in photovoltaic research as both organic and perovskite solar cells.

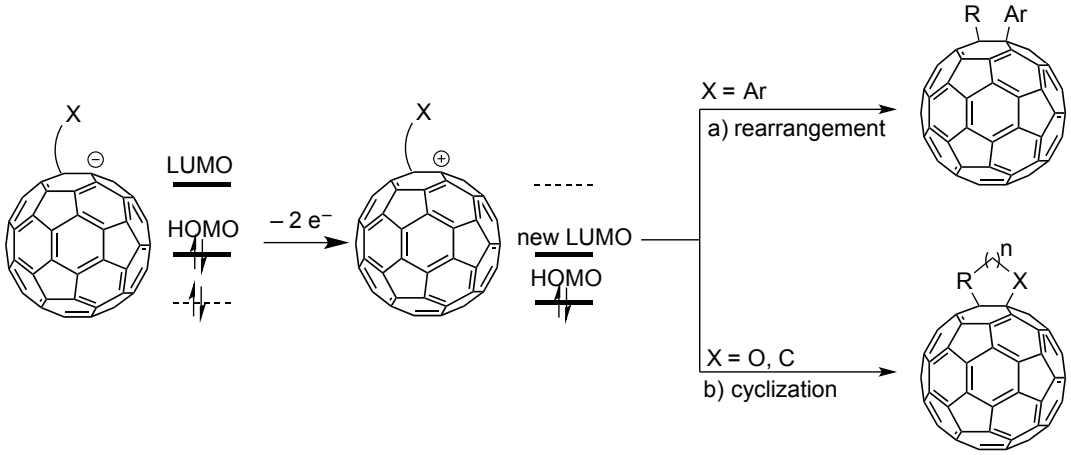

Figure. Concept of the newly LUMO for the further derivatization

References

[1] Y. Matsuo *et al.*, *J. Mater. Chem. A* **2017**, *5*, 2774.

Corresponding Author: Y. Matsuo

Tel: +81-3-5841-0978, E-mail: matsuo@ustc.edu.cn; matsuo@photon.t.u-tokyo.ac.jp

Molecules inside Fullerenes as Magnetic Probes for the Detection of Specific Intramolecular Interactions

○Yoshifumi Hashikawa and Yasujiro Murata

Institute for Chemical Research, Kyoto University, Uji, Kyoto 611-0011, Japan

Encapsulation of a small molecule inside fullerene C_{60} has an effect on the nature and chemical reactivity of the outer sphere of C_{60}. Recently, Martín and co-workers reported that the entrapped H_2O and HF molecules interact with the anionic cage (RC_{60}^-) via an intramolecular hydrogen bonding, which resulted in the accelerated reaction rate relative to empty one.[1] However, there still remain issues how to elucidate and experimentally detect the specific intramolecular interactions in endohedral fullerenes.

In this context, to demonstrate the existence of such interactions, we have focused on the magnetic relaxation for nuclear spins of the corresponding molecules entrapped inside C_{60}. In general, relaxation times are changeable by the influence of the degree of spin-spin interactions as well as the molecular motion. Thus, we expected that the entrapped molecules with the NMR-active nuclei would act as a probe to evaluate magnetic and electrostatic interactions between the carbon cage and the entrapped molecule.

Our recent study showed that the proton relaxation times of entrapped H_2O sensitively respond to the introduction of a heteroatom on the C_{60} cage, suggesting the restricted rotational motion of the water molecule via electrostatic attraction.[2] Such specific interaction was also observed in $H_2O@RC_{59}N$ by replacing a carbon atom in $H_2O@C_{60}$ with the nitrogen atom even though the intramolecular interaction in $H_2O@C_{60}$ was concluded to be negligible by the measurements of longitudinal and transverse relaxation times, T_1 and T_2,[3] as well as the single molecule junction study.[4] In addition, the electrostatic attraction was found to be drastically enhanced by the oxidation of $H_2O@C_{59}N$ dimers.[5] Surprisingly, at the temperature of 280 K, $H_2O@C_{59}N^+$ has much larger value (T_1/T_2 = 6) compared with $H_2O@C_{59}N$ dimers (T_1/T_2 = 2.5) and the T_1/T_2 curve is shifted by a factor of +40 K, indicating the strong $C_{59}N^+\bullet\bullet\bullet O^{\delta-}H_2$ interaction which was also supported by the DFT calculations (Figure 1).

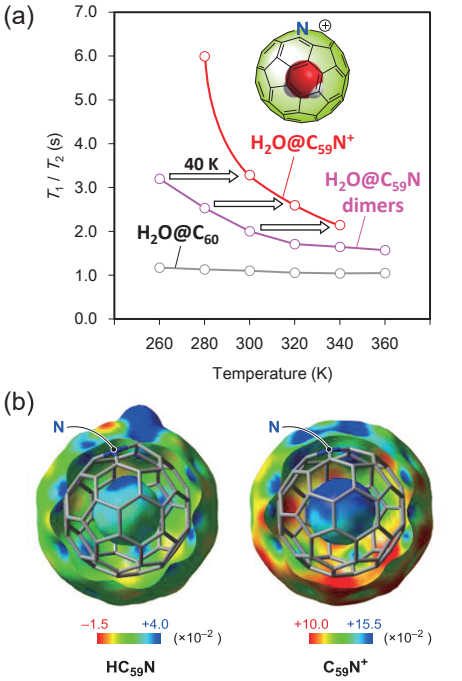

Figure 1. (a) Relaxation times and (b) electrostatic potential maps calculated at MP2/6-31G(d,p)//M06-2X/6-31G(d,p).

[1] (a) Maroto, E. E.; Mateos, J.; Garcia-Borràs, M.; Osuna, S.; Filippone, S.; Herranz, M. Á.; Murata, Y.; Solà, M.; Martín, N. *J. Am. Chem. Soc*. **2015**, *137*, 1190–1197. (b) Vidal, S.; Izquierdo, M.; Alom, S.; Garcia-Borràs, M.; Filippone, S.; Osuna, S.; Solà, M.; Whitby, R. J.; Martín, N. *Chem. Commun*. **2017**, *53*, 10993–10996.
[2] Hashikawa, Y.; Murata, M.; Wakamiya, A.; Murata, Y. *Angew. Chem., Int. Ed*. **2016**, *55*, 13109–13113.
[3] Hashikawa, Y.; Murata, M.; Wakamiya, A.; Murata, Y. *J. Am. Chem. Soc*. **2016**, *138*, 4096–4104.
[4] Kaneko, S.; Hashikawa, Y.; Fujii, S.; Murata, Y.; Kiguchi, M. *Chem. Phys. Chem*. **2017**, *18*, 1229–1233.
[5] Hashikawa, Y.; Murata, Y. *J. Am. Chem. Soc*. **2017**, *139*, 18468–18471.
Corresponding Author: Y. Murata
Tel: +81 774-38-3172, Fax: +81 774-38-3178,
E-mail: yasujiro@scl.kyoto-u.ac.jp

Characterization of the spin system in $GdM@C_n$ anion (M=Sc, Y, La; n=78, 80)

○Takuji Mitani[1], Ko Furukawa[2], Tatsuhisa Kato[3, 4], Koichi Kikuchi[1], Yohji Achiba[1], Takeshi Kodama[1]

[1]*Department of Chemistry, Tokyo Metropolitan University, Tokyo 192-0397, Japan*
[2]*Center for Coordination of Research Facilities, Niigata University, Niigata 950-2181, Japan*
[3]*Graduate School of Human and Environmental Studies, Kyoto University, Kyoto 606-8501, Japan*
[4]*Institue for Liberal Arts and Sciences, Kyoto University, Kyoto 606-8501, Japan*

In $(Gd_2@C_{80}(I_h))^-$, an excess electron (S=1/2) is located on the internal Gd dimer and two Gd atoms take the trivalent state (S=7/2). From the ESR study, the ferromagnetic interaction between three spins was suggested and the resultant spin state of $(Gd_2@C_{80}(I_h))^-$ is S=15/2[1]. On the other hand, for $Gd@C_{82}(C_{2v})$, it was reported the antiferromagnetic interaction between an octet spin of the encapsulated Gd^{3+} and a doublet spin of an unpaired electron on the π orbital of the carbon cage[2]. To clarify the magnetic interaction between the spins of Gd^{3+} and an excess electron on the internal metal dimer, we synthesized $(GdY@C_{80}(I_h))^-$ that has a nonmagnetic ion Y^{3+} instead of one Gd^{3+} of $(Gd_2@C_{80}(I_h))^-$ [3]. In the previous symposium, we reported the UV-vis-NIR absorption and the ESR spectra of $(GdY@C_{80}(I_h))^-$, but we couldn't analyze the ESR spectrum in detail. In this work, we report the spin system of new hetero-dimetallofullerenes $(GdM@C_n)^-$ (M=Sc, La; n=78, 80).

GdM-metallofullerenes (M=Sc, Y, La) were produced and extracted by the method previously reported[3], and was separated by multi-step HPLC using acetone with an ion-pair reagent, tetrabutylammonium bromide, as an eluent. The UV-vis-NIR absorption spectra of $(GdMC_{78})^-$ (M=Sc, Y, La) (Fig.1) and $(GdLaC_{80})^-$ are very similar to those of $(Gd_2@C_{78}(D_{3h}))^-$ and $(Gd_2@C_{80}(I_h))^-$, respectively. Then, it was suggested that the cages of $GdMC_{78}$ (M=Sc, Y, La) and $GdLaC_{80}$ are $C_{78}(D_{3h})$ and $C_{80}(I_h)$, respectively. By the analysis of the W-band ESR spectra (Fig.2), the spin state of $(GdM@C_{78}(D_{3h}))^-$ (M=Sc, La) was found to be S=4, that is, the ferromagnetic interaction between an octet spin of the encapsulated Gd^{3+} and a doublet spin of an unpaired electron on the metal-dimer was suggested.

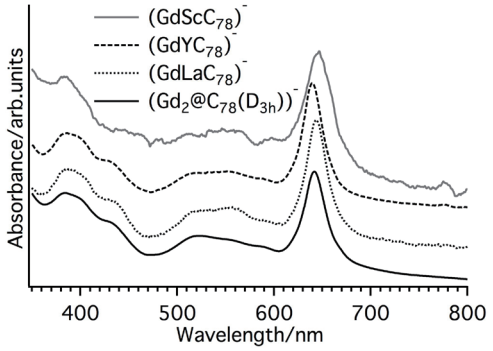

Fig.1 UV-vis-NIR absorption spectra of $(GdMC_{78})^-$ (M=Sc, Y, La) and $(Gd_2@C_{78}(D_{3h}))^-$.

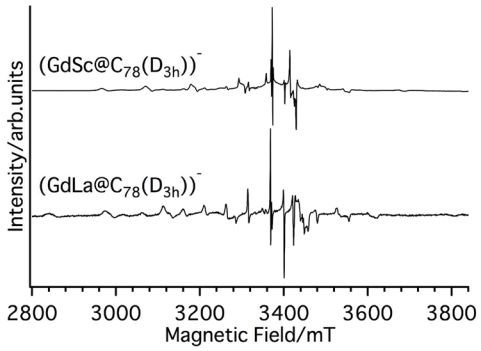

Fig.2 W-band ESR spectra of $(GdM@C_{78}(D_{3h}))^-$ (M=Sc, La) observed at 20 K.

[1] T. Mitani, et al. *The 50th Fullerenes-Nanotubes-Graphene General Symposium* 95 (2016).
[2] K. Furukawa, et al. *J. phys. Chem. A* **107**, 10933-10937 (2003).
[3] T. Mitani, et al. *The 52nd Fullerenes-Nanotubes-Graphene General Symposium* 92 (2017).

Corresponding Author: Takeshi Kodama
Tel:+81-42-677-2530, Fax:+81-42-677-2525
E-mail: kodama-takeshi@tmu.ac.jp

Highly Stabilized Perovskite Solar Cells by Li^+-Encapsulated [60]Fullerene as Both Dopant and Anti-Oxidant

○Hiroshi Ueno[1], Il Jeon[2], Seungju Seo[2], Ryosuke Nishikubo[3], Hiroshi Okada[2], Akinori Saeki[3], Shigeo Maruyama[2,4], Yutaka Matsuo[1,2]

[1] *School of Chemistry, Northeast Normal University, Changchun, Jilin 130024, China*
[2] *Department of Mechanical Engineering, School of Engineering, The University of Tokyo, Bunkyo-ku, Tokyo 113-8565, Japan*
[3] *Department of Applied Chemistry, Graduate School of Engineering, Osaka University, Suita, Osaka 565-0871, Japan*
[4] *Energy NanoEngineering Laboratory, National Institute of Advanced Industrial Science and Technology (AIST), Tsukuba 305-8564, Japan*

With excellent power conversion efficiency (PCE) beyond 20%, lead halide perovskite solar cells (PSCs) have attracted growing attention as a promising solar energy source in recent years. Despite the high PCE comparable to silicon solar cell, low stability of PSCs has been the most serious drawback, which is in dire need of resolution.[1] Previously we reported that Li^+-encapsulated [60]fullerene salt ($[Li^+@C_{60}]TFSI^-$) can be used as an alternative to Li^+TFSI^- as a dopant for spiro-MeOTAD in $MAPbI_3$-based PSCs. The device exhibited ca. 7 times higher stability than LiTFSI-used conventional device, however, the PCE dropped significantly from 17.0% to 13.1 %.[2]

In this work, formamidinuim and methylammonium mixed $(FAPbI_3)_{0.85}(MAPbBr_3)_{0.15}$-based PSCs was fabricated using $Li^+@C_{60}$ salt as a dopant for spiro-MeOTAD. A higher PCE of 16.8% was achieved, and such improvement can be attributed to higher V_{OC} and *FF*, coming from much reduced degradation of the perovskite active layer (Figure 1a). The device showed 10 times higher stability than LiTFSI-used device (Figure 1b), which ascribed to the hydrophobic nature and anti-oxidant activity of $Li^+@C_{60}$ and $Li@C_{60}$.

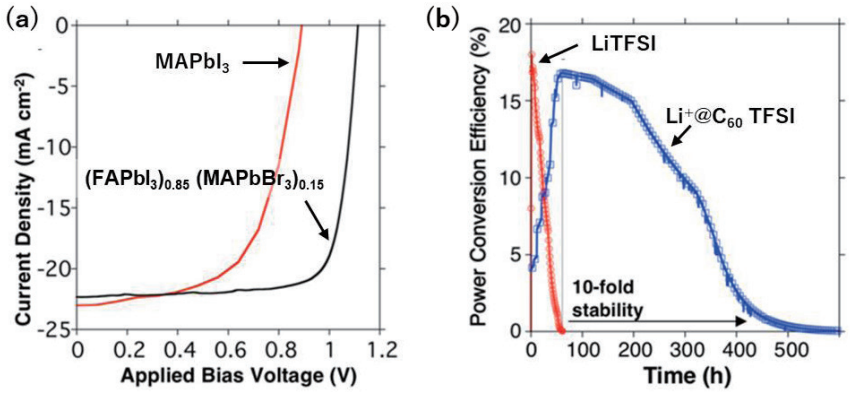

Figure 1. (a) Optimum J–V curves of $MAPbI_3$- and $(FAPbI_3)_{0.85}(MAPbBr_3)_{0.15}$-PSCs using $[Li^+@C_{60}]TFSI^-$ under 1 sun. (b) Stability data of the $(FAPbI_3)_{0.85}(MAPbBr_3)_{0.15}$-PSCs with $[Li^+@C_{60}]TFSI^-$ and those with Li^+TFSI^-, the test condition was that the devices were unencapsulated in air under constant illumination.

[1] Ahn, N. *et al. Nat. Commun.* **2016**, *7*, 13422.
[2] Jeon, I. *et al. 53rd FNTG general symposium*, 1P-4.

Corresponding Author: Y. Matsuo
Tel: +81-3-5841-0978, E-mail: matsuo@photon.t.u-tokyo.ac.jp

Matrix approach to calculation of phonon group velocities from MD transient dispersion relation as applied to graphene

○Tatiana Zolotoukhina[1], Kentaro Kumaki [1], Kenta Tawara [1]

[1] *Department of Mechanical Engineering, University of Toyama, Toyama 930-8555, Japan*

For calculation of thermal properties of nanoconfigured materials, knowledge of transport phonon group velocities, and lifetime characteristics is essential. Molecular dynamics (MD) estimation of transient dispersion relation evaluates matrix D(ω,k) distribution. To extract modes and their velocities through an automated procedure, we propose mode selection on the matrix obtained by differentiation in k-space [1] and spline fitting of modes from the edges of Brillouin zone along selected ΓM path on grid. The spline fitting was tested on the results of MD calculation of thermally excited graphene nanoribbon. The dispersion relation for graphene sample shows presence of basic and transient phonon modes in the 1st Brillouin zone [2]. We extract phonon branches from the dispersion matrix by differentiation in k space and spline approximation of branches to functional ω(k) form that are easily differentiable by k value to get group velocity of present phonon modes.

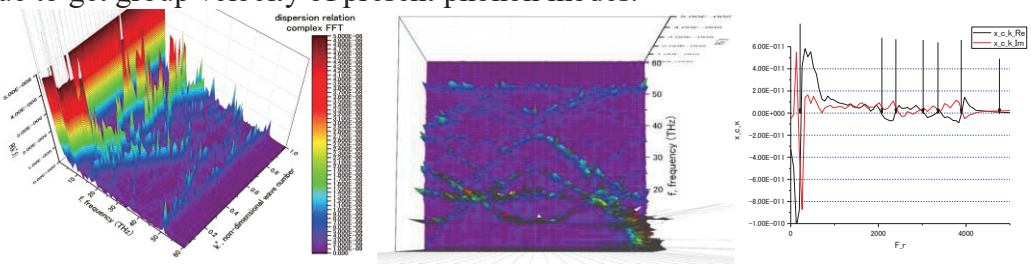

Fig.1 The transient dispersion map D(ω,k) in the ΓM direction of the 1st Brillouin zone (left and center), k-space derivative (right) along one of the k cross-section with the 0 values at the place of peak values.

MD estimation of dispersion relation in regions of interest evaluates ω(k) distribution as a matrix. To extract ω(k) for passing modes from the matrix, we use the intensity-dependent mode cut-off on the transient dispersion matrix and k-space peak selection for approximation points. The spline fitting of ω(k) functions is attempted by 2-step fitting of the second and third order by the automatic point selections from the opposite edges of Brillouin zone along the ΓM path on matrix grid. The spline fitting was applied to the results of MD calculation of thermally excited graphene nanoribbon with the presence of basic and transient phonon modes along the ΓM path in the dispersion relation for graphene sample. We utilized points of the second order approximation to build linear approximation of the search area to the points of the third order approximation to functional ω(k) form that are required to get group velocity of transient phonon modes. The error of such spline approximation can be brought to be close to 4 - 5% in our estimation.

[1] K. Firouzi, J. Acoust. Soc. Am. 132 , 2012, 1271
[2] T. Zolotoukhina, Proc. of the 15th Int. Tech. Conf. on Packaging and Integration of Electronic and Photonic Microsystems, 2015, 48297.

Corresponding Author: T. Zolotoukhina
Tel: +81-76-445-6739, Fax: +81-76-445-6739,
E-mail: zolotu@eng.u-toyama.ac.jp

High-yield production of thin layer materials by solid phase ball milling

○Ahmad Tayyebi, Gang Liu, Naoko Ogino, Naoki Komatsu

Graduate School of Human and Environmental Studies, Kyoto University, Sakyo-ku, Kyoto 606-8501, Japan

Two dimensional (2D) materials have attracted much attention due to their potential applications in energy, environment, optoelectronics, and biomedicine [1]. Several production methods have been developed in both top-down and bottom-up approaches, in which liquid phase exfoliation of the bulk layered materials might be the most appropriate in terms of scalability and simplicity [1]. Recently, our group developed a facile, scalable and high-yield production of 2D nanosheets using solid phase exfoliation of ball milling [2,3]. It is important to find out what controls the morphology and amount of exfoliated 2D materials. For this reason, we investigate the ball milling exfoliation of bulk molybdenum disulfide (MoS_2) in the presence of sodium cholate (SC) as a surfactant to study the effect of different operational conditions of ball milling process such as ball size, surfactant/initial MoS_2 weight ratio (SC/MoS_2), and ball milling duration and speed.

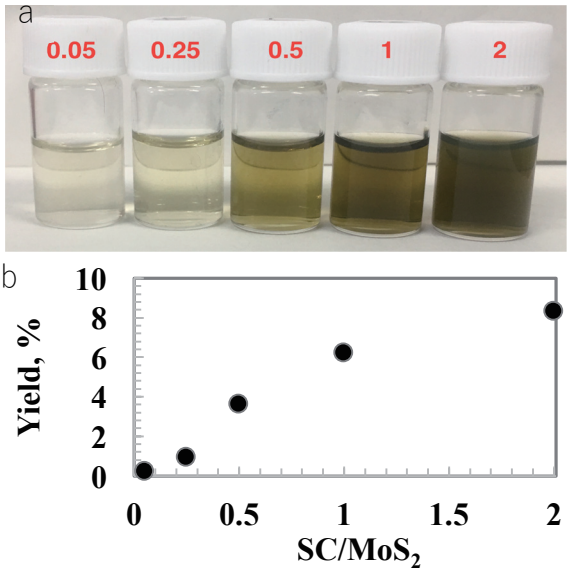

Figure 1. (a) Image of MoS_2 dispersion with different SC amount, and (b) plots of dispersed MoS_2 yield versus initial weight ratio of SC/MoS_2.

First, the effect of surfactant amount in the ball milling process was studied; the amount of MoS_2 was fixed at 0.20 g and the amount of SC was varied from 0.010 to 0.40 g. The powder obtained after ball milling was dispersed in deionized water (100 mL) and the resulting dark-greenish suspension was centrifuged at 3000 rpm (1025*g*) for 60 min. The top 75% of the supernatant (Figure 1a) was subjected to UV/vis spectroscopic analysis. The yield, the mean number of layers, and lengths of the nanosheets were calculated using the extinction and the reported coefficient at 345 nm [4], the wavelength of the exciton peak (λ_A), and the ratio of the extinction at 605 and 345 nm (Ext_{605}/Ext_{345}), respectively. As shown in Figure 1a and 1b, the yield of MoS_2 increased according to the increase of the weight ratio of SC/ MoS_2. The yield of 9% obtained at the SC/MoS_2 weight ratio of 2 is much larger than that obtained by liquid phase sonication. The morphology of MoS_2 nanosheets was determined to be two layers and 60 - 80 nm in size, from the λ_A observed at 658 nm and the value of Ext_{605}/Ext_{345}.

[1] V. Nicolosi, *et al.* Science, **340**, 1420 (2013). [2] G. Liu *et al.* ChemNanoMat. **35**, 9467 (2016). [3] G. Liu *et al.* ChemPhysChem **17**, 1557 (2016). [4] E. Varrla *et al.* Chem of Mat. **27**, 1129 (2015). [5] C. Bakes *et al.* Nat. Commun. **5**, 4576 (2014).

Corresponding Author: A. Tayyebi
Tel, Fax: +81-75-753-6833, E-mail: ahmad.tayyebi.28e@st.kyoto-u.ac.jp

Automated searching and assembly of atomic layers: a robotic building system of van der Waals superlattices

○Satoru Masubuchi [1], Masataka Morimoto [1], Momoko Onodera [1], Sei Morikawa [1], Kenji Watanabe [2], Takashi Taniguchi [2], and Tomoki Machida [1,3]

[1]*Institute of Industrial Science, University of Tokyo, Japan,*
[2]*National Institute for Materials Science, Japan,* [3]*CREST-JST, Japan*

Since the advent of van der Waals (vdW) heterostructures, random nature in the shape, thickness, and positions of exfoliated 2D crystals insist researchers for repetitive manual tasks of optical microscopy-based searching and subsequent mechanical transfer. To solve the long-standing problems, we developed a robotic system, which enables automated fabrication of vdW heterostructures. The system performance was demonstrated by finding 1200 monolayer graphene in 4 hours, stacking 30 alternative layers of atomically thin graphite and hexagonal boron nitride (hBN) in 8 hours, and 7 sets of hBN/graphene/hBN heterostructures in 3 hours. The system frees up researchers from the repetitive tasks, and provides a feasible platform for prototyping various types of vdW heterostructures.

Our optical microscopy system automatically searches atomically thin two-dimensional crystals on SiO_2/Si. After searching, the catalog of available 2D crystals are developed in a database system. vdW heterostructures are designed by selecting 2D crystals from database. Designated 2D crystals are assembled into vdW heterostructures by automated stamping machine. The entire system was developed in glove box enclosure with inert gas atmosphere, which enables handling easily-oxidized 2D crystals.

Corresponding Author: S. Masubuchi
Tel: +81-3-5452-6847, Fax: +81-3-5452-6157,
E-mail: msatoru@iis.u-tokyo.ac.jp

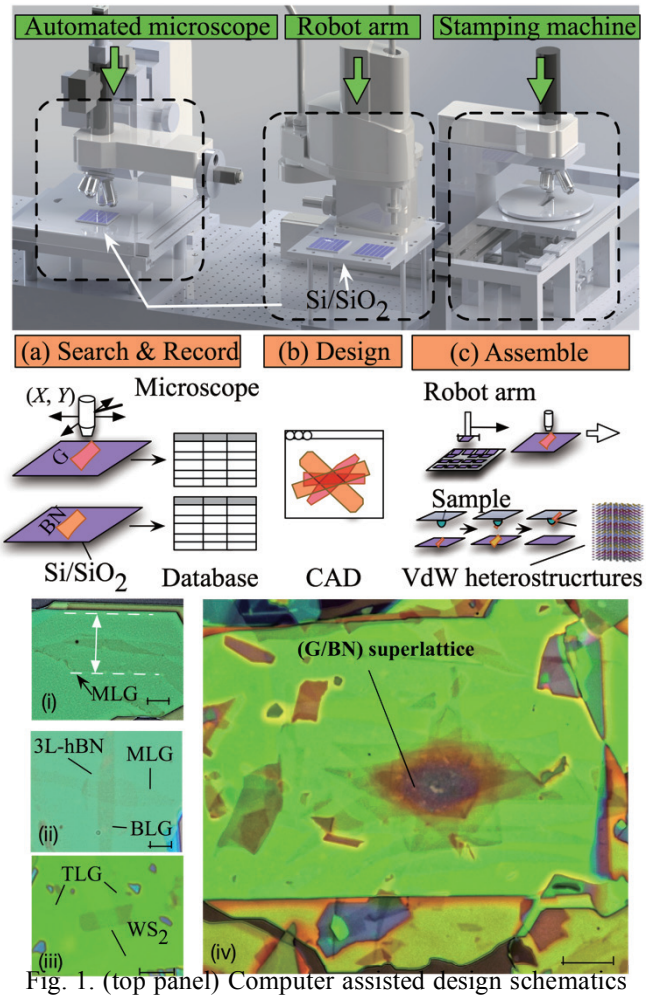

Fig. 1. (top panel) Computer assisted design schematics of automated assembly system. (middle panel) Schematics for fabrication process. (a) Atomically thin two-dimensional crystals on SiO_2/Si are searched by automated optical microscope and their information are stored in database. (b) The combination of 2D crystals for vdW heterostructures are designed by CAD software. (c) The designed vdW heterostructures are assembled by stamping machine. (bottom panel) optical microscopy images of fabricated vdW heterostructures. (i) monolayer graphene encapsulated in h-BN with crystallographic alignment. (ii) monolayer graphene/3L-hBN/bilayer graphene tunnel device. (iii) WS_2 contacted by trilayer graphene. (iv) $(graphene/hBN)_{14}$ superlattice structure. Scale bar corresponds to 5 µm.

Fast and precise imaging of structural defects in large area graphene films via lock-in thermography

○Hideaki Nakajima[1], Takahiro Morimoto[1], Yoshiue Ikuta[1], Yuki Okigawa[1], Takatoshi Yamada[1], Kenji Kawahara[2], Hiroki Ago[2], and Toshiya Okazaki [1]

[1] *National Institute of Advanced Industrial Science and Technology, Tsukuba 305-8565, Japan*
[2] *Global Innovation Center, Kyushu University, Fukuoka 816-8580, Japan*

Large area graphene synthesis by chemical vapor deposition (CVD) method has rapidly progressed for realizing scalable device applications. Nevertheless, the existence of local defects such as domain boundaries seriously degrade its superior physical properties. Although several experiments based on scanning tunneling microscopy have shown the influence of defects on the electrical transport properties, only the limited area were investigated in those reports due to long measurement times. Here, we demonstrate the fast and precise electrical characterization of large area CVD graphene sheets by using lock-in thermography (LIT) technique.

Figure 1 shows the measurement setup. The sample was the single-layer CVD graphene film epitaxially grown on a sapphire substrate. After transferring the graphene onto a quartz substrate, LIT was carried out by applying a 25 Hz AC bias between two electrodes. By using lock-in technique, Joule heat component from the biased sample was detected separately from background heat storage [1].

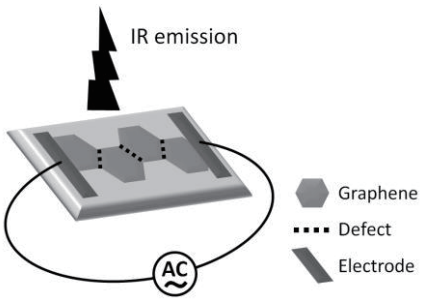

Fig. 1 Schematic diagram of electrical characterization with LIT.

Figure 2 (a) shows an optical microscope image of the sample. Individual graphene domains and boundary lines can be identified. The LIT image is indicated in Fig. 2 (b). The heat generation behaviors are clearly exhibited at the boundary locations 1 and 2. Since both locations show intense D-bands in Raman mapping (not shown), it is found that the observed thermal features are originated from boundary defects. In contrast, the boundary 3 shows a featureless thermal pattern. There is no D-band signature in the region, indicating to be a seamless boundary. These results indicate that the LIT successfully images the electrical properties of domain boundaries over a mm-sized graphene film within a reasonable time frame (10 min.). The detailed analysis of thermal properties to individual boundary characteristics will be discussed in the symposium.

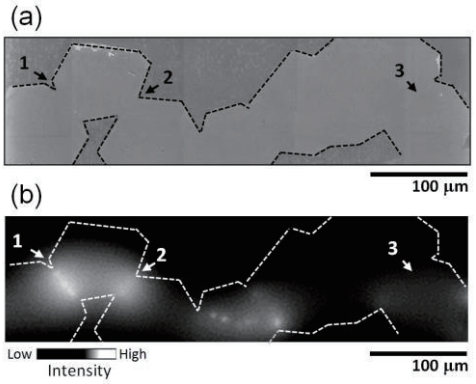

Fig. 2 (a) Optical microscope and (b) LIT images. The LIT image was obtained in 10 minutes.

[1] T. Morimoto *et al*., The 52nd FNTG general symposium, 2-4 (2017).

Corresponding Author: Toshiya Okazaki
Tel: +81-29-861-4173 / E-mail: toshi.okazaki@aist.go.jp

Direct Observation of Cross-Polarized Excitons in Aligned and Chirality-Enriched Single-Wall Carbon Nanotubes

○ Fumiya Katsutani,[1] Weilu Gao,[1] Xinwei Li,[1] Yota Ichinose,[2] Yohei Yomogida,[2]
Kazuhiro Yanagi,[2] and Junichiro Kono[1]

[1]*Department of Electrical and Computer Engineering, Rice University, Houston, Texas 77005, USA*
[2]*Department of Physics, Faculty of Science and Engineering, Tokyo Metropolitan University, Hachioji, Tokyo 192-0397, Japan*

Single-wall carbon nanotubes (SWCNTs) show strong absorption peaks due to subband-index-conserving exciton transitions (E_{ij}, $i = j$) for light polarized parallel to the nanotube axis. For light polarized perpendicular to the nanotube axis, absorption peaks are expected at E_{ij}, where $i - j = \pm 1$, but they are significantly suppressed by the depolarization effect [1,2]. These "cross-polarized" excitons (especially E_{12} and E_{21}) have been previously observed in circular dichroism and polarized photoluminescence excitation spectroscopy studies on aqueous suspensions of SWCNTs. However, their *direct observation* in optical absorption, combined with *quantitative analysis*, has been elusive due to the unavailability of suitable samples.

Here, we report a direct observation of the E_{12}/E_{21} peak in a (6,5)-enriched aligned SWCNT film. We prepared a pure (6,5) suspension through pH-controlled gel chromatography [3], and fabricated an aligned film through slow vacuum filtration [4]. Figure 1(a) shows polarization-dependent absorption spectra. For parallel polarization, strong E_{11} and E_{22} peaks are observed. As the polarization angle increases, these peaks gradually decrease in intensity while the E_{12}/E_{21} peak appears and grows at the lower energy side of the E_{22} peak. Figure 1(b) compares the parallel ($A_{\parallel}$) and perpendicular ($A_{\perp}$) spectra after multiplying $A_{\perp}$ by 3.2, whereas Figure 1(c) shows the normalized difference between $A_{\parallel}$ and $3.2A_{\perp}$. The E_{12}/E_{21} peak is observed at 1.88 eV, which is 660 meV higher than E_{11} and 250 meV lower than E_{22}. The integrated intensity of the E_{12}/E_{21} peak in $A_{\perp}$ is ~10% of that of the E_{11} peak in $A_{\parallel}$.

[1] H. Ajiki *et al*, Physica B **216**, 358 (1996).
[2] S. Uryu *et al*., Phys. Rev. B. **74**, 155411 (2006).
[3] Y. Ichinose *et al*, J. Phys. Chem. **121** 13391 (2017).
[4] X. He *et al*, Nat. Nanotech. **11**, 633 (2016).

Corresponding Author: Junichiro Kono
Tel: +1-713-348-2209, Fax: +1-713-348-3091,
E-mail: kono@rice.edu

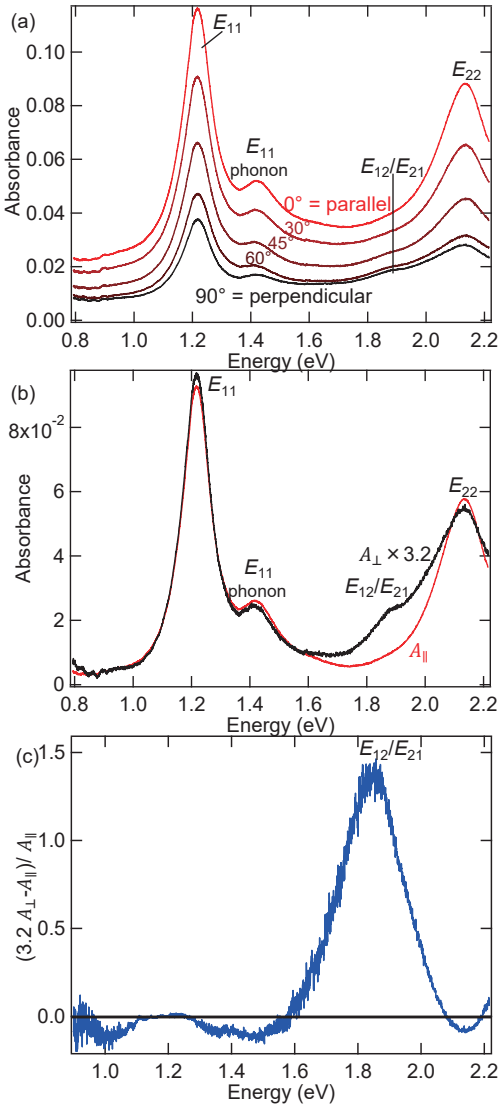

Fig. 1 (a) Absorption spectra for an aligned (6,5) SWCNT film for various angles between the light polarization and the nanotube alignment direction. (b), (c) Comparison of absorbance spectra for parallel and perpendicular polarizations.

Bilayer Plots for Accurately Determining the Chirality of Single-Walled Carbon Nanotubes Under Complex Environments

Juan Yang*, Daqi Zhang, Yuecong Hu, Chenmaya Xia, Sida Sun, Yan Li

College of Chemistry and Molecular Engineering, Peking University, Beijing 100871, China

The chirality (n,m) determines all the structures and properties of a single-walled carbon nanotube (SWNT), therefore, accurate and convenient (n,m) assignments are vital in nanotube-related science and technology [1]. In 1999, H. Kataura *et al.* [2] first proposed a calculated E_{ii}–d_t plot to explain the absorption and Raman spectra of SWNTs. Later, this plot was named after him as the Kataura plot, and was widely utilized by the researchers in the carbon nanotube community. However, the facts that both E_{ii} and the calculated d_t from ω_{RBM} are subject to interactions with the environments make it inconvenient to accurately determine the (n,m) under complex environments. Here, we propose a series of bilayer plots that take into account the interactions between the SWNTs and the environments so that the (n,m) of SWNTs can be accurately determined [3]. These plots are more concise, with less data overlapping, suitable to be used under complex environments, and can distinguish individual and bundled SWNTs. We strongly encourage the researchers in the carbon nanotube community to utilize the bilayer plots for all (n,m)-related studies, especially for accurate and convenient (n,m) determination. We have also launched an (n,m) assignment program on our group website (www.chem.pku.edu.cn/cnt_assign) to assist the researchers in accurately and conveniently determining the (n,m) of various SWNT samples under complex environments based on the bilayer plots.

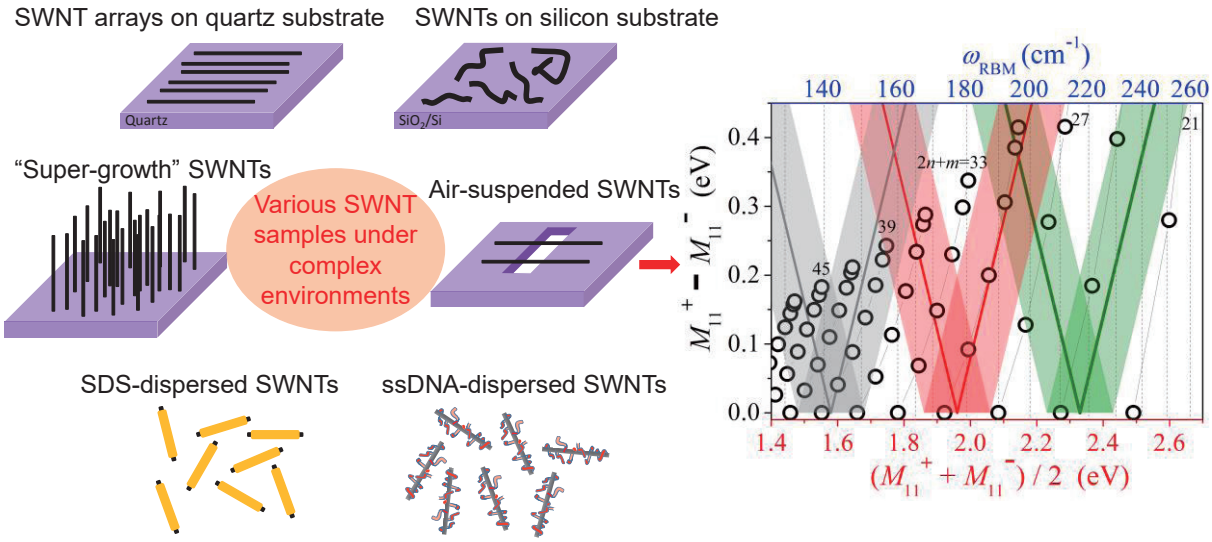

Fig.1 Bilayer plots for accurately determining the chirality of SWNTs under six different environments

[1] D. Zhang, J. Yang, Y. Li, small **9**, 1284 (2013).
[2] H. Kataura *et al.* Synth. Met. **103**, 2555 (1999).
[3] J. Yang, D. Zhang, Y. Hu *et al.* ACS Nano, **11**, 10509 (2017).

Corresponding Author: J. Yang
Tel: +86-10-62755357
E-mail: yang_juan@pku.edu.cn

Spectral tuning of optical coupling between air-mode nanobeam cavities and individual carbon nanotubes

○Hidenori Machiya[1,2], Takushi Uda[1,3], Akihiro Ishii[1,4], Yuichiro K. Kato[1,4]

[1] *Nanoscale Quantum Photonics Laboratory, RIKEN, Saitama 351-0198, Japan*
[2] *Department of Electrical Engineering, The University of Tokyo, Tokyo 113-8656, Japan*
[3] *Department of Applied Physics, The University of Tokyo, Tokyo 113-8656, Japan*
[4] *Quantum Optoelectronics Research Team, RIKEN Center for Advanced Photonics, Saitama 351-0198, Japan*

We design high quality factor air-mode nanobeam cavities by finite-difference time-domain simulations, and utilize the cavities to enhance the emission of air-suspended carbon nanotubes [1]. The cavities are fabricated from silicon-on-insulator wafers, and nanotubes are synthesized over the cavities by chemical vapor deposition. Photoluminescence spectroscopy is performed on the devices, where we observe optical coupling when the nanotube emission energy is close to the cavity resonance. Taking advantage of laser-heating-induced blueshifts of the nanotube emission, we can reduce the detunings [2]. We derive and numerically calculate the generalized expression for the spectral overlap, and good correlation to the enhancement factors is obtained.

Work supported by JSPS (KAKEIHI JP16H05962, JP16K13613), and MEXT (Photon Frontier Network Program, Nanotechnology Platform). H.M. is supported by RIKEN Junior Research Associate Program, and T.U. is supported by ALPS and JSPS Research Fellowship.

[1] R. Miura, S. Imamura, R. Ohta, A. Ishii, X. Liu, T. Shimada, S. Iwamoto, Y. Arakawa, and Y. K. Kato, *Nature Commun.* **5**, 5580 (2014).
[2] H. Machiya, T. Uda, A. Ishii, and Y. K. Kato, *Appl. Phys. Lett.* **112**, 021101 (2018).

Corresponding Author: Yuichiro K. Kato
Tel: +81-48-462-1111 (ext. 3432)
E-mail: yuichiro.kato@riken.jp

ポスター発表
Poster Preview

1P – 1 ～ 1P – 38
2P – 1 ～ 2P – 39
3P – 1 ～ 3P – 39

Electronic structures of solid phases of chemically functionalized C_{60}

Sho Furutani[1], Yutaka Matsuo[2,3], and Susumu Okada[1]

[1]*Graduate School of Pure and Applied Sciences, University of Tsukuba 305-8571, Japan*

[2]*Hefei National Laboratory for Physical Sciences at Microscale, University of Science and Technology of China, Hefei, Anhui 230026, China*

[3]*Department of Mechanical Engineering, The University of Tokyo, Tokyo 113-8656, Japan*

Chemically functionalized fullerenes are known to possess unusual electronic structure, which is totally different from the pristine fullerene. Therefore, they are commonly used as electron acceptor in organic photovoltaic devices since the energy level alignment around the Fermi level can be tunable by functionalization resulting in high open voltage to electron donor materials. Silylmethyl[60]fullerene (SIMEF) and methano indene fullerene (MIF) are representative fullerene derivatives which provide the remarkable conversion efficiency. In the photovoltaic devices, chemically functionalized fullerenes form bulk heterojunction with the donor molecules. Because of the asymmetric molecular shape of these functionalized fullerenes, molecular arrangements in their bulk phases crucially affect the carrier mobility that determines the conversion efficiency. Although the crystalline structures of SIMEF and MIF have been experimentally determined, the electronic structures solid phases of SIMEF and MIF are not elucidate yet. Thus, we clarify the electronic structures of crystalline SIMEF and MIF to give the guiding principle to enhance the electron transport in their bulk phases, using the density functional theory with the local density approximation.

Fig. 1 shows the electronic band structure of SIMEF and MIF in condensed phase. Our calculations show that crystalline SIMEF and MIF exhibit strong anisotropic electronic energy band in their condensed phases owing to the various intermolecular spacing and orientation between adjacent molecules. The calculated effective mass of SIMEF is ranging from 1.37 to 7.91m_e depending on molecular conformations. Effective electron mass of MIF is ranging from 0.57 to 4.23m_e.

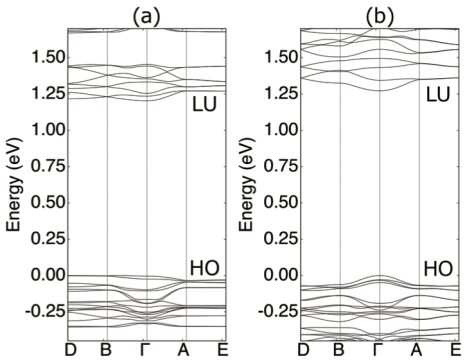

Fig. 1 Electronic band structure of (a)SIMEF and (b)MIF, respectively. The LU and HO indicate the lowest branch of the conduction band and the highest branch of the valence band, respectively

Corresponding author: S. Furutani (sfurutani@comas.frsc.tsukuba.ac.jp)

Temperature dependence of anisotropic transient conductivity of a La@C_{2v}-C_{82}(Ad) crystal

○Michio Yamada[1], Satoru Sato[2], Wookjin Choi[3], Shu Seki[3], Tsuneyuki Abe[2], Mitsuaki Suzuki[1,4] Yutaka Maeda[1], Shigeru Nagase[5], Takeshi Akasaka[1,2,6,7]

[1] Department of Chemistry, Tokyo Gakugei University, Tokyo 184-8501, Japan
[2] Life Science Center of Tsukuba Advanced Research Alliance, University of Tsukuba, Ibaraki 305-8577, Japan
[3] Department of Molecular Engineering, Kyoto University, Kyoto 615-8510, Japan
[4] Department of Chemistry, Josai University, Saitama 350-0295, Japan
[5] Fukui Institute for Fundamental Chemistry, Kyoto University, Kyoto 606-8103, Japan
[6] Foundation for Advancement of International Science, Ibaraki 305-0821, Japan
[7] State Key Laboratory of Materials Processing and Dye and Mold Technology, School of Materials Science and Engineering, Huazhong University of Science and Technology, Wuhan 430074, P. R. China

Endohedral metallofullerenes (EMFs) and their derivatives have attracted attention due to their potential for use in organic electronics [1-3]. La@C_{2v}-C_{82}, a typical monometallic EMF, is a stable neutral radical, in which the spin density is distributed over the carbon sphere. The open-shell electronic structure is derived from the transfer of three electrons from the encaged La atom to the C_{82} cage. As a result, the redox potentials are much smaller than those of C_{60}. Recently, we found that high electron mobility is achievable by aligning La@C_{2v}-C_{82} molecules in an orderly fashion [4,5]. The adamantylidene (Ad) adduct of La@C_{2v}-C_{82} (denoted as La@C_{2v}-C_{82}(Ad)), which retains its open-shell electronic structure, forms orderly aligned nanostructures in crystals where the Ad moiety facilitates crystal growth [6]. Flash-photolysis time-resolved microwave conductivity (FP-TRMC) measurements of a La@C_{2v}-C_{82}(Ad) crystal exhibited anisotropic (and extremely high) electron mobility of μ = 10 ± 5 cm^2 V^{-1} s^{-1} along the *c*-axis at room temperature. In this presentation, temperature-dependent conductivity measurements of a La@C_{2v}-C_{82}(Ad) crystal is provided to prove that the electron transport can be described by the electronic band-conduction model instead of the electron-hopping model [7].

[1] Y. Yasutake *et al*. Nano Lett. **5**, 1057 (2005).
[2] M. Iwamoto *et al*. J. Phys. Chem. C **114**, 14704 (2010).
[3] S. Kaneko *et al*. Phys. Rev. B **86**, 155406 (2012).
[4] S. Sato *et al*. J. Am. Chem. Soc. **133**, 2766 (2011).
[5] S. Sato *et al*. Angew. Chem. Int. Ed. **51**, 1589 (2012).
[6] Y. Maeda *et al*. J. Am. Chem. Soc. **126**, 6858 (2004).
[7] M. Yamada *et al*. Chem. Lett. **46**, 973 (2017).

Corresponding Authors: M. Yamada, S. Seki, T. Akasaka
Tel & Fax: +81-32-329-7493 (M.Y.)
E-mail: myamada@u-gakugei.ac.jp (M.Y.)

Spectroscopic studies of dimetallofullerene anions encapsulating Nd

○Shinya Nishimoto, Koichi Kikuchi, Yohji Achiba, Takeshi Kodama

Department of Chemistry, Tokyo Metropolitan University, Tokyo 192-0397, Japan

So far, emission from the encapsulated metal ion in metallofullerenes has been reported only for Er-metallofullerenes [1] and Tm-metallofullerenes [2]. Around 2006, we searched for Nd-metallofullerenes, which had the emission around 1 μm from the encapsulated Nd ion, and the very weak emission for $LaNd@C_{72}$ at 77 K was reported [3]. In general, the mechanism of emission from the encapsulated metal ion is supposed that, at first, the fullerene cage is excited by light, and then the energy transfers from the excited fullerene-cage to the metal ion, and finally the excited ion emits a photon. For Nd^{3+}, emission near 1 μm is due to the transition of $^4F_{3/2} \rightarrow {}^4I_J$(J=15/2, 13/2, 11/2, 9/2), and the shortest wavelength is about 900 nm. Therefore, to be observed the emission of Nd ion, the onset of the absorption spectrum for Nd-metallofullerenes should be shorter than 900 nm, which correspond to the lowest cage excitation energy. Fortunately, the onset for dimetallofullerenes is thought to be shorter than that for monometallofullerenes, so that the dimetallofullerenes might be more suitable for observing emission from encapsulated metals.

Recently, we succeeded in the isolation of $(M_2@C_{78}(D_{3h}))^-$ and $(M_2@C_{80}(I_h))^-$ using the method combining ion-pair chromatography with the extraction by a mixed solvent of triethylamine and acetone [4]. In this study, by using the method, we synthesized and isolated the novel Nd-dimetallofullerenes that are stable only as an anion form. Moreover, we investigated the emission properties of the obtained Nd-dimetallofullerenes.

Soot containing Nd-metallofullerenes was produced by direct-current (60 A) arc discharge of Nd/C composite rods (Nd:C=2:98) under a 500 Torr He atmosphere. $(Nd_2C_{78})^-$ and $(Nd_2C_{80})^-$ were extracted and isolated by the previously reported method [4]. For the obtained Nd-dimetallofullerenes, the UV-vis-NIR absorption and emission spectra were measured. As shown in Fig.1 and Fig.2, the UV-vis-NIR absorption spectra of $(Nd_2C_{78})^-$ and $(Nd_2C_{80})^-$ were very similar to those of $(La_2@C_{78}(D_{3h}))^-$ and $(Ce_2@C_{80}(I_h))^-$, respectively. Therefore, $(Nd_2C_{78})^-$ and $(Nd_2C_{80})^-$ were found to be $(Nd_2@C_{78}(D_{3h}))^-$ and $(Nd_2@C_{80}(I_h))^-$. The results of emission measurements will be discussed in the presentation.

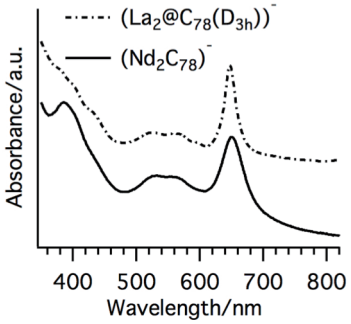

Fig.1 UV-vis-NIR absorption spectra of $(Nd_2C_{78})^-$ and $(La_2@C_{78}(D_{3h}))^-$.

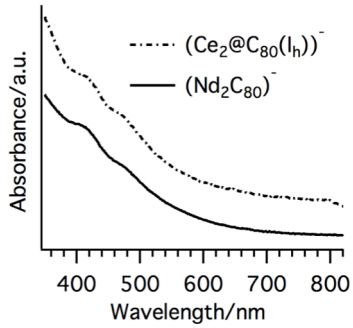

Fig.2 UV-vis-NIR absorption spectra of $(Nd_2C_{80})^-$ and $(Ce_2@C_{80}(I_h))^-$.

[1] X. Ding, et al. *Chem. Phys. Lett.* **269**, 72 (1997).
[2] Z. Wang, et al. *ACS Nano* **10**, 4282 (2016).
[3] N. Murata, et al. *The 30th Fullerenes-Nanotubes-Graphene General Symposium* 106 (2006).
[4] N. Nakatori, et al. *The 49th Fullerenes-Nanotubes-Graphene General Symposium* 46 (2015).

Corresponding Author: Takeshi Kodama
Tel: +81-42-677-2530, Fax: +81-42-677-2525
E-mail: kodama-takeshi@tmu.ac.jp

Isolation and Characterization of $Tm_2@C_n$(n=78, 80) anion

○Kazuhiro Kobayashi[1], Ko Furukawa[2], Tatsuhisa Kato[3, 4], Koichi Kikuchi[1], Yohji Achiba[1], Takeshi Kodama[1]

[1]*Department of Chemistry, Tokyo Metropolitan University, Tokyo 192-0397, Japan*
[2]*Center for Coordination of Research Facilities, Niigata University, Niigata 950-2181, Japan*
[3]*Graduate School of Human and Environmental Studies, Kyoto University, Kyoto 606-8501, Japan*
[4]*Institue for Liberal Arts and Sciences, Kyoto University, Kyoto 606-8501, Japan*

Recently, we succeeded in the isolation of the so-called missing metallofullerenes, $Y_2@C_{80}(I_h)$[1] and $Gd_2@C_{80}(I_h)$[2], as an anion form using the method combining the ion-pair chromatography (IPC) with the mixed solvent extraction. Therefore, it was shown a possibility of the production of unknown $M_2@C_{80}(I_h)$ containing other metals. At first, we tried to produce $Yb_2@C_{80}(I_h)$ because Yb^{3+} has the same J value, 7/2, as Gd^{3+}, but the different L and S values (L=3 and S=1/2 for Yb^{3+}; L=0 and S=7/2 for Gd^{3+}). We intended to compare the spin states of $(Yb_2@C_{80}(I_h))^-$ and $(Gd_2@C_{80}(I_h))^-$, but, unfortunately, $Yb_2@C_{80}(I_h)$ could not be produced. As the reason of the missing production, rather large ionization potential (IP) of Yb was suspected. So, next, we tried to produce $Tm_2@C_{80}(I_h)$ because Tm is an element on the left side of Yb in the periodic table and has rather large IP like Yb but slightly smaller than that of Yb. So far, Tm-monometallofullerenes, $Tm@C_n$(n=74, 82, 84, etc.), were isolated and Tm takes the divalent state in the cage. The situation is the same for Yb. On the other hand, though no dimetallofullerenes were reported for Yb, Tm-dimetallofullerenes, $Tm_2@C_{82}$ and $HoTm@C_{82}$, were isolated and Tm takes the trivalent state in the cage[3]. A Tm^{3+} ion has two holes on the 4f-shell, so Tm^{3+} has J value 6 (L=5, S=1) in the ground state. So, if $Tm_2@C_{80}(I_h)$ exists, the spin state of $Tm_2@C_{80}(I_h)$ anion which encapsulates two Tm^{3+} ions would be interesting. In addition, $Tm_2@C_{78}$ anion was also targeted in this work.

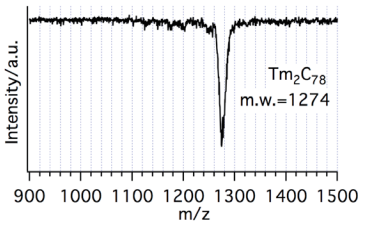

Fig.1 LD-TOF-MS spectrum of Tm_2C_{78}.

We carried out direct-current arc discharge of Tm/C composite rods under a He atmosphere. The obtained raw soot was extracted with a mixed solvent of triethylamine and acetone. The extract was separated by multi-step IPC. Fig.1 shows LD-TOF-MS spectrum of Tm_2C_{78}. From this spectrum, the isolation of Tm_2C_{78} is confirmed. As shown in Fig.2, the UV-vis-NIR absorption spectra of $(Tm_2C_{78})^-$ and $(La_2@C_{78}(D_{3h}))^-$ are very similar. Then it is suggested that the $(Tm_2C_{78})^-$ has a $C_{78}(D_{3h})$ cage, Tm takes a trivalent state, and an excess electron is located on the dimer like $(La_2@C_{78}(D_{3h}))^-$.

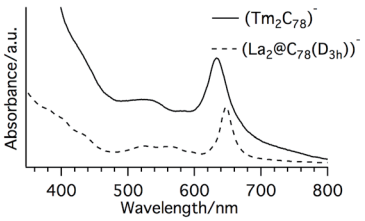

Fig.2 UV-vis-NIR spectra of $(Tm_2C_{78})^-$ and $(La_2@C_{78}(D_{3h}))^-$.

As for Tm_2C_{80}, we will discuss at the symposium.

[1] N. Nakatori, et al. *The 49th Fullerenes-Nanotubes-Graphene General Symposium* 46 (2015).
[2] T. Mitani, et al. *The 50th Fullerenes-Nanotubes-Graphene General Symposium* 95 (2016).
[3] K. Kikuchi, Endofullerenes, eds. by T. Akasaka and S. Nagase, Kluwer Academic Publishers, 217-230 (2002).

Corresponding Author: Takeshi Kodama
Tel: +81-42-677-2530, Fax: +81-42-677-2525
E-mail: kodama-takeshi@tmu.ac.jp

Energetics and Electronic Structure of Endohedral C_{60} Fullerenes

○Yuki Sugaya[1], Masayuki Toyoda[1], Susumu Saito[1], Tomonari Wakabayashi[2], Yasuyuki Kanai[3], Noboru Sasao[4], Motohiko Yoshimura[4]

[1] *Department of Physics, Tokyo Institute of Technology, Tokyo 152-8551, Japan*
[2] *Department of Chemistry, Kindai University, Higashi-Osaka 577-8502, Japan*
[3] *Nishina Center for Accelerator-Based Science, RIKEN, Wako 351-0198, Japan*
[4] *Division of Quantum Universe, RIIS, Okayama University, Okayama 700-8530, Japan*

Various fullerenes including C_{60} have hollow structure. Therefore, fullerene is expected to be a cage that realizes an isolated atomic system by trapping the atom. So far metal atoms (Y, Sc, La, etc.), noble gas atoms (He, Ne, Xe, etc.), nitrogen (N), etc. are validated as the encapsulated atom (X).

We study the energetics and electronic structure of endohedral C_{60} fullerenes ($X@C_{60}$) in the framework of the density-functional theory (DFT) in order to identify the ideal elements X for producing the coherent cluster of isolated atoms by laser, which is to be used for detecting the neutrino double beta decay.

We use nitrogen (N) [1], oxygen (O), xenon (Xe), copper (Cu) and gold (Au) as the encapsulated atom X, and calculate total energies and the electronic structures of X, C_{60} and $X@C_{60}$ by using the local density approximation (LDA) and local spin density approximation (LSDA):

1. Energy levels (X,C_{60}, $X@C_{60}$: X = N, O, Xe, Cu and Au)
   First, we calculate energy levels of X, C_{60} and $X@C_{60}$. Figure.1 shows energy levels of C_{60} and $Xe@C_{60}$. It is found that there is no electron transition between X and C_{60} for all X atoms studied. Therefore, these X atoms are good candidates for coherent cluster of isolated atoms.

2. Energetics ($X@C_{60}$: X = N, Cu and Au)
   We calculate total energies of $X@C_{60}$ as a function of X atom's position from C_{60}'s center. Following these results, we discuss energetical stabilities of $X@C_{60}$, and also the energy barrier for X to pass through the C_{60}'s shell.

3. Photoabsorption Cross section
   (X,C_{60}, $X@C_{60}$: X = N and Xe)
   We study the photoabsorption cross section by using time-dependent local density approximation (TDLDA) to discuss the laser excitation for coherent cluster of atoms.

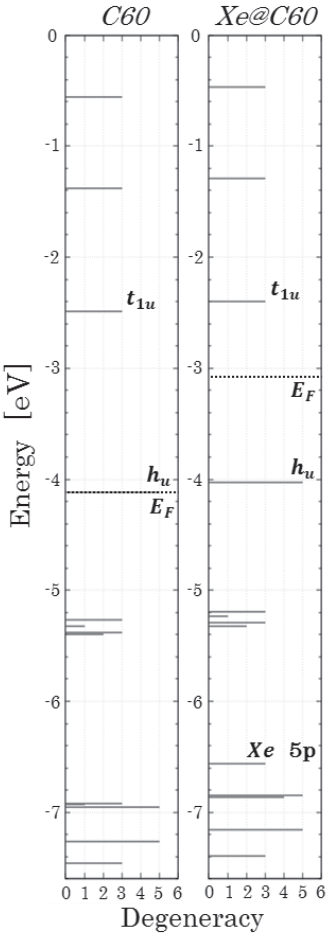

Fig.1 Energy levels of C_{60} and $Xe@C_{60}$ (0[eV] is vacuum level)

[1] T. Wakabayashi *et al.*, submitted to the 54th FNTG General Symposium, Tokyo (2018)

Corresponding Author: Y. Sugaya
Tel: +81-3-5734-2703, Fax: +81-3-5734-2739,
E-mail: sugaya@stat.phys.titech.ac.jp

$N@C_{60}$ produced from C_{60} by irradiation with N^+ and N^{2+} ion beam

○Tomonari Wakabayashi[1], Yasuyuki Kanai[2], Noboru Sasao,[3] Yuki Sugaya,[4]
Masayuki Toyoda[4], Susumu Saito[4], Motohiko Yoshimura[3]

[1]*Department of Chemistry, Kindai University, Higashi-Osaka 577-8502, Japan*
[2]*Nishina Center for Accelerator-Based Science, RIKEN, Wako 351-0198, Japan*
[2]*Division of Quantum Universe, RIIS, Okayama University, Okayama 700-8530, Japan*
[2]*Department of Physics, Tokyo Institute of Technology, Tokyo 152-8551, Japan*

Nitrogen-doped fullerene C_{60}, namely $N@C_{60}$, is known for its unique properties of electron spin systems which can maintain extremely long coherence time [1]. The discovery of $N@C_{60}$ in 1996 stimulated following researches on the application of the electron spin states to quantum computation and quantum information processing [2,3]. Methodological modifications have been invented for increasing the production yield of $N@C_{60}$, including ion implantation, plasma discharge, and ion bombardment. However, quantity of the material accessible in the laboratory is still limited at most to a few tens of micrograms. For further improvement to obtain macroscopic amount of $N@C_{60}$, the formation mechanism is to be clarified under the systematically controlled experimental conditions. In consideration of the mechanism, applications to the formation of novel species such as $X@C_{60}$ where X represents an atom other than nitrogen may follow for coherent control of radiation processes [4].

Ion beam of N^+ or N^{2+} was obtained by an electron cyclotron resonance ion source, Capris ECRIS at Nishina Center in RIKEN. Sediment of C_{60} on a copper substrate was irradiated by the ion beam at desired incident energy at 100 eV or 5 keV. After the 2-4 hours of irradiation of C_{60} in vacuum with N^+ or N^{2+} ion beam at the current of 17-30 microamperes, the C_{60} sediment was collected in the air by dissolving it into a small amount of carbon disulfide. The solution was filtered to remove undissolved solid particles and subjected to the X-band ESR spectrometer for the detection of the magnetic species.

Figure 1 shows ESR spectra of the solution containing ion-beam irradiated C_{60}. The triplet signal with the hyperfine splitting of 15.8 MHz indicates the presence of $N@C_{60}$. The electron spin of atomic nitrogen at the configuration of $2p^3$, $S = 3/2$, couples with the nuclear spin of the isotope of ^{14}N, $I = 1$, providing the triplet. In comparison with the result from two types of experiment, it turned out that *in situ* co-deposition of C_{60} was crucial for high yield of $N@C_{60}$. The penetration depth of the accelerated ions into the C_{60} sediment will be discussed.

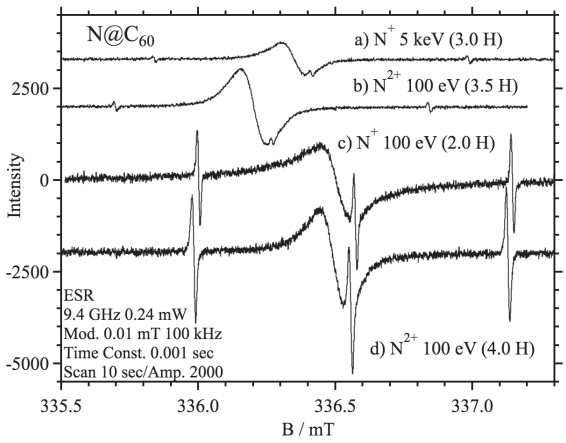

Figure 1. ESR spectra of $N@C_{60}$ produced by irradiation of mass-selected N^+ or N^{2+} ion beam to pre-deposited film of C_{60} (a,b) or to co-deposited film of C_{60} (c,d).

[1] T. Almeida-Murphy *et al*. Phys. Rev. Lett. **77**, 1075 (1996).
[2] W. Harneit, Phys. Rev. A **65**, 032322 (2002).
[3] J. J. L. Morton *et al.* Nature Phys. **2**, 40 (2006).
[4] A. Fukumi *et al.* PTEP, 04D002 (2012).
Corresponding Author: T. Wakabayashi
Tel: +81-6-4307-3408, Fax: +81-6-6723-2721,
E-mail: wakaba@chem.kindai.ac.jp

Self-patterning of C_{60} sheet like crystals by liquid-liquid interfacial precipitation method

○Yuto Funamori [1], Saori Yamamoto [1], Hiromichi Gonnokami [1], Hidenobu Murata [1], Yuko Kaneda [2], Makoto Tanimura [2], Masaru Tachibana [1]

[1] *Department of Materials System Science, Yokohama City University, Kanagawa 236-0027, Japan*
[2] *Instrumental Analysis Center, Yokohama National University, Kanagawa 240-8501, Japan*

C60 nano/micro crystals have attracted much attention due to their unique shapes and properties [1]. They have been effectively grown by liquid-liquid interfacial precipitation (LLIP) method with good and poor solvents. The shape and structure depend on the solvents used. In the LLIP method, alcohol has been mainly used as poor solvent. Recently we obtained hexagonal sheet like crystals by LLIP method using not alcohol but CCl4 as poor solvent. Additionally, it was found that the crystals exhibit an interesting change called a self-patterning. In this paper, we report the growth of hexagonal sheet like crystals and their self-patterning.

C60 nano/micro crystals have attracted much attention due to their unique shapes and properties [1]. They have been effectively grown by liquid-liquid interfacial precipitation (LLIP) method with good and poor solvents. The shape and structure depend on the solvents used. In the LLIP method, alcohol has been mainly used as poor solvent. Recently we obtained hexagonal sheet like crystals by LLIP method using not alcohol but CCl4 as poor solvent. Additionally, we found that the crystals exhibit an interesting change called a self-patterning. In this paper, we report the growth of hexagonal sheet like crystals and their self-patterning.

C60 sheet like crystals were grown by LLIP method with CCl4 and toluene as poor and good solvents, respectively. In the procedure, CCl4 was poured in a glass bottle, and then, C60-saturated toluene was gently added. The crystals were nucleated from the interface of both of the solutions, and was grown for 24 hours in 278 K. Consequently, hexagonal sheet like crystals were obtained with several micrometers in thickness. The crystals were placed on the slide glass, and were observed in open air using an optical microscope. Interestingly, the partition in each crystal appears with the evaporation of solvent while keeping the original hexagonal outline (Fig.1). Each partitioned shape exhibits rod-like one. The long-axis orientations of partitioned rod-like crystals are arranged along any edges of the original hexagonal shape. We call such change a self-patterning. The origin of the self-patterning is discussed in light of the desolvation of CCl4 with the results of FT-IR, XRD and TEM.

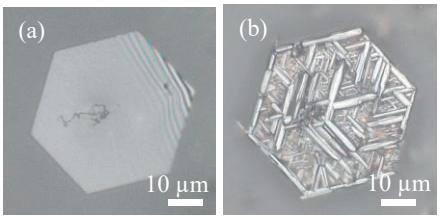

Fig.1 (a) Crystal placed on the slide glass, and (b) after self-patterning

[1] "Fullerene nanowhiskers", 2nd ed. edited by K. Miyazawa, Y. Ochiai, M. Tachibana, T. Kizuka, S. Nakamura, Pan Stanford Publishing (2018)

Corresponding Author: Y. Funamori
Tel: +81-45-787-2162, Fax: +81-45-787-2162,
E-mail: author@domain.jp

Third-harmonic generation process in a thin film of (6,5) single-wall carbon nanotubes

○Takahiro Yokoyama, Takeshi Koyama, Hideo Kishida

Department of Applied Physics, Nagoya University, Nagoya 464-8603, Japan

It is expected that single-wall carbon nanotubes (SWCNTs) show large optical nonlinearities due to their one-dimensional electronic structure [1]. In Ref. [2], the third-order nonlinear optical susceptibility ($\chi^{(3)}$) of SWCNTs was evaluated using the third-harmonic generation (THG) method. However, resonant processes and excitonic effects on the THG process in SWCNTs are still open questions. In this study, we measured the $|\chi^{(3)}|$ spectrum for (6,5) SWCNTs using the THG method.

(6,5) enriched dispersion was made by the method previously reported [3]. After vacuum filtration of the dispersion, we obtained a thin film and transferred it onto an SiO_2 substrate. The measured $|\chi^{(3)}|$ spectrum displays a resonance at around 0.64 eV. A comparison with the absorption spectrum indicates that the resonance at around 0.64 eV is attributed to two-photon resonance. This result suggests that processes including a transition to a one-photon forbidden state affect THG in the SWCNTs. By a discrete-level model, we analyzed the THG spectrum and revealed the dominant THG processes in the observed photon energy region.

[1] V. A. Margulis, T. A. Sizikova, Physica B **245**, 173 (1998).
[2] D. T. Morris *et al.*, Phys. Rev. B **87**, 161405 (2013).
[3] H. Liu *et al.*, Nat. Commun. **2**, 309 (2011).

Corresponding Author: H. Kishida
E-mail: kishida@nagoya-u.jp

Tuning of the Thermoelectric Properties of High-Purity Single-Chirality (6,5) Single-Walled Carbon Nanotubes by Electrolyte Gating

○Yota Ichinose, Kengo Fukuhara, Junko Eda, Yohei Yomogida, Kazuhiro Yanagi

Department of Physics, Tokyo Metropolitan University, Tokyo 192-0397, Japan

One-dimensional materials have potential to exhibit extremely high thermoelectric performance [1]. One of suggested approaches to achieve the high thermoelectric performance is to tune the Fermi level of the 1D materials with sharp van Hove singularity (vHS). Single-walled carbon nanotubes (SWCNTs) are a model for 1D system with sharp vHS, and thus we can investigate how the location of Fermi level influences their thermoelectric properties. Previously, we have investigated the thermoelectric properties of SWCNTs as a function of Fermi-level using an electrolyte gating technique [2]. However, the observed relationships between the Fermi level and the Seebeck coefficients of semiconducting SWCNTs were not in agreement with theoretical predictions. It is suggested that even a small amount of impurities (~1%) affects the thermoelectric properties [3]. Recently, we established a separating technique, which controls pH of solutions using CO_2 bubbling in gel-column chromatography, to obtain extremely high-purity single-chirality SWCNTs (6,5) with purity of more than 99% [4]. Therefore, in this study, we investigated the relationships between thermoelectric properties and location of Fermi levels of high-purity single-chirality SWCNTs.

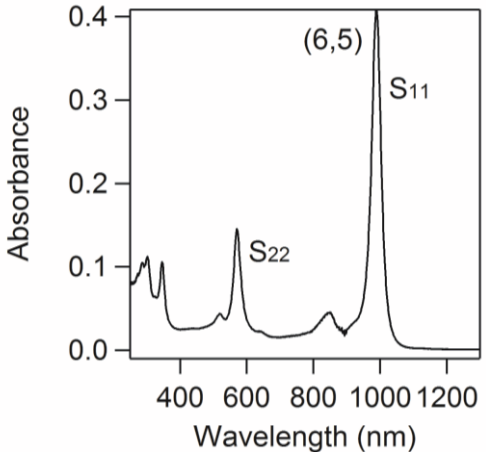

Fig.1 Optical absorption spectrum of (6,5) SWCNTs

As shown in Figure 2, we found very large Seebeck coefficient (above 10mV/K), which is about 10^2 times larger than previous reported values. The power factor was also enhanced and about 10 times lager. We found that the improvement of semiconducting SWCNTs purity strongly enhances the film thermoelectric properties.

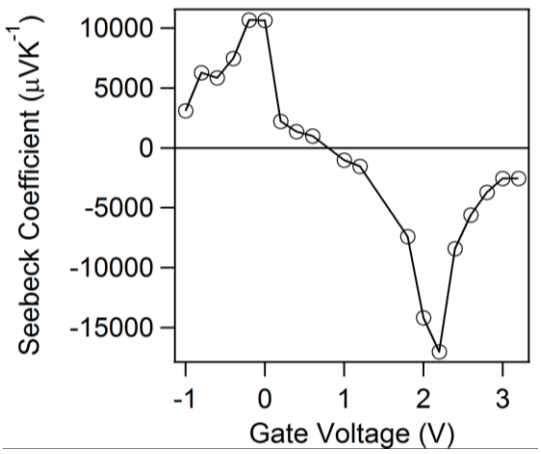

Fig.2 Seebeck coefficient of (6,5) using electrolyte gating

[1] Hicks & Dresselhaus, PRB 47, 16631 (1993)
[2] K. Yanagi *et al*. Nano letters, **14(11),** 6437 (2014).
[3] D. Hayashi *et al*. Applied Physics Express, **9(2)**, 025102 (2016)
[4] Y. Ichinose *et al*. J. Phys. Chem. C, **121 (24)**, 13391 (2017)

Corresponding Author: K. Yanagi Tel: +81-42-677-2493, E-mail: yanagi-kazuhiro@tmu.ac.jp

Optimizing photothermoelectric effects in semiconducting and metallic carbon nanotubes

○ Ahmad R.T. Nugraha, Nguyen T. Hung, Riichiro Saito
Department of Physics, Tohoku University, Sendai 980-8578, Japan

Carbon nanotubes (CNTs) are known to absorb electromagnetic waves in a wide spectral range, including THz regime [1]. THz detectors are required for many applications in astronomy, sensing, spectroscopy, imaging, defense, and communications. Using CNTs as a THz detector has been shown by some researchers to be promising due to the intrinsic polarization sensitivity of the CNTs as the absorbing materials with the THz-light-induced thermoelectric effect (or photothermoelectric effect), which is assigned as the origin of the THz signal in the THz detector [1-2]. However, the reported thermoelectric efficiency is quite low, about a thousand times less efficient than commercial thermoelectric generator.

In this work, we investigate the photothermoelectric effects in CNTs by considering combinations of semiconducting and metallic CNTs under illumination of THz light. We propose that the metallic and semiconducting CNTs play independent roles in the photothermoelectric effect. The metallic CNTs are responsible for absorbing THz light and convert it into heat, which results in a temperature distribution along the device. On the other hand, the semiconducting CNTs are responsible for generating voltage difference from the temperature distribution due to Seebeck's effect. Since the Seebeck coefficient of CNTs is chirality-dependent [3], we expect that there should be some optimized structures and also optimized ratios of semiconducting and metallic CNTs to improve the efficiency of the photothermoelectric effect in the CNT THz detector [4].

[1] L. Ren et al., Nano Lett. 12, 787–790 (2012)

[2] X. He et al., Nano Lett. 14, 3953–3958 (2014).

[3] N. T. Hung, A. R. T. Nugraha, et al., Phys. Rev. B 92, 165426 (2015).

[4] A. R. T. Nugraha, N. T. Hung, R. Saito, unpublished.

Corresponding Author: A.R.T. Nugraha
Tel: +81-22-795-6442, Fax: +81-22-795-6447, E-mail: nugraha@flex.phys.tohoku.ac.jp

Ferric ions affect surfactant assembly structures on carbon nanotubes

○Atsushi Hirano [1], Tomoshi Kameda [2], Takeshi Tanaka [1], Hiromichi Kataura [1]

[1] *Nanomaterials Research Institute, National Institute of Advanced Industrial Science and Technology (AIST), Ibaraki 305-8565, Japan*
[2] *Artificial Intelligence Research Center, National Institute of Advanced Industrial Science and Technology (AIST), Tokyo 135-0064, Japan*

Carbon nanotubes (CNTs) are grown on metal catalyst particles. Ions originating from the catalyst particles are dissolved into aqueous phases when the CNTs with the catalyst particles are dispersed into aqueous solutions using surfactants. In this study, we demonstrated that the ferric ions (Fe^{3+}) from iron catalyst particles modify surfactant assembly structures on the CNTs, which is determined by adsorption experiments of CNTs onto hydrogel surfaces and molecular dynamics (MD) simulations. We suggest that the coexisting ferric ions affect colloidal properties of the CNTs including quality of CNT separation using hydrogels.

We used CNTs produced by the HiPco process in this study. We prepared CNT dispersion using sodium dodecyl sulfate (SDS). Iron ions from the catalyst particles can thus coexist with the SDS-dispersed CNTs. Figure 1 shows spectra of the adsorbed CNTs onto the hydrogel (Sephacryl S-200) surfaces at various concentrations of the chelating agent (ethylenediaminetetraacetic acid disodium salt, EDTA-2Na) or NaCl as a control, which were collected by an eluent (sodium deoxycholate). EDTA-2Na even at 10 μM was found to enhance the adsorbability of the CNTs onto the hydrogel surfaces, whereas NaCl was inert in the same range of sodium concentrations. This result indicates the coexisting iron ions weaken the CNT adsorbability onto the hydrogel surfaces.

The weakening effect on the CNT adsorbability onto the hydrogel surfaces should be attributed by the surfactant density on the CNT surfaces [1]. To provide a realistic model of this effect, we performed MD simulations of SDS molecules around a CNT in the presence of ferric ions (Fe^{3+}) or ferrous ions (Fe^{2+}) (Figure 2). Ferric ions interacted with the SDS molecules on the CNT, whereas ferrous ions marginally interacted with them. We thus concluded that the coexisting ferric ions increase SDS density on the CNT surfaces, leading to the attenuation of the CNT adsorbability onto the hydrogel surfaces. This is the first report of the effect of ferric ions originating from the catalyst particles on the surfactant assembly structures.

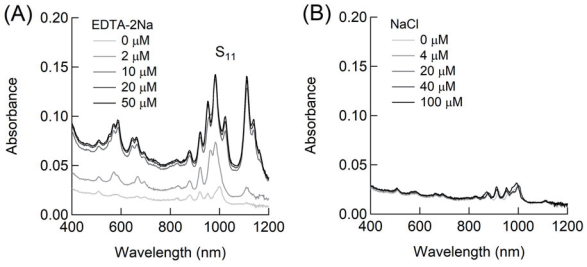

Fig.1 Absorption spectra of the CNTs adsorbed on the hydrogel surfaces in the presence of different concentration of EDTA-2Na (A) and NaCl (B).

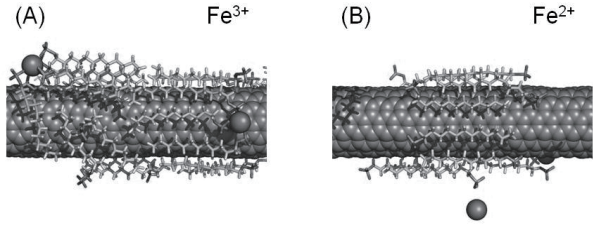

Fig.2 Conformations of SDS assembly on the CNT in the presence of Fe^{3+} ions (A) and Fe^{2+} ions (B) provided by the MD simulations. Iron ions are represented by spheres.

[1] A. Hirano *et al*. ChemNanoMat 2, 911 (2016).

Corresponding Author: A. Hirano
Tel: +81-29-849-1064, Fax: +81-29-861-2786,
E-mail: hirano-a@aist.go.jp

Near-infrared luminescence thermometric imaging using carbon nanotubes

○Kengo Hachiya[1], Saki Okudaira[1], Yui Konno[2], Yutaka Maeda[2],
Kazunari Matsuda[1], and Yuhei Miyauchi[1]

[1] *Institute of Advanced Energy, Kyoto University, Uji 611-0011, Japan*
[2] *Department of Chemistry, Tokyo Gakugei University, Koganei, Tokyo 184-8501, Japan*

Single-walled carbon nanotubes (SWNTs) have been considered as nearly ideal luminescent probes for deep tissue bioimaging because of their photoluminescence in near-infrared range known as the second optical window of biological tissues [1]. Furthermore, availability of efficient phonon-assisted up-conversion photoluminescence (UCPL) in SWNTs, for which the excitation light wavelength can be longer than the emission one, has recently been discovered [2]. With increasing temperature, the UCPL intensity increases while Stokes PL (hereafter, just referred to as PL) intensity decreases [2]. Thus, the temperature dependent variation of the intensity ratio of the UCPL and PL may potentially be used for optical thermometry applicable to deep inside of biological tissues. Recently, hyperthermia using nanoparticles has been considered to be effective for the treatment of tumors [3]. In the hyperthermia treatment, strict control of the tumor temperature is required. However, the exact temperature control still remains a challenge because of the difficulty in measuring the temperature of the tumor in deep tissue. Therefore, development of an effective method for the deep tissue optical thermometry has been strongly desired.

In this study, we observed UCPL and PL images of SWNTs that were chemically functionalized in order to enhance both the UCPL from the free excitons and the longer wavelength PL from the localized excitons [4,5]. The SWNTs were dispersed in water, and it was sealed in a thin circular cell, and their UCPL and PL were measured by changing the filters with an InGaAs near-infrared camera. The temperature of the dispersion was directly controlled using a rubber-heater and a thermostat, and the luminescence image of the UCPL (980 nm) and the PL (1100 nm) were obtained under epi-illumination using a 1064 nm laser. The PL and UCPL images were taken under the same temperature, and the ratio of the PL and UCPL intensities at each spatial position were obtained to construct a ratiometric image. As the temperature of SWNTs increased, the luminance intensity of UCPL (I_{UCPL}) increased but the PL (I_{PL}) counterpart decreased. Consequently, the value of the ratio (I_{UCPL}/ I_{PL}) increased as shown in Figure 1. Clear increase of the intensity ratio indicates high sensitivity of this method to a small temperature variation. Performance evaluation for the deep-tissue optical thermometric imaging will be discussed.

[1] K. Welsher *et al.*, Nat. Nanotechnol. **4**, 773 (2009).
[2] N. Akizuki *et al.,* Nat. Commun. **6**, 8920 (2015).
[3] Jelena Kolosnjaj-Tabi et al., Pharm. Res. **126**, 123 (2017).
[4] Y. Maeda, *et al.*, Nanoscale **8**, 16916 (2016).
[5] Y. Maeda, *et al.*, Chem. Eur. J. **23**, 1789 (2017).

Corresponding Author: Y. Miyauchi
Tel: +81-774-38-3463, Fax: +81-774-38- 3467,
E-mail: miyauchi@iae.kyoto-u.ac.jp

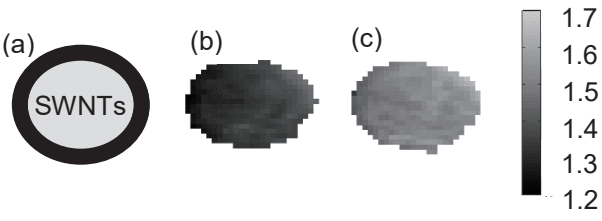

Fig.1: (a) Schematic of a thin circular cell filled with an aqueous dispersion of SWNTs (top view). (b) I_{UCPL}/ I_{PL} image at 21.5 ° C and (c) at 35.8 ° C. Color bar indicates the value of the I_{UCPL}/ I_{PL} in an arbitrary unit.

Polymeric p-Type Dopant showing Permanent Doping Durability for Transparent Carbon Electrodes

○Clement Delacou [1], Il Jeon [2], Ahmed Shawky, Rong Xiang, Anton Anisimov, Esko I. Kauppinen, Yutaka Matsuo, Shigeo Maruyama [1]
[1] *Department of Mechanical Engineering, The University of Tokyo, Tokyo 113-8656, Japan*
[2] *Department of Chemistry, The University of Tokyo, Tokyo 113-8656, Japan*

Transparent electrodes are vital components for touch panels, displays, and photovoltaic cells. Widely used indium tin oxide (ITO) transparent electrodes are not suitable for use in flexible electronics because of their brittleness, high cost, and diffusion of impurities within devices. Carbon nanotube (CNT) has shown considerable promise as replacements for ITO-based electrodes, but they fall short in terms of conductivity. To offset this weakness, dopants are used to increase the conductivity by increasing the concentration of free carriers and reducing the resistance. As reported by Lee and colleagues, trifluoromethanesulfonic acid (TFMS) displayed nearly ideal durability when used to dope graphene in organic light emitting diodes.[1] However, TFMS nonetheless does not exhibit permanent durability and has an issue regarding handling safety when used as a dopant in carbon electrodes.

We investigated the use of high molecular weight polymeric dopant (sulfonated tetrafluoroethylene-based fluoropolymer-copolymer sulfonic acid i.e., Nafion®) in transparent conductive CNT films. We expected that entanglement of the CNT network and the long chains of the polymeric acid would stabilise the donated protons, which in turn would provide an exceptionally durable doping effect. The polymeric acid doped CNT films satisfied other key requirements for transparent carbon electrode, including transparency, smooth morphology, and safety of handling. In this work, various analyses were conducted to compare the polymeric acid with the established acid dopants HNO_3 and TFMS. This study showed that the polymeric acid had similar doping effectiveness but superior durability in comparison with the other dopants. This excellent durability came from the low volatility and high stability of the acid and its conjugate base, as demonstrated by a number of analytical techniques and comparison of the doping effects between CNT and graphene. Accordingly, we revealed that the polymeric acid dopant has nearly permanent (1 year) doping durability. Furthermore, organic solar cells (OSCs) were fabricated using the polymeric acid-doped CNT films and a mixture of PBTZT-stat-BDTT and $PC_{71}BM$. The *p*-type polymeric acid-doped CNT-based OSCs initially produced a PCE of 8.0%, which was retained for more than 60 days, while the ITO-based OSCs had an initial PCE of 9.1%, which dropped below 8.0%, because of suspected degradation of ITO by poly(3,4-ethylenedioxythiophene)-poly(styrenesulfonate) (PEDOT:PSS) and metal diffusion. The devices using the polymeric acid dopant were the most durable when compared with the devices using other dopants.

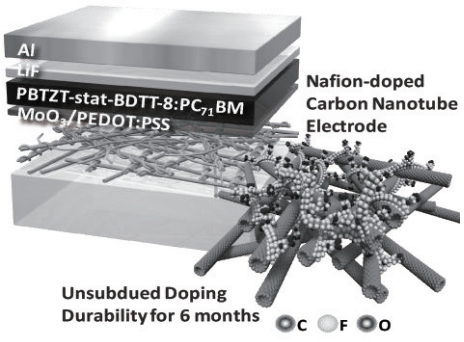

Fig.1 Illustration of Nafion-doped CNT-based organic solar cell.

[1] T.-H. Han *et al*. Angew. Chem. Int. Ed. **55**, 6197 (2016).
Corresponding Author: S. Maruyama
Tel: +81-3-5841-6421, Fax: +81-3-5800-6983,
E-mail: maruyama@photon.t.u-tokyo.ac.jp

Transparent and flexible triboelectric generator based on carbon nanotube

○Masahiro Matsunaga[1], Jun Hirotani[2], Shigeru Kishimoto[2], Yutaka Ohno[2,3]

[1]*Venture Business Laboratory, Nagoya University, Nagoya 464-8603, Japan*
[2]*Department of Electronics, Nagoya University, Nagoya 464-8603, Japan*
[3]*Institute of Materials and Systems for Sustainability, Nagoya University, Nagoya 464-8603, Japan*

A self-powered device which harvests electrical energy from surrounding environment has been required for future society. One of the typical energy sources is mechanical vibration. Several principles such as electromagnetic and piezoelectric effect have been studied for converting the mechanical vibration into electricity. Recently, the triboelectric generators (TG) have attracted much attention for the energy harvesting device due to many advantages such as high output voltage, low cost, and simple structure [1,2]. The TG generates electricity using triboelectrification and electrostatic induction. Here, we report transparent and flexible TG with carbon nanotube (CNT) thin film and Polydimethylpolysiloxane (PDMS).

Figure 1 shows a schematic TG. The TG was fabricated by sandwiching a CNT thin film grown by floating-catalytic chemical vapor deposition with PDMS layers. Cu wire was connected by a silver paste for electrical measurement. To enhance the output performance, the surface of the TG was treated with CF_4 plasma for increasing surface charges. The size of the TG is 5 cm × 5 cm. The fabricated CNT TG is highly transparent and flexible as shown in Fig. 2. The voltage generation was performed by tapping the surface of TG with fingers with a nitrile grove. The output voltage across the external load resistance (R = 10 k ~ 1 GΩ) was measured.

The peak power density (P) at various load resistance from 10 kΩ to 1GΩ was shown in Fig. 3. The maximum P was ~500 mW/m^2 at 300 MΩ. The peak voltage and current density were ~600 V at 1 GΩ and ~2.8 mA/m^2 at 10 kΩ, respectively. These value are much higher than the previous transparent and flexible TG which was fabricated using hydrogel [2]. The generated power was sufficient to drive 30 blue light emitting diodes (LED) as shown in Fig. 4.

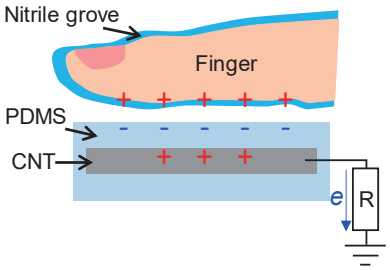

Fig. 1 Schematic CNT TG.

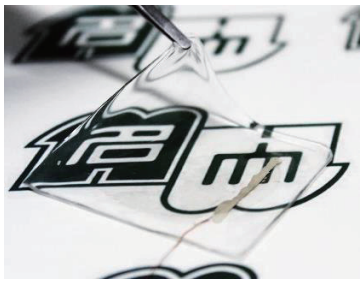

Fig. 2 Photograph of fabricated CNT TG.

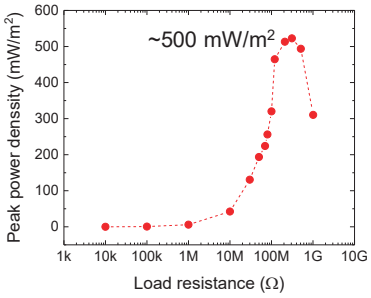

Fig. 3 Peak power density versus load resistance.

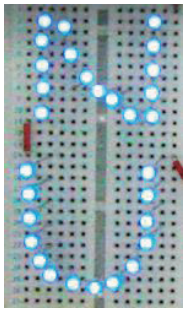

Fig. 4 Photograph of 30 blue LEDs drived by CNT TG.

Acknowledgment: This work was supported by JST/CREST (JPMJCR16Q2).

[1] Z. L. Wang, Mater. Today **20**, 74 (2017). [2] S.-H. Shin *et al*., ACS Nano **9**, 4621 (2015)
[3] X. Pu *et al*., Sci. Adv. **3**, e1700015 (2017).

Corresponding Author: Y. Ohno
Tel & Fax: +81-52-789-5387, E-mail: yohno@nagoya-u.jp

Preparation of MWNT/HDPE Composites *via* Melt Blending

○Atsushi Onodera [1], Masaru Sekido [2]

[1] *Advanced Course of Production System Engineering ,National Institute of Technology, Sendai College, Natori 981-1239, Japan*
[2] *Department of Materials Science and Engineering, National Institute of Technology, Sendai College, Natori 981-1239, Japan*

We have been studying to optimize the conditions to prepare MWNT/Polyethylene(PE) composites by melt blending. Last year we have reported that tensile strength of MWNT/High Density Polyethylene(HDPE), functionalized-MWNT(f-MWNT)/HDPE, MWNT/Low Density Polyethylene(LDPE) and f-MWNT/LDPE composites prepared by melt-blending was not increased with 1/100(MWNT/PE) weight ratio. In this work, we focused on MWNT/HDPE composites and studied various CNT/PE weight ratio to optimize MWNT/HDPE weight ratio to get higher tensile strength than HDPE itself. The influence of functionalization of MWNT was also studied.

f-MWNT were prepared by using 1,3-dipolar cycloaddition reaction. The mixture of MWNT (0.5 g), sarcosine (1.5 g) and 3,4-dihydroxybenzaldehyde (1.5 g) in DMF (250 ml) were refluxed. After 3days DMF was removed by rotary evaporator and remaining powder were washed by water and acetone to obtain f-MWNT (1.9 g). MWNT/HDPE composites were prepared by melt blending at 220 °C, screw speed of 100 rpm and a recycle time of 10 minutes. Weight ratio of MWNT/HDPE were 1/100, 3/100, 5/100 and 10/100. f-MWNT/HDPE composites were also prepared with 1/100 and 3/100 weight ratio. Tensile strength of MWNT/HDPE and f-MWNT/HDPE composites were measured by tension tester (Dak System INC., UTB9052-TT).

The tensile strength of various weight ratio is shown in Fig 1. Tensile strength of 1/100 composites did not increase as expected. While tensile strength of 3/100, 5/100 and 10/100 composites increased about 50%. When using f-MWNT, tensile strength of 1/100 composites did not change while 3/100 composites were increased about 30% compared with HDPE itself. We will discuss the reason why f-MWNT did not increase the tensile strength compared with MWNT.

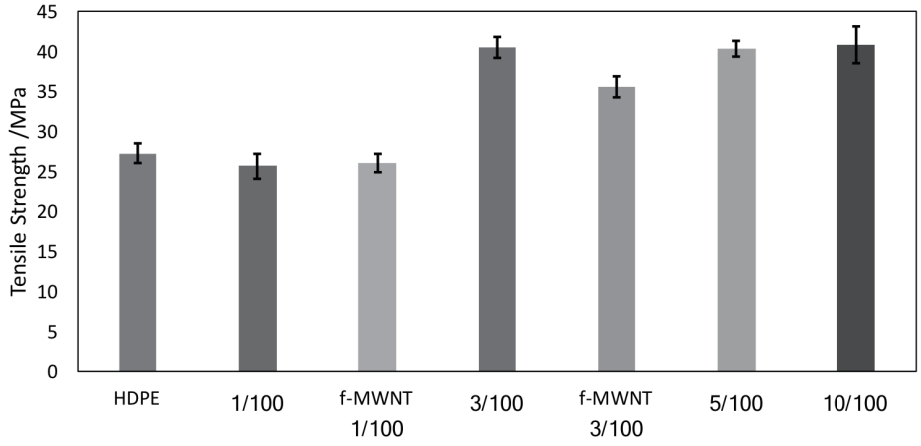

Fig 1. Tensile strength of MWNT/HDPE and f-MWNT/HDPE composites.

Corresponding Author: A. Onodera
Tel: +81-22-381-0329, Fax: +81-22-381-0329
E-mail: a1601008@sendai-nct.jp

In situ XANES investigation of Co and Ni Catalysts during Single-Walled Carbon Nanotube Growth

○Takahiro Maruyama [1], Makoto Kumakura [2], Takahiro Saida [1], Shigeya Naritsuka [2]

[1] *Department of Applied Chemistry, Meijo University, Nagoya 468-8502, Japan*
[2] *Department of Materials Science and Engineering, Meijo University, Nagoya 468-8502, Japan*

In general, 3d transition metals, such as Fe, Co and Ni, are widely used as catalysts for single-walled carbon nanotubes (SWCNTs) growth by chemical vapor deposition (CVD). However, growth mechanism of SWCNTs from these metal catalysts is still unclear. So far, several groups reported *in situ* observations for SWCNT growth using transmission electron microscopy (TEM) [1, 2]. However, TEM can detect only a few catalyst particles, and it is difficult to characterize chemical states of the overall catalyst particles. In this study, we carried out *in situ* X-ray absorption near edge structure (XANES) to investigate the chemical bonding states of Co and Ni catalyst during SWCNT growth.

Using Co and Ni catalysts, SWCNTs were grown on $Al_2O_3/SiO_2/Si$ substrates by alcohol catalytic CVD. The growth temperature and the ethanol pressure were 650 °C and 50 Pa, respectively. During SWCNT growth, Co and Ni K-edge XANES spectra were measured every 7-8 min. In addition, just before and after heating the catalysts at 650 °C, XANES spectra were measured. All XANES measurements were carried out at BL5S1 of Aichi SR (Japan) in the fluorescence mode.

Fig. 1 shows K-edge XANES spectra of Ni catalysts. Before SWCNT growth, Ni catalysts were partially oxidized, but they were reduced during heating and remained metallic during SWCNT growth. On the other hand, some portions of Co catalysts became carbide during SWCNT growth, although they were metallic before the start of growth. Our observation was consistent with previous density functional tight-binding/MD simulation [3].

The XANES measurement was conducted with the support of the Aichi Synchrotron Radiation Center “Project for publishing outcomes for graduate students 2016.” This study was partially supported by the Program for the Strategic Research Foundation at Private Universities supported by MEXT, Japan and Daiko Foundation. Part of this study was conducted at the Institute for Molecular Science (IMS), supported by the “Nanotechnology Platform” of MEXT.

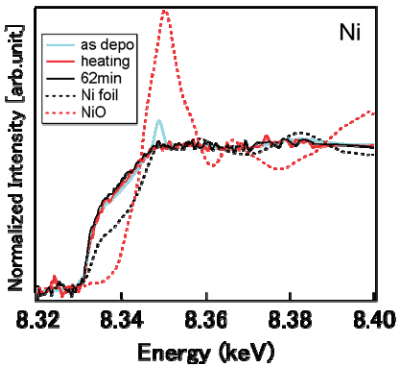

Fig.1 *In situ* Ni K-edge XANES spectra of Ni catalysts during SWCNT growth.

[1] Y. Kohigashi *et al*. Appl. Phys. Lett. **105**, 073108 (2014).
[2] M. Picher *et al*. Nano Lett. **14**, 6104 (2014).
[3] Y. Okamoto *et al*. J. Comp. Theor. Nanosci. **8**, 1755 (2011).

Corresponding Author: T. Maruyama
Tel: +81-52-838-2386, Fax: +81-52-838-1179,
E-mail: takamaru@meijo-u.ac.jp

Repeated CNT synthesis by resetting $CoAl_2O_4$ and $NiAl_2O_4$ catalysts

○Toshihiro Sato[1], Hisashi Sugime[2], Bin Liang[3], Eongyu Yi[3], Richard M. Laine[3], Suguru Noda[1, 4]

[1] Department of Applied Chemistry, School of Advanced Science and Engineering, Waseda University, 3-4-1 Okubo, Shinjuku-ku, Tokyo 169-8555, Japan
[2] Waseda Institute for Advanced Study, Waseda University, 1-6-1 Nishiwaseda, Shijuku-ku, Tokyo 169-8050, Japan
[3]Department of Materials Science and Engineering and the Macromolecular Science and Engineering Center, University of Michigan
[4]Waseda Research Institute for Science and Engineering, Waseda University, Tokyo 169-8555, Japan.

We achieved repeated synthesis of carbon nanotubes (CNTs) by resetting the catalyst nanoparticles (NPs). It is well known that the catalyst NPs get coarsened through Ostwald ripening [1] during chemical vapor deposition (CVD), resulting in CNT growth termination, and no way has been known to reset the coarsened catalyst nanoparticles (NPs). We had Co and Ni NPs segregating out from their spinel films under reducing environment and dissolving in the spinel films under oxidizing environment.

$CoAl_2O_4$ and $NiAl_2O_4$ nanopowders were synthesized by liquid-feed flame spray pyrolysis [2] and sintered in air to yield flexible, dense films (30±10 μm in thickness) without any NPs on surface. The films were then reduced at 1100 ˚C in H_2/Ar, on which NPs were found. Then CNTs were grown by CVD by flowing C_2H_2/H_2/Ar at 1100 ˚C (① in Figures 1 and 2). The oxidation treatment of the CNTs/spinel samples O_2/N_2 at 1100 ˚C yielded the spinel films without CNTs nor NPs (② in Figures 1 and 2). We repeated the reduction-CVD-oxidation treatment for three cycles, and confirmed similar CNT growth on the spinel.

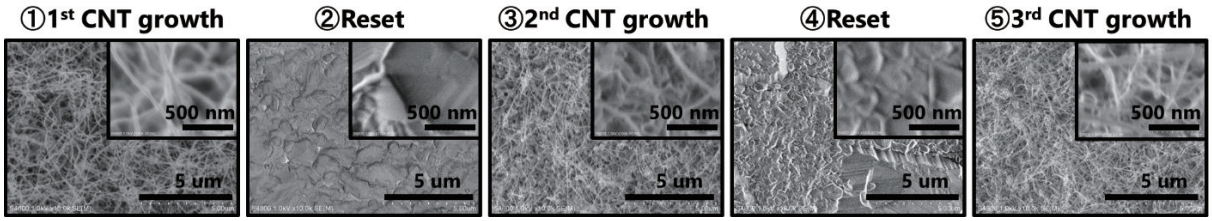

Figure 1. Repeated CNT growth on $NiAl_2O_4$ film

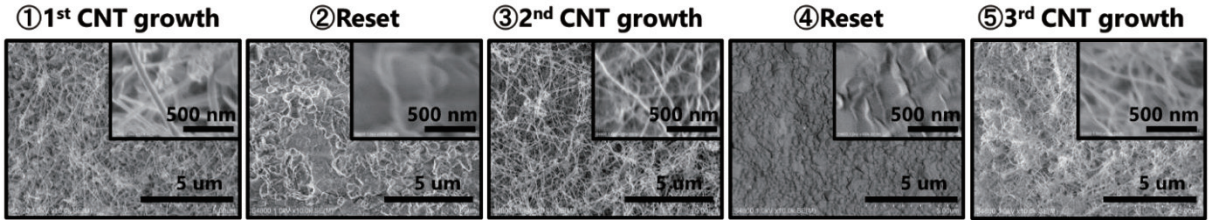

Figure 2. Repeated CNT growth on $CoAl_2O_4$ film

[1] K. Hasegawa, S Noda, *Carbon* **49**, 4497 (2011).
[2] J. Azurdia et al., JACS **89**, 2749 (2006).
Corresponding Author: S. Noda, Tel: 03-5286-2769, E-mail: noda@waseda.jp

1P-18

Controlled Growth of SWNTs Using $CoWO_4$ Nanoparticles as Catalyst Precursor

○ Xu Liu, Feng Yang, Yan Li*

College of Chemistry and Molecular Engineering, Peking University, Beijing 100871 China

Single-walled carbon nanotubes (SWNTs) with special structure and excellent performance are regarded as one of the most promising candidates as building blocks in the next generation electronics. The Controlled synthesis of the structure and properties enriched SWNT samples for large-scale integrated carbon nanotube devices is a great challenge. We have developed a novel tungsten-based intermetallic compound catalyst by using heteropolyacid containing W and Co as a precursor. The catalyst has a high melting point and a lower crystal structure symmetry, acting as a structural template for the growth of carbon nanotubes with specific chirality [1-4]. However, the complex preparation process and the pH sensitivity of the specific composition of tungsten heteropolyacid is not conducive to large-scale production in the future. Therefore, it is important to find a catalyst precursor with simple preparation procedure and good stability.

Recently, we have tried to use uniform $CoWO_4$ nanoparticles, which were prepared in water-in-oil microemulsions, as catalyst precursor. By adjusting the conditions of chemical vapor deposition, we achieved the diameter, conductivity and chirality controlled growth of SWNTs on Si / SiO_2 substrates.

[1] F. Yang, Y. Li *et al*. Nature **510**, 522 (2014).
[2] F. Yang, Y. Li *et al*. Acc. Chem. Res. **49**, 606 (2016).
[3] F. Yang, Y. Li *et al*. J. Am. Chem. Soc. **137**, 8688 (2015).
[4] F. Yang, Y. Li *et al*. ACS Nano, **11**, 186 (2017).

Corresponding Author: Yan Li
Tel: +86-10-6275-6773
E-mail: yanli@pku.edu.cn

Mechanism of preferential synthesis of (6,4) single-walled carbon nanotube using surface state control of Co catalyst

○ Bin Xu[1], Toshiro Kaneko[1], Yasushi Shibuta[2], Toshiaki Kato[1,3]

[1] *Department of Electronic Engineering, Tohoku University, Sendai 980-8579, Japan*
[2] *Department of Materials Engineering, University of Tokyo, Tokyo 113-8656, Japan*
[3] *JST-PRESTO*

Single-walled carbon nanotubes (SWNTs) are promising candidate for high performance optoelectrical devices due to the unique 1-dimension structure. Since the physical properties of SWNTs strongly depend on the chirality, obtaining SWNTs with particular chirality remains as a critical issue in this scientific community. Based on the previous studies, the catalyst size [1], component [2], and crystal structure [3] are proven to be contributed to decide SWNTs chirality. However, effect of catalyst surface state on chirality control is seldom being studied.

In this study, we find out that the catalyst surface state can be very sensitive to nucleate specific type of chirality species and significant change of chirality from (6,5) to (6,4) SWNTs are observed by controlling the surface state of catalyst [4]. The surface state of catalyst is controlled by our newly established catalyst pretreatment process. The annealing of catalyst nanoparticles under the high vacuum condition with slightly adding small amount of reactive gas species can control the oxidation degree of catalyst surface.

To elucidate the mechanism of chirality selective nucleation by changing the surface state of catalyst, systematic investigations have been carried out. The detailed measurements with X-ray absorption fine structure (XAFS) shows about 50 % of oxidized Co catalyst (CoO_x) were reduced by the pretreatment. The activation energy of SWNTs growth near the lower threshold of growth temperature increases with the catalyst pretreatment, which is consistent with the results of first-principle calculations, where the binding energy between cap structure of SWNTs and CoO_x catalyst increase by reducing catalyst surface. Theoretical calculation also reveals that the most preferred chiral angel shift to a smaller chiral angle through the reduction of Co catalyst. This is also in good accordance with the experimental results. Based on these results, it is revealed that the combination of diameter (to small diameter) and chiral angle (to small angle) shift through the change of catalyst surface state can cause the drastic shift of chirality species from (6,5) to (6,4) SWNTs (Fig. 1(a)(b)).

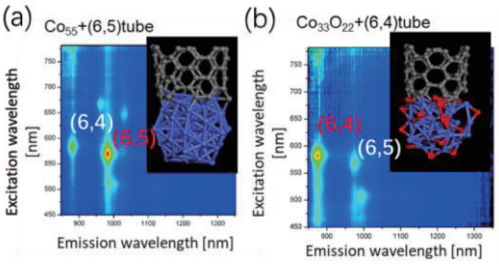

Fig. 1: Photoluminescence-excitation (PLE) map and corresponding first principle calculation model of SWNTs grown from catalyst (a) without and with pretreatment.

[1] M. Picher, E. Anglaret, R. Arenal and V. Jourdain, ACS Nano **5** (2011) 2118.
[2] W.-H. Chiang and R.M. Sankaran, Nat. Mater. **8** (2009) 882.
[3] F. Yang, et al., Nature **510** (2014) 522.
[4] B. Xu, T. Kaneko, Y. Shibuta, and T. Kato, Sci. Rep. **7** (2017) 11149.

Corresponding Author: B. Xu
Tel: +81-22-795-7046, Fax: +81-22-263-9225
E-mail: xu12@ecei.tohoku.ac.jp

Separation of CoMoCAT-SWNTs by utilizing aqueous two immisible solution phase (ATP) technique and Raman/fluorescence spectroscopy

Tatsuki Watase, Tokinaru Matsuoka, ○Shinzo Suzuki,

Department of Physics, Kyoto Sangyo University, Kyoto 603-8555, Japan

In the previous symposium [1], we showed that Raman spectroscopy could have been applied for evaluating the ratio of metal/semiconductive single-wall carbon nanotubes (SWNTs) in aqueous two immiscible solution phase (ATP) technique, especially for those made by using arc-burning technique. This separation technique by using two immiscible solution phases (e.g., in polyethylene glycol (PEG) and dextran (DX) solution) has been first reported by C.Y. Khripin et al. [2], where metal/semiconductive SWNTs of large diameter (> 1.2 nm) were shown to be successfully separated.

In this presentation, we reported about the separation of CoMoCAT-SWNTs utilizing ATP technique combined with Raman spectroscopy, in order to investigate how thinner SWNTs were separated in ATP solution, since the separation mechanism for those thinner nanotubes in ATP solution was considered to be different from the case of SWNTs made by arc-burning technique [2]. Additionally, by using 785nm laser as an excitation wavelength, it was found that some thinner semiconductive nanotubes show fluorescence, indicating that SWNTs are well mono-dispersed in each solution phase [3]. Further experimental findings will be presented and discussed.

References:

[1] K. Uratani et al., *Proc. of the 52nd Fullerene-Nanotube-Graphene General Symposium.* **3P-15**(2017).

[2] C.Y. Khripin et al., *J. Am. Chem. Soc.*, **135**, 6822-6825(2013).

[3] M.S. Strano et al., *J. Nanoscience and Nanotechnology,* **3**, 81-86(2003).

Corresponding Author: Shinzo Suzuki

Tel: +81-75-705-1631, Fax: +81-75-705-1820,

E-mail: suzukish@cc.kyoto-su.ac.jp

Atomistic simulations of formation processes of in-plane heterostructures of h-BN and graphene

○Hisaki Sawahata[1], Ayaka Yamanaka[2], Mina Maruyama [1], Susumu Okada [1]

[1] *Graduate School of Pure and Applied Sciences, University of Tsukuba, Tsukuba 305-8571, Japan*
[2] *Research Organization for Information Science and Technology (RIST), Shinagawa, Tokyo 140-0001, Japan*

In these days, h-BN and graphene have attracted much attention at nanoscience and nanotechnology, because they have unique geometric and electronic properties. Owing to the structural similarity between graphene and h-BN, they can form in-plane heterostructures with a border between them. An experimental work reported that the zigzag edge of graphene prefer B atoms with the formation of BC heterobond rather NC heterobond [1]. Our previous work also corroborated that the BC bond is energetically stable compared with the NC bond. On the other hand, because of the competition between polarity at the border near the zigzag shape and the BC bond energy gain, we also demonstrated that the BC dominant border with the angle of 8 degree is the most stable border structure [2]. However, it is still unclear the microscopic mechanism of preferential formation of the zigzag border with BC bond at the graphene edges.

In the present work, to give a theoretical insight into the energetics of the formation process of the border between graphene and h-BN, we studied the energetics of the graphene with BN adsorbates and the formation energy of the borders under various conditions, using the density functional theory combined with the generalized gradient approximation and the effective screening medium method. Our calculation shows the chemisorption energy of BN to the zigzag graphene edges indicate that the BC bond is energetically stable compared with the NC bond, indicating that BN preferentially growth from zigzag edges of graphene have BC bonds at the border. Furthermore, the preferential formation of BC bond at the border prevents h-BN growth from the armchair portion of graphene. On the other hand, from the h-BN edges under the high vacuum condition, we found that both zigzag borders with NC and BC bonds are generated in terms of their border formation energy. Our calculations indicate that the border shape and structure strongly depend on the formation condition of in-plane heterosheet of graphene and h-BN.

References
[1] E. Maeda *et al*. Appl. Phys. Express. **10**, 055102 (2017).
[2] H.Sawahata *et al*. Abstract of 53rd FNTG general symposium, 3P-24, September (2017).

Corresponding Author: H. Sawahata
E-mail: hsawahata@comas.frsc.tsukuba.ac.jp

Selective Growth of AB-Stacked Bilayer Graphene

○Yuri Terao,[1] Kenji Kawahara,[2] Kenshiro Suenaga,[1] Keisuke Yamamoto,[1]
Hiroshi Nakashima,[1,2] Kosuke Nagashio,[3] Hiroki Hibino,[4] Hiroki Ago[*,1,2]

[1] *Interdisciplinary Graduate School of Engineering Sciences, Kyushu University*
[2] *Global Innovation Center (GIC), Kyushu University*
[3] *Department of Materials Engineering, University of Tokyo*
[4] *School of Science and Technology, Kwansei Gakuin University*

Bilayer graphene (BLG) with AB stacking shows a tunable band gap by a vertical electric field, which promises the applications to semiconductor devices [1]. Although the CVD growth of BLG on Cu catalyst has been reported [2-4], it is still difficult to synthesize large-area BLG due to the self-limiting growth mechanism on Cu surface which generally gives monolayer graphene. Recently, we reported that a Cu-Ni alloy catalyst deposited on sapphire substrate can catalyze the uniform growth of BLG [5]. The added Ni metal increases the carbon solubility in the alloy, increasing the bilayer coverage up to 93% [5]. However, the AB-stacking ratio of the BLG was about 70%, while the remaining 30% was twisted BLG. The twisted BLG can be useful for intercalation [6], but the semiconductor applications require AB-stacked BLG. Here, we present that the AB-stacking ratio can be dramatically improved by controlling the reaction time, reaching to ~100% AB stacking.

BLG was synthesized by ambient pressure CVD using Cu-Ni alloy (Ni 20%) film deposited on c-plane sapphire. We investigated various growth parameters, such as the Ni concentration, temperature, and methane/hydrogen concentrations. Interestingly, the growth time was found to greatly influence the AB/twist ratio. As shown in Figure 1, the AB ratio increased from ~70% to 98% by simply extending the growth time. We speculate that the twisted BLG grains are less stable than AB-stacked BLG, thus the former can be etched during the growth period. As the BLG coverage did not show substantial change, we think that BLG grains are regenerated by carbon atoms supplied from the alloy or vapor. Our finding offers a new strategy to tune the stacking order of BLG for future applications. Transport properties will be also discussed in the Symposium.

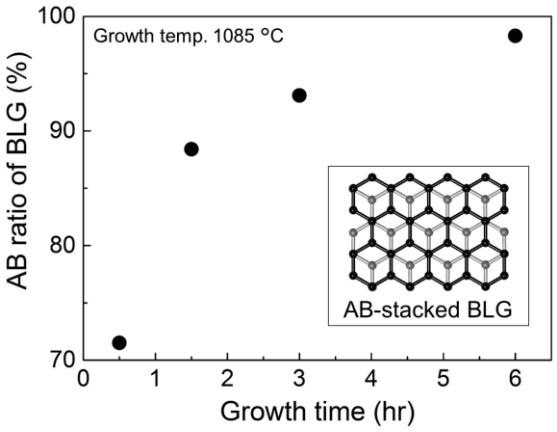

Fig. 1 Effect of growth time on the AB stacking ratio.

[1] Y. Zhang *et al*., *Nature*, **459**, 820 (2009). [2] L. Liu *et al*., *ACS Nano*, **6**, 8241 (2012).
[3] X Chen *et al*., *Carbon*, **107**, 852 (2016). [4] Y. Hao *et al*., *Nat. Nanotech.*, **11**, 426 (2016).
[5] Y. Takesaki *et al*., *Chem. Mater.*, **28**, 4583 (2016). [6] H. Kinoshita *et al*., *Adv. Mater.*, 1702141 (2017).

Corresponding Author: H. Ago (Tel&Fax: +81-92-583-8975, E-mail: h-ago@gic.kyushu-u.ac.jp)

Fabrication of graphene nanoribbon transistors with high on/off ratio using advanced plasma CVD

○Yuta Wato[1], Hiroo Suzuki[1], Toshiro Kaneko[1], and Toshiaki Kato[1,2]

[1]*Department of Electronic Engineering, Tohoku University, Sendai 980-8579, Japan*
[2] *JST-PRESTO*

Graphene nanoribbons (GNR) combine the unique electronic and spin properties of graphene with a transport gap that arises from quantum confinement and edge effects. Although GNR can be made in a variety of ways, the reliable site and alignment control of GNR with high on/off current ratios remains a challenge.

Up to now, we have developed a novel method based on the advanced plasma CVD with nanoscale Ni catalyst (Ni nanobar) for directly fabricating suspended GNR devices [1, 2]. Although this method has outstanding advantages in terms of precise site and alignment controlled growth of suspended GNR, there remain a space to be studied about this method, especially for on/off current ratio. At the current state, GNR grown by Ni nanobar has relatively low on/off ratio (~5). GNR devices with on/off ratio higher than 10^3 are useful for the various semiconductor applications.

In this study, we attempted to improve on/off ratio of field-effect transistor with GNR grown by advanced plasma CVD. It is known that the band gap of GNR is inversely proportional to the width of GNR, indicating narrower GNR can obtain higher on/off ratio. To narrow down the width of GNR, GNR growth was carried out with various kinds of metal nanobars such as Ni, Cu, Fe, Co, and Ge as catalysts. It was found that there is a clear correlation between GNR width and melting point (MP) of nanobars. The nanobars with relatively low MP such as Cu and Ge can grow narrower GNR than that of higher MP materials such as Ni. Based on our previous study about the growth model of GNR, it is found that the nanobar structure becomes liquid phase during plasma CVD [2]. Although the initial width of nanobars was same for all kinds of nanobars, Cu and Ge nanobars may shrink before GNR nucleation due to the relatively low MP, resulting in the growth of narrower width of GNR. The electrical measurement was also carried out for the GNR grown from various kinds of nanobars. The on/off ratio of GNR grown from Ge nanobar (Fig. 1(b)) shows very high on/off ratio (~10^4) at room temperature compared to that of GNR grown from Ni nanobar (Fig. 1(a)). This result shows that GNR grown from Ge nanobar includes higher potential for the future application of GNR for various semiconductor devices.

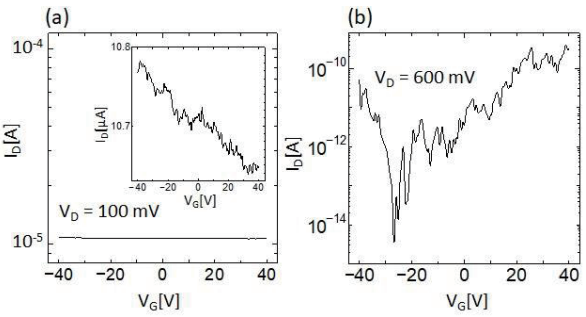

Fig.1 Typical drain-source current (I_D) -gate bias voltage (V_G) curves of GNR devices fabricated with (a) Ni and (b) Ge nanobars.

[1] T. Kato and R. Hatakeyama, Nature Nanotechnology **7**, 651 (2012).

[2] H. Suzuki, T. Kaneko, Y. Shibuta, M. Ohno, Y. Maekawa and T. Kato, Nature Communications **7**, 11797 (2016).

Corresponding Author: Y. Wato

Tel: +81-22-795-7046, E-mail:yuta.wato.s8@dc.tohoku.ac.jp

Energetics of water migration through unstitched grain boundaries of graphene

○Kenta Yasuraoka, Susumu Okada

Graduate School of Pure and Applied Sciences, University of Tsukuba, Tsukuba 305-8571, Japan

Further miniaturization and integration of electronic devices demand us to design the stable and reliable Cu interconnect structures against the oxidization. Atomic-layer materials, such as graphene and boron nitride (h-BN), are possible coating materials for Cu interconnect to prevent their conductivity deterioration by surface oxidization, because of their stiff and flexible covalent network with atom-scale mesh which hinder water migration through the coating sheet. On the other hand, it has been pointed out that graphene and other atomic-layer materials usually possesses grain boundary at which the covalent networks possess structural imperfection, such as topological defects, atomic defects, and unstitched borders. In particular, unstitched grain boundaries severely affect the water migration through the atomic layer materials. Thus, in this work, we aim to give theoretical insight into the energetics of water migration through the unstitched grain boundaries for providing guiding principles for designing the high efficient and stable coating layer structures.

All calculations are conducted using the density functional theory with the local density approximation. To investing the energetics of water migration through the unstitched grain boundary in terms of the overlap length of graphene layers, we consider the structural model in which the unstitched grain boundary is simulated by the partially stacked graphene ribbons (Fig. 1). Water migrations through the boundaries depend on the area of interlayer overlap: For the boundaries without interlayer overlap, water can migrate through the boundary without energy barrier. On the other hand, the barrier for the migration through the boundary increases with increasing the interlayer overlap up to 0.9 eV. The results indicate that graphene with unstitched grain boundaries are not stable and reliable coating materials for Cu interconnect, because water molecules can migration through the boundaries.

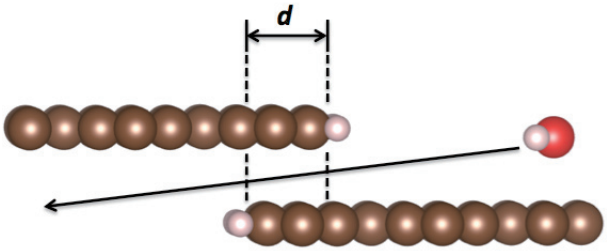

d (A)	0	1.22	2.45	3.66
ΔE (eV)	0.0	-0.5	0.8	0.9

Fig. 1 A structural model of unstitched gram boundary of graphene and migration energies (ΔE) as a function of interlayer overlap (d).

Corresponding Author: K. Yasuraoka and S. Okada
E-mail: soakda@comas.frsc.tsukuba.ac.jp

Computational Simulation of Edge-Roughness Effects on GNR-based FETs

○Kengo Takashima[1], Takahiro Yamamoto[1, 2]

[1] *Department of Engineering, Tokyo University of Science, Tokyo 125-8585, Japan*
[2] *Department of Liberal Arts, Tokyo University of Science, Tokyo 125-8585, Japan*

Graphene is expected to be a channel material of field effect transistors (FETs) because of its high carrier mobility. However, no band gap of the graphene is a serious problem for its FET application. One possible way to overcome the gap-opening problem is to process it in the form of a nanometer width ribbon, referred as graphene nanoribbons (GNRs). They have been successfully applied to FETs with high on-off ratio. Although the resistance of GNR is known to increase dramatically with edge disorder[1][2], the effects of edge roughness on the FET characteristics (e.g., on-off ratio and subthreshold) have not been clarified yet.

In this study, we have investigated the coherent electronic transport in edge-disordered armchair GNR FETs (ED-AGNR-FETs) using the nonequilibrium Green's function method combined with a tight-binding model[3]. In our simulation model, the edge vacancy is modeled by adding or removing pairs of carbon atoms at the edges (Fig. 1). We calculated drain current(I_d) versus gate voltage(V_g) characters of ED-AGNR-FETs by changing the roughness concentration P from 0% to 30% and the ribbon-width from 2.21nm (Fig. 2). We confirmed that average values of device characteristics deteriorated with increasing of P. However, even for P = 30%, some GNR-FETs show that sub-threshold slope values are smaller than 60mv/dec which is the limit value of planer FET as considered here. Furthermore, we investigate optimal position of edge roughness to improve FET characteristics. Details will be discussed at the symposium.

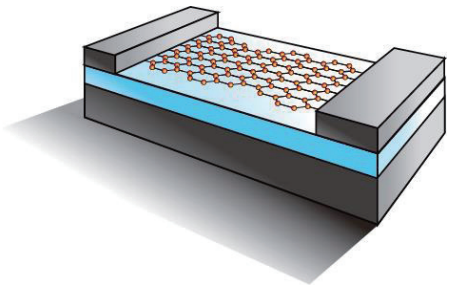

Fig. 1 Edge-disordered AGNR-FET

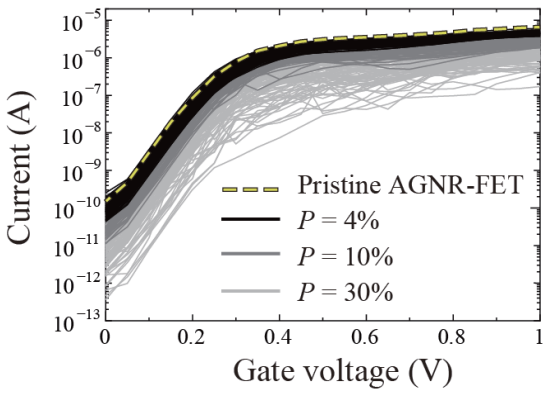

Fig. 2 I_d-V_g curves of edge-disordered AGNR-FETs

References:
[1] K. Takashima and T. Yamamoto, APL., **104**, 093105 (2014).
[2] K. Takashima, S. Konabe and T. Yamamoto, JAP., **119**, 024301 (2016).
[3] P. Koskinen and V. Mäkinen, Computational Materials Science, **47**, 237 (2009)

Corresponding Author: T. Yamamoto
E-mail: takahiro@rs.tus.ac.jp

Synthesis of Novel $IrRuO_x$ / Graphene Catalyst for Oxygen Evolution Reaction

○Masanori Hara, Badam Rajashekar, Hsin-Hui Huang, Masamichi Yoshimura

Toyota Technological Institute, Nagoya 468-8511, Japan

1. Introduction

Recently, environmental issues such as global warming and depletion of fossil fuels have become important topic for progress toward sustainable societies. To utilize renewable energies effectively, conversion of surplus energies to hydrogen via water electrolysis has attracted attention as energy storage method. However, activity, durability, and cost of catalysts are insufficient for practical application in water electrolysis systems due to high over-potential and low kinetics of electrode reactions, especially, oxygen evolution reaction (OER) on the anode [1-3]. In the present study, we have synthesized novel alloy nanoparticle catalysts of iridium oxide (IrO_2) and ruthenium oxide (RuO_2) on the graphene, both of which are active catalysts for OER. The $IrRuO_x$ / graphene catalyst was characterized and evaluated in catalytic activity for OER in sulfuric acid solution.

2. Experimental

The $IrRuO_2$ / graphene (or reduced graphene oxide, rGO) catalyst was synthesized by hydrothermal method. Briefly, required amount of metal complexes, H_2IrCl_6 and $RuCl_3$, and graphene oxide were dispersed in ethanol/water mixture and the mixture was heated at 80 °C for 6 h under constant stirring. Then, the mixture was heated at 150 °C in hydrothermal autoclave for 4 h. The $IrRuO_x$ / rGO catalyst was characterized by TEM, SEM-EDX, XPS, XRD and electrochemical methods (LSV and RDE) in 0.5 M H_2SO_4 solution.

3. Results and discussion

Figure 1 shows a TEM image of the $IrRuO_x$ / rGO catalyst. The $IrRuO_2$ nanoparticles were dispersed on the surface of rGO substrate and an average size of the nanoparticles was 1.5 ~ 5 nm. The wide distribution of the particle size is due to the difference of solubility of the catalyst metal salts. The characterization by SEM-EDX and XPS reveals that the ratio of Ir to Ru is promotional to the ratio of starting materials for the synthesis. The XRD measurement shows the (200) peak of $IrRuO_x$ was shifted to small angle and became broader with increasing Ir ratio of the catalysts. It suggests that nanoparticles of the catalyst form alloy of two metal oxides, RuO_2 and IrO_2. Thus, we successfully prepared the alloy catalysts of IrO_2 and RuO_2 supported on nanocarbon substrate, and can be a promising candidate as anode for water electrolysis.

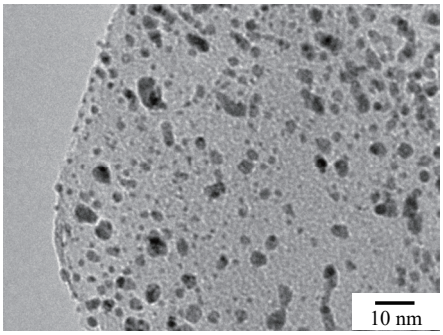

Fig. 1 TEM image of $IrRuO_2$ / rGO.

[1] M. Carmo, D. L. Fritz, J. Mergel, D. Stolten, Int. J. Hydrogen Energy 38 (2013) 4901.
[2] E. Antolini, ACS Catal. 4 (2014) 1426.
[3] J. Cheng, H. Zhang, H. Ma, H. Zhong, Y. Zou, Electrochim. Acta 55 (2010) 1855.

Corresponding Author: M. Hara
Tel: +81-52-809-1850, Fax: +81-52-809-1851,
E-mail: haram@toyota-ti.ac.jp

Ab initio study of double-layered graphene with ethylenic linkage structures

Hiroyuki Yokoi

Department of Materials Science and Engineering, Faculty of Advanced Science and Technology, Kumamoto University, Kumamoto 860-8555, Japan

Graphene has no energy gap, which is unfavorable to the application to semiconductor devices. However, theoretical studies have predicted that modification to the graphene sheet, such as stripping to ribbon or periodic formation of pores could open the energy gap. In addition, the emergence of magnetism related to the formation of a pore or adsorption of a hydrogen atom has been investigated intensively both theoretically and experimentally. These preceding studies suggest that we could create novel graphene-based materials through introducing a variety of modulating substructures to the honeycomb structure. In this study, we propose a novel double-layered graphene interconnected with ethylenic chains, and investigated the electronic states in the framework of ab initio calculations. We chose a hexagonal supercell with 6x6 hexagonal carbon rings. We designed double-layered graphene structures with 1-6 bridges per one supercell, where a carbon atom on the bridge connected with two carbon atoms at the outer sides of six hexagonal rings surrounding the hexagonal ring in the center of the basal plane in the supercell (Fig. 1). Ab initio calculation using the VASP code has revealed that their electronic states depend on the number of bridges dominantly. One of the most remarkable results is that the magnetic moment of $2\mu_B$ per one supercell emerges in the case of the structure with six bridges (Fig. 2). This material might be very interesting as it could be a magnetic atomic-layer material composed with carbon only.

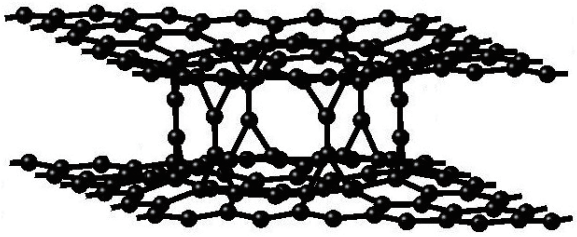

Fig. 1 Optimized structure of double-layered graphene with a six-fold ethylenic linkage structure.

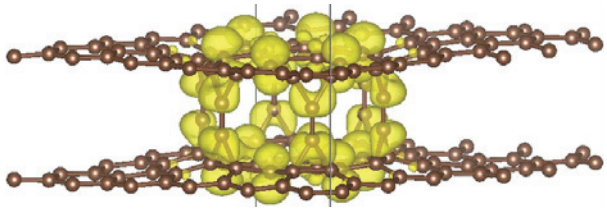

Fig. 2 Differential spin density distribution in the optimized structure of double-layered graphene with a six-fold ethylenic linkage structure.

Corresponding Author: H. Yokoi
Tel: +81-96-342-3727, Fax: +81-96-342-3710,
E-mail: yokoihr@kumamoto-u.ac.jp

Electronic structures of N-doped graphene nanoribbons with H-terminated armchair edges

○ Airi Yasuma, Mina Maruyama, and Susumu Okada

Graduate School of Pure and Applied Sciences, University of Tsukuba, 1-1-1 Tennodai, Tsukuba, Ibaraki 305-8571, Japan

Electronic structures of graphene nanoribbons (GNRs) are known to be sensitive their width and edge atomic arrangement: GNRs with armchair edges (AGNRs) are semiconducting of which band gap asymptotically decreases with increasing their width, while GNRs with zigzag edge (ZGNRs) are magnetic owing to the edge states. In our previous work, substitutional doping of N atoms with pyridinic structure in GNRs does not affect their electronic structure near the Fermi level except the appearance of the fully occupied dangling bond state of edge N atoms [1]. In the cases, N-doped AGNRs (N-AGNRs) and ZGNRs (N-ZGNRs) also possess semiconducting and magnetic electronic structures which are quantitatively the same with those of the pristine GNRs. However, on the other hand, hydrogenation of N atoms was found to modulate the electronic structure of N-AGNRs and N-ZGNRs. Thus, in this work, we aim to give comprehensive knowledge of the electronic structure of H-terminated N-AGNRs, by performing the systematic calculations based on the density functional theory.

Figure 1 shows the electronic structure of H-terminated N-AGNR with the width of N=5 and 30. For the wider N-AGNR, we found degenerated less dispersive states emerge in the energy gap between dispersive bonding and antibonding π states. By checking the squared wave function of the states at Γ and X points, the states are extended throughout the ribbon at Γ point, while they are slightly localized near the edge atomic site and extended along the ribbon direction. We also found that the bandwidth of these less dispersive states gradually decreases with increasing the ribbon width.

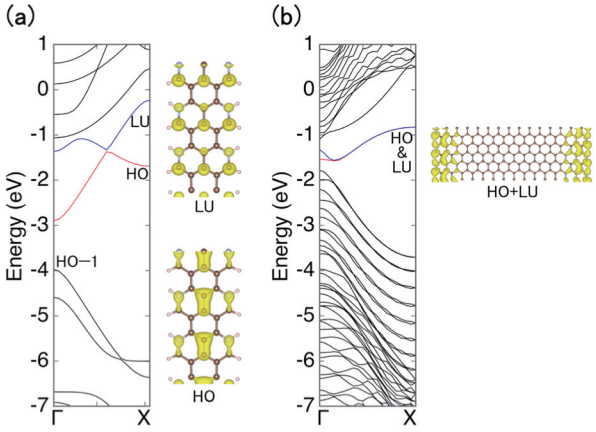

Fig.1 Electronic structures of H-terminated N-AGNR with the widths of (a) N=5 and (b) N=30. The squared wave function of the top of valence and the bottom of conduction bands at X point.

[1] A. Yasuma and S. Okada, Abstract of 53rd FNTG general symposium, 2P-27, September (2017).

Corresponding Author: A. Yasuma (ayasuma@comas.frsc.tsukuba.ac.jp)

Tuning of Kagome bands of 2D hydrocarbon networks by the molecular conformations

Y. Fujii, M. Maruyama, and S. Okada[1]

Graduate School of Pure and Applied Science, University of Tsukuba, 1-1-1 Tennodai, Tsukuba, Ibaraki305-8571, Japan

2D honeycomb networks consisting of oligoacene and fourfold coordinated hydrocarbon atoms possess peculiar electronic structures in their valence and conduction states. Because of the Kagome network of oligoacene connected through sp^3 C atoms, the networks possess the Kagome bands in their valence and conduction states, which consist of a flat dispersion band and a Dirac cone, owing to the substantial wave function overlap between the adjacent oligoacene moieties. The band gap and width were found to depend on the oligoacene length, while the Kagome band near the band edge are robust against the structural modulation. Here, we studied another possible 2D honeycomb network consisting of polyphenylene which are connected via sp^3 hydrocarbon interconnects, using the density functional theory (Fig. 1).

As the case of the networks consisting of oligoacene, the polypenylene networks are also semiconductor with the Kagome bands near the band edge. Furthermore, the network also possesses the Dirac band in the valence states. By rotating the phenyl unit, the Kagome band in the valence band edge shift downward while the Dirac band shift upward, resulting in the substantial electronic structure modulation near the valence band edge (Fig. 2).

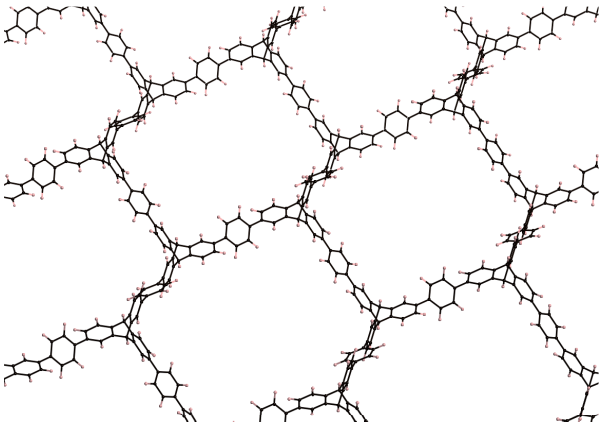

Fig.1 2D honeycomb network consisting of polyphenylene and sp^3 C atom

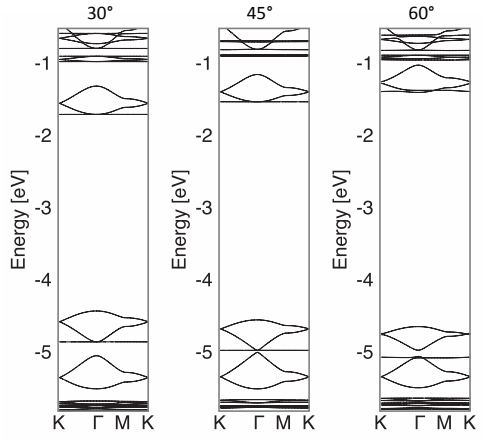

Fig.2 Electronic structure of a 2D network of polyphenylene connected via sp^3 hydrocarbons.

Corresponding author: Y. Fujii and S. Okada (sokada@comas.frsc.tsukuba.ac.jp)

Ultrafast photocarrier relaxation in monolayer graphene on SiC substrate due to phonons in the buffer layer

○Hirotaka Imaeda[1], Takeshi Koyama[1], Hideo Kishida[1], Kenji Kawahara[2], Hiroki Ago[2], Jianfeng Bao[3], Tomoo Terasawa[4], Wataru Norimatsu[5], Michiko Kusunoki[4]

[1] *Department of Applied Physics, Nagoya University, Japan*
[2] *Global Innovation Center, Kyushu University, Japan*
[3] *College of Physics and Electronics Information, Inner Mongolia University for Nationalities, China*
[4] *Institute of Materials and Systems for Sustainability, Nagoya University, Japan*
[5] *Department of Materials Chemistry, Nagoya University, Japan*

Photoexcited carriers (photocarriers) in graphene are cooled with emission of optical phonons via carrier-carrier scattering and carrier-optical phonon scattering [1]. When the temperatures of carriers and optical phonons in graphene become same, carrier cooling slows down because the cooling rate of carriers is limited by that of phonons (it is called hot phonon bottleneck) [2]. Reducing hot phonon bottleneck leads to fast photocarrier relaxation, resulting in enhancement of the properties for optical switches and saturable absorbers with graphene [3,4]. It is expected that photocarrier relaxation in epitaxial graphene becomes faster than that in transferred graphene because of the shorter distance between graphene and the substrate, which will cause faster energy flow to the substrate. In this study, we investigated the photocarrier dynamics in epitaxial and transferred monolayer graphene on a SiC substrate by means of femtosecond time-resolved photoluminescence spectroscopy.

The epitaxial monolayer graphene used in this study was grown on a Si face of a 4*H*-SiC substrate by a thermal decomposition method [5] (hereafter we call this sample epGr/buffer/SiC). The transferred monolayer graphene used in this study was first synthesized by chemical vapor deposition method [6] and then transferred onto a buffer layer on the SiC substrate (hereafter we call this sample trGr/buffer/SiC).

Measured photoluminescence decay in epGr/buffer/SiC at 0.7 eV is faster than that in trGr/buffer/SiC. In other words, photocarrier relaxation in epGr/buffer/SiC is faster than that in trGr/buffer/SiC. It is known that out-of-plane acoustic phonons at the M point in the buffer layer strongly scatter carriers in graphene [7]. The faster relaxation of photocarriers in epGr/buffer/SiC suggests that the interaction between the carriers in graphene and the phonons in the buffer layer for epGr/buffer/SiC is stronger than that for trGr/buffer/SiC, which is presumably caused by a short separation between them.

[1] D. Brida *et al*. Nat. Commun. **4**, 1987 (2013).
[2] L. Huang *et al*. Surf. Sci. **605**, 1657-1661 (2011).
[3] T. Husan *et al*. Adv. Mater. **21**, 3874-3899 (2009).
[4] Q. Bao *et al*. Adv. Funct. Mater. **19**, 3077-3083 (2009).
[5] W. Norimatsu and M. Kusunoki, Phys. Chem. Chem. Phys. **16**, 3501-3511 (2014).
[6] H. Ago *et al.* Appl. Phys. Express **6**, 075101 (2013).
[7] J. Bao et al. Phys. Rev. Lett. **117**, 205501 (2016).
Corresponding Author: T. Koyama
Tel: +81-52-789-4450, Fax: +81-52-789-4450,
E-mail: koyama@nuap.nagoya-u.ac.jp

Mechanism of photoresponse speed improvement on MoS_2-FET by Al_2O_3 buffer layer

○Yuga Miyamoto, Daiki Yoshikawa, Kuniharu Takei, Takayuki Arie, Seiji Akita

Department of Physics and Electronics, Osaka Prefecture University, Sakai 599-8531, Japan

It is known that MoS_2 field effect transistor (FET) using SiO_2 as an insulationg layer shows persistent photocurrent (PPC) resulting in the limitation of photoresponse speed. Recently, we have reported that the photoresponse speed of MoS_2 FET was greatly improved by inserting 2 nm-thick Al_2O_3 buffer layer at the MoS_2/SiO_2 interface.[1] Here, we investigate the mechanism of the improvement of the photoresponse speed.

The Al_2O_3 buffer layer was deposited by atomic layer deposition on n-type Si covered with SiO_2 (300 nm). The MoS_2 channel was prepared by the PDMS stamp method. The device was annealed at 120 °C in vacuum for 12 h to improve the contact resistance.

Figure 1 shows a comparison of the normalized transient photoresponses of I_{DS} under the irradiation of light pulse (623 nm, 860 μW/cm^2) with or without 2 nm-thick Al_2O_3. The decay characteristic can be expressed by $\exp(-(t/\tau)^{\alpha})$, which is explained by the released electrons from traps formed by local potential fluctuations (RLPF) at the SiO_2/MoS_2 interface.[2] The decay time constant τ drastically decreased from 1700 to 0.5 s. Based on the RLPF model, the electrons are well bounded around the positively charged traps and recombined at lower temperature. On the other hand, the bounded electrons are easily released at higher temperature, which results in PPC. This is consistent with the experimental results of the temperature dependence of τ shown in Fig. 2. Figure 3 shows the Al_2O_3 thickness dependence of decay time. The thinner Al_2O_3 enhances the electron trapping and recombination around the positively charged traps as well as low temperature. The thicker Al_2O_3 may prevent the bound of the electrons around positively charged trap, which results in the PPC. Thus, the Al_2O_3 layer controls the extrinsic origin of RLPF and enhances the neutralization process of trapped carrier, which results in the higher photoresponse speed.

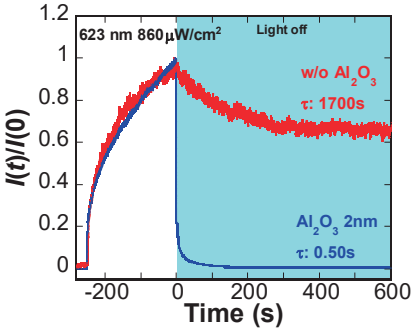

Fig. 1 Photoresponses of MoS_2-FETs with or without Al_2O_3 on SiO_2 gate insulator.

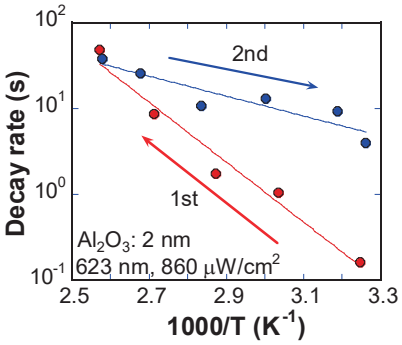

Fig. 2 Temperature dependence of decay rate.

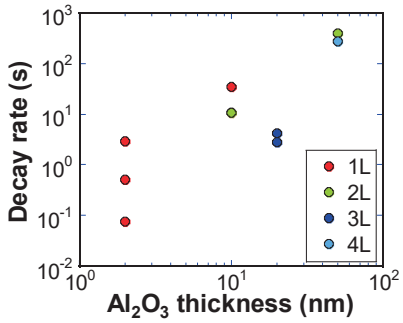

Fig. 3 Al_2O_3 thickness dependence of decay rate of photocurrent.

Acknowledgements This work was partially supported by KAKENHI Grant Number 16H00920, 16K14259, 16H06504 and 17H01040. **Reference** [1] Y. Miyamoto et al., submitted, [2] 1 Y. C. Wu et al., Sci. Rep. **5**, 11472 (2015). **Corresponding Author**: Y. Miyamoto, Tel: +81-72-254- 9261, E-mail: miyamoto-4@pe.osakafu-u.ac.jp

1P-32

Direct TEM/STEM imaging of 2D atomic layer crystals on SiO_2

○Rong Xiang[1], Akihito Kumamoto[2], Yu Kobayashi[3], Yasumitsu Miyata[3], Yuichi Ikuhara[2], Shigeo Maruyama [1, 4]

[1] *Department of Mechanical Engineering,The University of Tokyo, Tokyo 113-8656, Japan*
[2] *Institute of Engineering Innovation, The University of Tokyo, Tokyo 113-8656, Japan*
[3] *Department of Physics, Tokyo Metropolitan University, Hachioji, Tokyo 192-0397, Japan*
[4] *Energy NanoEngineering Laboratory, National Institute of Advanced Industrial Science and Technology (AIST), Tsukuba 305-8564, Japan*

We recently proposed a method of TEM imaging catalyst and single-walled carbon nanotubes (SWNTs) directly on a MEMS fabricated Si/SiO_2 grid. The strength of this method is that high temperature chemical vapor deposition (CVD) growth can be performed on this grid, and therefore SWNTs can be viewed in their original morphology without any post treatment or transfer. More importantly, nano-sized catalytic particles, which were previously difficult to characterize, become visible on SiO_2 film with atomic resolution and in a statistical manner. With this method, we demonstrated that Cu can epitaxially anchore Co in Co-Cu bimetallic system and promote growth of vertically aligned (VA-) SWNT with a sub-nm diameter.[1] Sputtering prepared Co-W catalyst, which produces (12, 6) SWNTs with a selectivity over 70%,[2] were confirmed to be junctions of metallic W and Co_6W_6C.[3] We also employed this method to characterize the zeolite support Fe-Co and on-substrate momo-metallic Co for ultra-low temperature growth of random and VA-SWNT arrays.[4, 5]

In this study, we further extend this method to a new system: 2D materials. Single crystal, triangle-shaped WS_2 flakes are directly synthesized on our Si/SiO_2 grid by metal-organic CVD (MOCVD). This strategy allows a convenient and transfer-free TEM/STEM investigation of WS_2 2D crystals. We confirm that mono- and multi-layer WS_2 can be viewed with an atomic resolution even through the thick SiO_2 film (Fig. 1). As the crystals are kept in an "as-grown" form, we can trace their formation mechanism by viewing the edges and surface of different layers. The atomic structure of the flakes center shows a different stacking order, and suggests a dislocation-induced formation of rhombohedral multilayers. The edge evolution and stability at high temperatures will also be discussed.

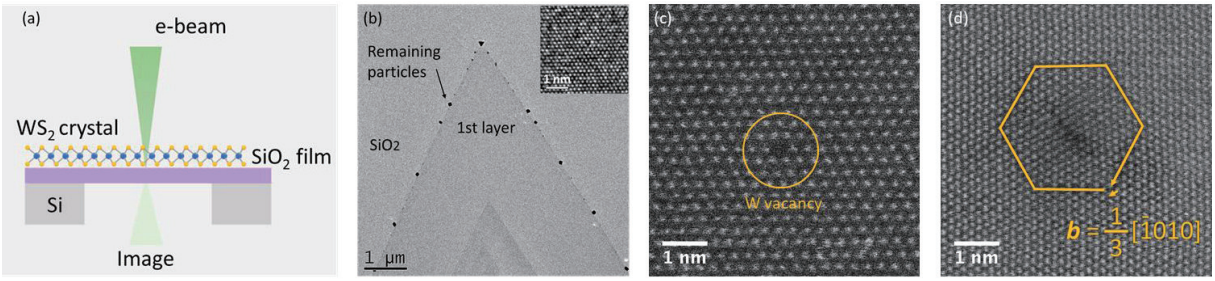

Figure 1 (a) Schematic of experimental setup; (b) (HR)TEM images of mono- and multi-layer WS_2 flakes on SiO_2; STEM image of WS_2 (c) mono-layer region and (d) dislocation at the rhombohedral stacking multi-layer region.

[1] K. Cui *et al*. *Nanoscale*, (2016), 8-3, 1608.
[2] H. An *et al*. *Nanoscale*, (2016), 8, 14523
[3] H. An *et al*. to be submitted (2018).
[4] B. Hou *et al.* Carbon, (2017), 119, 502
[5] M. Liu *et al*. *Phys. Rev. Appl.* (2018)

Corresponding Author: S. Maruyama
Tel: +81-3-5841-6421, Fax: +81-3-5841-6983,
E-mail: maruyama@photon.t.u-tokyo.ac.jp

Two-dimensional van der Walls p-n heterostructures: Two-step CVD growth and transport properties

○Masanori Izumoto,[1] Adha Sukma Aji,[1] Hiroki Ago,[1,2]

[1] *Interdisciplinary Graduate School of Engineering Sciences, Kyushu University*
[2] *Global Innovation Center (GIC), Kyushu University*

Van der Walls (vdW) heterostructures of semiconducting two-dimensional (2D) materials have attracted a great interest, because integration of 2D materials with a wide variety of electronic structures offers new opportunities to realize unique and excellent physical properties. In particular, 2D p-n heterojunctions with band alignment of type II are useful for electric and photonic devices, including p-n diodes, photodetectors, and tunneling field-effect transistors (TFETs) due to their staggered band structure [1-3]. Recently, the vdW heterostructures are fabricated by multiple transfer of exfoliated flakes. However, this process lacks scalability, and the interface can be contaminated with residue introduced during the fabrication processes.

Here, we have synthesized vertically stacked heterostructures of p-type tin sulfide (SnS) and n-type molybdenum disulfide (MoS_2) by two-step CVD method. An optical microscope image shows that square-shaped SnS grains partially overlap with triangular MoS_2 grains on SiO_2 substrate (Fig. 1a). To evaluate the electrical properties of SnS-MoS_2 p-n junctions, we fabricated back-gated FETs with Ni/Au as the electrodes (inset of Fig. 1b). Output curves presented in Fig. 1b show a clear rectifying behavior, confirming the formation of p-n heterojunction. The rectification ratio (ratio of forward and reverse bias current) is about 10^3 without given gate bias (Fig. 3c). We also evaluated the performance of SnS-MoS_2 p-n junction by calculating its ideality factor (n) from Shockley diode equation, $I=I_s(\exp(qV_D/nk_BT)-1)$, where I_s is the saturation current, q is the elementary charge, k_B is Boltzmann's constant, T is the temperature, and V_D is the applied voltage. The ideal factor of our SnS-MoS_2 device was 2.4. The ideal factors reported for 2D p-n junction devices are generally high (n=2.7 and 6.7) due to high-density trap states. However, our value is lower than these values, suggesting cleaner interface obtained by CVD than heterostructures made by exfoliation method [4-6].

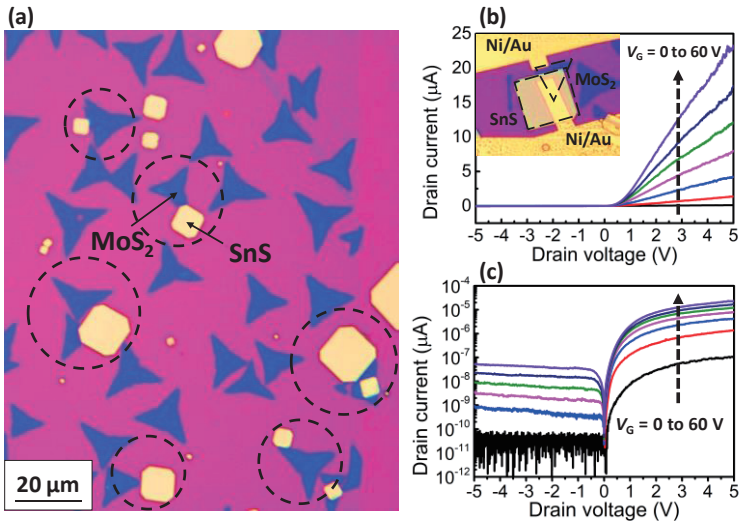

Figure 1. (a) Optical image of SnS-MoS_2 heterostructures. Output curves of SnS-MoS_2 at different gate voltages in (b) linear and (c) semi-log scales. The inset in (b) is an optical image of the SnS-MoS_2 heterostructure device.

[1] C.-H. Lee *et al*., *Nat. Nanotechnol*., **9**, 979 (2014). [2] K. Zhang *et al*., *ACS Nano*, **10**, 3852 (2016). [3] T. Roy *et al*., *Appl. Phys. Lett.*, **108**, 83111 (2016). [4] J-H. Ahn *et al*., *Nano Lett*., **15**, 3703 (2015). [5] Y. Deng *et al*., *ACS Nano*, **8**, 8292 (2014). [6] A. S. Aji *et al*., *Phys. Chem. Chem. Phys*., **20**, 889 (2018).

Corresponding Author: Hiroki Ago
Tel and Fax: +81-92-583-8852
E-mail: h-ago@gic.kyushu-u.ac.jp

Investigation on the influence of ball milling conditions to the morphology of exfoliated hexagonal boron nitride nanosheets

○Naoko Ogino, Gang Liu, Naoki Komatsu
Graduate School of Human and Environmental Studies, Kyoto University, Sakyo-ku, Kyoto 606-8501, Japan

Hexagonal boron nitride (h-BN) nanosheet is known to have a similar 2D structure to graphene and have been attracting extensive interest due to its unique physical and chemical properties. Therefore, the efficient method to produce h-BN nanosheets has been widely investigated.

Recently we reported that bulk molybdenum disulfide (MoS_2) and tungsten disulfide (WS_2) was exfoliated in the presence of sodium cholate through ball milling and resulting powder was readily dispersed in water [1]. Herein, we report the application of this method to the exfoliation of bulk h-BN. In addition, the ball milling conditions were studied thoroughly to control the thickness and size of the exfoliated h-BN nanosheet.

To prepare h-BN nanosheet and its aqueous dispersion, bulk h-BN and sodium cholate were ball milled for 6 hours. The resulting white powder (Fig. 1a) was readily dispersed in water by shaking by hand for a few seconds and the stable dispersions were obtained by centrifugation at 1000 rpm and 3000 rpm (3.78 mg/mL and 1.32 mg/mL, respectively, as shown in Fig. 1b).

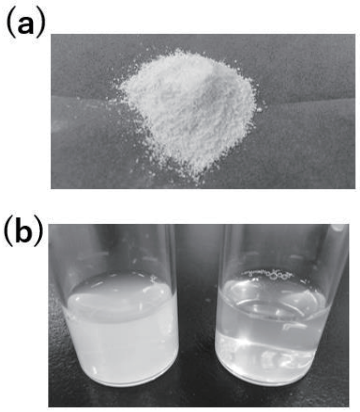

Fig. 1. Photographs of (a) ball-milled h-BN and (b) aqueous dispersion after the centrifugation at 1000 rpm (left) and 3000 rpm (right).

Although h-BN nanosheets were produced through ball milling, the conditions were not optimized. Therefore, we studied the relationship between the ball milling conditions and h-BN nanosheet morphology. In the preliminary experiments, the influence of ball size and milling duration on the size and thickness of h-BN nanosheets was investigated; the bulk h-BN and sodium cholate were ball milled at different durations and by using different ball sizes. After centrifugation of the aqueous dispersion, the resulting whitish supernatant was analyzed by AFM. From the result summarized in Fig. 2, we found that 1) smaller balls grind and exfoliate h-BN at a slower rate, 2) both size and thickness are gradually reduced as the ball milling proceeds, and 3) its size and thickness are maintained, once h-BN nanosheets becomes thin and small enough. We are going to make clear the influence of the other ball milling parameters such as speed, the amount of balls, the amount of starting material on the size and thickness of h-BN nanosheets.

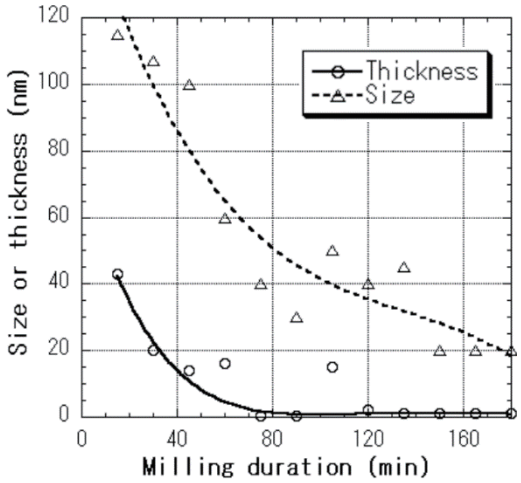

Fig. 2. Chronological change of the thickness and the size of h-BN nanosheets during ball milling.

[1] G. Liu and N. Komatsu, *ChemNanoMat*. **2**, 500 (2016); *ChemPhysChem*, **17**, 1557 (2016).

Corresponding Author: Naoki Komatsu
Tel, Fax: +81-75-753-6833,
Email: komatsu.naoki.7w@kyoto-u.ac.jp

Chemical doping of monolayer MoS_2 by crown ether complex salts

○Shintaro Yoshimura[1], Yu Kobayashi[1], Takahiko Endo[1],
Yutaka Maniwa[1], Yasumitsu Miyata[1]

[1]*Department of Physics, Tokyo Metropolitan University, Hachioji, 192-0397, Japan*

Transition metal dichalcogenide (TMDC) atomic layers have attracted much attention because of their unique two-dimensional structure and high electrical performance. For electronics applications, it is essential to develop a sophisticated way to control carrier density of materials. So far, several reports have used chemical doping through surface charge transfer for carrier control of TMDCs [1, 2]. For further improvement of doping concentration and air stability, it is highly desired to find a stable dopant for TMDCs. Recently, Nonoguchi *et al.* have reported the electron doping for carbon nanotubes by using crown ether complex salts [3]. In this study, we have applied this technique to MoS_2 monolayers (Fig.1a) and have investigated their transport and optical properties.

Monolayer MoS_2 single crystals were grown on SiO_2/Si substrates by using halide assisted chemical vapor deposition method [4]. For transport measurements, Au/Ni electrodes were deposited on the crystals by photolithography (Fig.1b). For the doping, the samples were immersed into methanol solution with 0.1~1 mol/L 15-Crown-5 and sodium chloride (NaCl). We found that the doped MoS_2 field-effect transistors (FETs) keep n-type behavior and have lower resistance compared with undoped samples (Fig.1c). These results suggest the electron doping from crown ether complex salts to monolayer MoS_2. In the presentation, the details of optical and transport properties will be discussed.

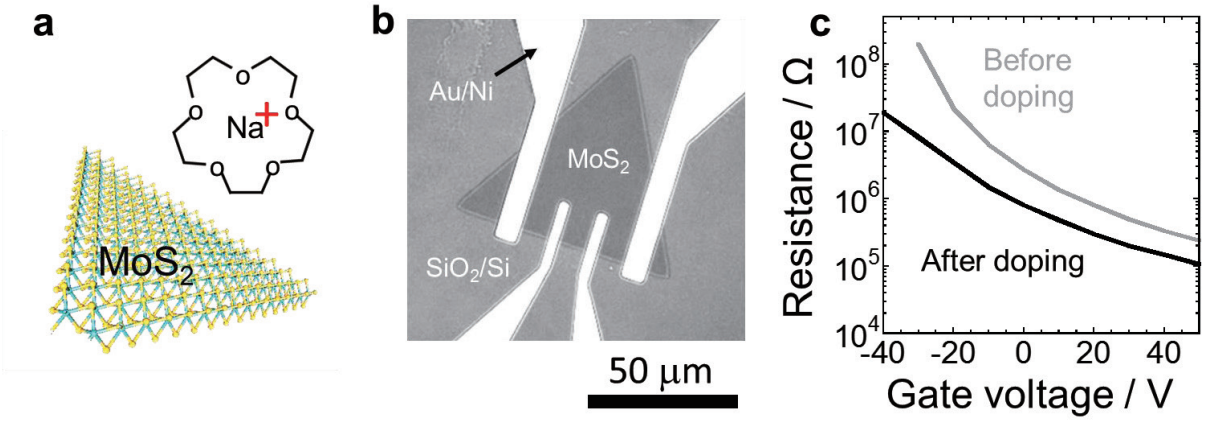

Fig.1 (a) Schematic illustration of monolayer MoS_2 and 15-Crown-5 with Na ion. (b) Optical microscope image of a monolayer MoS_2 FET and (c) Resistance-gate voltage curves of the device before and after the doping.

[1] S. Mouri *et al.*, Nano Lett., **13**, 5944 (2013).
[2] D. Kiriya *et al.*, J. Am. Chem. Soc., **139**, 7853 (2014).
[3] Y. Nonoguchi *et al.*, Adv. Fanct. Mater., **26**, 3021 (2016).
[4] S. Li *et al.*, Appl. Mater. Today, **1**, 60 (2015).
Corresponding Author: Yasumitsu Miyata, Tel: 042-677-2508, E-mail: ymiyata@tmu.ac.jp

In vivo behaviors of oxygen-doped carbon nanotube imaging probes after intravenous administration to mice

○Yoko Iizumi[1], Tsukasa Takeuchi[1,2], Masako Yudasaka[3], Toshiya Okazaki[1]

[1] *CNT-Application Research Center, National Institute of Advanced Industrial Science and Technology (AIST), 1-1-1 Higashi, Tsukuba 305-8565, Japan*
[2] *Shimadzu Corporation, 1-3 Kanda Nishiki-cho Chiyoda Tokyo 101-8448, Japan*
[3] *Nanomaterials Research Institute, National Institute of Advanced Industrial Science and Technology (AIST), 1-1-1 Higashi, Tsukuba 305-8565, Japan*

Because of bright fluorescence and low toxicity, single-walled carbon nanotubes (SWCNTs) are promising candidates as *in vivo* fluorescent imaging probes. Moreover, SWCNTs show fluorescence in long near-infrared (NIR-II) region, which is ideal for biological imaging due to the low tissue auto-fluorescence and low absorption coefficient of water. For a practical use of the CNT probes, the influence on a living body and the *in vivo* kinetics are necessary to be understood.

Recently, we found a very simple and efficient fabrication method of epoxide-type oxygen-doped single walled carbon nanotubes (ep-SWCNTs), in which the SWCNT thin film was exposed to ozone generated by a conventional UV ozone cleaner for a few minutes [1]. *In vivo* imaging of mice was successfully demonstrated using ep-SWCNTs as NIR fluorescent agents [1]. In this study, time-course of NIR fluorescence images of mice were observed for a long period (Figure 1) and the fluorescence intensities of liver and blood were analyzed (Figure 2). Further, the distribution of ep-SWCNT in liver tissue was clarified by Raman mapping measurements. The influence of ep-SWCNT on metabolomics & lipidomics were also analyzed. The details of *in vivo* kinetics of ep-SWCNT in mice body and the performance of the ep-SWCNT as the imaging probes will be discussed in the presentation.

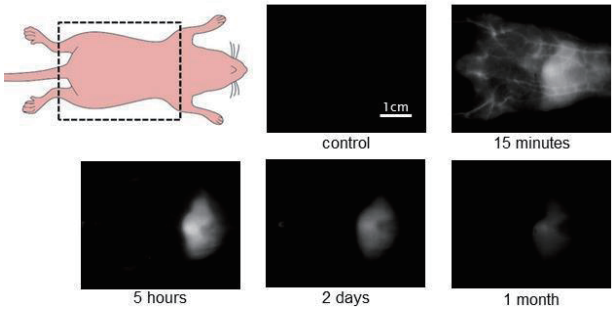

Figure 1. NIR fluorescence images of ep-SWCNT administered mouse, changing with time. Control: No ep-SWCNT injection.

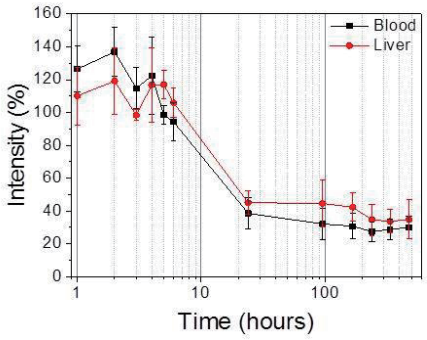

Figure 2. Time-course of the ep-SWCNT fluorescence intensities in blood and liver in mice.

[1] Y. Iizumi, M. Yudasaka, T. Takeuchi, T. Okazaki, The abstract of the 50th Fullerenes-Nanotubes-Graphene General Symposium 2016, #1-10, page 22.

Corresponding Author: Toshiya Okazaki, E-mail: toshi.okazaki@aist.go.jp

Experimental System for Testing Dynamics of Carbon Nanomaterials in Lymphatic Vessels

○Chika Kuroda[1], Kumiko Ajima[2,3], Hisao Haniu[2,4], Haruka Ishida[4], Katsuya Ueda[4], Kaoru Aoki[5], Hiroyuki Kato[1], Naoto Saito[2,4]

[1] *Graduate School of Medicine, Shinshu University, Nagano 390-8621, Japan*
[2] *Institute for Biomedical Sciences, Shinshu University, Nagano 390-8621, Japan*
[3] *The Department of Innovation of Medical and Health Sciences Research, Shinshu University, Nagano 390-8621*
[4] *Graduate School of Science and Technology, Shinshu University, Nagano 390-8621*
[5] *School of Medicine, Shinshu University, Nagano 390-8621*

1. Introduction

Numerous questions exist on the evaluation of *in vivo* dynamics in the development of a drug delivery system (DDS) using carbon nanohorns (CNHs). To investigate the influence of nanoparticles by means of an experimental system closely related to biological tissue, we have devised a novel method employing living lymphatic vessels (LVs) as a passageway for CNHs and other nanoparticles.

2. System

LVs excised from Wistar rats are isolated and then fixed using glass micropipettes mounted in a chamber (Figure). The LV wall monitoring system consists of video microscopy as well as an automatic guiding-type LV diameter measuring device that chronologically records the amplitude of spontaneous contractions. Continuous perfusion of Krebs solution is used for the external environment of the LVs. Inside the vessels, we induce spontaneous contractions using hydrostatic pressure.

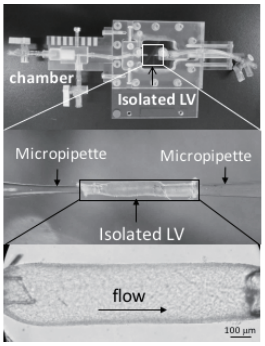

Figure. Isolated lymphatic vessel

3. Procedure

We verified normal functioning of the lymphatic endothelial and smooth muscle cells by adding an acetylcholine and thromboxane A_2 receptor agonist to the Krebs solution and were therefore able to construct a new isolated LV perfusion prototype system that could be used for assessment based on changes in spontaneous contractions. After perfusion, LVs were prepared for sectioning, histological evaluation of constituent cells, and evaluation of adhesion and uptake of nanoparticles by transmission electron microscopy.

4. Experiment

Compared with the perfusion of a dispersant control, it was possible to measure the change in LV diameter during the flow of CNHs and analyze the lymphatic tissue after particle perfusion. This experimental system will enable evaluation of the dynamics and safety of nanoparticles and fine particles considered for use as DDS carriers in LVs and other vessels.

Corresponding Author: N. Saito
Tel: +81-263-37-3547, Fax: +81-263-37-3549, E-mail: saitoko@shinshu-u.ac.jp

Quantification of Single-Walled Carbon Nanotubes in Mouse Feces: Phantom Experiments

○Mitsuko Takahashi[1], Yuko Okamatsu-Ogura[2], Takeshi Tanaka[1], Hiromichi Kataura[1], Masako Yudasaka[1, 3]

[1]*Nanomaterials Research Institute, National Institute of Advanced Industrial Science and Technology (AIST), Tsukuba, 305-8565, Japan*
[2] *Department of Biomedical Sciences, Graduate School of Veterinary Medicine, Hokkaido University, Sapporo 060-0818, Japan*
[3]*Graduate School of Science and Technology, Meijo University, Nagoya 468-8502, Japan*

Single-walled carbon nanotubes (CNTs) administered in mice are reportedly shown to be excreted in feces and urines, where the CNTs in feces and urines are detected by Raman scattering spectroscopy or transmission electron microscopy. These techniques are not suitable for the quantification of the CNTs in feces and urines. In this context, the methods for the CNT quantification in feces and urine should be developed, though it is not easy for the feces as it contains a vast amount of various undigested foods in addition to the CNTs excreted via biliary route. We show in this report a method for the extraction of CNTs from the mice feces, enabling the quantification of CNTs in feces.

Phantom test specimen was prepared by dispersing feces of mice (no CNT administration) in alkaline solution and mixing it with CNTs. From this test specimen, the CNTs were separated and concentrated by the interface precipitation method. In detail, mice feces were immersed in an alkaline detergent (non-phosphoric acid type for removal of oil, fat, protein, hydrocarbon) overnight and bath-sonicated for 3 hours at 25ºC. The feces dispersion solutions (1 mL) was mixed with sodium cholate-CNT aq. dispersion solutions (0.5 mg/mL, 0.01 mL), thus obtained the phantom specimen. For the separation of CNTs from the phantom specimen, 30% KOH solution (1 mL) were added and vigorously mixed and centrifuged. As a result, cotton like floating objects with gray color were obtained at the upper area of the supernatant. The cotton like objects were sucked (ca. 0.5 mL) and mixed with 30% KOH solution (0.5 mL), after that, isopropanol (1 mL) was poured and well mixed. After the centrifugation, the dispersion solution separated in two layers of KOH rich and isopropanol rich ones, and CNTs were precipitated at the interface of the two layers. Finally, the precipitated CNTs were taken out and its optical absorption spectra were measured. The spectra were similar to that of the original one, presenting some peak shifts probably due to the solution pH changes. From the intensity of CNT absorption peaks, the precipitated CNT quantity was estimated, which reasonably agreed with the initial CNT quantity.

Corresponding Author: M. Yudasaka, E-mail: m-yudasaka@aist.go.jp

Understanding Efficiency Enhancement in Solution-Processed C_{60}/C_{70} Mixed Fullerenes Perovskite Solar Cells

○Haosheng Lin [1], Il Jeon [1], Shigeo Maruyama [1], Yutaka Matsuo, [1,2]

[1] *Department of Mechanical Engineering,The University of Tokyo, Tokyo 113-8656, Japan*
[2] *Department of Chemistry, The University of Science and Technology of China, Hefei, Anhui 230026, P. R. China*

Organometal halide perovskite solar cells (PSCs) have emerged as next-generation thin-film solar energy harvesters with high efficiency owing to a long exciton diffusion length, high absorption coefficient and carrier mobility. Fullerenes, which have been used in organic solar cells for more than two decades, opened up a new exciting perspective as an electron transporting layer (ETL) in PSCs. Metal oxides ETLs, such as TiO_2 and SnO_2, have been used in PSCs, but they result in large hysteresis originating from charge accumulation and charge trap. Also, the high temperature process of metal oxide sintering limits flexible applications. These problems can be avoided by using fullerenes as the ETL in PSCs. Their intrinsic low chemical capacitance and high electron affinity realize PSCs with no hysteresis. In addition, the fullerenes are reported to act not only as ETLs but also as a passivation layer, reducing the surface trap density of the perovskite grains. To date, high power conversion efficiency (PCEs) were reported using fullerenes in which they were thermally deposited or over-coated on metal oxide. However, the thermal deposition is a costly process and the over-coating still relies on metal oxide which requires high temperature process. Solution deposition of fullerene is preferred over the thermal evaporation because of its simple and low cost process that allows large-size application. Fullerene derivatives are widely used in organic solar cells due main to the solubility issue. However, high concentration of fullerene solution is not necessary for PSCs, and pristine fullerenes without chemical modification is a better option for the synthesis and purification of fullerene derivatives are difficult and costly. Also, pristine fullerene films possess higher mobility and conductivity than fullerene derivatives, for example [6,6]-phenyl-C_{61}- butyric acid methyl ester (PCBM). Yet, the solution-processed fullerene PSCs do not produce PCEs as high as the thermal-evaporated fullerene PSCs.

In this work, we investigate the reason behind lower performance of the solution-processed fullerene PSCs over the thermal-evaporated fullerene PSCs, and provide an answer to obtaining a higher efficiency using the solution-processed fullerene. Crystalline domains and misaligned packing with remnant solvents are found to be the key difference between those two films. Based on this finding, we suppress the growth of crystalline domains in the solution-processed fullerene ETLs by adding a small amount of C_{70} into a pool of C_{60}, which improved the PSC performance. The mixture of C_{60} and C_{70} (mixed fullerene) film was then dried in vacuum to remove the remaining solvent and enhance the fullerene packing, which further improve the PCE to even exceed that of the thermal-evaporated fullerene PSCs.

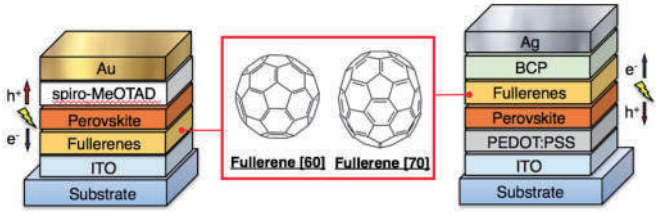

Figure 1. Illustration of our C60/C70 perovskite solar cell.

Corresponding Author: Y. Matsuo
Tel: + 81-3-5841-0978,
E-mail: matsuo@photon.t.u-tokyo.ac.jp

Preparation of [C_{60}]fullerene nanowhisker-cadmium sulfide nanoparticle composites and their photocatalytic activity for degradation of Rhodamine B

○Jeong Won Ko [1], Weon Bae Ko [1,2]

[1] *Department of Convergence Science, Graduate School, Sahmyook University, Seoul 139-742, South Korea*

[2] *Department of Chemistry, Sahmyook University, Seoul 139-742, South Korea*

Cadmium sulfide(CdS) nanoparticles were synthesized by cadmium sulfate($CdSO_4$), sodium hydroxide(NaOH), and sodium sulfide(Na_2S) dissolved into distilled water, and the resulting solution was refluxed for 5 h. The precipitate was collected by centrifugation and was dried at 100 ℃ for 12 h to obtain solid state CdS nanoparticles. The CdS nanoparticles solution was prepared by dissolving powdered CdS nanoparticles in an aqueous solution with surfactant of polysorbate 20(Tween 20). [C_{60}]Fullerene nanowhisker-CdS nanoparticle composites were prepared by liquid-liquid interfacial precipitation(LLIP) method using C_{60}-saturated toluene, the CdS nanoparticles solution and isopropyl alcohol. The product of [C_{60}]fullerene nanowhisker-CdS nanoparticle composites was characterized by X-ray diffraction, scanning electron microscopy, Raman spectroscopy, and transmission electron microscopy. Photocatalytic activity of [C_{60}]fullerene nanowhisker-CdS nanoparticle composites through degradation of Rhodamine B was confirmed by UV-vis spectroscopy.

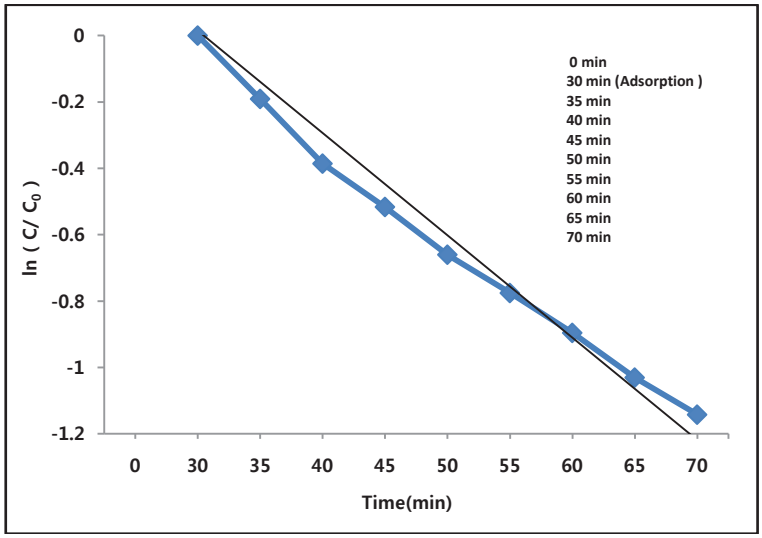

Fig.1 Kinetics study for Rhodamine B degradation with [C_{60}]fullerene nanowhisker- CdS nanoparticle composites at 254 nm.

[1] K. Miyazawa, J. Nanosci. Nanotechnol. **9**, 41 (2009).

[2] Q. Y. Liu *et al*. Bull. Mater. Sci. **40** (7), 1329 (2017).

Corresponding Author: W. B. Ko

Tel: +82-2-3399-1700, Fax:, +82-2-979-5318,

E-mail: kowb@syu.ac.kr

Search for Missing $Lu_2@C_{80}(I_h)$

○Ryoya Takai, Koichi Kikuchi, Yohji Achiba, Takeshi Kodama

Department of Chemistry, Tokyo Metropolitan University, Tokyo 192-0397, Japan

In the previous symposium, Nakatori et al. reported the separation of novel Lu-metallofullerenes, Lu_2C_{78} and Lu_2C_{80}, as an anion form[1]. $(Lu_2C_{78})^-$ was isolated, but $(Lu_2C_{80})^-$ was obtained as a mixture of $(Lu_2C_{78})^-$. Because the UV-vis-NIR absorption spectrum of $(Lu_2C_{78})^-$ is very similar to those of $(M_2@C_{78}(D_{3h}))^-$ (M=Y, Ce, etc.), it was found that $(Lu_2C_{78})^-$ is $(Lu_2@C_{78}(D_{3h}))^-$. For a mixture of $(Lu_2C_{80})^-$, and $(Lu_2C_{78})^-$, its UV-vis-NIR absorption spectrum is also very similar to those of $(M_2@C_{78}(D_{3h}))^-$ (M=Y, Ce, etc.), then it was suggested that the structure of $(Lu_2C_{80})^-$ is a carbide type: $(Lu_2C_2@C_{78}(D_{3h}))^-$, that is, $(Lu_2@C_{80}(I_h))^-$ was not found. In this work, we reexamined the separation procedure and tried to find $(Lu_2@C_{80}(I_h))^-$.

Lu-metallofullerenes were produced and extracted by an almost identical method previously reported[1]. They were extracted as an anion form, and the separation of obtained anions was accomplished by the multistage ion-pair chromatography (IPC). The IPC chromatogram at the first stage is shown in Fig.1. The fractions A and B contain $(Lu_2C_{80})^-$ and $(Lu_2C_{78})^-$, respectively. By the successive two-stage IPC, $(Lu_2C_{80})^-$ was almost isolated. The isolation was confirmed by LD-TOF-MS. As shown in Fig. 2, the UV-vis-NIR absorption spectrum of $(Lu_2C_{80})^-$ is featureless and different from those of $(Lu_2@C_{78}(D_{3h}))^-$ and $(Ce_2@C_{80}(I_h))^-$. Therefore, the cage structure of $(Lu_2C_{80})^-$ could not be determined. Moreover there is a possibility that $(Lu_2C_{80})^-$ obtained here differs from previously reported one. In addition, the ESR spectrum of $(Lu_2C_{80})^-$ was measured at low temperature, but only the broad signal was obtained.

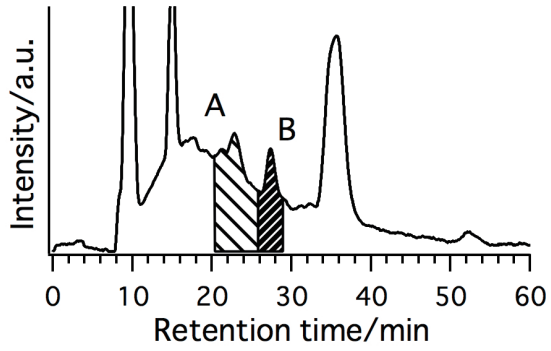

Fig. 1 IPC chromatogram at the first stage.

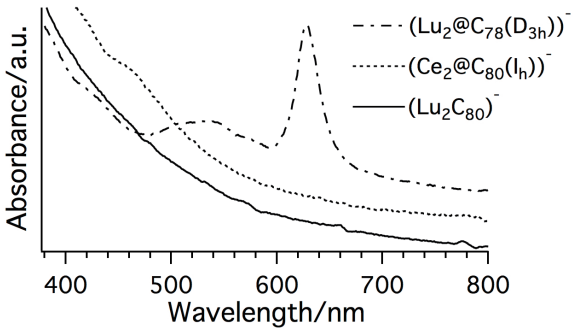

Fig. 2 UV-vis-NIR absorption spectra of $(Lu_2@C_{78}(D_{3h}))^-$, $(Ce_2@C_{80}(I_h))^-$ and $(Lu_2C_{80})^-$.

[1] N. Nakatori, et al. *The 52nd Fullerenes-Nanotubes-Graphene General Symposium* 27 (2017).

Corresponding Author: Takeshi Kodama

Tell: +81-42-677-2530, Fax: +81-42-677-2525

E-mail: kodama-takeshi@tmu.ac.jp

Chemical Reduction of Lithium-Ion-Encapsulated Fullerene to Li@C_{60}

○Hiroshi Okada,[1] Hiroshi Ueno,[2] Yasuhiro Takabayashi,[3] Takeshi Nakagawa,[3] Martina Vrankic,[3] Shinobu Aoyagi,[4] Ken Kokubo,[5] Kimio Akiyama,[6] Ioannis Arvanitidis,[3,7] Kosmas Prassides,[3] Yutaka Matsuo[1,2,8]

[1]*Department of Mechanical Engineering, School of Engineering, The University of Tokyo, Tokyo 113-8656, Japan.* [2]*Department of Chemistry, Northeast Normal University, Changchun, Jilin 130024, China.* [3]*Advanced Institute for Materials Research (AIMR), Tohoku University, Miyagi 980-8577, Japan.* [4]*Dapartment of Information and Basic Science, Nagoya City University, Nagoya 467-8501, Japan.* [5]*Division of Applied Chemistry, Graduate School of Engineering, Osaka University, Osaka 565-0871, Japan.* [6]*Institute of Multidisciplinary Research for Advanced Materials, Tohoku University, Miyagi 980-8577, Japan.* [7] *Department of Physics, Aristotle University of Thessaloniki, 54124 Thessaloniki, Greece.* [8]*University of Science and Technology of China, Hefei, Anhui 230026, China.*

Alkaline metal doping of C_{60} has been attracted much attention for its radical behavior,[1] super conductivity,[2] and chemical reactivities.[3] Neutral Li endohedral fullerene (Li@C_{60} ≡ $Li^+@C_{60}^{\cdot-}$) is, so to speak, ultimate 1 to 1 doping of C_{60}.

We have reported synthesis and isolation of Li@C_{60} by electrochemical reduction of lithium-ion-encapsulated fullerene $Li^+@C_{60}$ previously.[4] Its productivity was low (0.5–1 mg / 2–3 days) to investigate further research.

For more productive method to synthesize Li@C_{60}, chemical reduction was undertaken. The reaction of $[Li^+@C_{60}]TFSI^-$ and decamethylferrocene $FeCp^*_2$ in dichloromethane gave brown precipitate. A solution of the solid in *o*-dichlorobenzene showed NIR absorption peak corresponding to Li@C_{60}. XRD pattern for the solid indicated similarity with azafullerene dimer $(C_{59}N)_2$,[5] which suggests the formation of $(Li@C_{60})_2$ dimer in the solid state. In this presentation, comparison with Li@C_{60} obtained from electrochemical reduction and ESR data will be discussed.

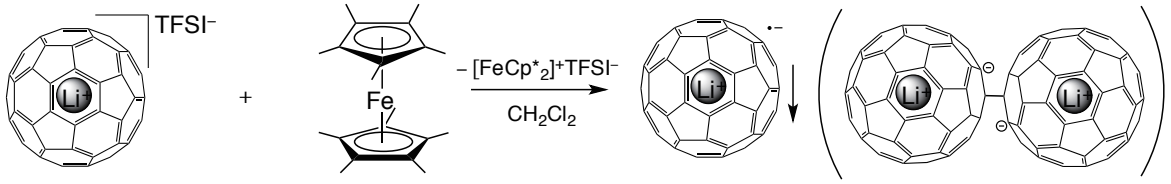

References

[1] P. Rapta *et al.*, *ChemPhysChem* **2002**, *3*, 351–356.

[2] P. W. Stephens *et al.*, *Nature* **1991**, *351*, 632–634.

[3] C. Caron *et al*., *J. Am. Chem. Soc.* **1993**, *115*, 8505–8506.

[4] H. Ueno *et al.*, *Chem. Sci.* **2016**, *7*, 5770–5774.

[5] K. Prassides *et al.*, *Chem. Mater.* **1996**, *8*, 2405–2408.

Corresponding Author: Y. Matsuo, Tel: +81-3-5841-0978, E-mail: matsuo@photon.t.u-tokyo.ac.jp

Thermoelectric Properties of Aligned Single-Wall Carbon Nanotube Films

○Kengo Fukuhara[1], Yota Ichinose[1], Yohei Yomogida[1], Weilu Gao[2],
Junichiro Kono[2], Kazuhiro Yanagi[1]

[1] *Department of Physics, Tokyo Metropolitan University, Tokyo 192-0397, Japan*
[2] *Department of Electrical and Computer Engineering, Rice University, Texas 77005, USA*

Since the seminal study by Hicks and Dresselhaus [1], it has been of great importance to experimentally clarify how the dimensionality of a material influences its thermoelectric properties and whether reduced dimensionality can enhance thermoelectric performance. Single-wall carbon nanotubes (SWCNTs) are one-dimensional materials with sharp van Hove singularities, and their thermoelectric properties have been intensively studied. However, we still do not understand the relationships between thermoelectric performance, current, and thermal flow directions with respect to the tube axis. For example, electrical conductivity along the axis is evidently higher than that in the perpendicular direction, but it is not clear whether thermoelectric performance in the parallel direction should be higher than that in the perpendicular direction. Since thermoelectric properties are strongly dependent on the location of the Fermi level [2], it is crucial to evaluate thermoelectric properties in particular current and thermal flow directions as a function of Fermi level in order to correctly answer the above question.

In this study, as a first step, we investigated Seebeck coefficients and electrical conductivities of aligned SWCNT films as a function of Fermi level using electrolyte gating techniques. We fabricated large-area films of aligned SWCNTs, a mixture of metallic and semiconducting types, using the slow filtration method reported by He *et al*. [3]. Then we investigated how the thermoelectric properties are influenced by current and thermal flow directions as a function of Fermi level.

We found that, although the electrical conductivity in the direction parallel to the tube axis is higher than that in the perpendicular direction, there is no significant difference in their Seebeck coefficients between the parallel and perpendicular directions. This fact indicates a unique an-isotropy of thermoelectric properties in aligned SWCNT films.

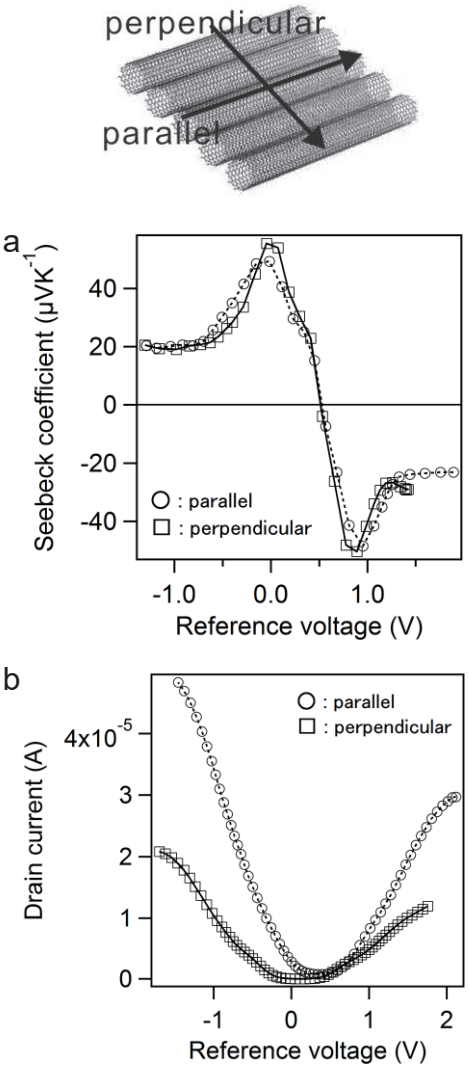

Figure 1. Difference of (a) Seebeck coefficient and (b) electrical current between parallel and perpendicular directions along the tube axis as a function of shift of the gate voltage.

References: [1] Hicks & Dresselhaus, PRB **47**, 16631 (1993) [2] Yanagi *et al*., Nano Lett. **14**, 6437 (2014)
[3] He *et al*., Nat. Nanotechnol. **11**, 1 (2016)
Corresponding Author: K. Yanagi, Tel: +81-42-677-2493,
E-mail: yanagi-kazuhiro@tmu.ac.jp

THz high harmonic generation from single wall carbon nanotubes

○Hiroyuki Nishidome [1], Kohei Nagai [2], Yota Ichinose [1], Kengo Fukuhara [1], Junji Nozaki [1], Junko Eda [1], Yohei Yomogida [1], Kazuhiro Yanagi [1], Koichiro Tanaka [2, 3]

[1] *Department of Physics, Tokyo Metropolitan University, Tokyo 192-0397, Japan*
[2] *Department of Physics, Kyoto University, Kyoto 606-8502, Japan*
[3] *Institute for Integrated Cell-Material Sciences, Kyoto University, Kyoto 606-8501, Japan*

Recent advancement of high power laser source in mid-infrared and terahertz (THz) region enables us to investigate the extreme nonlinear optics in solids where the ground state of solid becomes unstable due to strong light-matter interactions [1]. One of the unique phenomena in the extreme nonlinear optics is high-harmonic generation (HHG). HHG has been intensively studied in atomic gases, but observation of HHG phenomena in solid has long been difficult because of unavoidable damage on samples by extremely strong laser light. But since observation of HHG from ZnO [2] using THz light, HHG by intense THz light has been observed in various kinds of materials such as semiconductor crystals and two dimensional materials (graphene [3], MoS_2 [4], etc.). Physical background of HHG in solid is supposed to be fundamentally different from that in atomic gases, however, the essential feature of HHG has still been elusive because of the presence of various physical parameters in solids affecting nonlinear processes.

To tackle with this problem, we try to investigate HHG of single wall carbon nanotubes (SWCNTs) for the following reasons. SWCNTs have unique one-dimensional structure, and are mechanically and chemically very stable for strong THz light, and we can systematically change electronic structure of SWCNTs from gap-less metallic to semiconductor with different band-gap. Therefore, we assumed we can clarify how the electronic structure of SWCNTs influences HHG.

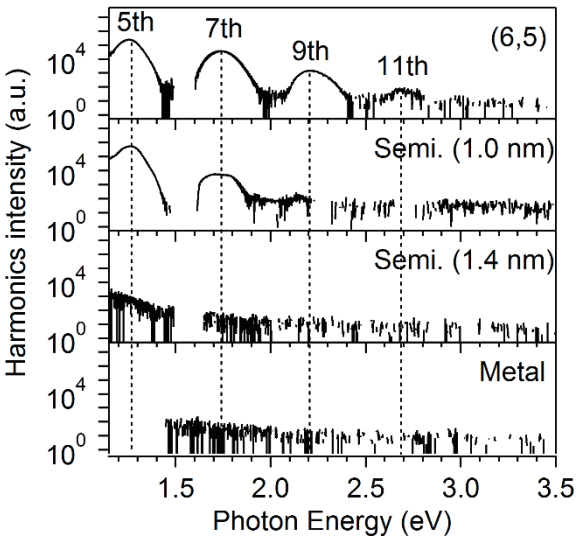

Fig.1 HHG spectra from a series of SWCNTs with different electronic structure by using 4800 nm (≈ 60 THz) laser.

We prepared SWCNT thin films with a systematically different electronic structures, and investigated HHG using 60 THz laser. The type of SWCNTs is metal, semiconductor (diameter is 1.4nm), semiconductor (diameter is 1.0nm), and single-chirality (6,5). The results are shown in Figure 1. We observed HHG from (6,5) and semi. (1.0 nm), and slight 5th HHG from semi. (1.4 nm), but didn't find any HHG from metal. These results indicate that electronic structure of samples strongly influences on HHG. In this poster, the physical background of HHG from SWCNTs will be discussed.

[1] K. Tanaka, Hikaribussei kenkyukai tutorial (2017)
[2] S. Ghimire *et al.,* Nature Physics, 7, 138 (2010)
[3] N. Yoshikawa *et al.*, Science **356**, 736 (2017)
[4] H. Liu *et al.,* Nature Physics, 13, 262 (2016)

Corresponding Author: K. Yanagi, Tel: +81-42-677-2494, E-mail: yanagi-kazuhiro@tmu.ac.jp

Growth of Individually-Suspended Single-Walled Carbon Nanotubes toward Thermal Conductivity Measurement and Manipulation

○Takumi Inaba[1, 2], Ryuunosuke Shima[1, 2], Maki Shimizu[1, 2],
Tomohiro Yamaguchi[2], Koji Ishibashi[2], Yoshikazu Homma[1]

[1] *Department of Physics, Tokyo University of Science, Tokyo162-8601, Japan*
[2] *Advanced Research Laboratory, RIKEN, Saitama 351-0198, Japan*

Thermal management of integrated devices becomes more and more important as the Joule heating per unit area increases. Single-walled carbon nanotubes (SWCNTs) attracted great interest in the field of thermo-mechanics possibly owing to their high thermal-conductivity or one-dimensional unique structure.

In this presentation, the fabrication procedure of ultra-clean and individually-suspended SWCNTs with electrode contacts, which is applicable to the thermal-conductivity measurement of individual SWCNTs,[1] will be introduced. Chirality assignment of such samples can be achieved by photoluminescence measurement for the suspended segment. Left and right images of Fig. 1 show typical scanning electron and atomic force microscopy (AFM) images of such samples, respectively. Cross sectional drawing is shown in the bottom of the right image. Two SWCNTs grown laterally and suspended on platinum electrodes and the trench can be clearly observed in both images.

The observation of SWCNTs using AFM were successfully achieved on a trench with the width below 500 nm. Availability of AFM for those samples enables us to dynamically control the physical properties of SWCNTs via van der Waals force exerts between suspended SWCNTs and AFM tip. Some experimental studies have already shown that the electronic conductivity of suspended carbon nanotubes decrease when the suspended region is pulled down by AFM tip,[2] while the thermal conductivity of those does not.[3] Robust thermal conductivity of SWCNTs under bending was also theoretically predicted.[4] However, no studies examined experimentally how the electronic and thermal conductivity of an individually suspended SWCNT changes when the SWCNT is touched by AFM.

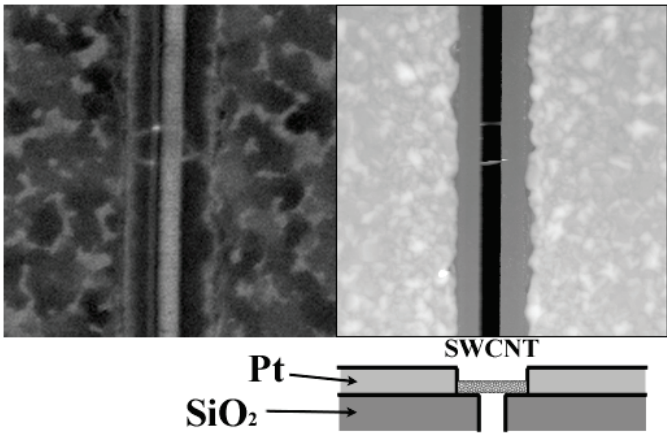

Fig. 1 (Left) Scanning electron microscopy image and (Right) atomic force microscopy image of two individually-suspended SWCNTs. Scanned areas of two images are the same and 5×5 μm. The schematics shown in the bottom is the cross sectional image of scanned areas.

[1] E. Pop, *et al.*, *Nano Lett.* **6**, 96 (2006)
[2] E. D. Minot, *et al.*, *Phys. Rev. Lett.* **90**, 156401 (2003)
[3] C. W. Chang, *et al.*, *Appl. Phys. Lett.* **99**, 045901 (2007)
[4] F. Nishimura, *et al.*, *Appl. Phys. Exp.* **2**, 035003 (2009)

Corresponding Author: T. Inaba
E-mail: takumi.inaba.63@rs.tus.ac.jp

Voltage generation by electrolyte droplet on carbon nanotube thin film: Dependence of output power on carrier density

°Ryohei Nishi[1], Shigeru Kishimoto[1], Jun Hirotani[1], Hiromichi Kataura[2], and Yutaka Ohno[1,3]

[1]*Department of Electronics, Nagoya University*
[2]*National Institute of Advanced Industrial Science and Technology*
[3]*Institute of Materials and Systems for Sustainability, Nagoya University*

Recently, it has been reported that the voltage generation is caused by the movement of the electrolyte in contact with graphene or carbon nanotube (CNT) thin film [1-3]. These reports show that it is possible to harvest electric energy from a small flow in the environment. Previously, we have reported that the output power was enhanced by increasing the sheet resistance of the CNT film on the basis of the equivalent circuit analysis. In this work, we have further increased the output power by changing the carrier density of the CNT thin film by the field effect.

We used semiconducting CNTs separated by gelchromatography [5]. Semiconducting CNTs dispersed in the surfactant solution were collected on a membrane filter by suction filtration, and transferred on a Si/SiO_2 substrate. Ag-paste electrodes were formed at both ends of a rectangular (30 mm x 5 mm) CNT thin film. The sheet resistance of the CNT thin film was 111.5 kΩ/sq. As shown in Fig. 1, a droplet of NaCl aqueous solution (0.01 mol/l) was reciprocated on the CNT film at 10 cm/s. The generated open-circuit voltage and short-circuit current were measured by a semiconductor device parameter analyzer (Agilent, B1500A). The carrier density of the CNT thin film was changed by applying a voltage to the substrate which was used as the back-gate electrode.

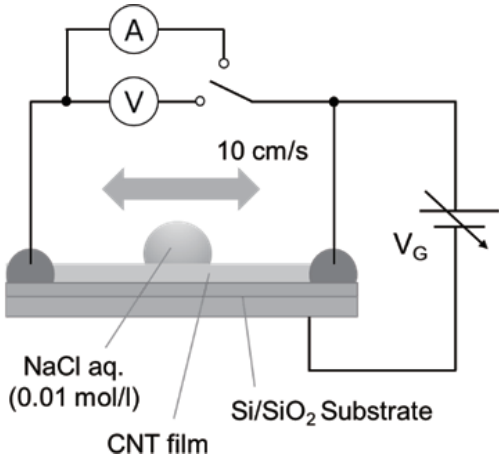

Fig. 1 Experimental setup.

Figure 2 shows the gate voltage dependence of the output power. As the gate voltage increased, the output power increased. This suggests a possibility of an enhancement of output power by controlling carrier density.

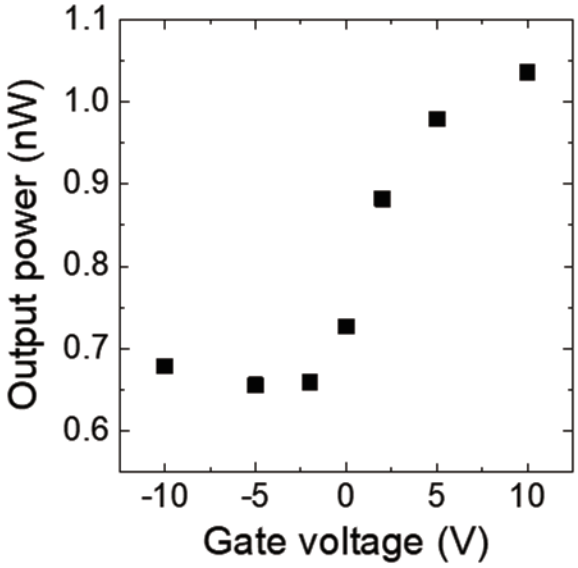

Fig. 2 Gate voltage dependence of output power.

Acknowledgment: This study was partially supported by JST/CREST (JPMJCR16Q2).

[1] P. Dhiman *et. al.*, Nano Lett. **11**, 3123, (2011).
[2] J. Yin *et. al.*, Nat. Nanotechnol. **9**, 378, (2014).
[3] S. Ghosh *et. al.*, Science **299**, 1042 (2003).
[4] R. Nishi *et. al.,* The 53rd Fullerenes-Nanotubes-Graphene General Symposium, 2P-13 (2016).
[5] T. Tanaka *et al.*, Anal. Chem. **87**, 9467-9472 (2015).

Corresponding Author: Y. Ohno
Phone & Fax: +81-52-789-5387
E-mail: yohno@nagoya-u.jp

Preparation of SWNT/PE Composites by Melt Blending

○Koichi Utsugi[2], Nao Otsuki[2], Ryota Yamada[2], Riku Ota[2], Atsushi Onodera[1], Masaru Sekido[2]

[1] *Advanced Course of Production System Engineering ,National Institute of Technology, Sendai College, Natori 981-1239, Japan*
[2] *Department of Materials Science and Engineering, National Institute of Technology, Sendai College, Natori 981-1239, Japan*

Due to their combination of outstanding mechanical characters, extremely large interfacial contact area, high aspect ratio, and low mass density CNTs are considered as the ideal reinforcement fillers for the nanocomposite materials. As CNT reinforced nanocomposites we have prepared MWNT/Polyamide(PA)-6 composites and MWNT/Polyethylene(PE) composites by melt blending methods. 35% increase of tensile strength has been observed in MWNT/PA-6 nanocomposites while no significant increase has been observed in MWNT/PE nanocomposites.

In this work, we focused on SWNT/PE composites and studied various SWNT/PE weight ratio to increase tensile strength. SWNT/PE composites were prepared by melt blending at 220 °C, screw speed of 100 rpm and a recycle time of 10 minutes. Weight ratio of SWNT/PE were 1/100, 3/100, 5/100 and 10/100. Tensile strength of SWNT/PE composites were measured by tension tester (Dak System INC., UTB9052-TT).

In another work we have studied with MWNT/PE composites and observed that the tensile strength of MWNT/HDPE(3/100) composites increased about 50%(Fig.1). We will discuss the difference of SWNT and MWNT as a reinforcement filler with PE matrix.

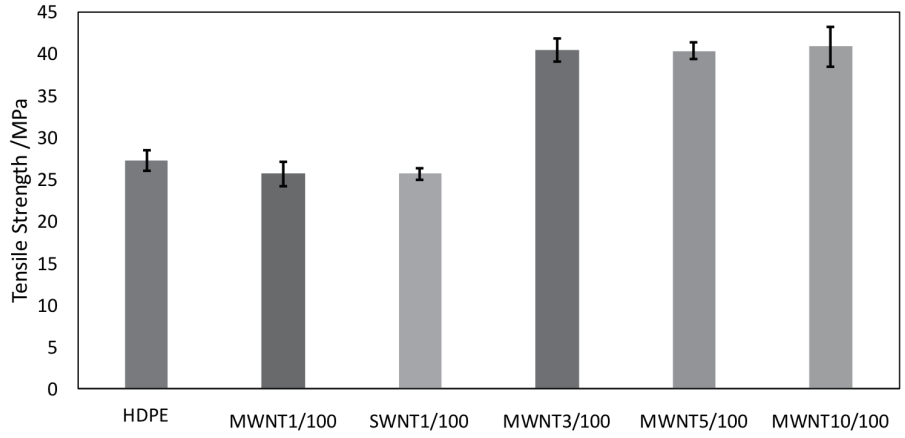

Fig 1. Tensile strength of MWNT/HDPE and SWNT/HDPE composites.

Corresponding Author: A. Onodera
Tel: +81-22-381-0329, Fax: +81-22-381-0329
E-mail: a1601008@sendai-nct.jp

Computational Study on Optimization of Sheet Conductance of Carbon Nanotube Transparent Films

○Masaaki Tsukuda[1] and Takahiro Yamamoto[1]

[1] *Department of Electrical Engineering, Tokyo University of Science, Niijuku 6-3-1, Katsushika-ku, Tokyo 125-8585, Japan*

Carbon nanotube (CNT) thin films are expected as flexible transparent conductive films. However, the details of electrical transport properties of CNT thin films have not been clarified yet because network structures in CNT films are extremely complicated. To increase the electric conductivity of CNT thin films with keeping their transparency, it is essential to understand relation between the network structure with the nanotube densities, alignment, length and diameter, and its electrical transport property. In this study, we thus theoretically explored how nanotube alignment affects electrical transport properties of CNT thin films.

First, we generated two-dimensional random networks in a film with the fixed values of the film length of $L = 5$ μm, the film width $W = 5$ μm, and the nanotube length $l_{\mathrm{CNT}} = 500$ nm (Fig1). When nanotubes are distributed, the angle between the axis of nanotube and *x* axis takes a uniformly random value between $-\theta_{\max}$ and $\theta_{\max}$. We then calculated the sheet conductance by solving network equations [1, 2] for the CNT network by changing the value of alignment angle $\theta_{\max}$ for several different nanotube densities *N*. The obtained results are summarized as follows.

1. The more density increases, the more sheet conductnace increases because nanotubes can contact each other.
2. When $\theta_{\max}$ exceeds the threshold value, the sheet conductance increases, depending on the increase of $\theta_{\max}$.
3. There is a drop of the sheet conductance at specific alignment angle.
4. The sheet conductance decreases at the high alignment angle region.

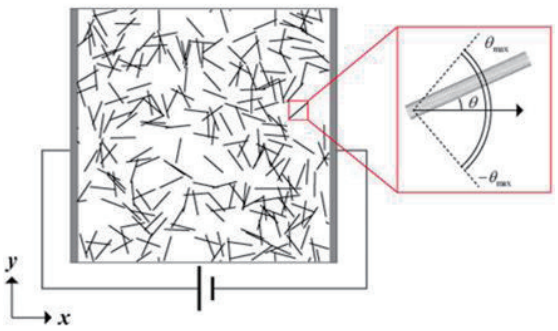

Fig1. Schematics of a random network consisting of CNTs

References:

[1] K. Ishizeki, K. Sasaoka, S. Konabe, S. Souma, and T. Yamamoto, Phys. Rev. B, **96**, 035428 (2017).

[2] A. Buldum, J. Ping Lu, Phys. Rev. B **63**, 161403(2001).

Corresponding Author: T. Yamamoto
Tel: +81-3-5876-1492
E-mail: takahiro@rs.tus.ac.jp

Production and Characterization of Double-wall Carbon Nanotubes by High-temperature Pulsed-arc Discharge: Dependence on Distance between Discharge Electrodes

○Yuya Tanaka, Toshiki Sugai

Department of Chemistry, Toho University, Chiba 274-8510, Japan

Double wall carbon nanotubes (DW) can be used to various fields with their unique properties. DW have been produced with highly graphitized homogeneous structures by a high-temperature pulsed-arc discharge (HTPAD)[1]. However the purity of DW realized by HTPAD has been limited with impurities such as amorphous carbon and single wall carbon nanotubes (SW) even if various production parameters have been optimized[2]. Here we present an enhanced production of DW by controlling the distance between electrodes.

The details of HTPAD system were described elsewhere[1,2]. The pulsed-arc discharges vaporized the electrodes with catalytic metals and produced nanotubes in Ar at the temperature and the pressure of 1250 ℃ and 300 Torr, respectively. The distance between discharge electrodes was controlled from 1 mm to 10 mm. The products were characterized by Raman with 633 nm laser and TEM.

Fig. 1 shows the dependence on the distance of the ratio between G and D-bands of the Raman spectra of the products. The peak around 8 mm reveals that nanotubes were produced with less amorphous carbon, which was also confirmed by the TEM observations. This distance is suitable not only for less amorphous carbon but also for DW. Fig. 2 shows the production ratio between DW and SW. At 8 mm the ratio was enhanced to 70 %, which is the best selectivity ever achieved. Those results can be understood with the dependence of the temperature and the carbon density distribution on the electrode distance recently observed with a steady-arc discharge[3].

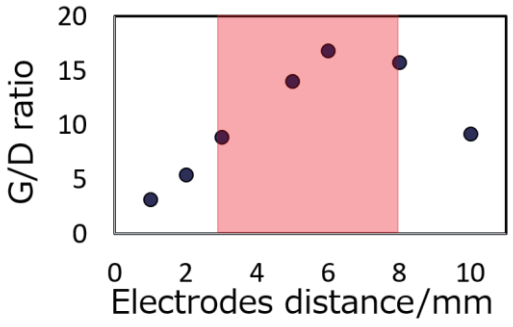

Fig.1 G/D ratio at each electrodes distance

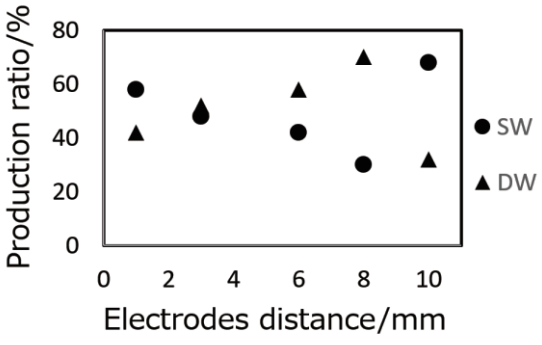

Fig.2 Diameter distribution

[1] T. Sugai *et al*., *Nano Lett*. **3**, 769 (2003).

[2] Y. Hikichi *et al.* The 50th FNTG General Symposium. 1P-22.

[3] Feng Liang *et al* *Mater. Res. Bull.,* **60** 158–165 (2014)

Corresponding Author: T. Sugai Tel: 047-472-4406 E-mail: sugai@chem.sci.toho-u.ac.jp

Purification of SWNT-porous glass (PG) composite by using heat treatment

○Tokinaru Matsuoka[1], Yoshiki Hayashi[1], Hiroshi Nagasawa[2], Shinzo Suzuki[1],

[1]Department of Physics, Kyoto Sangyo University, Kyoto 603-8555, Japan
[2]Kankyo Resilience Co. Ltd., Yokohama 240-8501, Japan

ACCVD technique has been widely used in the field of single-wall carbon nanotube (SWNT) growth, partly because that the ambient temperature suitable for the formation of SWNTs is relatively lower (typically, less than 800°C), and the purity of SWNTs in as-grown material is better than those obtained by other technique, e.g. arc-burning procedure.

In 2005, Aoki et al., reported about the formation of SWNTs in the porous glass (PG) material by using ACCVD technique [1], where metal particles (e.g. Co particles) were deposited on the PG material before ethanol was introduced as carbon source for making SWNTs in the PG material. The advantage of using PG material is that, it is very easy to make any kind of shape (rod, sheet.., etc.) made of PG, which implies that the as-grown SWNT-PG complex itself is expected to be used as an optical or other kind of device [2].

In this presentation, the effect of heat treatment aimed for further purification of SWNT-PG composite, is investigated. A preliminary search for thermal gravimetric (TG) analysis combined with Raman spectroscopy shows the best condition for heat treatment of the film made of mono-dispersed SWNT in solution, which indicates SWNT-PG composite also can also be purified furthermore by similar heat treatment. Further experimental findings are presented and discussed.

References:

[1] Y. Aoki et al., *Chem. Lett.*, **34**, 562(2005).
[2] K. Nagao et al., *Proceeding of the 46th fullerenes-nanotubes-graphene general symposium*, **3P-15**(2014).

Corresponding Author: Shinzo Suzuki
Tel: +81-75-705-1631, Fax: +81-75-705-1820,
E-mail: suzukish@cc.kyoto-su.ac.jp

Growth simulation of chirality-assignable single-walled carbon nanotubes with perfect cap structure by molecular dynamics

○Hiroyuki Ukai [1], Ryo Yoshikawa [1], Shohei Chiashi [1], Shigeo Maruyama [1,2]

[1] *Department of Mechanical Engineering, The University of Tokyo, Tokyo 113-8656, Japan*
[2] *Energy NanoEngineering Laboratory, National Institute of Advanced Industrial Science and Technology (AIST), Ibaraki 305-8564, Japan*

Single-walled carbon nanotube (SW-CNT) is an allotrope of carbon, and it is composed of cap and side wall parts. Ideal CNT has exactly six 5-membered rings and no 7-membered ring in the cap part, and it has only 6-membered rings in the side wall part. If 7-membered rings or extra 5-membered rings exist, they are regarded as defects. Molecular dynamics (MD) simulation is used to simulate CNT growth. Although CNTs with chirality-assignable side wall part were obtained in our former study [1,2], no ideal CNT has been obtained yet.

In this study, we tried to grow ideal CNTs by MD simulation, focusing the supply ratio of carbon atom. Cobalt was used as catalyst and CVD temperature was 1400 K. Carbon supply ratio was 1.35 atom/ns at the beginning. After the formation of graphitic structure on the catalyst surface and its lift-off, carbon supply frequency was gradually reduced from 1.35 to 0.0625 atom/ns. The cap part slightly continued to grow up and it became the ideal cap structure with six 5-membered rings. And then, perfect side wall part, which was composed of only 6-membered rings, grew following the ideal cap, and ideal CNT with no defects was obtained, as shown in Fig. 1.

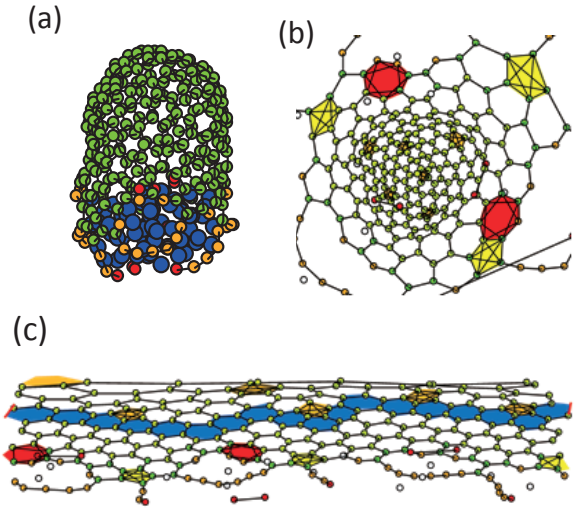

Fig. 1. (a) Snapshot of MD simulation of ideal CNT growth. The chirality is (13, 5). Calculation time is 1200 ns. (b) Development of the cap and (c) side wall part.

[1] K. Hisama *et al.* Proceedings of 46th FNTG general symposium, 2-1 (2014).
[2] R. Yoshikawa *et al.* Proceedings of 48th FNTG general symposium, 2P-22 (2015).

Corresponding Author: S. Maruyama
Tel: +81-3-5841-6421, Fax: +81-3-5841-6421,
E-mail: maruyama@photon.t.u-tokyo.ac.jp

Stability of isomerized forms of photoisomerizable molecules complexed with carbon nanotubes

○Keisuke Hamajima[1], Takeshi Koyama[1], Takeshi Saito[2], Hideo Kishida[1]

[1] *Department of Applied Physics, Nagoya University, Nagoya 464-8603, Japan*
[2] *National Institute of Advanced Industrial Science and Technology, Tsukuba 305-8501, Japan*

Photoisomerizable molecules change their conformations (Figure 1) and absorption bands by light absorption [1,2]. Application of photoisomerizable molecules to optical recording materials is expected for high-speed data writing and has been studied for decades [3]. For this application, it is needed that both forms before and after isomerization are stable. However, there is a problem that the thermal stability of the isomerized form is low. For this issue, we propose to compound photoisomerizable molecules with π conjugated system and carbon nanotubes (CNTs). It is expected that both forms of the molecules are stabilized by van der Waals forces between CNT wall and the molecules [4,5]. In this study, we used azobenzene and spiopyran as the photoisomerizable molecules.

For preparation of the composites, we used a gas phase reaction [6]. The CNTs were dispersed in water using a surfactant after ring opening treatment. By vacuum filtration of the dispersion, the CNTs were formed into a thin film, and the film was transferred onto a quartz substrate. Thereafter, the film and powder of the photoisomerizable molecules were sealed in vacuum in a Pyrex tube and heated in a furnace.

The lifetime of *cis* form of azobenzene was evaluated by measuring the time dependence of absorption change. The lifetime in the azobenzene-CNT composite is longer than that in organic solution. Similarly, the lifetime of merocyanine form of spiropyran is long in the composite. In this study, the composites of photoisomerizable molecules and CNTs enhance the thermal stability of the isomerized forms of the molecules.

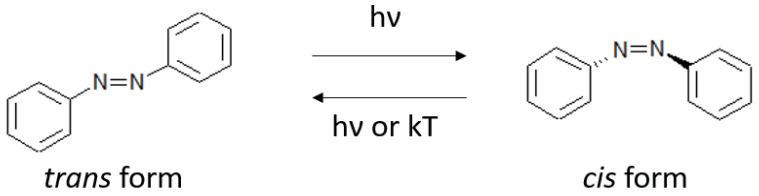

Figure 1: Isomerization of a typical photoisomerizable molecule, azobenzene.

[1] G. Zimmerman *et al.* J. Am. Chem. Soc. **80**, 3528 (1957).
[2] E. Fisher *et al.* J. Chem. Soc. **868**, 4522 (1952).
[3] Z. F. Liu *et al.* Nature **347**, 658 (1990).
[4] A. Setaro *et al.* Phys. Status Solidi B **251**, 2356 (2014).
[5] P. Bluemmel *et al.* J. Phys.: Condens. Matter **24**, 394005 (2012).
[6] H. Kataura *et al.* Synth. Met. **121**, 1195 (2001).

Corresponding Author: Takeshi Koyama
Tel: +81-52-789-4450, Fax: +81-52-789-4450,
E-mail: koyama@nuap.nagoya-u.ac.jp

Energetics of perylene molecules encapsulated in carbon nanotubes

○Yuya Nagasawa[1], Takeshi Koyama[2], and Susumu Okada[1]

[1]*Graduate school of Pure and Applied Sciences, University of Tsukuba Tennodai, Tsukuba 305-8571, Japan*
[2]*Department of Applied Physics, Nagoya University, Chikusa, Nagoya 464-8603, Japan*

Carbon nanotubes (CNTs) can encapsulate foreign atoms or molecules inside their tubular spacing where encapsulated guest materials form unusual structures. Polycyclic aromatic hydrocarbons (PAHs), coronene and perylene, form not only a stacking columnar structure as their bulk structure but also a lying double-decker structure in which the encapsulated PAHs are parallelly arranged with respect to the CNT wall. Experiments reported that coronene and perylene can forms these two different molecular conformations inside CNTs depending on the CNT species and the tiny difference in synthesis conditions [1~3]. However, it is still unclear that physical and chemical mechanisms of multiple conformations of PAHs in CNTs. Thus, the purpose of this work is to computationally investigate the detailed energetics of perylene molecule encapsulated into a metallic (11,11)CNT and a semiconducting (19,0)CNT for unraveling the physical and chemical mechanism of various metastable conformations of PAH inside CNT experimentally observed. All calculations are based on the density functional theory with the generalized gradient approximation in which the van der Waals correction is taken into account.

Our first-principles total-energy calculations reveal that cooperation between the encapsulation energy of a perylene molecule in CNT and the intermolecular interaction renders the potential energy landscape with double minimum structures in terms of the molecular orientation to the CNT wall. The lying molecular conformation energetically competes with the stacking conformation with the tilting angle of 70 degree with respect to the CNT axis (Fig. 1). A standing conformation with respect to the CNT wall is the ground state conformation for a semiconducting (19,0)CNT, while a lying conformation is the ground state for a metallic (11,11)CNT. In addition to these two conformations, perylene possess the other metastable molecular conformation of which energy is higher by 0.1 eV per molecule than that of the lying and stacking conformations.

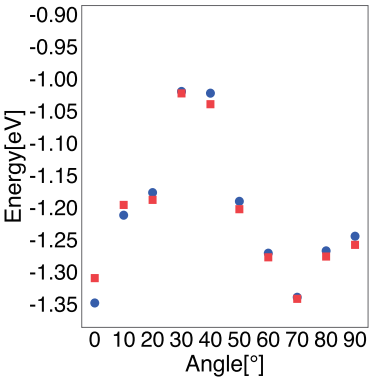

Fig. 1, Formation energy of perylene chains inside CNTs as a function of the tilting angle with respect to the tube axis. Circle and squares denote the energies for (11,11) and (19,0) CNTs, respectively.

References
[1] T. Okazaki et al. Angew. Chem. Int. Ed. **50**, 4853 (2011).
[2] M. Fujihara et al. J. Phys. Chem. C **116**, 15141 (2012).
[3] T. Koyama et al. unpublished.

Corresponding Author: Y. Nagasawa
E-mail: ynagasawa@comas.frsc.tsukuba.ac.jp

Local structure and properties of polycyclic aromatic hydrocarbon molecule encapsulated in single-walled carbon nanotubes studied by molecular dynamics simulations(II)

○Ryo Nagai[1], Yosuke Kataoka [2] and Hironori Ogata [1,2,3]
[1]*Dept. Chem. Sci. and Technol., Hosei University, Koganei, 184-8584, Japan*
[2] *Graduate School of Sci. and Engin., Hosei University, Koganei, 184-8584, Japan*
[3]*Research Center for Micro-Nano Technology, Hosei University, Koganei, 184-0003, Japan*

Carbon nanotubes (CNTs) is one of the most promising material because of their superior electronic, thermal and mechanical properties. One of the applications of Single-Walled Carbon Nanotube (SWNTs) is their use as a template to synthesize novel nanostructure materials. Synthesis of graphene nanoribbons (GNRs) encapsulated CNTs was reported by fusion reaction of encapsulated polycyclic aromatic hydrocarbon (PAH) molecules such as coronene in CNTs as a one-dimensional reactor for fusion [1]. Columnar stacked coronene molecules encapsulated in a single-walled carbon nanotubes(SWNTs) and their unique luminescence properties are reported[3-6]. In this study, molecular dynamics simulation was performed to clarify the local structure and properties of various kinds of PAH molecules encapsulated in SWNTs systematically. Figure 1. shows the snapshots of (a)coronene and (b) perylene encapsulated (10,10)SWNT at 298 K. We will report the detailed results of simulations several kinds of PAH molecules encapsulated SWNTs.

(a) (b)

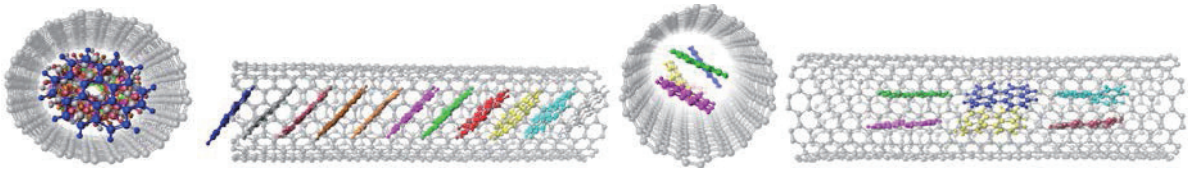

Fig.1: Snapshots of (a)coronene and (b)perylene encapsulated (10,10)SWNT at 298 K.

References:

[1] A. V. Talyzin *et al., Nano Lett.***11**(2011)4352-4356.

[2]Miho Fujihara, *et al*., *J. Phys. Chem.* C **116**(2012)15141−15145.

[3]B. Botka *et al., Phys. Status Solidi* B **249**(2012)2432–2435.

[4]Alexander I. Chernov *et al., Phys. Status Solidi* B **251**(2014)2372–2377.

[5]Ilya V. Anoshkin *et al., ChemPhysChem.* **15**(2014)1660 – 1665.

[6]Y. Sakane, *et al., AIP ADVANCES* **5** (2015)117113.

[7]Y.Joko, *et al., Phys. Chem. Chem. Phys*.**19**(2017)27704-27715.

Corresponding Author: H. Ogata
Tel: +81-42-387−6229, Fax: +81-42−387−6229, E-mail: hogata@hosei.ac.jp

Fast Synthesis of Graphene in Three-Dimensional Reaction Field by Chemical Vapor Deposition

○Yukuya Nagai[1], Hisashi Sugime[2], Suguru Noda[1,*]

[1]*Department of Applied Chemistry, Waseda University, Tokyo 169-8555, Japan*
[2]*Waseda Institute for Advanced Study, Waseda University, Tokyo 169-8050, Japan*

Chemical vapor deposition (CVD) using copper (Cu) as catalyst has become the mainstream for the synthesis of graphene [1]. Synthesis of 30-inch graphene films was reported, however with a long process time including 30 min for CVD and 30 min for annealing [2]. Recently, graphene synthesis using "rolled-Cu" foils was reported with careful pretreatments of electrochemical polishing, oxidation, and reduction of Cu foils and quick CVD in 5–20 min using typical carbon source of CH_4 [3]. The idea of rolled-Cu is excellent because it can utilize the reactor volume and convert carbon source more efficiently than the conventional layout. However, it is essential to make processes simpler and time shorter for both pretreatment and CVD toward practical production of graphene.

Here we used a roll of 5×30 cm^2-sized Cu foils with simple pretreatment of immersion in HNO_3 aq. for 3 min followed by annealing during heating up the furnace to 975 ºC within 15 min. For the CVD, we used ethylene (C_2H_4), which is often used for the growth of carbon nanotubes [4], as a more reactive carbon source than CH_4. Within 90 s of CVD, a continuous graphene film was obtained on the rolled-Cu (Fig. 1a), with a small discontinuous part at the bottom of the roll. Raman spectra of the film showed a sharp G-band peak with a strong 2D-band peak with a negligibly small D-band peak (Fig. 1b). The graphene transferred with the size of ~1×1 cm^2 to quartz glass substrates showed optical transmittances of 94.8−96.7% and sheet resistances of 0.8−3.6 kΩ/sq without doping. Graphene synthesis using rolled-Cu was compared with the conventional CVD using flat Cu foils.

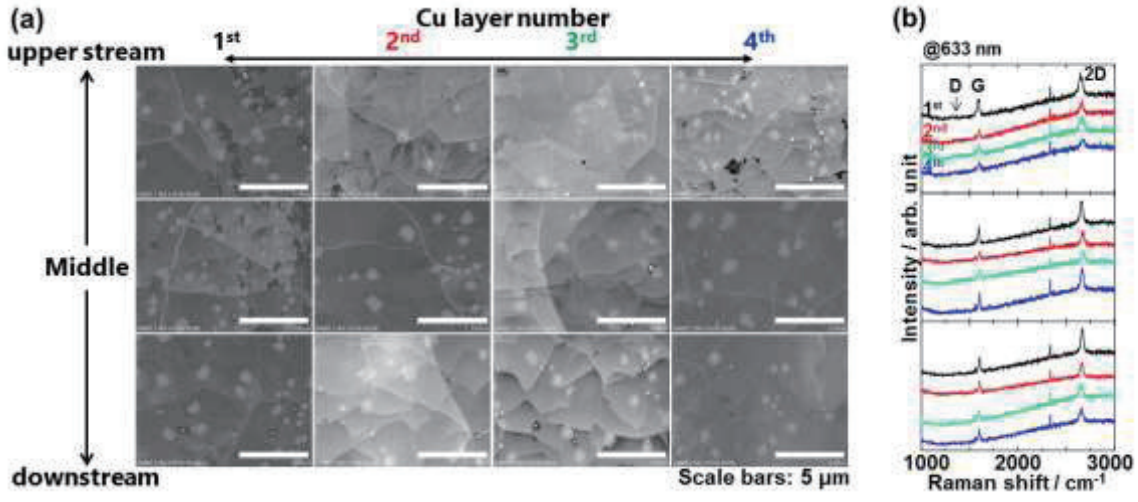

Fig.1 Graphene obtained on rolled Cu. (a) SEM images. (b) Raman spectra.

[1] X. Li, et al., *Science* **324**, 1312 (2009).
[2] S. Bae, et al., *Nat. Nanotechnol.* **5**, 574 (2010).
[3] H. Wang, et al., *Adv. Mater.* **28**, 8968 (2016).
[4] G. Eres, et al., *J. Phys. Chem. B.* **109**, 16684 (2005).

Corresponding Author: S. Noda, Tel&Fax: +81-3-5286-2769, E-mail: noda@waseda.jp

Characterization of size controlled graphite by O_2 plasma etching and its application to liquid phase exfoliation

○Yasushi Ishiguro[1], Genki Hirobe[1], Kazuyuki Takai[1,2]

[1] *Dept. of Chemical Science and Technology, Hosei University, Tokyo 184-8584, Japan*
[2] *Graduate School of Science and Engineering, Hosei University, Tokyo 184-8584, Japan*

Development of a method for producing high-quality graphene in large scale is essential for actual achievement of graphene applications. In this view point, the liquid-phase exfoliation of graphite have been investigated for graphene production due to its simple and scalable process. Control of size and form of graphite in the liquid phase exfoliation process is interesting in view of controlling the structure and properties of graphene, in spite of few examples reported [1,2]. In this study, the size of highly oriented pyrolytic graphite (HOPG) was controlled thorough plasma etching treatment using oxygen (O_2) gas. The change in geometry and electronic structure of the etched HOPG was investigated. In addition, the liquid phase exfoliation of graphite by sonication in organic solvent was examined.

The plasma etching treatment was carried out by using RIE-101iPH (ICP 150 W, Bias 50 W) with cupper grid-shaped mask (□7.5 μm^2). Raman mapping analysis was measured by LabRAM HR Evolution (532 nm).

According to optical microscope image, the grid-shaped mask pattern is well transcribed on the etched HOPG. Raman D-band intensity mapping is also agreement with the shape of the etched HOPG (Fig. 1). The Raman G-band position is almost remains even after etching, indicating the Fermi level does not change. Whereas, the D-band / G-band intensity ratio and the FWHM of the G-band increases after the etching, suggesting the increment in carrier scattering at defect and edges (Fig. 2).

References:
[1] X. Lu *et al.*, *Appl. Phys. Lett.*, **75**, 2, 193 (1999). [2] H. Fredriksson *et al.*, *Carbon*, **47**, 1335 (2009).

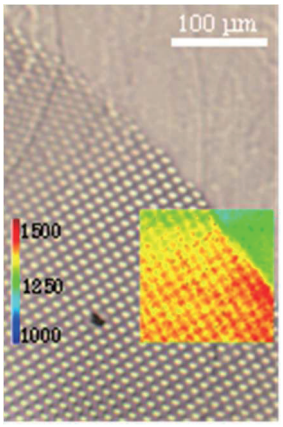

Fig. 1. Optical microscope image of HOPG. The inset shows the Raman D-band intensity mapping.

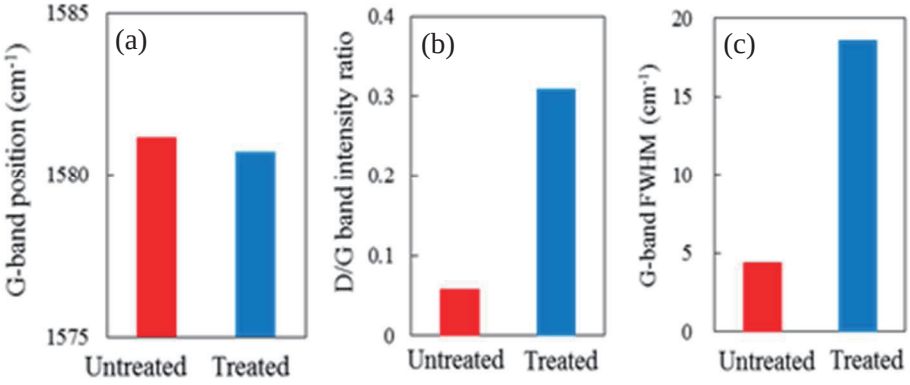

Fig. 2. Raman peaks for graphite with / without etching. (a) G-band position, (b) D-band / G-band intensity ratio and (c) FWHM of G-band.

Persistent photo conductivity in functionalized graphene nanoribbons

○Hiroo Suzuki[1], Toshiro Kaneko[1], and Toshiaki Kato[1,2]

[1]*Department of Electronic Engineering, Tohoku University, Sendai 980-8579, Japan*
[2] *JST-PRESTO*

Graphene nanoribbons (GNRs) combine the unique electronic and spin properties of graphene with a transport gap that arises from quantum confinement and edge effects. This makes them an attractive candidate material for the channels of next-generation transistors.

Up to now, we developed a novel method based on the advanced plasma CVD [1] with nanoscale Ni catalyst (Ni nanobar) for directly fabricating suspended GNRs devices [2]. Through the comparison of molecular dynamics simulation and phase diagram calculation with the systematically obtained experimental results, the growth dynamics of GNRs in our method has been also elucidated. By following this growth model, the yield of suspended GNR growth can be drastically improved (~98%) and wafer-scale synthesis of 1,000,000 suspended GNRs has been realized [3].

Recently, we found that our suspended GNRs include unique optoelectrical features. The current in GNR can be drastically changed by photo irradiation (Fig. 1a) and the current change can be maintained for a long time (over 3 days) even after stopping the photo irradiation, which is known as a persistent photoconductivity (PPC). To further improve the PPC features such as sustain time and response speed, we attempted to elucidate the detailed mechanism of PPC in GNR. The PPC was often observed in samples which were kept in air for long period (Fig. 1b). Functionalized GNRs by O_2 plasma irradiation were also showed clear PPC features. These indicate that surface reaction of GNR device (GNR itself or Ni electrode) with oxygen and related species should be a key to cause PPC. To identify the surface structures of GNR device after O_2 plasma functionalization, detailed measurements were carried out by X-ray photoelectron spectroscopy (XPS), atomic force microscopy (AFM) (Fig. 1c-d), and optical absorption spectroscopy. These measurements reveal that the Ni electrode is converted to $Ni(OH)_2$, and the interface between GNR and $Ni(OH)_2$ can work as a carrier trapping center, causing the PPC. These results indicate the wafer-scale suspended GNRs array can be useful as a novel optical-memory device using interface control between metal and suspended GNRs.

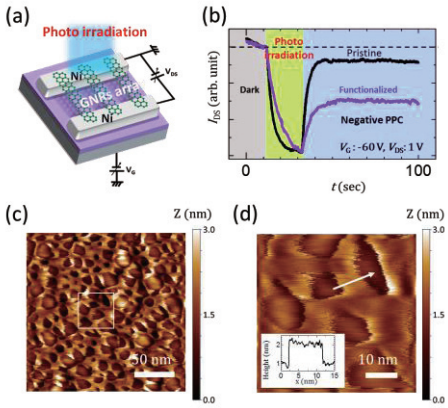

Fig. 1: (a) Schematic image of GNR array-FET under photo irradiation. (b) Comparison of photoresponce of pristine and functionalized suspended GNRs array. (c) Low and (d) high magnification AFM image of O_2 plasma irradiated Ni electrodes. Inset in (d) shows height profile along the arrow.

[1] H. Suzuki, T. Kato and T. Kaneko, Plasma and Fusion Res. **9,** 1206079 (2014).

[2] T. Kato and R. Hatakeyama, Nature Nanotechnology **7**, 651 (2012).

[3] H. Suzuki, T. Kaneko, Y. Shibuta, M. Ohno, Y. Maekawa and T. Kato, Nature Communications **7**, 11797 (2016).

Corresponding Author: H. Suzuki
Tel: +81-22-795-7046
E-mail: suzuki12@ecei.tohoku.ac.jp

First-Principles Calculation of Carrier Injection and Work Function in Graphene/Ferroelectrics Hybrid Material

○Hikaru Horii[1], Satoru Konabe[1], Takahiro Yamamoto[1]

[1] *Faculty of Engineering, Tokyo University of Science, Tokyo 125-8585, Japan*

Thermoelectric conversion is a key technology for recovering energy from waste heat. To obtain high thermoelectric performance, it is required that both the electrical conductivity and the Seebeck coefficient are high. Currently, graphene has attracted attention as a potential material for exhibiting such performance. Thermoelectric performance has an optimum value for a carrier density due to the trade-off relation between the conductivity and the Seebeck coefficient. Nontheless the chemical doping, on the one hand, is difficult to control the carrier density and also reduces the mobility of graphene. On the other hand, the electric field doping uses an external electric source, which is not suitable for energy harvesting.

We thus propose a new carrier injection method using spontaneous polarization of ferroelectric materials, which does not need an external electric source. To validate this new method, we used first-principles calculation based on density functional theory (DFT) and non-equilibrium Green's function (NEGF) method to theoretically analyze the carrier injection to graphene by the spontaneous polarization of Polyvinylidene Fluoride (PVDF). The calculation models are shown in Fig. 1.

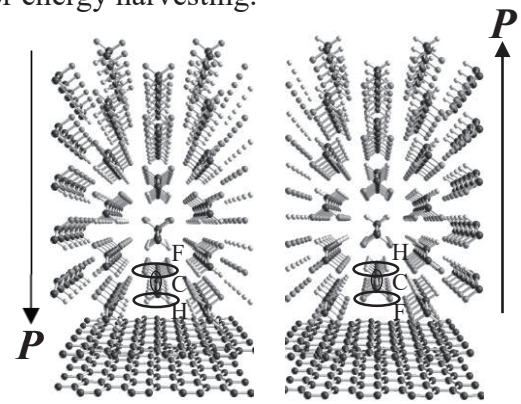

(a) positive (b) negative

Fig. 1 Two simulation models

Our simulation shows that, when graphene contacts a surface of positive (negative) polarization of PVDF, electrons (holes) are injected into graphene and those carriers penetrate up to the third layer of multilayer graphene from the interface.

It is then necessary to optimize a carrier density to improve thermoelectric performance of graphene. The optimum value of the carrier density in monolayer graphene is known as approximately 10^{12} cm^{-2} [1]. On the other hand, a carrier density of 7×10^{13} cm^{-2} was injected in our calculation. Therefore, it is possible to optimize thermoelectric performance by adjusting the spontaneous polarization.

In addition, it is found that such carrier injection is caused by charge transfer from two layers of PVDF interface. Therefore, not only the field effect by the polarization but the difference of the work function (WF) between PVDF and graphene surfaces must be considered. We thus calculated WF of graphite and PVDF surfaces by NEGF method. Consequently, we found that WF of graphite surface was 4.52 eV and that of hydrogen- and fluorine-terminated of PVDF surface ware 1.68 eV and 8.81 eV, respectively. According to the WF difference, electrons (holes) are transferred from hydrogen (fluorine) of PVDF surface to graphene. These are in excellent agreement with the results of the carrier injection.

[1] E. H. Hwang *et al.*, Phys. Rev. B **80**, 235415 (2009).

Corresponding Author: T. Yamamoto
Tel: +81-3-5876-1492
E-mail: takahiro@rs.tus.ac.jp

First Principles Calculations of Electrical Structure of Water Absorbed Graphene

○Yusei Kioka[1], Yuki Maekawa [2], Kenji Sasaoka [3], Takahiro Yamamoto [1,2,3]

[1] Department of Electrical Engineering, Tokyo University of Science, Tokyo, 125-8585, Japan
[2] Department of Liberal Arts, Tokyo University of Science, Tokyo, 125-8585, Japan
[3]Water Frontier Science & Technology Research Center, RIST, Tokyo University of Science, Tokyo, 125-8585

It has long been believed that water molecules cannot adsorb on graphene because it is a hydrophobic material. However, the existence of water layers on a graphene surface was theoretically confirmed by performing classical molecular dynamics (MD) simulations [1,2]. These previous works suggested that water molecules spread out on the graphene surface. Before these observations and simulations, Homma *et al*. discovered that similar water molecular layers can exist around a carbon nanotube (CNT) by both photoluminescence measurements and classical MD simulations [3]. Although the structure of surface water along the surface normal on a graphene has been systematically and rigorously investigated, the microscopic structure of surface water parallel to a graphene surface has not yet been fully characterized despite its importance. In addition, the influence of surface water on the electronic states of a graphene remains to be elucidated yet.

In this study, we thus theoretically investigate the microscopic structure of surface water on a free-standing graphene using classical MD simulations and the influence of surface water on the electronic states of a graphene using *ab initio* calculations based on the density functional theory. We found that the surface water exhibits a single or double layered structures on graphene depending on the water vapor pressure. In particular, we clarify the two-dimensional hydrogen-bond network is formed on the water layers on graphene surface [4]. In addition, we found that there is no electron transfer between the surface water and the graphene and that the low-energy electronic state near the Dirac points is unaffected by the surface water.

[1] T. A. Ho and A. Striolo, J. Chem. Phys. **138**, 054117 (2013).

[2] A. Akaishi, T. Yonemaru, and J. Nakamura, ACS Omega **2**, 2184 (2017).

[3] Y. Homma, *et al*., Phys. Rev. Lett. **110**, 157402 (2013).

[4] Y. Maekawa, K. Sasaoka, and T. Yamamoto, accepted in Jpn. J. Appl. Phys.

Corresponding Author: Takahiro Yamamoto,
Tel&FAX: +81-3-5213-0990,
E-mail: takahiro@rs.tus.ac.jp

Defect introduction and hydrogen termination in Epitaxial graphene

○Yoshinori Obata[1], Kazuyuki Takai[1, 2]

[1] *Graduate School of Science and Engineering, Hosei University, Tokyo 184-8584, Japan*
[2] *Research Center of Ion Beam Technology, Hosei University, Tokyo 184-0002, Japan*

Although defect introduction is one of the important strategies to tune the properties of graphene [1], the number of defects is usually focused, and the chemical structure of defects has been not well considered. Actually, vacancies in graphene become magnetic depending on the number and position of termination hydrogen atoms [2]. In this study, atomic vacancies are introduced into graphene, and its hydrogen termination is investigated in order to clarify the chemical structure of vacancies in graphene.

Atomic vacancies were introduced into the surface of epitaxial graphene grown on SiC by Ar ion beam sputtering at 100 eV after pre-annealing, followed by exposing to hydrogen molecules, or air atmosphere. Raman spectroscopy and XPS were measured by LabRAM HR Evolution (532 nm) and ESCA 5600, respectively.

The increase of XPS composition ratio of O to C indicates that defects and its termination atoms gradually increase upon ion beam irradiation (Fig.1). The decrease of oxygen content by 28% in average for hydrogen adsorption case compared to air adsorption one suggests that the termination atoms of defects are controlled by exposure gas after defect introduction into graphene. Raman intensity ratio of D band to G band increases upon irradiation time for both of adsorption conditions, but hydrogen adsorption shows a smaller D band as compared to the air exposure condition (Fig.2). This reveals that the probability of carrier scattering might depend on the chemical structure of the defect.

This project was supported by JSPS and RFBR under the Japan - Russia Research Cooperative Program.

[1] Chen, et al., *Nat. Phys*. **7**, 535 (2011). [2] G. Sunnardianto, et al, *J. Adv. Sci. Eng. Med*. **8**, 421-426 (2016).

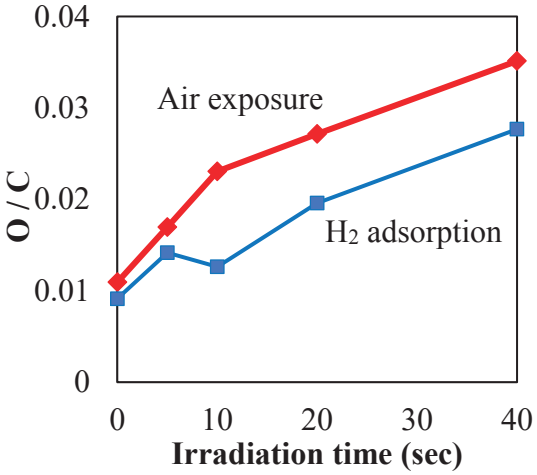

Fig. 1 XPS O / C composition ratio

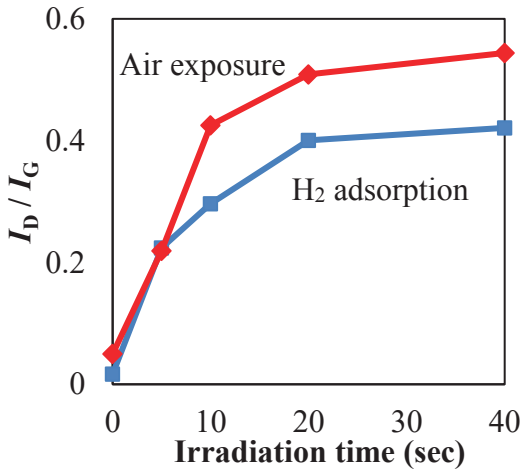

Fig. 2 Raman D / G intensities ratio

Diffusion of Li Atom on Graphene Sheet through V_6 Vacancy: First Principles Calculations

○Kento Shiota, Takazumi Kawai

Graduate School of Pure and Applied Sciences, University of Tsukuba, Tennodai 305-8571, Japan

Since nano-carbon materials generally have large pore structures, they have attracted much attention as a negative electrode material for Li ion batteries with high electrical capacity. Recent studies show large battery capacities in comparison with the conventional graphite negative electrode. However, the atomic scale understanding of the Li atom diffusion with some defects is still not clear, where such diffusion through the vacancy defect possibly affect the charge/discharge rate and also increase of the battery capacity. Here, we investigated the adsorption and diffusion of Li atom on the graphene with V_6 defect with various H termination configurations at the defect edge using first principles electronic state calculations. We calculated Li diffusion path through the defect toward backside of the graphene. For V_6 terminated with 4 hydrogen, 0.70eV is required for Li to diffuse through the defect as shown in Fig.1(a). Although there is little diffusion barrier for clean edge (Fig.1(b)), Li atom could be trapped at the deep potential hollow at the defect due to strong interaction between Li atom and dangling bond. We also investigated the Li atom diffusion through V_6 defect when the Li atoms are trapped at the defect site. We found that the trapped Li atoms reduce the attractive potential for a diffusing Li atom and enable the Li atom to diffuse by way of exchange diffusion.

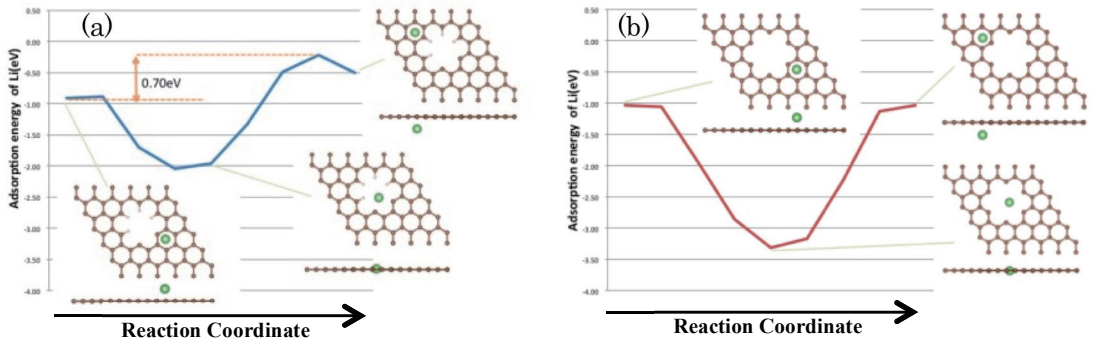

Fig.1 The variation of adsorption energy during diffusion through the V_6 defect (a) terminated with 4 hydrogen atoms and (b) without termination.

Fabrication and Electrical Resistance Mesurement of Graphene Nanoribbons on SiC (0001)

○Masashi Horibe[1], Seichiro Ito[1], Yuya Mizuno[1], Chenxing Wang[1], Hitoshi Nakahara[1], and Yahachi Saito[1]

[1] *Department of Quantum Engineering,The University of Nagoya, Nagoya 464-8603, Japan*

Graphene nanoribbon shows metalic and semiconducting properties depending on the structure of edges and is expected to be applied to electronic devices[1,2]. Epitaxial graphene nanoribbons with few defects can be fabricated by growth on a SiC substrate. However, since the sides of a nanoribbon are connected to a buffer layer [Fig. 1 (a)], the effect of the edge is not exhibited and it becomes an obstacle to device application. Therefore, we developed a technology to etch the buffer layer connected to the sides of the nanoribbon selectively by heating the SiC substrate in a low pressure oxygen atmosphere [3] [Fig. 1 (b)]. In this study, resistance measurement using the 4 probe method was peformed in order to investigate the difference in electrical conduction characteristics depending on the presence or absence of the buffer layer. In the resistance mesurement, the distance between the current application probes was fixed at 15 μm, and the distance between the voltage measurement probes was changed.

Figure 2 shows probe distance vs. resistance characteristics of a nanoribbon with a width of 78 nm with a buffer layer and a nanoribbon with a width of 64 nm without a buffer layer. In both cases, the change of the resistance is small when the probe distance for the voltage measurement is less than 4 μm, and for the larger distance it shows a rapid increase with the increase of the distance. However, when the resistance values of nanoribbons with and without the buffer layer at the probe distance of 5 μm or more are compared with each other, the nanoribbon with a buffer layer show remarkably small resistance value of 1/10 or less. As a cause of this, we consider that when the buffer layer is oxygen-etched, defects are generated in the buffer layer under the single-layer graphene, the current flowing through the nanoribbon may leak to the SiC substrate through the defects.

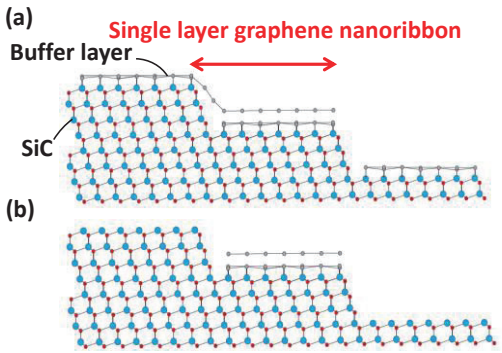

Figure 1: Schematic diagrams of the dfferences In a graphene nanoribbon structure on a SiC substrate. (a) With a buffer layer. (b) Without a buffer layer.

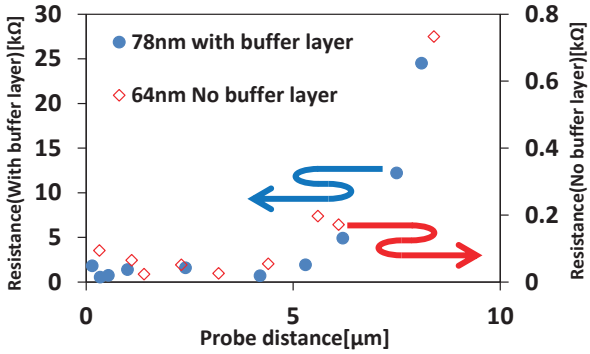

Figure 2: Probe distance vs. resistance characteristics of graphene nanoribbons with and without buffer layer.

[1] Young-Woo Son et al., Phys. Rev. Lett. **97**, 216803 (2006).

[2] Melinda Y. Han et al., Phys. Rev. Lett. **98**, 206805 (2007).

[3] Chenxing Wang et al., e-J. Surf. Sci. Nanotech. **15**, 13-18 (2017).

Corresponding Author: M. Horibe
Tel: +81-90-6646-7578,
E-mail: h.m030605@gmail.com

2P-25

Ion-beam irradiation into Graphene via sacrificial layers

○Kosuke Nakamura[1], Tomoaki Nishimura[2], Kazuyuki Takai [1, 2]

[1] *Graduate School of Science and Engineering, Hosei University, Tokyo 184-8584, Japan*
[2] *Research Center of Ion Beam Technology, Hosei University, Tokyo 184-8584, Japan*

In view of defect-introduction and chemical modification, irradiation of ion-beam into graphene is an interesting strategy. Indeed, hole doping to graphene was achieved by Au^+ ion irradiation into SiO_2 / Si substrate supporting graphene [1]. In this study, we attempted to inject Au ion directly to graphene, where the irradiation to bear graphene will cause damage, so a sacrificial layer protecting graphene was designed and evaluated to prevent damaging bear graphene by irradiation using Raman spectroscopy (LabRAM HR), Rutherford Backscattering Spectrometry (RBS), and XPS (ESCA5600).

At first we adopted the resist thin-film as a sacrificial layer, however Au ion irradiation has changed the structure of the sacrificial layer, which become not removable without introducing damage to graphene.

Next, ZnO and NaCl thin-film was applied for an alternative sacrificial layer, where it has been confirmed ZnO can be removed by HCl, and NaCl can be removed by water even after Au ion irradiation. However, Raman spectroscopy indicates ZnO deposition damages the top most layer of graphene even before Au ion irradiation, where the degree of damage depends on the thickness of graphene (**Fig.1**).

On the other hand, depositing NaCl for sacrificial layer gives little damage to graphene. Irradiating Au ion to graphene covered with NaCl thin-film had successfully performed at 200 keV at dosage of 1 x 10^{13} ions / cm^2. Raman spectroscopy of Au irradiated graphene with NaCl thin-film as a sacrificial layer, shows clear G band near 1580 cm^{-1}, indicating honeycomb lattice structure of graphene remained even after irradiation (**Fig.2**). A significant Raman D band (1340 cm^{-1}) and D' band intensity (1620 cm^{-1}) suggests a successful introduction of defects causing intervalley scattering and intravalley scattering after irradiation, respectively.

This project was supported by JSPS and RFBR under the Japan - Russia Research Cooperative Program.

[1] K. Nakamura, et al, FNTG symposium (2017)

Corresponding Author: Kazuyuki Takai
Tel: +81-42-387-6138, Fax: +81-42-387-7002, E-mail: takai@hosei.ac.jp

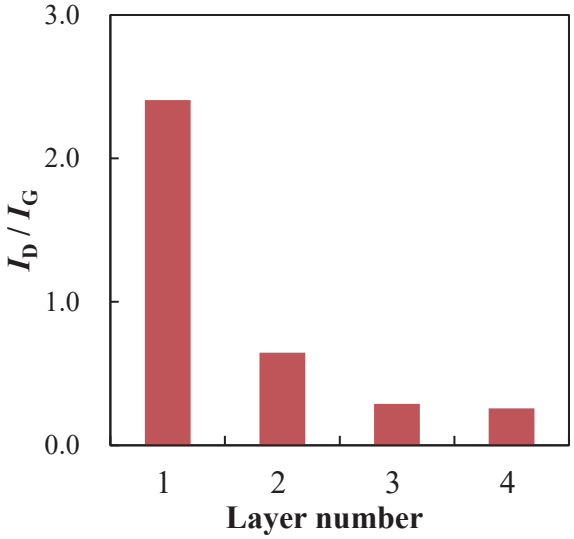

Fig. 1 Raman I_D / I_G ratio for Graphene after ZnO deposition

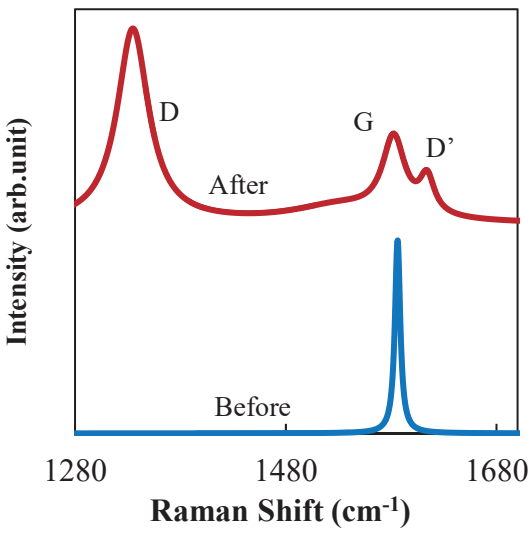

Fig. 2 Raman spectra of graphene before / after irradiation

2P-26

Near-Field Electron-Photon Matrix Element of Monolayer Graphene

F.R. Pratama[1], M. Shoufie Ukhtary[1], R. Saito[1]
[1]Department of Physics, Graduate School of Science, Tohoku University

In the typical experimental set-up of tip-enhanced Raman spectroscopy (TERS), a tip whose radius around 10 nm is placed near the sample of the characterized material. The presence of tip enhances the intensity of Raman signal [1] due to the localization of electric field around the tip that is called near-field [1, 2]. In this study, we calculate electric near-field enhancement around Au parabolic tip of radius 10 nm irradiated by light with wavelength of 520 nm. Considering the quasi-static approximation which is valid when the spatial dimension of the object is much smaller than the wavelegth of the light [3, 4] the calculation is performed by solving the Laplace's equation numerically with finite-difference method.

A monolayer graphene is placed 2 nm below the tip. We calculate the electron-photon matrix element which describes the interaction of electrons with the near-field. The calculated results show that the magnitude of near-field electron-photon matrix element is significantly higher (by the factor ~4) compared to the case of the far-field, thus explaining the origin of the enhanced Raman intensity in the interband transition between the initial and the final states in graphene TERS [5]. We also found that while in the case of far-field spectroscopy the optical transition of electron from valence to conduction bands occurs vertically (with no change of electron's wave vectors) [6], [7] the presence of the near-field on the graphene plane induces the change of electron's wave vectors in the optical transition.

References:

[1] E.C. Le Ru & P.G. Etchegoin, *Principles of Surface-Enhanced Raman Spectroscopy*, Oxford: Elsevier (2009).
[2] J. Cui et al., *Laser Phys*., **23**, 076003 (2013).
[3] S.A. Maier, *Plasmonics*, New York: Springer (2007).
[4] J. Larsson, *Am. J. Phys*., **75** No. 3 (2007).
[5] M. Ghislandi et al., *Appl. Spectrosc. Rev*. **47**, pp. 371-381 (2012).
[6] A. Grüneis et al., *Phys. Rev. B* **67**, 165402 (2003).
[7] A. Ferreira et al., *Phys. Rev. B* **84**, 235410 (2011).

Valley relaxation in monolayer WSe_2 studied by ultrafast spectroscopy

○Keisuke Shinokita, Xiaofan Wang, Yuhei Miyauchi, Kazunari Matsuda
Institute of Advanced Energy, Kyoto University, Uji 611-0011, Japan

Atomically thin transition metal dichalcogenides (TMDs) possess novel physical properties originating from the extreme low dimensionarity, making monolayer TMDs an ideal platform to investigate fundamental physics in two-dimensional system. In addition, strong spin-orbit interaction and no inversion symmetry endow monolayer TMDs with optical band gaps at the K and K' valleys with opposite spin configuration. This valley-spin locking results in the ability to control valley degrees of freedom using circular polarized light [1]. Realization of optoelectronic application based on manipulation of the valley-spin polarization of charged carries, *valleytronics,* requires the understanding of valley depolarization process to achieve long-lived valley polarization. Here we report valley relaxation dynamics of electron and hole in monolayer TMDs.

We investigated ultrafast valley depolarization dynamics in monolayer WSe_2 at 5 K using circularly polarized pump-probe reflectivity spectroscopy. Figure 1(a) shows reflectance contrast of monolayer WSe_2 with A exciton and B exciton transition, as shown in Figure 1(b). Figure 1(c) and (d) show time development of pump-probe differential reflectivity probed around A and B exciton transition, respectively. The circularly polarized pump pulse with a photon energy of 1.879 eV creates electron-hole pairs in one valley, inducing bleaching of both A and B exciton transition because of phase-space filling effect. Figure 1(c) shows A excition transition has almost no circular polarization dependence of time-resolved reflectivity change even at 0 ps, which is contrast with circularly polarized time-integrated photoluminescence (PL) measurement, where valley polarization of 40 % was observed (not shown). It suggests that A exciton transition in unexcited valley is suppressed by either electron or hole equally populated in the both valleys after ultrafast valley relaxation, and the other carrier is preferentially populated in the excited valley. Figure 1(d) also shows no valley dependence of differential reflectivity of B exciton transition, identifying the equally populated carrier is *electron*. The combinations of pump-probe and PL results conclude the dissimilar intervalley scattering of electron and hole: The *electron* suffers ultrafast intervalley scattering and is populated equally in K and K' valleys, while the *hole* is robust against intervalley scattering [2].

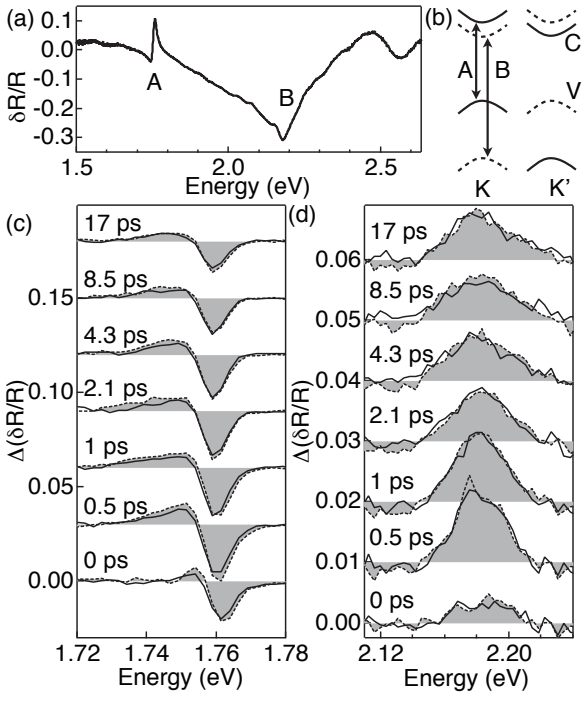

Fig.1: (a) Reflectance contrast of monolayer WSe_2 on Si/SiO_2 substrate. (b) Energy level diagram showing A and B exciton transition. Pump-probe differential reflectivity for same (solid lines) and opposite (dotted lines) circular polarization of pump and probe pulses as a function of delay time around A exciton (c) and B exciton (d) transition.

[1] X. Xu *et al*., Nature Physics. **10**, 343 (2014).
[2] A. Molina-Sánchez *et al*., Nano Letters 17, 4549 (2017).

Corresponding Author: K. Shinokita
Tel: +81-774-38-3465, FAX: +81-774-38-4567,
E-mail: shinokita.keisuke.4r@kyoto-u.ac.jp

Layer-by-layer growth of single crystalline transitional metal dichalcogenide thin films by molecular beam epitaxy

○Y. Wang[1], M. Nakano[1], Y. Kashiwabara[1], Y. Iwasa[1,2]

[1]*Department of Applied Physics, The University of Tokyo, Tokyo 113-8656, Japan*
[2] *RIKEN Center for Emergent Matter Science (CEMS), Saitama 351-0198 Japan*

The discovery of graphene has opened research gate on two-dimensional (2D) materials due to their novel properties from both fundamental and applied viewpoints. To date, main approach of making 2D materials is "top-down" mechanical exfoliation, with sample typically several micrometer level, which is not enough for further research development. Therefore "bottom-up" synthesis, which means deposition by both physical and chemical ways on substrates with millimeter-level size, is getting considerable attention.

We have been developing a growth process by molecular-beam epitaxy (MBE) for high quality transition-metal dichalcogenide (TMDC) thin films, which are composed of various 2D materials with properties ranging from semiconducting to metallic. Recently we succeeded in establishing a versatile route to layer-by-layer epitaxial growth of millimeter-scale TMDC thin films on commercially-available insulating sapphire substrate by MBE. Especially our semiconducting WSe_2 and semi-metallic $TiSe_2$ showed single crystallinity evaluated by x-ray diffraction measurements both for out-of-plane and in-plane directions. These films also show high performance in transport properties. The obtained WSe_2 epitaxial thin films exhibited ambipolar transistor operation upon electrolyte gating with clear Hall signals for hole-accumulation regime with the maximum mobility of about 3 cm^2/Vs at T = 150 K[1], which was in the highest level reported for the first-generation MoS_2 thin films grown by chemical-vapor deposition. Obtained 10-monolayer-thick $TiSe_2$ epitaxial thin films exhibited clear CDW transition at around T = 200 K with the sign change in the Hall coefficient, which is consistent to the behavior reported for bulk $TiSe_2$.

[1] M. Nakano, Y. Wang, Y. Kashiwabara, H. Matsuoka, and Y. Iwasa. Nano Letters, 17, 5595-5599 (2017)
Corresponding Author: Y.Wang Tel: 03-5841-6822 E-mail: wangyue@mp.t.u-tokyo.ac.jp

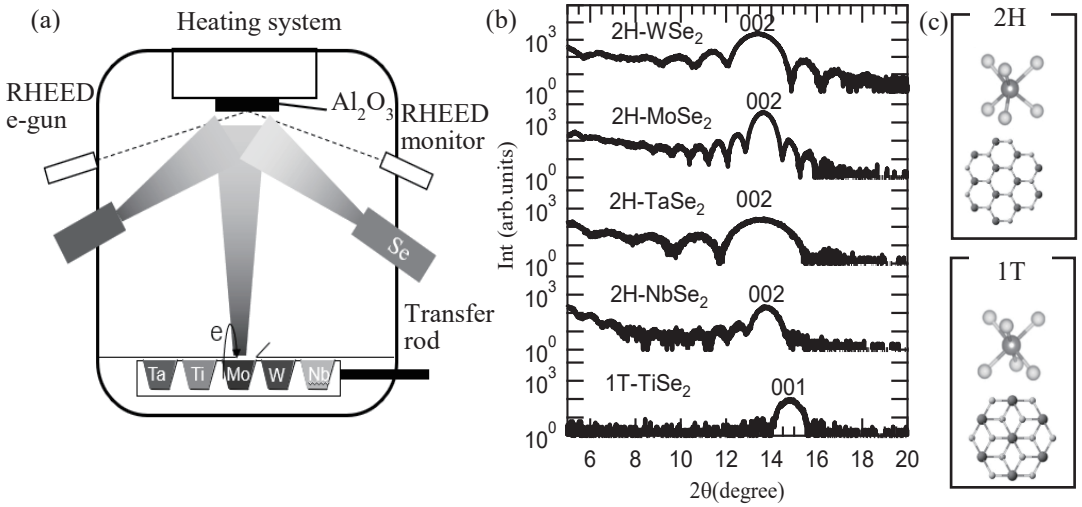

Figure 1: (a) Schematic image of MBE system in this project. (b) Out-of-plane XRD patterns of various TMDC thin films with different structure. (c) Schematic image of two main polytypes in TMDC material. In each column, upper figure shows atomic structure and lower figure shows top view.

Preparation and optical properties of suspended monolayer MoS_2

○Kana Kojima[1], Zhang Wenjin[2], Yuhei Miyauchi[2], Tetsuki Saito[1], Yu Kobayashi[1], Takahiko Endo[1], Kazunari Matsuda[2], Yutaka Maniwa[1], Yasumitsu Miyata[1]

[1]*Department of Physics, Tokyo Metropolitan University, Hachioji, 192-0397, Japan*
[2]*Institute of Advanced Energy, Kyoto University, Uji, 611-0011, Japan*

The optical properties of transition metal dichalcogenide (TMDC) atomic layers have attracted much attention because of their unique spin-valley coupling and excitonic optical responses. Recently, to probe their intrinsic properties, several groups have used the suspended atomic layers to suppress the unintentional doping and lattice strain induced by supporting substrates [1,2]. However, the conventional preparation processes usually require multistep complex processes and lead to the contamination of polymer for transfer of atomic layers. To solve these problems, we have developed a facile, clean method to prepare suspended TMDCs and have investigated their optical properties.

MoS_2 monolayers were grown on SiO_2/Si substrates by chemical vapor deposition (CVD). As-grown samples were separated from the substrates by putting a water droplet on the substrate, and then the monolayers floating on water were transferred onto another substrate with holes or trenches. We found that the suspended monolayers show bright photoluminescence (PL) without broadening compared with samples on SiO_2 (Fig.1a). The PL peak also has high-energy shift for suspended samples due to the release of tensile strain induced by supported substrates. Furthermore, time-resolved PL measurements reveals the increase of PL lifetime from less than ~10 ps on SiO_2 to 50 ps for the suspended samples, indicating the suppression of non-radiative decay process (Fig.1b). In the presentation, the details of sample preparation and optical properties of suspended monolayers will be discussed.

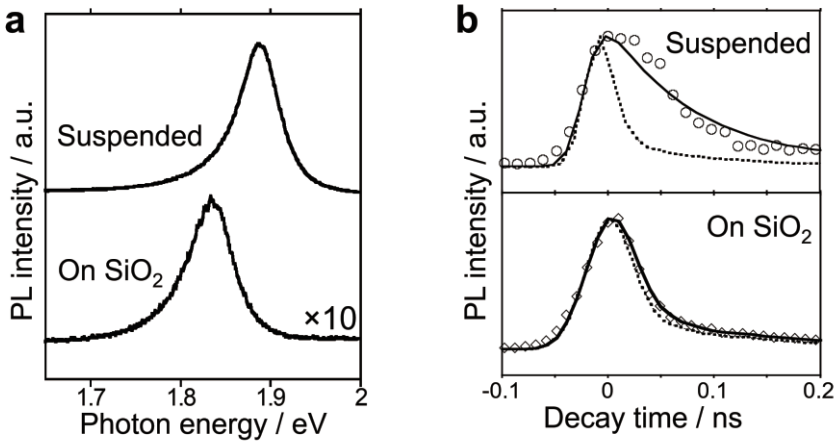

Fig.1 (a) PL spectra and (b) time-resolved PL decay profiles of as-grown monolayer MoS_2 on SiO_2 and suspended monolayer MoS_2. In (b), Solid and dotted lines correspond to fitting results and instrument response function (IRF), respectively.

[1] T. Kato, *et al*. ACS Nano, **10**, 9687 (2016).
[2] W. Jin, *et al*. Phys. Rev. B, **91**, 121409 (2015).

Corresponding Author: Y. Miyata, Tel: 042-677-2508, E-mail: ymiyata@tmu.ac.jp

Surface segregation of Ge crystal on metal thin films

○Seiya Suzuki, Tatsurou Inaba, Masamichi Yoshimura

Graduate School of Engineering, Toyota Technological Institute, Nagoya 468-8511, Japan

Germanene is a single atomic sheet of germanium (Ge). Ge atoms in germanene are arranged in buckled honeycomb structure, which provides massless Dirac fermions and tunable band gap [1]. Although germanene can be epitaxially grown on single crystal surface of metals such as gold (Au), aluminum, and platinum in ultra-high vacuum [2], the costly growth method limits practical electronic applications. Thus, a practical large scale growth of germanene is desirable.

To achieve large scale germanene growth, we have studied surface segregation of Ge crystal on metal thin films. First, we deposited Ge following by Au (or Au/Ag) thin film on crystalline Si with thin layer oxide through piranha etching. After that, the samples were annealed under medium vacuum condition (~2 Pa). Then, the sample surface was characterized by Raman spectroscopy, X-ray photoelectron spectroscopy (XPS), atomic force microscopy (AFM), and tip-enhanced Raman spectroscopy (TERS).

Figure 1 shows Raman spectra of Au/Ge/Si before and after heating at 350 ºC for 1 min. A sharp peak was observed at ~299 cm^{-1} after heating, indicating that Ge was segregated and crystallized on the sample surface. Figure 2(a) shows an AFM image of the sample surface after heating. Aggregated particles with the height of 5 ~ 10 nm are observed. Figure 2(b) shows a TERS map at ~300 cm^{-1}, taken at the same area in Fig. 2(a). Figure 2(c) shows three representative Raman spectra in Fig. 2(b). The results indicate that crystallization of Ge is occurred around the aggregated particles. In addition, we measured Au/Ge/Si samples before and after heating by XPS. The XPS results indicate Ge was segregated and Ge oxide (GeO_x) was formed even at room temperature, which also potentially prevents the germanene formation. To suppress GeO_x formation at room temperature, we used Au/Ag where Ag has higher solubility of Ge compared to Au. By using Au/Ag instead of Au, the Ge segregation at room temperature was completely suppressed, which may lead germanene formation by the segregation method.

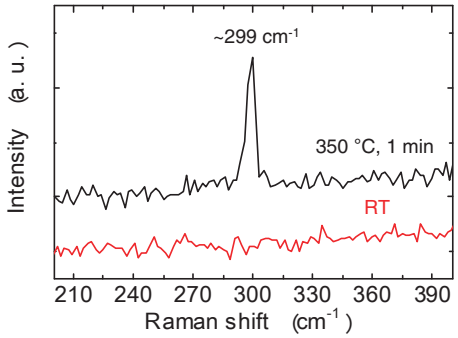

Fig. 1. Raman spectra of Au/Ge/Si before and after heating

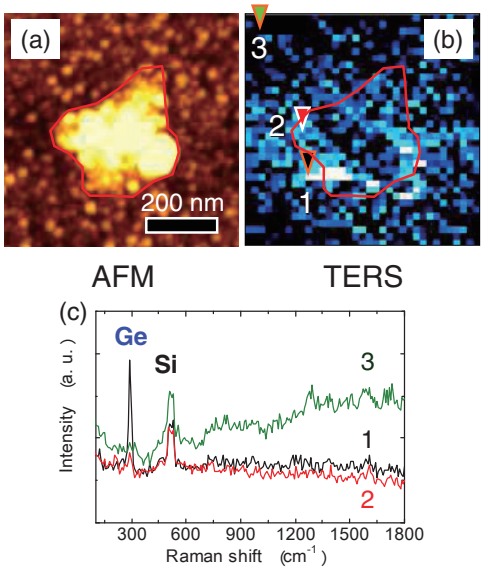

Fig. 2. (a) AFM image, (b) TERS map at ~300 cm^{-1} of Au/Ge/Si after heating, and (c) Representative Raman spectra in (b).

[1] Z. Ni *et al*., Chem. Nano Lett. **12**, 113 (2012).
[2] J. Zhuang *et al*., ACS Nano **11**, 3553 (2017).

Corresponding Author: S. Suzuki
Tel: +81-52-809-1852
E-mail: seiya09417@gmail.com

Photoluminescence properties of twisted bilayer transition metal dichalcogenides

○Masafumi Shimasaki[1], Wenjin Zhang[1], Xiaofan Wang[1], Takashi Taniguchi[2], Kenji Watanabe[2], Kazunari Matsuda[1], and Yuhei Miyauchi[1]

[1]*Institute of Advanced Energy, Kyoto University, Kyoto 611-0011, Japan*
[2]*National Institute for Materials Science, Tsukuba, Ibaraki 305-0044, Japan*

Atomically-thin transition metal dichalcogenides (TMDCs, MX_2, M=Mo, W and X = S, Se, etc.), which are two dimensional semiconductors with a few atom thicknesses, have been attracting much attention due to their distinctive electronic and optical properties promising for future optoelectronic applications. Monolayers of TMDCs are direct gap semiconductors [1] that exhibit sharp optical absorption and luminescence peaks arising from excitons with binding energy of more than a few hundred meV. Recently, their heterostructures consisting of various kinds of monolayer TMDCs stacked on each other have intensively studied because the stacking leads to completely new optical properties [2,3]. In contrast to the hetero-bilayers, however, the effect of the stacking of the same TMDC monolayers on their optical and excitonic properties still remains unclear.

In this study, we examined photoluminescence (PL) properties of twisted bilayer $MoSe_2$, which are artificially structured homo-bilayer materials fabricated by stacking two $MoSe_2$ monolayers on each other with an arbitral twist angle of the honeycomb lattice directions between the layers. This stacking retains the direct gap nature of each monolayer in the twisted bilayer, and enables to study the effect of the interactions between the two extremely close-set direct gap semiconductors. Interestingly, the twisted bilayer sample showed a few to several times higher PL intensity and less PL nonlinearity than those observed in the monolayer samples. We will discuss the detailed procedure of these experiments and the possible mechanism for the observed phenomena.

[1] K. F. Mak, C. Lee, J. Hone, J. Shan, and T. F. Heinz, Phys. Rev. Lett. **105**, 136805 (2010).

[2] A. K. Geim, and I. V. Grigorieva, Nature **499**, 419 (2013).

[3] S. Mouri, W. Zhang, D. Kozawa, Y. Miyauchi, G. Eda, and K. Matsuda, Nanoscale **9**, 6674 (2017).

Corresponding Author: Y. Miyauchi

Tel: 81-774-38-3463, Fax: +81-774-38- 3467,

E-mail: miyauchi@iae.kyoto-u.ac.jp

Monolayer WSe_2-MoS_2 Lateral Heterojunction Light-Emitting Diodes

○Jiang Pu [1], Ming-Yang Li [2], Jing-Kai Huang [2], Yuhei Miyauchi [3], Kazunari Matsuda [3]
Lain-Jong Li [2], and Taishi Takenobu [1]

[1] *Department of Applied Physics, Nagoya Univ., Nagoya 464-8603, Japan*
[2] *Physical Sciences and Engineering Division, KAUST, Thuwal 23955-6900, Saudi Arabia*
[3] *Institute of Advanced Energy, Kyoto Univ., Kyoto 611-0011, Japan*

Recent advances of heterostructure fabrications based on transition metal dichalcogenides (TMDCs) yield atomically regulated interfaces due to their intrinsically passivated surfaces, allowing us to explore unusual electrical and optical phenomena and to make outstanding improvements to device performance [1]. Although, numerous experimental demonstrations of vertically stacked heterostructures have been realized using scotch-tape approach, the investigation of physical properties of lateral heterojunctions, in which dissimilar TMDCs are artificially stitched together, has been still limited. In particular, lateral heterojunctions are easier to tune band offset for designing p-n junction because of their spatial separation. Moreover, compared with manual transfer of vertical heterostructures, lateral heterojunctions is ideally adopted for the scalable approach of chemical vapor deposition (CVD) for creating atomically sharp heterojunctions [2]. Here, we developed a scalable fabrication process for WSe_2-MoS_2 lateral heterojunction films and firstly realized its light-emitting device arrays.

WSe_2-MoS_2 lateral heterojunction films were synthesized by two-step CVD process. As shown in Fig. 1, W electrodes were firstly patterned for the subsequent location-selective growth of WSe_2 monolayers. And then, epitaxial growth of MoS_2 monolayers was performed to form heterojunctions. Finally, additional Mo pads were deposited, followed by spin-coating ion gel films for building light-emitting device [3,4]. As applying voltage, holes (electrons) are injected and accumulated in WSe_2 (MoS_2) mediated by electric double layers to form p-n junction (Fig.1). Figure 2 obviously indicates electroluminescence (EL) image generating along junction interface. Interestingly, the comparison between photoluminescence (PL) and EL spectra shown in Fig. 3 revealed inconsistent behavior. Although both contributions of WSe_2 and MoS_2 were observed in PL, EL only showed MoS_2 luminescence. This suggests band structure evolution at junction interface; thus we will discuss this physical picture based on recent scanning tunneling spectroscopy study. Importantly, we firstly realized lateral heterojunction light-emitting devices and achieved the improvements of their external quantum efficiency compared to reported homojunction devices, providing a new platform for high-performance optoelectronic device applications.

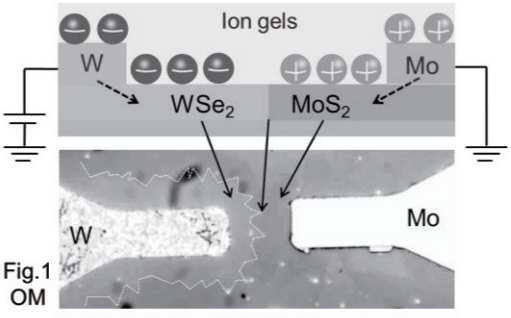

Fig.1 OM

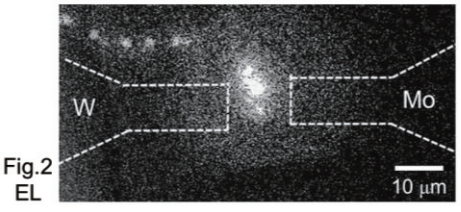

Fig.2 EL

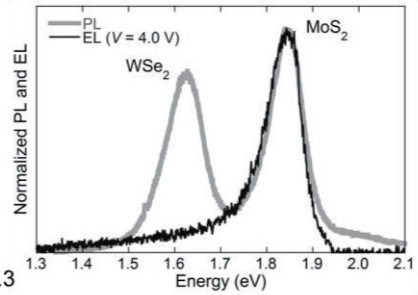

Fig.3

[1] K. S. Novoselov *et al*., *Science* **353**, 461 (2016).
[2] M.-Y. Li *et al*., *Science* **349**, 524 (2015).
[3] J. Pu, *et al*. *Adv. Mater.* **29**, 1606918 (2017).
[4] M.-Y. Li, J. Pu, *et al*. *Adv. Func. Mater.* under review.

Corresponding Author: J. Pu, T. Takenobu
Tel/Fax: +81-52-789-5165,
E-mail: jiang.pu@ngoya-u.jp, takenobu@nagoya-u.jp

Absorption spectra from exciton effect of atomic layer materials

○ Toshiya Shirakura[1], Yuki Tatsumi[1], Riichiro Saito[1]

[1]*Department of Physics, Tohoku University, Sendai 980-8578, Japan*

In this work, we discuss the absorption of light considering exciton effect with spin orbit coupling in atomic layer materials. We focus on monolayer molybdenum diselenium ($MoSe_2$). $MoSe_2$ is one of the semiconducting transition metal dichalcogenides (TMD) which have interesting optical properties. When an electron in the valence band obtain incident light, the electron is excited to the conduction band. At the same time, exciton is generated by Coulomb interaction from electron in the conduction band and hole in the valence band. In order to make exciton wave function, the electron and hole wave functions in the different states are mixed to each other. Then, we can make exciton wave function that is localized in the real space. Previous works show that the so-called A peak and B peak appear in TMD from spin orbit coupling around the K and K' points [1]. Also, peak positions shift from bandgap to low energy region which matches to binding energy of exciton. Then, also show how important relative permittivity affect to absorption spectra, reproducing the previous work [2].

We calculate the absorption spectra by using Wannier function (WF) which is based on tight binding model. Therefore we develop a code of optical absorption spectra with exciton and spin orbit coupling effect for WF that is calculated by Wannier90 and used it for numerical calculation.

In this work, we numerically calculate Coulomb interaction as a function of relative permittivity. We consider not only the direct Coulomb interaction between the bottom conduction band of electron and the top valence band of hole but also the Coulomb repulsion between the bottom conduction band of electron and the valence band which is occupied by all electrons except for the top valence band that is called self-energy. We also show absorption spectra with exciton and spin orbit coupling effect.

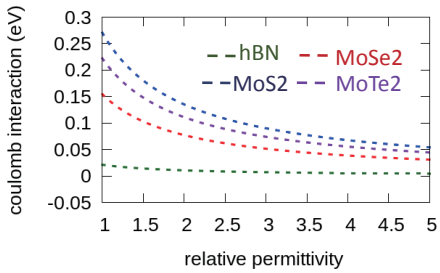

Fig.1 electron-electron interaction which comes from self-energy as a function of relative permittivity with different materials. Coulomb interaction seem to change invers proportional to relative permittivity [3].

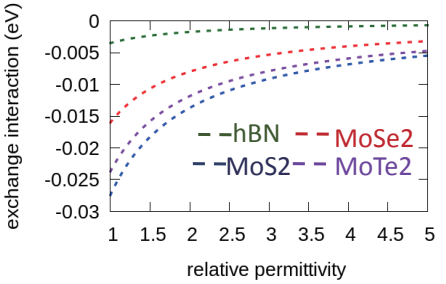

Fig.2 electron-electron interaction which comes from the direct exchange interaction as a function of relative permittivity with different materials. Minus sign means that these materials have a property as diamagnetism [3].

[1] W. G. Gerber, *et al*., 2D Materials. **2**, 4 (2015).
[2] J. Z. Liu, *et al*., Phys. Rev. Let. **118**, 266401 (2017).
[3] W. Zi-Wu, et al., Journal of Physics D: **50.47** (2017): 475306.

Corresponding Author: T. Shirakura,
E-mail: shirakura@flex.phys.tohoku.ac.jp

Aqueous dispersion of carbon materials inspired by Japanese Ink II

○Kaito Ishido, Kazuki Nakamura, Koki Taniyama, Kento Hujita, Junpei Hayakawa*

Science Team, Nara Prefectural Seiwaseiryo Senior High School, Sango 636-0813, *Japan*

Japanese ink have been made from susu(soot) and nikawa(glue) unceasingly from Nara Period. It is well known that ink is a protective carbon colloid prepared from soot and glue.

Solubilization or dispersion of carbon materials such as, fullerenes, carbon nanotubes and graphene in water is of great importance because of interesting biological application[1~3].

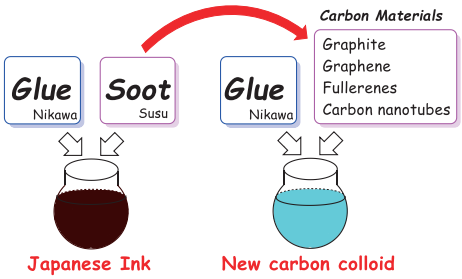

Fig.1: Aqupus dispersion of carbon materials utlitizing a glue

On these backgrounds, we studied aqueous dispersion of carbon materials, such as [60]fullerene, graphite, graphene and carbon nanotubes, utilizing a glue[4] (Fig. 1).

we considered several kinds of dispersant to clarify the mechanism of dispersion of carbon materials to water (Table 1). First, we examined an agar which is a gelling agent similar to glue, as a dispersant. In the case of using agar which is a polysaccharide, not a black colloidal solution but a colorless transparent liquid was obtained (entry 2). On the other hand, in the case of cook gelatin (type-B gelatin), type-A gelatin, and collagen peptide with molecular weight of about several thousand as a dispersant, black dispersion was obtained. After centrifugation, we measured the particle size and zeta potentials indicating colloidal stability. When cook gelatin was used, a result similar to glue was obtained although the particle diameter was somewhat larger (entry 3). When type-A gelatin was added, the zeta potential was positively charged and the particle diameter was polydispersed (entry 4). In the case of using collagen peptide, the zeta potential was low, the particle diameter was smaller than when glue was used (entry 5). From these results, it can be expected that proteins with some molecular weight are effective for dispersion of carbon materials in water, irrespective of whether the dispersed material is charged to positive or negative.

entry	carbon mateiral	dispersant	color	particle size (nm)	zeta potentic
1	graphene	glue	black	412	-10.5
2	graphene	agar	colorless	-	-
3	graphene	cook gelatin	black	615	-11.4
4	graphene	gelatin A type	black	polydisperse	7.2
5	graphene	collagen peptide	black	255	-5.5

Table 1: Examination of dispersant

Next, we conducted food analysis and amino acid composition analysis of a glue. The component of the glue was found to be 84.4% protein, 11.7% moisture, 2.8% saccharide. Amino acid composition analysis revealed that the glue is a glycine - rich protein that closely resembles gelatin.

Although details of the mechanism of dispersion with glue have not been elucidated, it was found that proteins with some molecular weight are effective.

[1] S. Deguchi *et al*. Sci. Rep, **3**, 2094 (2013)

[2] M. EstiliS, A. Khademhosseinia *et al*. Nanoscale, **7**, 6436 (2015)

[3] N. Nakashima and T. Shiraki. Nippon Gomu Kyoukaishi, **1**, 3 (2016).

[4] The 53rd Fullerenes-Nanotubes-Graphene General Symposium, 1-14 (2017)

Corresponding Author: Junpei Hayakawa

Tel: +81- 0745-72-4101, Fax: +81-0745-32-9819

E-mail: hayakawa.j@nps.ed.jp

Applicability of DLS to Diluted Nanodiamond Colloidal Solutions

○Takumi Sato[1], Toshihiko Tanaka[1,3], Yasuhiro F. Miura[2], Tetsuya Aoyama[3], Eiji Osawa[4]

[1] Department of Chemistry and Biochemistry, National Institute of Technology, Fukushima College, 30 Aza-nagao, Tairakamiarakawa, Iwaki, Fukushima, 970-8034, Japan
[2]Hamamatsu University School of Medicine, 1-20-1 Handayama, Higashi-ku, Hamamatsu city, Shizuoka, 431-3192, Japan
[3]Elements Chemistry Laboratory, RIKEN, 2-1 Hirosawa, Wako, Saitama, 351-0198, Japan
[4]Nano Carbon Research Institute Ltd., Asama Research Extension Center, Shinshu University, 3-15-1 Tokida, Ueda, Nagano, 386-8567 Japan

We previously reported that ultrathin rectangular nanosheets were precipitated on the surface of a 0.005% nanodiamond (ND) colloidal solution carrying a Langmuir monolayer of a fatty acid.[1] The degree of diluting aggregation[2] in the solution determines what are their starting particles and their thickness should depend on the degree.

However, dynamic light scattering (DLS) measurements have intrinsic difficulties when they are applied to such diluted ND solutions and we must be cautious there. ND aggregated particles are usually 2.6 ~ 100 nm in size for such cases, thus their Rayleigh scattering taking place there. Rayleigh scattering intensity is proportional to the sixth power of a particle size (the third power of a particle size per volume). Hence, even if a trace of aggregation contaminates a main component in a single nanometer range, the intensity from contaminants often exceeds significantly that from the main component. The size resolution from a fitted autocorrelation function is quite limited in such cases and main component peaks are often disappeared. For example for a 0.25wt.% ND solution, **Fig. 1a** shows the average of the 9 high resolution data selected from 50 measurements and **Fig. 1b** shows that of the 50. The former procedure is able to detect the main peak of ~10 nm, whereas the latter is not: we can estimate that the volume from the main peak is 92%, assuming that a scattering intensity per volume are proportional to the third power of its peak particle size. In DLS, undesirable measurements such as ones having accidentally strong scattering are often excluded in calculating an average from a set of many measurements.

We have further examined with a Malvern zetasizer the dependence of optional measurement conditions[2] (a high speed fitting mode and a statistical discarding process) on the peak resolution (or main particle sizes) in order to clarify the applicability and limit of the options. Then we will discuss the degree of diluting aggregation in the solutions. Probably the degree[2] was overestimated previously.

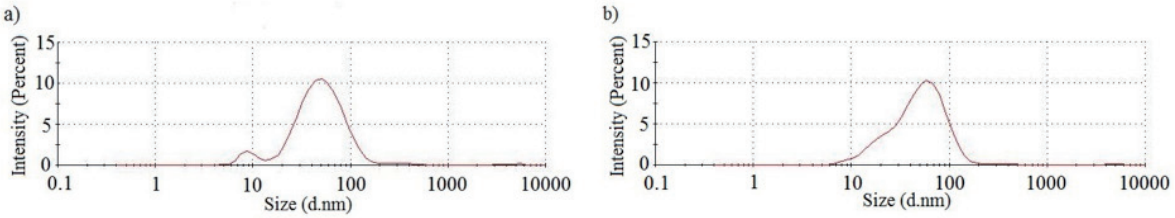

Fig.1 DLS spectra of scattering intensity for a 0.25wt.% ND solution: a) the average of 9 measurement sets showing a good peak resolution ; b) that of 50 measurement sets including the 9.

[1] T. Tanaka, Y.F. Miura, T. Sato, E. Osawa; *Abstract of the 53th FNTG Symposium*, 66(2017)
[2] N. O. Mchedlov-Petrossyan, N. N. Kamneva, A. I. Marynin, A. P. Kryshtalc, E. Osawa, *Phys. Chem. Chem. Phys.*,17, 16186-16203(2015).
Corresponding Author:Toshihiko Tanaka / Tel: +81-246-46-0810 / E-mail: ttanaka@fukushima-nct.ac.jp

Suppression of carbon nanotube redox reaction caused by protein adsorption

○Tomohito Nakayama[1,2], Takeshi Tanaka[2], Kentaro Shiraki[1], Muneaki Hase[1], Atsushi Hirano[2]

[1] *Division of Applied Physics, Faculty of Pure and Applied Sciences, University of Tsukuba, Tsukuba, Ibaraki 305-8573, Japan*
[2] *Nanomaterials Research Institute, National Institute of Advanced Industrial Science and Technology (AIST), Tsukuba, Ibaraki 305-8565, Japan*

Physicochemical properties of single-wall carbon nanotubes (CNTs) such as redox reaction are affected by adsorbed molecules on the CNT surfaces [1]. In this study, we show that protein adsorption causes suppression of CNT redox reaction in aqueous solutions by using bovine serum albumin (BSA) as a model protein. We suggest that protein molecules form thicker layers on the CNT surfaces compared with ordinary surfactant molecules such as sodium dodecyl sulfate (SDS).

We measured absorption and Raman spectra of HiPco–CNTs at different pH values. The inflection point of the absorbance in the S_{11} region (e.g. absorbance at 1275 nm) for BSA adsorbed CNTs (CNT–BSA) was shifted to a more acidic pH value compared with that for SDS adsorbed CNTs (CNT–SDS) (Fig.1), which indicates suppression of the redox reaction of the semiconducting CNTs by the adsorbed BSA molecules. We also investigated redox reaction of the metallic CNTs by a measurement of Raman spectra with excitation at 532 nm. The Raman spectral intensities of the radial breathing mode for the CNT–BSA were higher than those for CNT–SDS (Fig.2), an indication of suppression of the redox reaction of the metallic CNTs by the BSA molecules. These findings provide a new understanding of redox chemistry of CNT–protein complex materials and their behavior in biological systems.

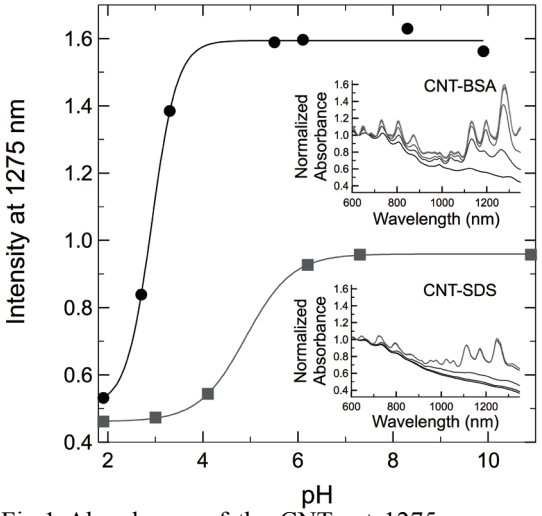

Fig.1 Absorbance of the CNTs at 1275 nm as a function of pH value; the CNTs were dispersed by BSA (circle) and SDS (square). Insets show the corresponding absorption spectra.

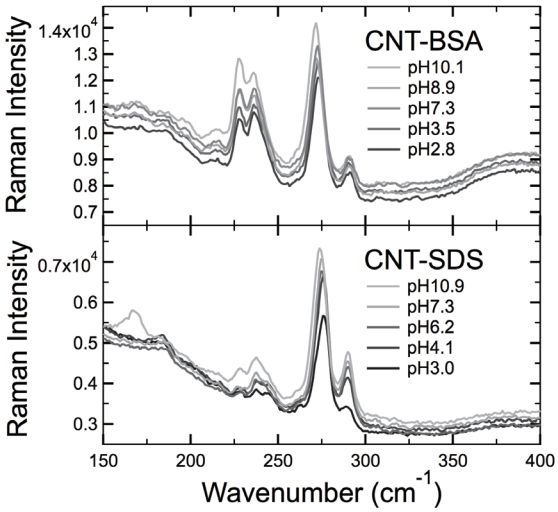

Fig.2 Raman spectra of the CNTs with excitation at 532 nm, which were dispersed by BSA (upper panel) and SDS (lower panel).

[1] Z. Gao *et al*. J. Hazard. Mater. **167**, 357 (2009).

Corresponding Author: A. Hirano
Tel: +81-29-849-1064, Fax: +81-29-861-2786,
E-mail: hirano-a@aist.go.jp

Biodistribution of carbon nanotubes after local implantation of mice

○Eri Hirata[1], Masako Yudasaka[2], Yukari Maeda[1], Takeshi Tanaka[2], Hiromichi Kataura[2], Atsuro Yokoyama [1]

[1] Graduate School of Dental Medicine, Hokkaido University, Sapporo 060-8586, Japan
[2] Nanomaterials Research Institute (NMRI), National Institute of Advanced Industrial Science and Technology (AIST), Tsukuba Central, Tsukuba 305-8565 Japan.

Carbon nanomaterials (CNMs) are used in the development of various functional materials and products as well as in the basic research mainly in engineering field. In addition, due to its high biocompatibility, application to biomaterials is widely expected. We have been studying the application of CNMs to the biomaterials for bone regeneration [1] [2]. These biomaterials are implanted in the bone defects, and the local effect is expected. Many researches have intravenously administered CNMs to examine their kinetics and toxicity. On the other hand, little research on the in vivo kinetics of CNMs implanted locally has been reported.

Therefore, single-walled carbon nanotube (SWNT) [3] were implanted in bone and, in vivo kinetics was observed by near-infrared (NIR) fluorescence imaging (excitation 730 nm, emission >1000 nm) as shown in Fig.1. In NIR region, the light is highly transparent in body and, auto-fluorescence level is low, therefore NIR fluorescence is suitable for bio-imaging. SWNTs in the subcutaneous tissue and medullary cavity were visible.

Fluorescence was observed at the implanted part of SWNTs embedded in the bone marrow cavity, and the fluorescence intensity gradually decreased in 24 hours. Similar results were obtained when SWNTs were implanted subcutaneously in the cranial region. Fluorescence was not observed in any other organs (liver, spleen, lung, etc.) by the whole-body imaging. No fluorescence was observed in the liver tissue section by the NIR microscopy. After 56 days, the fluorescence was weakly but clearly observed at the implanted area. The fluorescence becomes weak with time perhaps because the SWNTs were bundled or adsorbed certain fluorescence-quenching materials in the tissue. These results suggested that locally implanted SWNTs hardly migrated to other organs and remained in the site of implant.

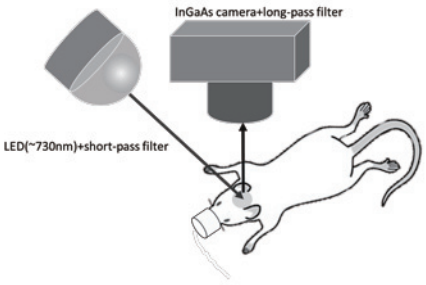

Fig.1 Schematic representation of the imaging setup.

[1] E. Hirata *et al*. Chem. Carbon. **49**, 3284 (2011).
[2] E. Hirata *et al*. Nanoscale. **30**, 14514 (2016)
[3] Y. Yomogida *et al*. Nat. Commun.,**7**, 12056 (2016)
Corresponding Author: E Hirata
Tel: +81-11-706-4270
E-mail: erieri@den.hokudai.ac.jp

Carrier accumulation on functionalized diamond (111) surfaces by an external electric field

○Yanlin Gao, Susumu Okada

Graduate School of Pure and Applied Sciences, University of Tsukuba, Tsukuba, 305-8571, Japan

Diamond has attracted significant interest due to its promising application to the high-power and high-frequency electronic devices arising from its excellent electronic and thermal properties, such as the wide band gap, high thermal conductivity, high breakdown field, and symmetric carrier mobility. Indeed, it has been demonstrated that the diamond surfaces work as the conducting channels of the field effect transistors. In such devices, the surfaces of the diamond are chemically functionalized depending on the environmental conditions. Such surface functionalization certainly affects the electronic properties of the surfaces under carrier injection by the gate electrode. However, microscopic mechanism of the carrier accumulation on the functionalized diamond surface is still unclear. Therefore, in this work, we aim to elucidate the electronic properties of diamond (111) surfaces under the external electric field, of which surfaces are functionalized by H, O, COH, and OH functional groups, based on the density functional theory combined with the effective screening medium method.

Our calculations show that the distribution of accumulated carriers strongly depends on the functional group and carrier species. For the surfaces functionalized by O and COH groups, the electron and hole are mainly induced on the attached functional groups, which causes the almost constant capacitance for the applied gate voltage. In contrast, for both surfaces functionalized by H and OH, hole is injected into the functional groups and C atoms at the vicinity of the surfaces, making the constant capacitances for the positive gate voltage, while electron is spilled over the vacuum region outside the surfaces with the nearly free electron (NFE) nature, since the NFE state shifts downward and crosses the Fermi level by the negative gate voltage and the surface dipole.

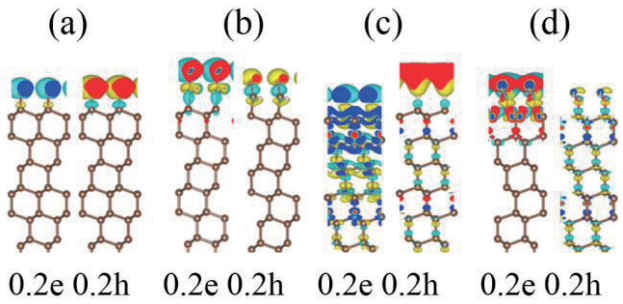

Fig. 1 Isosurfaces of induced carriers on diamond (111) surfaces functionalized by (a) O, (b) COH, (c) H, and (d) OH functional groups under the electric field.

Corresponding Author: Y. Gao
TEL: +81-29-853-5921, FAX: +81-29-853-5924
E-mail: ylgao@comas.frsc.tsukuba.ac.jp

Catalytic Activity of Several Carbons with Different Structures and By-Produced Carbons for Methane Decomposition

○Dai miyamoto[1], Haruki Nishii[1], Yoshito Umeda[2], Hiroaki Hamaguchi[3], Masashi Suzuki[3], Toru Harigai[1], Tsuyoshi Tanimoto[1], Hirofumi Takikawa[1], Yoshiyuki Suda[1]

[1] *Department of Electrical and Electronic Information Engineering, Toyohashi University of Technology, Toyohashi, Aichi 441-8580, Japan*
[2] *Toho Cryogenics Co., Ltd, Nagoya, Aichi 456-0004, Japan*
[3] *Aichi Center for Industry and Science Technology, Toyota, Aichi 470-0356, Japan*

Thermo-catalytic decomposition (TCD) of methane is the attractive hydrogen production process to mitigate CO_2 emissions commonly associated with the conventional processes. However, the problem of the process is catalyst deactivation by carbon deposition. [1] The purpose of this study is to investigate the relationship between the catalysts structure and the catalytic activity of produced carbon during TCD of methane by using four types of carbon catalysts with different structures. Four types of carbon catalysts were tested in the TCD of methane: activated carbon (AC), mesoporous carbon (MC), carbon black (CB), and carbon nanofiber (CNF). Experiments were carried out in a fixed-bed reactor using 1.7 g of the catalysts with space velocity of 360 h^{-1}, at a reaction temperature of 1173 K. The produced gas was analyzed by a hydrogen detector and gas chromatography. Carbon catalysts before and after the experiments were analyzed by Raman spectroscopic analysis. The methane conversion ratio was derived from the following formula using the hydrogen concentration obtained by gas analysis.

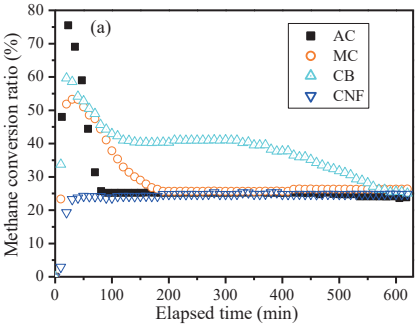

Fig. 1. Temporal change of methane conversion ratios.

$$Methane\ conversion\ ratio = \frac{Produced\ H_2\ concentration}{2 - Produced\ H_2\ concentration} \quad (1)$$

Temporal change of methane conversion ratio of each catalysts is shown in Fig. 1. Methane conversion ratios of all the tested catalysts eventually reached about 25%. We also investigated the temporal change of I_D/I_G that obtained from Raman spectrum of the produced carbon by reaction. I_D/I_G is the intensity ratio of the G band and the D band in Raman spectrum and, it is used to evaluate the degree of graphitization of the carbonaceous material. [2] After 600 min elapsed, I_D/I_G of the produced carbon of all the tested catalysts was about 1.5. Therefore, we found that the produced carbon by reaction shows the same activity and degree of graphitization regardless of the structure of catalysts. We also found that Raman spectroscopy is an effective method for evaluating initial catalytic activity for methane decomposition.

Acknowledgements

A part of this work was supported by "Development project of near-term hydrogen economy forming technology" for priority of research project of Knowledge Hub Aichi. The authors would like to thank K. Asato for emeritus Prof. of Gifu Univ. and H. Yamashita for emeritus Prof. of Nagoya Univ. with discussion about correlation between produced carbon and methane conversion.

[1] Lee Eun Kyoung, *et al*, Carbon., **42**, 12-13, 2641-48 (2004)
[2] L. Malard *et al*, Physics Reports., **473**, 51 (2009).

Corresponding Author: Y. Suda
Tel: +81-532-44-6726
E-mail: suda@ee.tut.ac.jp

Chromatographic Separation of FeCl-Fullerene Complexes

○Yuri Tanuma[1], Seiji Hosoda[2] Toru Maekawa[1,2,3], Takashi Uchida[1,3]

[1] *Graduate School of Interdisciplinary New Science, Toyo University, Kawagoe 350-8585, Japan*
[2] *Faculty of Science and Engineering, Toyo University, Kawagoe 350-8585, Japan*
[3] *Bio-Nano Electronics Research Centre, Toyo University, Kawagoe 350-8585, Japan*

We previously reported the synthesis of iron and chlorine (FeCl)-fullerene complexes, which are supported to posess interesting magnetic properties and be utilised for drug delivery or spintronics, by low energy ion irradiation [1]. For a large scale synthesis of the FeCl-fullerene complexes, we also developed a dc arc discharge setup and confirmed $FeClHC_{60}$ in discharged soot by mass spectrometry [2]. In this study, we focused on high performance liquid chromatography (HPLC) separation of $FeClHC_{60}$ from other components.

FeCl-fullerene complexes were synthesised by an arc discharge using an $FeCl_2$-impregnated carbon anode, as described elsewhere [2]. Soxhlet-refluxed soot solution was investigated by liquid chromatography-mass spectrometry (LC-MS), equipped with a liquid chromatograph (Prominence series, SHIMADZU) and ion trap-type mass spectrograph (amaZon speed -TYU, Bruker Daltonics). We investigated several operational conditions such as columns, mobile phase, oven temperature, and polarity of detected ions to find the optimal conditions for separating FeCl-fullerene complexes.

As a result, FeCl-incorporated C_{60}, which is considered to be $FeClHC_{60}$, eluted earlier than empty C_{60} as shown in Fig.1. Furthermore, the isotopic pattern of the detected $FeClHC_{60}$ showed almost the same feature as the simulated one, as shown in Fig. 2. However, the $FeClHC_{60}$ eluted with unassigned components, as shown in Fig.3. We observed change in relative retention time of the $FeClHC_{60}$ and unassigned components by changing columns and composition of mobile phase, i.e., ratio of *n*-hexane to toluene. We will discuss the separation of the $FeClHC_{60}$ in more detail.

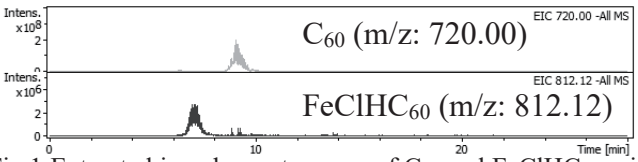

Fig.1 Extracted ion chromatograms of C_{60} and $FeClHC_{60}$ using a buckyprep column and pure toluene mobile phase at 30°C.

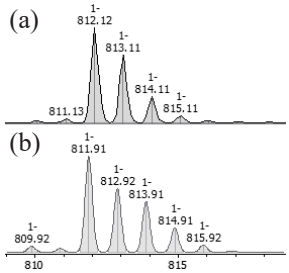

Fig.2 Isotopic distribution patterns of (a) detected and (b) simulated $FeClHC_{60}$.

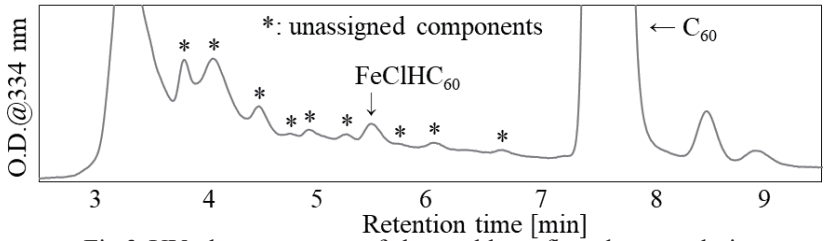

Fig.3 UV chromatogram of the soxhlet-refluxed soot solution.

[1] T. Uchida *et al*. Rev. Sci. Instrum. **87**, 02A720 (2016).

[2] Y. Tanuma *et al*. The 53rd Fullerene-Nanotube -Graphene General Symposium. 2P-6 (2017)

Corresponding Author: T. Uchida, Y. Tanuma
Tel: +81-49-239-1940, Fax: +81-49-239-1940,
E-mail: uchida_t@toyo.jp, s3r101700039@toyo.jp

Separation and Characterization of Sc-dimetallofullerenes: Sc_2C_n(n=76, 78, 80, 82)

○Shun Yoshida, Koichi Kikuchi, Yohji Achiba, Takeshi Kodama

Department of Chemistry, Tokyo Metropolitan University, Tokyo 192-0397, Japan

In the previous symposium, Nakatori et al. reported the production and extraction of Sc_2C_n (n=76, 78, 80) as an anion form [1]. $(Sc_2C_{76})^-$ and $(Sc_2C_{78})^-$ were obtained as a mixture of them because $(Sc_2C_{76})^-$ and $(Sc_2C_{78})^-$ eluted at the almost same retention time in HPLC separation. Therefore, it was suggested that $(Sc_2C_{78})^-$ would not be $(Sc_2@C_{78})^-$ but $(Sc_2C_2@C_{76})^-$. In addition, $(Sc_2C_{80})^-$ was isolated, but its UV-vis-NIR absorption spectrum was different from those of other $(M_2@C_{80}(I_h))^-$ (M=Y, Ce, etc.), so its cage structure could not be determined. Here, we report the partial isolation of $(Sc_2C_{76})^-$ and $(Sc_2C_{78})^-$, and finding $(Sc_2C_{82})^-$. Moreover, the ESR spectrum of $(Sc_2C_{80})^-$ was measured and analyzed.

Sc-dimetallofullerenes were produced by the direct-current arc discharge (60 A) of Sc/C composite rods (Sc:C=2:98) under a 500 Torr He atmosphere. The raw soot was extracted for 8 h with a mixed solvent of triethylamine and acetone. The separation of a mixture of $(Sc_2C_{76})^-$ and $(Sc_2C_{78})^-$ was accomplished by three-stage HPLC using acetone with an ion-pair reagent, tetrabutylammonium bromide (TBABr), as an eluent. On the other hand, the isolation of $(Sc_2C_{80})^-$ or $(Sc_2C_{82})^-$ was accomplished by one-stage HPLC. For $(Sc_2C_n)^-$ (n=76, 78, 80, 82), the UV-vis-NIR absorption spectra were measured. Furthermore, for $(Sc_2C_{80})^-$, the ESR spectrum was also measured at the room temperature.

The UV-vis-NIR absorption spectrum of the isolated $(Sc_2C_{78})^-$ was different from that of $(Sc_2C_{76})^-$. In addition, the UV-vis-NIR absorption spectra of $(Sc_2C_{78})^-$ is different from these of other $(M_2@C_{78}(D_{3h}))^-$ (M=Y, Ce etc.), so the cage structures could not be determined. For the same reason, the cage structure of $(Sc_2C_8)^-$ could not be determined. Fig. 1 shows the UV-vis-NIR absorption spectra of $(Sc_2C_{80})^-$ and $(Ce_2@C_{80}(I_h))^-$. This indicates that $(Sc_2C_{80})^-$ is not $(Sc_2@C_{80}(I_h))^-$ or electronic state of $(Sc_2@C_{80}(I_h))^-$ is different from that of $(Ce_2@C_{80}(I_h))^-$. Fig. 2 showed the ESR spectrum of $(Sc_2C_{80})^-$, which is very complex, and a large number of peaks over 100 was observed although the nuclear spin of Sc is I=7/2. These results suggest that $(Sc_2C_{80})^-$ was consisted of at least two kind of component, which were cage structural isomers or metal position isomers.

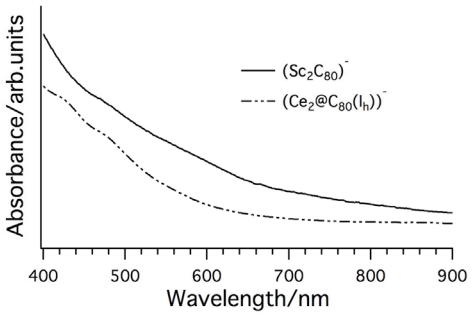

Fig. 1 UV-vis-NIR absorption spectra of $(Sc_2C_{80})^-$ and $(Ce_2@C_{80}(I_h))^-$.

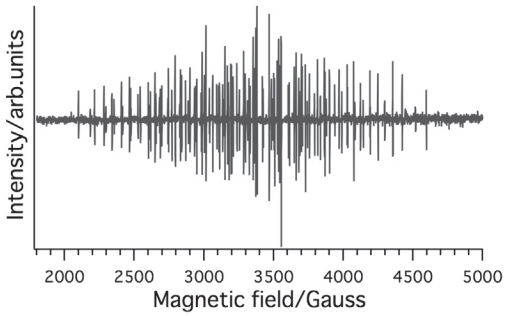

Fig. 2 X-band ESR spectrum of $(Sc_2C_{80})^-$ at 294 K in TBABr/acetone.

[1] N. Nakatori, et al. *The 52nd Fullerenes-Nanotubes-Graphene General Symposium* 27 (2017).

Corresponding Author: Takeshi Kodama
Tel:+81-42-677-2530, Fax:+81-42-677-2525
E-mail: kodama-takeshi@tmu.ac.jp

Crystal structure analysis of $[Li^+@C_{60}](TFSI^-)\cdot CH_2Cl_2$

Kazuhira Miwa[1], Shinobu Aoyagi[1], Hiroshi Okada[2], Hiroshi Ueno[3], Yutaka Matsuo[2,3,4]

[1]*Dapartment of Information and Basic Science, Nagoya City University, Mizuho-ku, Nagoya 467-8501, Japan*
[2]*Dapartment of Mechanical Engineering, School of Engineering, The University of Tokyo, Bunkyo-ku, Tokyo 113-8656, Japan*
[3]*Dapartment of Chemistry, Northeast Normal University, Changchun, Jilin 130024, China*
[4]*Hefei National Laboratory for Physical Sciences at the Microscale, Univarsity of Science and Technology of China, Hefei, Anhui 230026, China*

Endohedral metallofullerenes with electric and magnetic properties have a potential to be used for molecular devices such as molecular memories. Lithium ion endohedral metallofullerene $Li^+@C_{60}$ is commercially available and a promising material for the application. $Li^+@C_{60}$ forms salts with anions such as PF_6^-, and shows a fast response to an alternating electric field by a free rotational motion of the Li^+ cation inside the C_{60} cage [1-3]. The motion of Li^+ cations in the PF_6^- salt $[Li^+@C_{60}](PF_6^-)$ is suppressed at low temperature, and antiferroelectrically ordered below 24 K [3,4]. The antiferroelectric Li^+ ordering is caused by interactions among electric dipole moments formed between the Li^+ cations inside and the PF_6^- anions outside the C_{60} cages. It is expected that the Li^+ cations also show a ferroelectric ordering in a $Li^+@C_{60}$ salt.

As a candidate for a ferroelectric $Li^+@C_{60}$ salt, we investigate a single crystal of $Li^+@C_{60}$ with bis(trifluoromethanesulfonyl)imide ($TFSI^-$) anion in this study. $TFSI^-$ is an asymmetric polar anion, while PF_6^- is a symmetric non-polar anion. The polar $TFSI^-$ anion is a prospective counter anion to obtain a polar ferroelectric $Li^+@C_{60}$ crystal. The solubility of the $TFSI^-$ salt is substantially higher than that of the PF_6^- salt [5]. The dielectric property and crystal structure of the $TFSI^-$ salt would be also rather different from that of the PF_6^- salt.

A single crystal of $[Li^+@C_{60}](TFSI^-)$ was obtained from the dichloromethane (CH_2Cl_2) solution by a vapor diffusion method. The single crystal X-ray diffraction measurement was performed at SPring-8 to determine the crystal structure. A structural phase transition was found below 150 K. The crystal structure analysis revealed that the high-temperature phase at 150 K has an orthorhombic polar structure with the space group of $Pmc2_1$. The crystal contains CH_2Cl_2 solvent molecules with the ratio of $[Li^+@C_{60}](TFSI^-) : CH_2Cl_2 = 1 : 1$. The determined molecular structure is shown in Fig. 1. A complicated orientation disorder of the C_{60} cages in the structure is omitted in the figure. Unfortunately, the Li^+ cations have an antiferroelectric arrangement in the structure despite the polar space group. Further study will reveal the crystal structure in the low-temperature phase and the dielectric property of $[Li^+@C_{60}](TFSI^-)\cdot CH_2Cl_2$.

[1] S. Aoyagi *et al.* Nature Chem. **2**, 678-683 (2010).
[2] S. Aoyagi *et al*. Angew. Chem. Int. Ed. **51**, 3377-3381 (2012).
[3] S. Aoyagi *et al.* J. Phys. Soc. Jpn. **85**, 094605 (2016).
[4] H. Suzuki *et al.* Phys. Chem. Chem. Phys. **18**, 31384 (2016).
[5] H. Okada and Y. Matsuo Fuller. Nanotub. Car. N. **22**, 262-268 (2014).
Corresponding Author: S. Aoyagi
E-mail: aoyagi@nsc.nagoya-cu.ac.jp

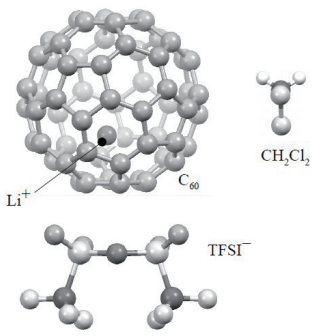

Fig.1 $[Li^+@C_{60}](TFSI^-)\cdot CH_2Cl_2$

Photoreaction of $Sc_3N@I_h$-C_{80} with Disilirane: Formation and Isomerization of 1,2-, 1,3-, and 1,4-Adducts

○Shinpei Fukazawa[1], Yuichi Sato[1], Masahiro Kako[*,1], Masanori Yasui[1], Michio Yamada[2], Yutaka Maeda[2], Takeshi Akasaka[2,3,4]

[1]*Department of Engineering Science, The University of Electro-Communications, Chofu, Tokyo 182-8585, Japan*
[2]*Department of Chemistry, Tokyo Gakugei University, Tokyo 184-8501, Japan*
[3]*Life Science Center of Tsukuba Advanced Research Alliance, University of Tsukuba, Tsukuba, Ibaraki 305-8577, Japan*
[4]*Foundation for Advancement of International Science, Ibaraki 305-0821, Japan*

The functionalization of endohedral metallofullerenes (EMFs) has attracted considerable attention because of their unique structures encapsulating metal atoms and metallic clusters. Until now, many researches of exohedral functionalization of EMFs were conducted to disclose their diverse properties of EMFs, indicating their potential applications in biochemistry, nanomaterials sciences, and molecular electronics [1]. In previous studies, we demonstrated that the photoreaction of $Sc_3N@I_h$-C_{80} with 1,1,2,2-tetramesityl-1,2-disilirane resulted in the formation of 1,2- and 1,4-addition products [2]. The structural and electronic properties of the 1,4-adduct were characterized using spectroscopic, electrochemical, and crystallographic techniques, as well as theoretical calculations. However, those of the 1,2-adduct have not been fully characterized because this compound was not isolated [2]. Recently, similar photoreactions of $Lu_3N@I_h$-C_{80} with disiliranes were reported to produce the corresponding 1,4-adducts. Although high-performance liquid chromatography (HPLC) analysis suggested the formation of less stable intermediates during the photoreactions, further structural analyses of the intermediates were unsuccessful due to their lability [3,4]. These results prompted us to further clarify the addition pattern in the reactions of $Sc_3N@I_h$-C_{80} with disiliranes because the properties of EMF derivatives depend on the regiochemistry of exohedral functionalization. We present a detailed report of the photoreaction of $Sc_3N@I_h$-C_{80} with 2,6-diethylphenyl(Dep)-substituted disilirane **1**, which include adducts **2**, **3**, and **4**, as the 1,2-, 1,3-, and 1,4-adducts, respectively (Scheme 1). In addition, the isomerization between **2** and **3** was observed at 50 °C in $CDCl_3$. At 100 °C, both adducts **2** and **3** were quantitatively converted to **4**. The details of the structural and electronic properties of adducts **2**, **3**, and **4** will be discussed.

Scheme 1.

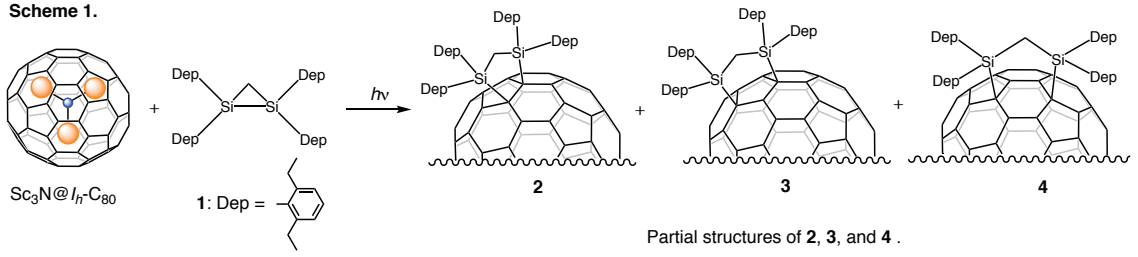

Partial structures of **2**, **3**, and **4** .

[1] L. Dunsch *et al.* Chem. Rev. **134**, 5989–6113 (2013). [2] Y. Iiduka *et al.* J. Am. Chem. Soc. **128**, 9919–9925 (2006). [3] K. Sato *et al.* Org. Lett. **14**, 5908–5911 (2012). [4] M. Kako, *et al.* Chem. Eur. J. **21**, 16411–16420 (2015).

Corresponding Author: Masahiro Kako Tel: +81-42-442-5570 E-mail: kako@e-one.uec.ac.jp

Rotational dynamics of a H_2O molecule encapsulated in a fullerene C_{60} at low temperature

○Hal Suzuki[1], Motohiro Nakano[1], Yoshifumi Hashikawa[2], Yasujiro Murata[2]

[1] *Graduate School of Science, Osaka University, Osaka 560-0043, Japan*
[2] *Institute for Chemical Research, Kyoto University, Kyoto 611-0011, Japan*

Fullerene C_{60} has a highly symmetric (almost spherical) vacancy inside with radius of ~3.7 Å, in which atoms or small molecules can be encapsulated. The encapsulated atoms/molecules are "isolated", so that their dynamics (especially the rotational dynamics) resemble those in the gas phase. It is of our interest how these isolated atoms/molecules behave at low temperature. In our previous works, we have investigated the dynamics of a Li^+ ion encapsulated in a fullerene C_{60} by using terahertz spectroscopy[1] and calorimetry. We revealed that the Li^+ ion is circulating in the C_{60} cage above 100 K, but is localized into two positions below 100 K.

In this work, we have investigated the dynamics of a H_2O molecule encapsulated in a fullerene C_{60} and $C_{60}O$ by heat capacity measurements between 0.6 and 100 K. Fig. 1 shows the heat capacity obtained for $H_2O@C_{60}$ in a double logarithmic plot. A broad peak is observed at ~ 1 K, which becomes smaller as the sample is annealed at 2.5 K for several tens of hours. Based on the previous spectroscopic works[2], it is concluded that the peak corresponds to the excitations between the split sublevels of the triplet ground rotational (*ortho*-) states of the H_2O molecule. The annealing effect is explained to be due to the nuclear spin conversion from the triplet (*ortho*-) to the singlet rotational (*para*-) state. Kinetics of the *ortho*-/*para*- conversion was investigated through the time variation in heat capacity, and two relaxation components were found: τ_1 ~ 6,000 s and τ_2 ~ 47,000 s at 1.8 K (Fig. 2). Heat capacity of $H_2O@C_{60}O$ also showed a broad peak at ~1 K, however the relaxation phenomenon due to the nuclear spin conversion was found to be very slow compared with that of $H_2O@C_{60}$. It was indicated that the dipole moments of the epoxide group in the carbon cage significantly affect the conversion rate of the H_2O molecule.

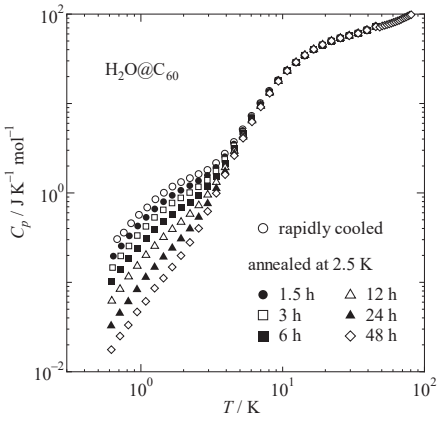

Fig. 1 Heat capacity of $H_2O@C_{60}$

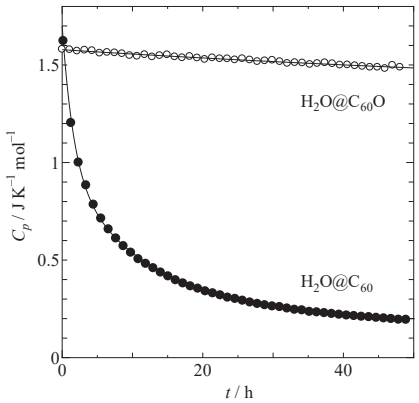

Fig. 2 Time variation in heat capacity of $H_2O@C_{60}$ and $H_2O@C_{60}O$

[1] H. Suzuki *et al*. Phys. Chem. Chem. Phys., **18**, 31384 (2016).
[2] C. Beduz, *et al.*, Proc. Natl. Acad. Sci. USA, **109**, 12894 (2012).

Corresponding Author: H. Suzuki
Tel: +81-6-6850-5526, Fax: +81-6-6850-5526,
E-mail: h_suzuki@chem.sci.osaka-u.ac.jp

Electronic structure of carbon nanotube thin films under an external electric field

Donghao Wang and Susumu Okada

Graduate School of Pure & Applied Sciences, University of Tsukuba, Tsukuba 305-8571 Japan

Individual and mat structures of carbon nanotubes (CNTs) can work as conducting channels of flexible electronic devices. In such devices, CNTs intrinsically feel the external electric field, which affect their electronic properties. Several theoretical works have elucidated fundamental properties of individual CNT under the external electric field. On the other hand, it is still unclear a microscopic insight into the electronic properties of CNT thin films under the external field, which are essential in the CNT-based electronic devices under the operation. Thus, in this work, we aim to elucidate the electronic properties of CNT thin films with the bilayer structure of (12,0), (13,0), (14,0), (15,0), (16,0), and (17,0) CNTs under the external electric field, using the density functional theory combined with the effective screening medium method. In particular, we give clarify how the electronic properties depend on the CNT combination.

Our calculations showed that the electrostatic properties in CNT thin films strongly depend on the electric field and constituent CNT species. We found the induced electric filed of which direction is opposite to the applied electric field for the thin film consisting of (12,0) and (15,0) CNTs under the electric field of 0.2 V/A (Fig. 1). In contrast, inversion filed is absent in the thin films comprising metallic and semiconducting CNTs and semiconducting CNTs.

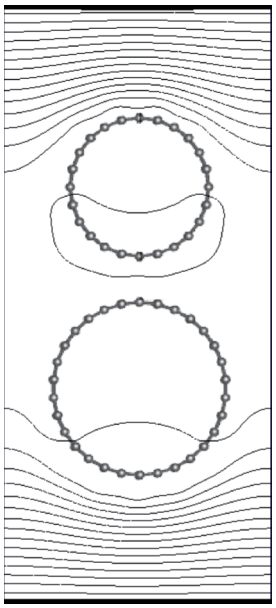

Fig.1 Electrostatic potential of the CNT thin film consisting of (12,0) and (15,0) CNTs under the external electric field.

Corresponding authors: Donghao Wang and S. Okada
E-mail: sokada@comas.frsc.tsukuba.ac.jp

Structural Isomer-induced spectral changes in near infrared photoluminescence of locally-functionalized single-walled carbon nanotubes

○Tomohiro Shiraki[1,2], Shunsuke Uchimura[1], Tomonari Shiraishi[1], Fumiyuki Toshimitsu[2], Naotoshi Nakashima[2]

[1] *Graduate School of Engineering, Kyushu University, Fukuoka 819-0395, Japan*
[2] *WPI-I2CNER, Kyushu University, 744 Motooka, Fukuoka 819-0395, Japan*

Defect doping to semiconducting single-walled carbon nanotubes (SWNTs) is a key approach to produce new near infrared photoluminescence (NIR PL) properties. Therein, the doping achieves local functionalization of the tubes that provides red-shifted PL with enhanced quantum yields (E_{11}*) in comparison to the PL (E_{11}) of the pristine SWNTs.[1-8] In the locally functionalized SWNTs (lf-SWNTs), diazonium chemistry allows us to introduce various chemical structures of the aryl groups on the doped site and, as a result, it is found that the chemical structures of the modified molecules play an important role to determine and control the E_{11}* PL wavelengths and their functionalities. For example, we have succeeded in generation of remarkably red-shifted PL on the basis of proximal modification using synthesized bisdiazonium compounds [5] and development of dynamic wavelength shift systems driven by molecular recognition using saccharide binding with introduced phenylboronic acid groups at the doped sites [6].

Here, we report a new structural factor of structural isomers that modulate the E_{11}* PL properties of the aryl functionalized lf-SWNTs; that is, when positional isomeric structures of the substituted aryl groups are introduced for the doped sites of lf-SWNTs (Fig. 1), we observe significantly different PL of these lf-SWNTs from that of typical para-aryl modified lf-SWNTs.[8] The meta-aryl modified lf-SWNTs show deviation from the reported liner relationship between the Hammett substituent constants and $\Delta E = E_{11}$*-E_{11} of the para-aryl modified lf-SWNTs. For the ortho-aryl modified lf-SWNTs, two PL peaks are generated by the functionalization and one of them appears in the largely red-shifted region compared to typically observed E_{11}* PL.

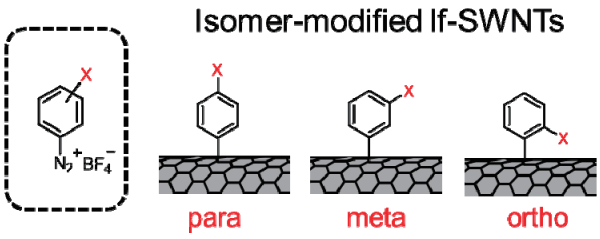

Fig. 1 Structure images of the synthesized diazonium compounds and the prepared isomer modified lf-SWNTs.

The present findings, therefore, are expected to provide new designs for the PL modulation of lf-SWNTs on the basis of the molecular structures of modifiers, which should lead to the development of novel nanomaterials whose NIR PL properties are applicable to advance photonic devices and bio/medical diagnostic tools.

[1] R. B. Weisman *et al.*, Science, **330**, 1656 (2010); [2] Y. Miyauchi *et al.*, Nat. Photon., **6**, 715 (2013); [3] G. C. Schatz and Y. Wang *et al.*, J. Am. Chem. Soc., **138**, 6875 (2016); [4] Y. Maeda *et al.*, Nanoscale, **8**, 16916 (2016); [5] T. Shiraki and N. Nakashima *et al.*, Sci. Rep., **6**, 28393 (2016); [6] T. Shiraki and N. Nakashima *et al.*, Chem. Commun., **52**, 12972 (2016); [7] T. Shiraki and N. Nakashima *et al.*, Nanoscale, **9**, 16900 (2017); [8] T. Shiraki and N. Nakashima *et al.*, Chem. Commun., **53**, 12544 (2017)

Corresponding Author: T. Shiraki
Tel: +81-92-802-2841, Fax: +81-92-802-2840
E-mail: shiraki.tomohiro.992@m.kyushu-u.ac.jp

Response of Localized Carriers to Terahertz Radiation in a Carbon Nanotube Film

○Takuya Okamoto[1], Naoki Fujimura[1], Xiaowei He[2], Weilu Gao[2], Junichiro Kono[2,3,4], and Yukio Kawano[1]

[1] *FIRST, Tokyo Institute of Technology, Tokyo 152-8552, Japan*
[2] *Department of Electrical & Computer Engineering, Rice University, Houston, Texas, USA*
[3] *Department of Physics & Astronomy, Rice University, Houston, Texas, USA*
[4] *Department of Materials Science & NanoEnginnering, Rice University, Houston, Texas, USA*

Carbon nanotubes (CNTs) exhibit significant ultrabroadband absorption from the microwave to the ultraviolet range. They can be used to build a sensitive detector that works at room temperature in the terahertz (THz, 10^{12} Hz) band [1]. However, at low temperatures, carrier localization occurs due to the presence of disorder such as intertube potential barriers, impurities, and random chiralities. To improve the performance as a THz detector, it is required to deeply understand the interaction of such localized carrier with THz waves.

In this work, we have investigated electrical transport properties of a highly aligned p-n junction single-wall CNT film under THz irradiation. We first measured the resistance of this sample as a function of temperature, T, in a range between 2.86 K and 295 K. With decreasing T, the resistance drastically increased at about 10 K, as shown in Fig. 1(a), indicating a transition from fluctuation-induced tunneling (FIT) to two-dimensional variable range hopping (2D-VRH) transport.

To understand how THz irradiation affects this VRH transport, we performed magnetoresistance (MR) measurements under THz irradiation at 3 K (Fig. 1(b)). The dark MR showed a negative conductance correction, which is a typical VRH behavior. THz irradiation then modified this MR curve in a strongly frequency-dependent manner. At high frequencies (2.52 and 3.11 THz), irradiation shifted up the MR curve, whereas low frequencies (1.39 and 1.63 THz) irradiation shifted down the MR curve. Through a fitting analysis [2], we estimated the localization length to be 8 nm at zero frequency and 12 nm at 1.63 THz, as shown in Fig. 1(c). These results lead us to conclude that the THz waves directly affected the conduction mechanism of localized carriers, providing a first step toward not only a high-sensitivity THz detector but also new functional THz devices.

[1] X. He *et al*., Nano Lett. **14**, 3953-3958 (2014). [2] U. Sivan *et al*., Phys. Rev. Lett. **60**, 1566 (1988).
Corresponding Author: Y. Kawano Tel & Fax: +81-3-5734-2542 E-mail: kawano@pe.titech.ac.jp

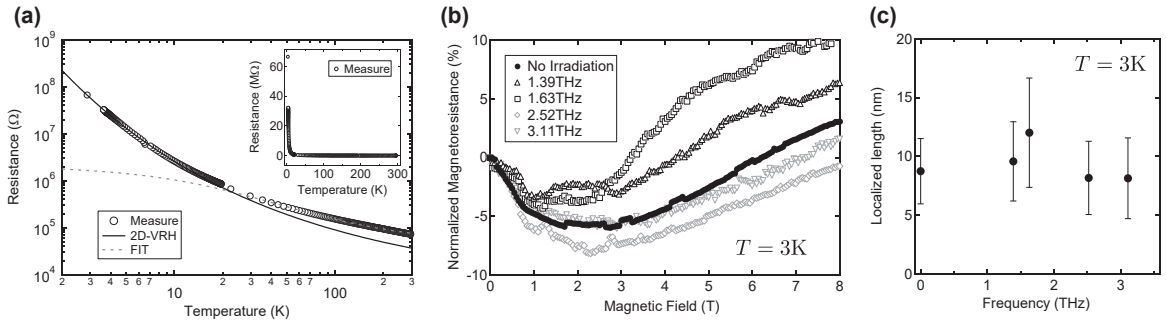

Fig.1 (a) Temperature dependence of the resistance. Inset: non-logarithmic plot. (b) Magnetoresistance with/without various-frequency THz irradiation at 3 K. (c) Localization length as a function of frequency.

Exciton effect of circular dichroism in single-wall carbon nanotubes

○Yuya Iwasaki and Riichiro Saito

Department of Physics, Tohoku University, Sendai 980-8578, Japan

Circular dichroism (CD) is defined by a difference of optical absorption for left- and right-handed circular polarized light. Recently, measurements of the CD spectra for single chirality of single-wall carbon nanotubes (SWNTs) are reported in separation of an enantiomer for a pair of chiralities by the agarose gel column chromatography method [1] and the two-phase method with DNA [2]. Sato, *et al.* [3] shows analytic and numerical calculations of CD spectra of SWNTs based on electron-photon interaction by the tight binding method. They explained the structure of CD spectra and chirality dependence for metal and semiconductor SWNTs. However, they cannot discuss CD value quantitatively because their calculations do not consider exciton effects. Exciton effects in low dimensional materials are strong due to confinement of electrons and holes in the systems. By the exciton effect, optical absorption of SWNTs for E_{11}, E_{22}, E_{12} and so on are enhanced, but the enhancement factors for these peaks may be different one by one [4,5].

In order to discuss the exciton effect of the CD in SWNTs quantitatively, we improve the program to calculate the CD spectra of SWNT including exciton effects by the tight binding method. The optical absorption intensity, which is given by the Fermi golden rule, is proportional to square of the matrix element. We obtain the exciton-photon matrix elements from the exciton wave function calculated by the Bethe-Salpeter equation (BSE) [4,5]. The BSE is used to make exciton wave function by a superposition of the electron and hole wave functions.

In this presentation, we present analytical formula for the CD of SWNTs including exciton effects and show numerical calculated results. We compare the calculated results with experiments, and also with previous CD spectra which does not consider the exciton effects. We also evaluate how much the exciton effect comes out.

[1] X. Wei *et al*., Nat. Comm. **7**,12899 (2016)
[2] G. Ao et al., JACS **138**, 16677 (2016)
[3] N. Sato *et al*., Phys. Rev. B. **95**, 155436 (2017)
[4] J. Jiang *et al*., Phys. Rev. B. **75**, 035407 (2007)
[5] J. Jiang e*t al*., Phys. Rev. B. **75**, 035405 (2007)

Corresponding Author: Yuya Iwasaki
Tel: +81-22-795-6442, Fax: +81-22-795-6447,
E-mail: iwasaki@flex.phys.tohoku.ac.jp

Semiconducting Carbon Nanotubes as Charge-transporting Grain Boundary Protector of Perovskite Solar Cells

○Seungju Seo[1], Il Jeon [1], Zhang Hao[1], Takeshi Tanaka[2], Hiromichi Kataura[2], Yutaka Matsuo[1,3], Shigeo Maruyama [1,4]

1 Department of Mechanical Engineering, The University of Tokyo, Tokyo 113-8656, Japan
2 Nanomaterials Research Institute, National Institute of Advanced Industrial Science and Technology (AIST), Tsukuba, Ibaraki, 305-0046, Japan
3 Hefei National Laboratory for Physical Sciences at the Microscale, University of Science and Technology of China, Hefei, Anhui 230026, China
4 Energy NanoEngineering Lab, National Institute of Advanced Industrial Science and Technology(AIST), Ibaraki 305-8564, Japan

After the demonstration of prototype liquid-junction perovskite solar cells (PSCs), organo-lead halide perovskite photovoltaics research has gained momentum with the achievement of the solid-state PSCs in 2012. High absorption coefficient, long-range diffusion length and high defect tolerance of PSCs enable remarkable certified power conversion efficiencies (PCEs) over 20%. Although PSCs are proven to be promising next-generation solar devices, further breakthroughs in terms of efficiency and stability are necessary to supersede silicon solar cells. With regard to the performance and stability of PSCs, perovskite grain boundaries play a significant role. Structural disorders at these boundaries induce shallow trap states and non-radiative recombination of localised charge carriers which serve as limitations to PSC performance. At the same time, these areas are also responsible for the perovskite degradation, as the reaction with moisture in air has been found to initiate from the grain boundaries. Therefore, technologies aiming at large perovskite grains with protected boundaries are highly desired.

Over the last two decades, carbon nanotubes have generated a lot of excitement among researchers for their device applicability. Especially, single-walled carbon nanotubes (SWNTs) show an exceptional charge carrier property with outstanding chemical and mechanical stability, which is an ideal quality for electronic components. Depending on the chirality of SWNTs, they can possess either semiconducting or metallic properties. Semiconducting SWNTs (s-SWNTs) have a wide range of direct bandgap of up to 2 eV, qualifying for a light-harvesting medium with strong absorption and high carrier mobility. Because carbon nanotubes have high conductivity along the tube axis, s-SWNTs can function effectively, not only as a light-harvester, but also as a charge-transporter between perovskite grains. While there have been a few reports on phenyl-C61-butyric acid methyl ester (PCBM) as a charge-transporter at the grain boundaries of perovskite films, fullerenes have inherently low carrier mobility and low stability compared to SWNTs. It is demonstrated that hydrophobic and air-stable SWNTs can protect the perovskite layer successfully from the oxygen and moisture.

Here, we fabricated PSCs in which s-SWNTs are located at the perovskite boundaries, functioning as a charge-transporter, light-harvester, and protector from air. By incorporating aqueous s-SWNTs into the perovskite solution, we produced perovskite films containing large crystal grains with s-SWNTs in between. By adding a small amount of deionised water to the perovskite solution, 18.0% PCE of the reference PSCs increased to 19.0% due to the increased perovskite grain size arising from favourable vapour pressure of the solvent. Upon addition of s-SWNTs, the PCE further increased with improved hysteresis and air/light stability.

Corresponding Author: S. Maruyama
Tel: +81-3-5841-6421, Fax: +81-3-5841-6421,
E-mail: maruyama@photon.t.u-tokyo.ac.jp

Fabrication and characterization of self-aligned carbon nanotube thin film transistors

○Taiga Kashima[1], Tomoki Matsuura[1], Jun Hirotani[1], Shigeru Kishimoto[1], and Yutaka Ohno[1,2]

[1]*Department of Electronics, Nagoya University, Nagoya 464-8603, Japan*
[2]*Institute of Material and Systems for Sustainability, Nagoya University, Nagoya 464-8603, Japan*

Carbon nanotube thin film transistors (CNT TFTs) are promising active component for flexible electronics because of high carrier mobility and excellent mechanical flexibility. In recent years, it has become possible to fabricate CNT TFTs with high yield and uniform characteristics by using purified semiconductor CNTs. This would lead to the realization of functional integrated circuits of CNT TFTs. For flexible electronics applicatoins, devices are fabricated on the plastic substrate, which is likey to expand or shrinks in size during the fabrication process. Then, a large alignment margin in lithography process is necessary. This results in the degradation of operation speed of the circuits due to the large orverlap capacitances between the source/drain and the gate electrodes. In this study, we have fabricated CNT TFTs by self-alignment process, and confirmed drastic reduction of parasitic capacitance.

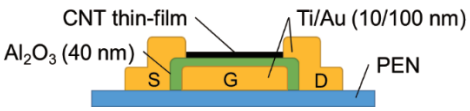

Fig. 1 Schematic device structure of self-aligned CNT TFT.

Figure 1 shows the structure of the self-aligned CNT TFT fabricated on the flexible substrate. The device has a bottom gate structure. The source and drain electrodes were self-aligned to the gate electrode by exposing UV light from the backside of the substrate in the lithography process.

The gate-capacitance verus gate-voltage (*C*-*V*) characteristics of the fabricated CNT TFTs with channel length (*L*) and channel width (*W*) of 100 μm is shown in Fig. 2. The capacitance at off state was reduced by a factor of 1/20 by introducing the self-alignment process, compared to the conventional process. In addition, since the driving current of the self-aligned CNT TFTs were comparable to that of the conventional devices. These results show that the operation speed of circuits can be improved by introducing the self-alignment process.

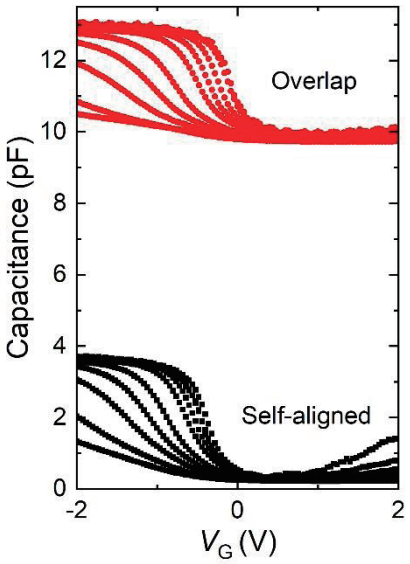

Fig. 2 *C*-*V* characteristics.

Acknowledgments: The semiconducting CNTs were provided by TASC. This work was partially supported by JST/CREST.

Corresponding Author: Yutaka Ohno, Phone & Fax: +81-52-789-5387, E-mail: yohno@nagoya-u.jp

CNT Supported Mn-doped ZnO Nanoparticles as Efficient Visible Light-Active Photocatalyst for Malachite Green Dye Degradation

○Ahmed Shawky[1,*,^], Reda M. Mohamed[1,2], I. A. Mkhalid[2]

[1] *Nanomaterials and Nanotechnology Department, Central Metallurgical R & D Institute, 11421 Helwan, P.O. Box, 87 Cairo, Egypt*
[2]*Chemistry Department, Faculty of Science, King Abdulaziz University, P.O. Box 80200, Jeddah 21589, Saudi Arabia*

Photocatalysis is photoreaction process occurs in the presence of semiconducting material resulting an electron-hole pair generation. These carriers are able to generate a free radical (e.g. OH·, O·) that can undergo secondary reactions. ZnO is well-known photocatalyst long time ago. However, the large band gap (~3.2 eV) and low surface area (40~50 m^2g^{-1}) are major problems for the real industrial applications. Doping of ZnO of transition metal (e.g. Mn) is one of effective ways to reduce the band gap to be applied in the visible light. On the other hand, Carbon nanotubes (CNT) represents an excellent carbon member in terms of optoelectronic properties and surface texture in which can introduce a higher surface area into ZnO. Moreover, CNT can enhance the photocatalytic activity due to the development of electron transfer from the surface of ZnO conduction band and reduce charge recombination.

In this regard, we introduce our recent work on in situ incorporation of CNT into Mn-doped ZnO nanoparticles that prepared through simple precipitation. It was found that the doping as well as the CNT induce a decrease of the band gap of ZnO and improve the charge transfer according to absorbance and photoluminescence spectroscopy measurements. The photocatalytic activity was applied for the degradation of Malachite green (MG) dye as an industrial model. The degradation efficiency reached up to 94% after just one hour under the ordinary bulb light. The effect of doping ZnO and adding CNT on the crystalline structure, surface texture, optical and electronic properties of the photocatalyst as well as the photocatalytic mechanism (See Fig. 1) and degradation kinetics will be presented in some details.

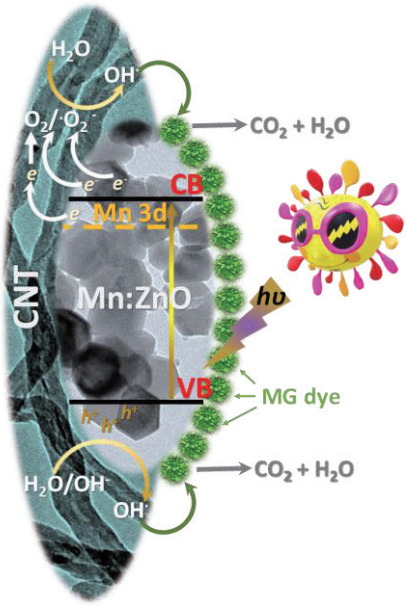

Fig. 1- Proposed photocatalytic mechanism for degradation of MG dye.

*Corresponding Author: Ahmed Shawky
^Current address: Department of Mechanical engineering, The University of Tokyo
7 Chome-3-1 Hongō, Bunkyō-ku, Tōkyō-to 113-0033, Tokyo, Japan
Tel: +81-80-9863-3037, Fax: +81-3-5800-6983,
E-mail: ahmed@photon.t.u-tokyo.ac.jp, phyashawky@gmail.com

Rapid and Efficient Removal of Water Soluble Polymers from ATP-extracted Semiconducting Single-Wall Carbon Nanotubes

○Kazuki Ueno[1], Haruka Omachi[1,2], Tomohiko Komuro[1], Jun Hirotani[3], Yutaka Ohno[3,4], Hisanori Shinohara[1,5]*

[1] Graduate School of Science, Nagoya University, Nagoya Nagoya 464-8602, Japan [2] Research Center for Materials Science, Nagoya University, [3] Graduate School of Engineering, Nagoya University, [4] Institute of Materials and Systems for Sustainability, and [5]Institute for Advanced Research, Nagoya University

Semiconducting single-wall carbon nanotubes (s-SWCNTs) are promising materials for electronic devices because of its high electronic mobility, mechanical durability, and so on. Recently, we developed a rapid and single-step aqueous two phase (ATP) extraction of highly enriched s-SWCNTs[1]. However, enriched s-SWCNT dispersion contained much amount of water-soluble polymers which caused the aggregation of s-SWCNTs and normally-on state of thin film transistor (TFT).

In this work, we accomplished rapid removal of water-soluble polymers from s-SWCNT dispersion. By mixing with halogenated solvent CH_2Cl_2, polyethylene glycol (PEG) was immediately precipitated out. ^{1}H NMR spectra indicate >99% of PEG polymer was removed (Fig. 1a). TFT measurements were also carried out and fabricated devices exhibits a high on/off ratio (>10^5) with normally-off state (Fig. 1b).

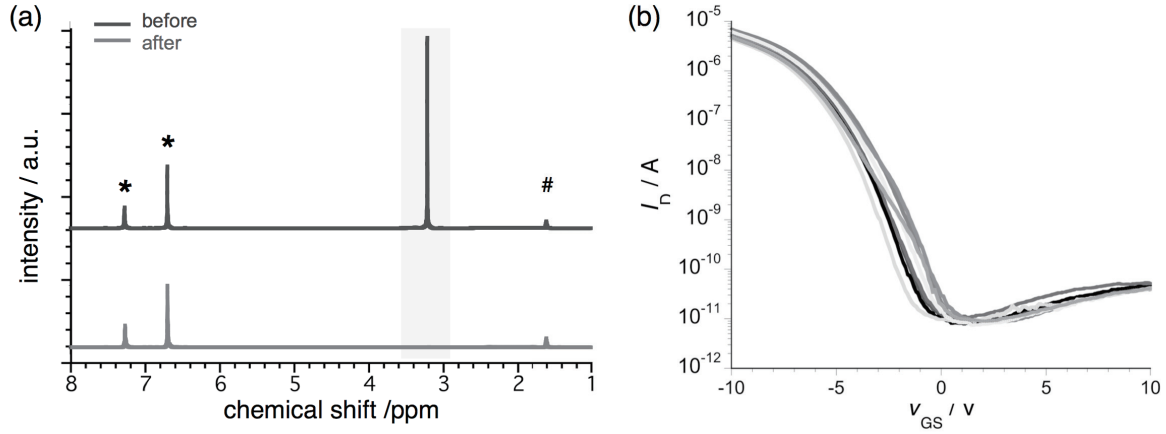

Fig.1 (a) ^{1}H NMR spectra of s-SWCNT dispersion before and after the treatment with CH_2Cl_2. Imidazole was used as internal standard (*) and peaks of acetonitrile solvent were observed at 1.92 ppm (#). (b) Transfer characteristics of thin film transistors using PEG-removed s-SWCNT dispersion (channel length = 100 μm, V_{ds} = –5 V).

[1] Omachi, H.; Shinohara, H. JP Patent 2017-066945.

Corresponding Author: Hisanori Shinohara
Tel: +81-52-789-2482, Fax: +81-52-747-6442
E-mail: noris@nagoya-u.jp

Computational Design for Thermoelectric Properties of Carbon Nanotubes Modified by Diazonium Salts

○Nayu Araki[1] and Takahiro Yamamoto [1]

[1] *Department of Electrical Engineering, Tokyo University of Science, Tokyo 125-8585, Japan*

Carbon nanotubes (CNTs) are expected to be high-performance thermoelectric materials with a large thermoelectric power factor [1]. However, the thermoelectric efficiency of a CNT is not so high because it has a high thermal conductivity. It is thus essential to develop experimental techniques to reduce the thermal conductivity of a CNT with maintaining the Seebeck coefficient and electrical conductivity. Recently, several techniques to reduce the thermal conductivity of a CNT have been theoretically proposed [2,3]. On the other hand, CNTs modified by a diazonium salt is hopeful for such a purpose since sp^3 bonding by a diazonium salt could lower thermal conductivity. In fact, it is experimentally shown that the thermal conductivity of CNTs is decreased by chemical modification of diazonium salts and eventually a figure of merit, ZT, for the thermoelectric efficient is succeeded to increase [4]. However, the details of influence of thermoelectric properties of CNTs by chemical modification of diazonium salts have not clarified yet. In addition, the optimal density of diazonium-salt modification has not been known.

In the present study, we thus investigate thermoelectric properties of CNTs modified by diazonium salts using the NEGF+DFT method [5]. One example of a simulation model is shown in Fig1. We calculated the electrical conductivity and Seebeck coefficient of a (10,0) CNT by changing the number of benzene rings, *i.e.*, the coverage of absorbed diazonium salts. Furthermore, we also calculated a thermoelectric power factor. In the presentation, we discuss the details of thermoelectric properties of CNTs modified by a diazonium salts and present the optimal coverage of absorbed diazonium salts.

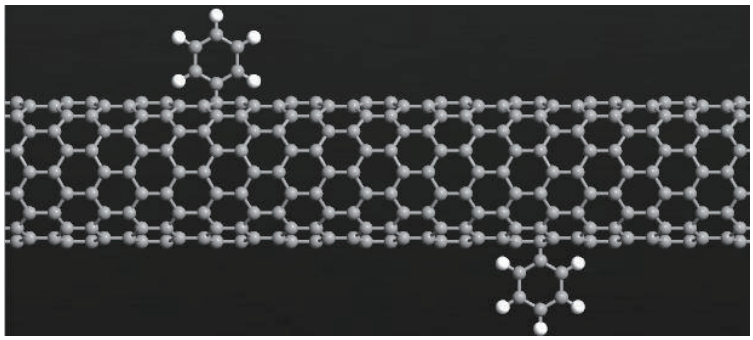

Fig 1: One example of two benzene rings modified a (10,0) CNT

[1] Y. Nakai, *et al*, Appl. Phys. Express **7**, 025103 (2014).
[2] T. Yamamoto, K. Sasaoka and S. Watanabe, Phys. Rev. Lett. **106**, 215503 (2011).
[3] M. Ohnishi, T. Shiga and J. Shiomi, Phys. Rev. B **95**, 155405 (2017).
[4] T. Fujigaya, *et al*., The 78th JSAP Autumn Meeting 2017 (7a-C22-9).
[5] https://quantumwise.co.jp/

Corresponding Author: T. Yamamoto
Tel: +81-3-5876-1492
E-mail: takahiro@rs.tus.ac.jp

Successive deposition of Al_2O_3, Fe and CNT forest by mist CVD

○Toshiya Kinoshita[1], Motoyuki Karita[2], Takayuki Nakano[2], Yoku Inoue[2], Hirokazu Nagaoka[3]

[1] *Graduate School of Science and Technology, Shizuoka Univ., Hamamatsu 432-8561*
[2] *Department of Electronics and Material Science, Shizuoka Univ., Hamamatsu 432-8561*
[3] *JNC Petrochemical Corp., Ichihara, 290-8551*

High density carbon nanotube (CNT) forest have been studied for various practical applications, such as interconnect, thermal interface material, super capacitor, lithium ion battery electrode, gas sensor and dry-spinning assembly. In these materials, CNT forest height (CNT length), areal density, diameter, wall number and crystal quality, play important roles. It is essential to control precisely catalyst formation and catalyst support layer during CNT chemical vapor deposition (CVD) to control these structural properties. We developed an *in-situ* CNT synthesis method on a substrate by mist CVD, including Al_2O_3 layer deposition, Fe catalyst nanoparticle formation and CNT growth. In this study, effects of mist-deposited Al_2O_3 support layer during *in-situ* CNT synthesis were investigated to control these CNT properties.

CNTs were grown on oxidized Si wafer by mist CVD method. In the synthesis procedure, Al_2O_3 support layer was first formed by flowing Al(III) acetylacetonate ($Al(acac)_3$)/ethanol mist generated by ultrasonic nebulizer. The mist was supplied with a carrier gas of Ar onto the substrate. Then, to form Fe catalyst nanoparticles on the support layer, the mist was switched to another mist formed from ferrocene/ethanol. After these depositions, acetylene was flown to grow CNT. Effects of the Al_2O_3 support layer were investigated at various thickness prepared by varying $Al(acac)_3$/ethanol mist deposition time.

Scanning electron microscopy (SEM) and transmission electron microscopy (TEM) images of grown CNTs on SiO_2 with no Al_2O_3 deposition and on mist-deposited Al_2O_3 layer are shown in Fig. 1 (a) and (b), respectively. In the case of no Al_2O_3 layer, spaghetti-like multi-walled CNTs (MWCNTs) with mean diameter of 9.5 nm and areal density of 3.6×10^{10} cm^{-2}, were grown. On the other hand, long and dense MWCNT forest with mean diameter of 7.0 nm and areal density of 7.0×10^{10} cm^{-2} was grown on mist-deposited Al_2O_3 layer with 6.0 nm in thickness. The Al_2O_3 thin layer made catalyst life time 10 times longer. In addition, as can be seen in TEM images, the CNTs on the Al_2O_3 resulted in smaller diameter and fewer wall number than on the SiO_2. These results indicate possibilities that the mist-deposited Al_2O_3 layer has effects on improvement of catalyst life time and suppression of catalyst nanoparticles agglomeration.

Corresponding Author: Toshiya Kinoshita
Tel: +81-53-478-1107, Fax: +81-53-478-1356
E-mail: kinoshita@cnt.eng.shizuoka.ac.jp

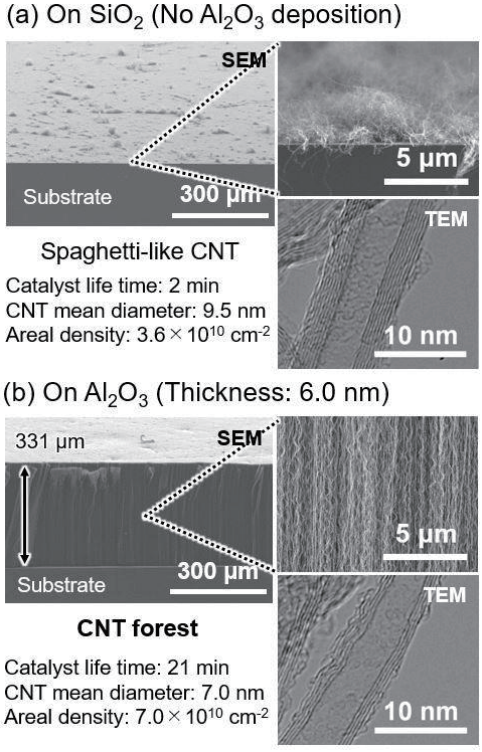

Fig. 1 SEM and TEM images of grown CNT on (a) SiO_2 with no Al_2O_3 mist deposition and (b) Al_2O_3 (6.0 nm in thickness).

Controlled Growth of Single-walled Carbon Nanotubes Using Graphene Oxide/$CoWO_4$ Hybrids as Catalyst Precursors

○Xiyan Liu, Feng Yang, Yan Li*
College of Chemistry and Molecular Engineering, Peking University, Beijing 100871 China

Preparation of the uniform and well-dispersed catalysts is crucially important for the controlled growth of single-walled carbon nanotubes on substrates [1]. Tungsten-based intermetallic catalyst with high melting points can act as the structural templates for chirality specific growth of SWNTs [2-4]. Graphene oxide (GO) have been widely used as dispersants and templates to prepare well-dispersed nanoparticles on surface [5].

Here, we used GO/cobalt tungstate hybrids as the catalyst precursors instead of the previously used molecular clusters to prepare tungsten-cobalt catalysts. The as-prepared catalyst precursors are well dispersed on the GO platforms with uniform size. The intermetallic W_6Co_7 structure of the catalysts after the annealing and reduction process was confirmed by X-ray diffraction (XRD) and high-resolution transmission electron microscopy (HRTEM). The SWNTs grown on W_6Co_7/GO platforms possess a uniform diameter. Semiconducting species of high purity were prepared at suitable conditions.

[1] M. Li, Y. Li *et al.* Top. Curr. Chem. **375**, 29 (2017).
[2] F. Yang, Y. Li *et al.* Nature **510**, 522 (2014).
[3] F. Yang, Y. Li *et al.* Acc. Chem. Res. **49**, 606 (2016).
[4] F. Yang, Y. Li *et al.* ACS Nano, **11**, 186 (2017).
[5] H. Wang, H. Dai *et al.* J. Am. Chem. Soc., **132**, 13978 (2010).
Corresponding Author: Yan Li
Tel: +86-10-6275-6773
E-mail: yanli@pku.edu.cn

Development of Interpenetrating Polymer Network Gel for the Separation of Single-Wall Carbon Nanotubes

○Guowei Wang, Takeshi Tanaka, Atsushi Hirano, and Hiromichi Kataura

Nanomaterials Research Institute, National Institute of Advanced Industrial Science and Technology (AIST), Tsukuba, Ibaraki 305-8565, Japan

Gel column chromatography has shown the potential for the large-scale metal/semiconductor (M/S) separation and further single-chirality separation of single-wall carbon nanotubes (SWCNTs) [1]. This method utilizes commercial dextran gel with three-dimensional structure as the separation medium. A highly reusable gel is desired for the sustainable SWCNT separation. However, the permanent trapping of various carbon species inside the gel causes the gel fouling. As a result, the separation efficiency of a gel decreases gradually with increasing number of reuse cycles.

In this study, we aim to synthesize a highly regenerable separation gel by introducing an interpenetrating polymer network (IPN) structure. This IPN gel contains two partially interlaced but not covalently bonded polymer networks: dextran network and poly (acrylic acid) network. The IPN gel can efficiently separate pristine HiPco SWCNTs to the M- and S-fractions (Fig. 1). This demonstrates that the dextran network in the IPN gel works as well as the dextran network in a commercially available gel does. At the same time, the poly (acrylic acid) network is highly pH responsive, enabling the easy controlling of the gel pore size. This function could be used for eluting all carbon species in the gel and regenerate the gel by increasing the pore size in the elution step.

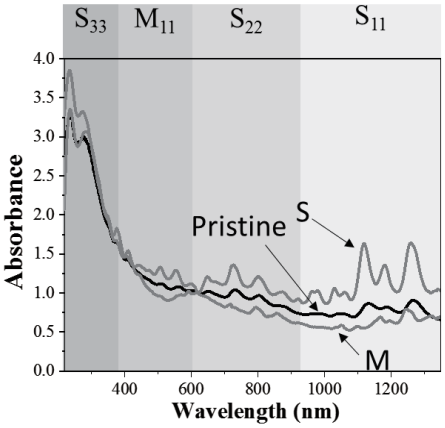

Fig. 1. Optical absorption spectra of pristine HiPco SWCNTs and separated M- and S-SWCNTs using IPN gel.

This work was supported by KAKENHI No. 25220602.

[1] H. Liu *et al*. Nat. Commun. **2**, 309 (2011).

Corresponding Author: H. Kataura
Tel: +81-29-861-2551, Fax: +81-29-861-2786,
E-mail: h-kataura@aist.go.jp

3P-18

Template-directed synthesis of coaxial structure of single-walled carbon nanotubes and boron nitride nanotubes by chemical vapor deposition

○Yongjia Zheng[1], Ming Liu[1], Taiki Inoue[1], Rong Xiang[1], Shigeo Maruyama[1,2]

[1] *Departure of Mechanical Engineering, The University of Tokyo, Tokyo 113-8656, Japan*
[2] *Energy Nano Engineering Lab., National Institute of Advanced Industrial Science and Technology (AIST), Ibaraki. 305-8564, Japan*

Graphene/h-BN interfaces have generated great interests recently due to the possibility of combining diverse atomic layers to create novel materials and devices [1-2]. In this work, we demonstrate a coaxial structure with similar interfaces that combines the single-walled carbon nanotubes (SWCNTs) with boron nitride nanotubes (BNNTs) in the radial direction. Ammonia borane (BH_3NH_3) as precursor was directly used to successfully synthesize BNNTs with the aid of SWCNTs as a template by a facile chemical vapor deposition (CVD) technique (Fig. 1a). Absorption spectra and Raman spectra confirmed not only the formation of BNNTs from BH_3NH_3, but also the undamaged condition of SWNTs (Fig. 1b and c). Furthermore, scanning electron microscopy (SEM) and transmission electron microscopy (TEM) were employed to examine the morphology and quality of the coaxial structure. As shown in Fig. 1e, with 30 min BH_3NH_3 growth, the number of walls increased to 3-5 with the diameter of ~5 nm wide. The heterostructure of coaxial SWNTs/BNNTs can be promising materials for modern integrated circuitry such as for field effect transistors (FETs) [3], resonant tunneling diode (RTD) [4], and interconnects. Formation mechanisms and electronic properties will be discussed.

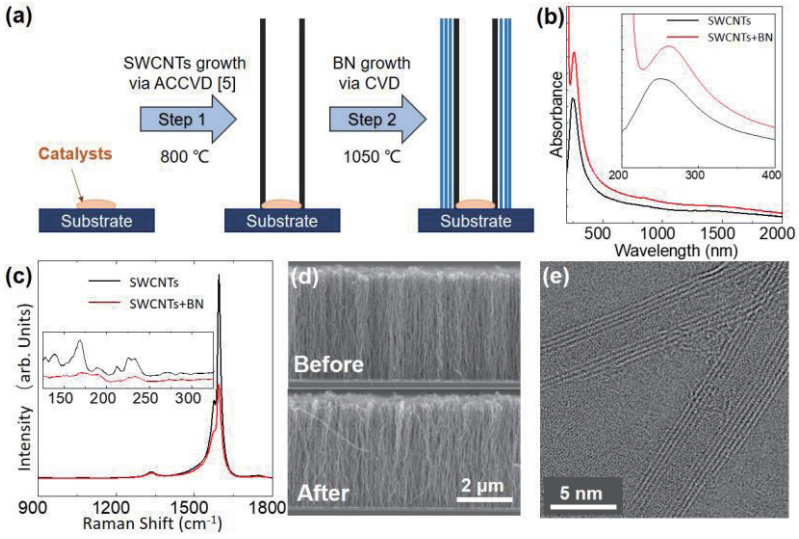

Fig. 1: (a) Schematic illustration of a fabrication of SWCNTs/BNNTs with coaxial hetero-structure. In step 1, SWCNTs were grown using alcohol catalytic CVD (ACCVD) [5]. In step 2, BN layers were coated onto surface of SWCNTs. (b) Absorption spectra and (c) Raman spectra of SWNTs and SWCNTs/BNNTs on quartz substrates. (d) SEM images of cross section of SWCNTs before and after BN growth. (e) TEM images of SWCNTs/BNNTs with more than one layer observed.

[1] M.P. Levendorf *et al., Nature,* **488,** 627 (2012).
[2] Z. Liu *et al., Nature Nanotechnology,* **8,** 119 (2013).
[3] R.Y. Tay *et al., Chemistry of Materials,* **27,** 7156 (2015).
[4] V.H. Nguyen *et al., Journal of Physics D: Applied Physics,* **45,** 325104 (2012).
[5] Y. Murakami *et al., Chemical Physics Letter,* **385,** 298 (2004).

Corresponding Author: S. Maruyama
Tel: +81-3-5841-6421, Fax: +81-3-5841-6983,
E-mail: maruyama@photon.t.u-tokyo.ac.jp

A study of Preparation Conditions of Carbon Nanobrushes: Influence of Target Types

○Ryota Yuge[1], Fumiyuki Nihey[1], Kiyohiko Toyama[1], and Masako Yudasaka[2, 3]

[1]*IoT Devices Research Laboratories, NEC Corporation, Tsukuba 305-8501, Japan*
[2]*Nanomaterials Research Institute, National Institute of Advanced Industrial Science and Technology (AIST), Tsukuba, 305-8565, Japan*
[3]*Graduate School of Science and Technology, Meijo University, Nagoya 468-8502, Japan*

Fibrous aggregates of single-walled carbon nanohorns, named as carbon nanobrushes (CNBs), were recently discovered [1]. The CNBs are expected as electrode materials of various devices such as actuators, electric double layer capacitors, and fuel cells since they show high dispersibility in solutions, large specific surface areas, and high electrical conductivity. CNBs are easily prepared by CO_2 laser ablation of Fe-containing carbon target at room temperature [1], but their yield is low and the major products are the spherical single-walled carbon nanohorn aggregates (CNHs). To increase the yield of CNBs, several preparation conditions such as Fe concentration in carbon targets, target rotation speed, and/or laser power density have already been investigated [2]. In this study, we tried to prepare CNBs by using carbon target containing different catalysts other than Fe. We also investigated the influence of the density of the carbon target itself.

A CO_2 laser ablated the catalyst-containing carbon targets at room temperature and ambient pressure. The laser power and target rotation speed were 3.2 kW and 1 rpm, respectively. The laser ablation was performed for 30 seconds. The gas pressure in the growth chamber was sustained at 700-800 Torr by controlling the evacuation rate while the buffer gas of nitrogen was kept at a flow rate of 10 L/min. The carbon target containing Fe (1 at. %, T1: 1.54 g/cm^3, T2: 1.73 g/cm^3), CoNi (T3: Co 0.9 at. %, Ni 0.3 at. %, 1.60 g/cm^3), or NiY (T4: Ni 4.2 at. %, Y 1.0 at. %, 1.60 g/cm^3) was used in our experiments.

The obtained carbon deposits after CO_2 laser ablation were 3.6, 1.7, 1.8, and 1.8 mg/s for T1, T2, T3, and T4, respectively. Fe-containing targets with lower density (1.54 g/cm^3) were evaporated easily during laser ablation and produced more carbonaceous deposits than that of higher density (1.73 g/cm^3). From scanning electron microscopy (SEM) and scanning transmission electron microscopy (STEM) observations, CNBs are prepared only for T1 target. Many amorphous carbons with a little CNHs were obtained for T2, T3, and T4 targets. Therefore, we found that target density rather than catalyst types such as Fe, Ni and Co is of importance for CNB formations. The details will be discussed in the presentation.

[1] R. Yuge *et al*. Adv. Mater. **28**, 7174 (2016).

[2] R. Yuge *et al*. The 52th FNTG General Symposium, 3P-24 (2017).

Corresponding Author: R. YugeTel: +81-29-850-1566, Fax: +81-29-856-6137, E-mail: r-yuge@bk.jp.nec.com

Energetics and electronic structures of corrugated graphene nanoribbons

○Kazufumi Yoneyama[1], Ayaka Yamanaka[2], and Susumu Okada[1]

[1] *Graduate School of Pure and Applied Sciences, University of Tsukuba, Tsukuba 305-8571, Japan*
[2] *Research Organization for Information Science and Technology (RIST), Shinagawa, Tokyo 140-0001, Japan*

The graphene nanoflakes and nanoribbons are attracting much attention as the constituent material for the functional devices, owing to their tunable electronic structure by controlling their sizes and shapes. Even though electronic structure of graphene nanoribbons has been elucidated by early theoretical works, a little is known about the energetics and electronic structure of nanoribbons with structural perturbations, such as edge roughness and corrugation, those are essentials for practical application of graphene nanostructure. Thus, in this work, we aim to investigate the energetics and electronic structure of graphene nanoribbons with structural corrugation, using the density functional theory with the generalized gradient approximation and pseudopotential procedure.

Figure 1 shows corrugation energies of graphene nanoribbons with armchair, chiral, and zigzag edges as function of the corrugation angle. The corrugation energy strongly depends on the edge shapes. For the zigzag nanoribbon, the energy keeps constant values up to the corrugation angle of about 9 deg. In contrast, for the armchair nanoribbon, the energy quickly increases with increasing the corrugation angle. The electronic structure modulation with respect to the corrugation also strongly depends on the edge shape of graphene nanoribbons.

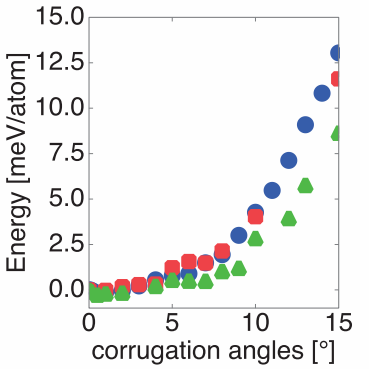

Fig. 1. Corrugation energies of graphene nanoribbons with armchair (circles), chiral (squares), and zigzag (triangles) edges as functions of corrugation angle.

Corresponding Author: K. Yoneyama
E-mail: kyoneyama@comas.frsc.tsukuba.ac.jp

Synthesis of Graphene by Oxidation and Reduction of Copper with Alcohol Chemical Vapor Deposition

○Yuya Ogata[1], Marina Tsujimoto[1], Hiromichi Gonnokami[1], Tyler Kurahashi[1], Hidenobu Murata[1], Masaru Tachibana[1]

[1] *Department of Materials System Science, Yokohama City University, Kanagawa 236-0027, Japan*

Graphene has attracted enormous attention due to its extraordinary mechanical, thermal, and electrical properties. Chemical vapor deposition (CVD) is a useful method for the amount synthesis of graphene. Many studies on CVD synthesis have been reported so far. However, most of reaction time on CVD synthesis has been limited to less than several hours. In this paper, we report the synthesis of graphene by oxidation and reduction of copper with alcohol CVD reaction for longer reaction times.

Graphene was synthesized on copper foil by using alcohol CVD where ethanol was used as carbon source. In the procedure, copper foil was annealed with Ar/H_2 gas, and then only ethanol was flown into the reaction chamber. The reaction times with ethanol flow at 900 ℃ was controlled in the range in 2 to 200 hours. After stopping the ethanol, the chamber was evacuated to 2 Pa, and then cooled down to room temperature to obtain a sample.

Many hollows are observed on copper surface after CVD process (Fig. 1(a)). Note that these hollows are not found in the original copper surface. Interestingly, single-layer graphenens are formed on only the bottom surface with square-like shape in each hollow (Fig. 1(b)). On the other hand, multi-layer graphenes are observed in all areas except for the hollows. Such hollows can be produced by the oxidation and reduction process beneath copper surface so that the clean copper surface with square-like shape is appeared at the bottom in each hollow. It is suggested that single-layer graphene is formed on the clean copper surface by the reprecipitation of dissoluved carbon beneath copper surface. This technique with the oxidation of copper will lead to the patterning of graphene

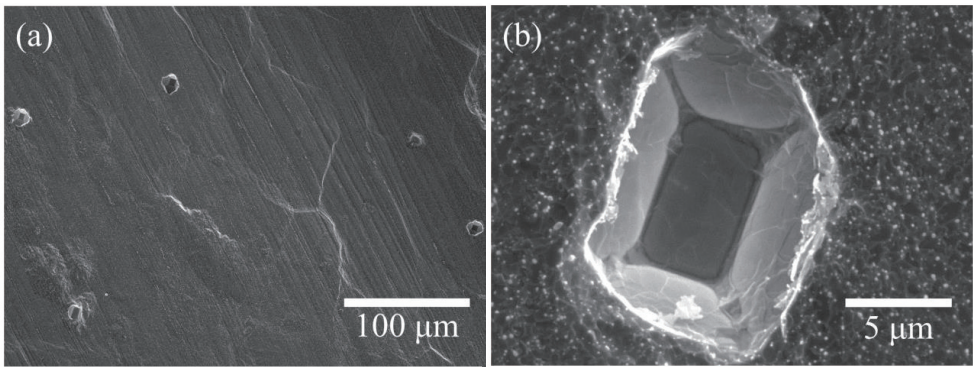

Fig. 1 The SEM images of sample with the growth time of 100hours.

(a)Low magnification (b)High magunification

Corresponding Author: Y. Ogata
Tel: +81-45-787-2162, Fax: +81-45-787-2162,
E-mail: n175210a@yokohama-cu.ac.jp

Sequential CVD growth of h-BN and graphene from ammonia borane and ethanol

○Kotaro Kashiwa[1], Naomasa Ueda[1], Hayato Arai[1], Taiki Inoue[1], Rong Xiang[1], Shohei Chiashi[1], Shigeo Maruyama[1,2]

[1] *Department of Mechanical Engineering, The University of Tokyo, Tokyo 113-8656, Japan*
[2] *Energy NanoEngineering Lab., National Institute of Advanced Industrial Science and Technology (AIST), Ibaraki 305-8564, Japan*

Hexagonal boron nitride (h-BN) is two-dimensional material with a hexagonal lattice. The lattice mismatch between h-BN and graphene is only 1.8% [1]. h-BN has a wide band gap of ~6 eV and can serve as an ideal supporting layer for graphene devices due to its planer structure without dangling bonds. Graphene has been a promising material due to its extraordinarily high mobility. However, graphene does not have band gap and is not easily applicable to transistors.

Some researchers proposed that by putting graphene on h-BN to form a van der Waals heterostructure, properties of graphene for device applications such as mobility, can be well improved compared with those of graphene on SiO_2 [2]. In addition, the superlattice potential induced by lattice mismatch can modify the electronic properties of graphene and lead to gap opening at Dirac cone. It was also reported that introduction of foreign atoms such as boron or nitrogen can modify the electronic properties and induce band gap to graphene [3]. Such kind of heterostructures of graphene and h-BN are obtained by CVD process using two kinds of source gasses for graphene and h-BN. However, the controllability of such CVD process needs to be improved.

In this study, we synthesized high-quality pristine h-BN and graphene and also demonstrated sequential CVD growth of them. We used a coper foil as the catalyst of CVD for h-BN and graphene. During growth, a CVD furnace was usually kept at 1050 ˚C. For h-BN and graphene growth, we used ammonia borane and ethanol as the precursors, respectively. Ammonia borane was kept at 80 ˚C. As shown in Fig. 1(a), single-layer h-BN was grown and possessed an ideal triangle shape. By supplying two different source gases sequentially, h-BNC was observed on copper surface (Fig. 1(b)). After transferred on SiO_2, h-BNC was identified by characteristic peaks of Raman spectra, and those spectra suggested the density of converted atoms were different between inside and outside of the triangle shape.

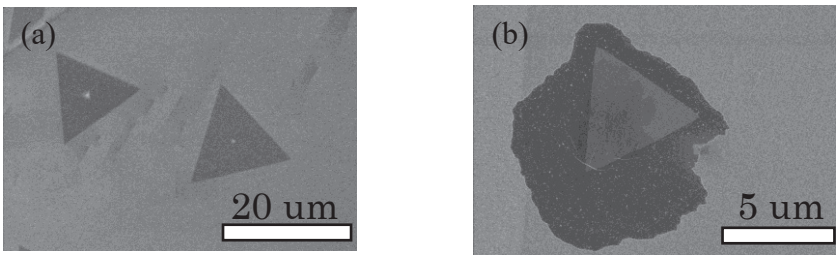

Fig. 1 (a) SEM image of h-BN. (b) SEM image of h-BNC.

[1] Z. Liu. *et al. Nat. Nano.* 8, 119 (2013).
[2] C. R. Dean. *et al. Nat. Nano*. 5, 722 (2010).
[3] W. Eryin. *et al. Nat. Phys*. 12, 1111 (2016)

Corresponding Author: S. Maruyama
Tel: +81-3-5841-6421 E-mail: maruyama@photon.t.u-tokyo.ac.jp

Transverse thermoelectric voltage in $^{12}C/^{13}C$-graphene heterostructures

○Yuta Mochizuki, Kuniharu Takei, Seiji Akita, and Takayuki Arie

Department of Physics and Electronics, Osaka Prefecture University, Osaka 599-8531, Japan

Graphene is expected as thermoelectric conversion elements due to its high career mobility and high power factor. However, the thermal conductivity of graphene is extremely high, resulting in small figure of merit (ZT) values. Therefore, the reduction in thermal conductivity of graphene has been investigated by using isotopes and defects in order to enhance ZT [1-3]. Another root of enhancing the thermoelectric performance of graphene may be transverse thermoelectric, where materials having different properties arranged alternately show anisotropic transport behavior, leading to transverse Seebeck and Peltier effects. Since the electrical and thermal properties of graphene are essentially isotropic, in this study we used isotopically modified heterostructures that enable devices to present transverse thermoelectric effect.

Graphene composed of ^{12}C and/or ^{13}C were synthesized by low-pressure chemical vapor deposition using $^{12}CH_4$ and/or $^{13}CH_4$ as carbon sources, respectively. After synthesizing and photolithographically patterning graphene composed of ^{13}C and ^{12}C (50%/50%), graphene with only ^{12}C was synthesized on the part of etched region to form isotopic heterostructures.

Transverse thermoelectric voltage appeared in the perpendicular direction to the temperature difference is expressed as

$$|\Delta V| = \left| \frac{\Delta T}{2} \frac{l}{d} \left(S_{\parallel} - S_{\perp} \right) \sin 2\theta \right| \qquad (1),$$

where ΔT, l/d, θ, $S_{\parallel}$, and $S_{\perp}$ are the temperature difference, aspect ratio of the device, tilt angle of the isotopic interface, and Seebeck coefficient of graphene heterostructures in the parallel and perpendicular directions to the interface, respectively (Fig. 1(a)). From our experiments using devices with various tilt angles, the measured transverse thermoelectric voltage takes the maximum value of approximately 12.0 μV at the tilt angle of 45° (Fig. 1(b)), which corresponds to Eq. 1. Thermovoltage was found to increase linearly with increasing the aspect ratio of the device, l/d, which is also consistent with Eq. 1. The transverse thermoelectric effect, therefore, can be utilized to improve the thermoelectric performance of graphene devices.

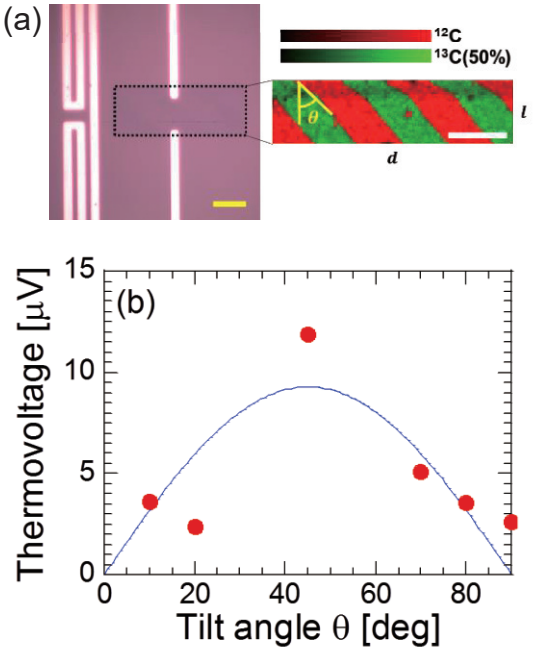

Fig. 1 Transverse thermoelectric voltage of graphene heterostructures as a function of tilt angle. Bars in (a) represent 10 μm.

[1] Y. Anno, K. Takei, S, Akita, T. Arie, Phys. Status Solidi RRL 8, 692 (2014).
[2] Y. Anno, K. Takei, S. Akita, T. Arie, Adv. Electron. Mater. 1, 1500175 (2015).
[3] Y. Anno, Y. Imakita, K. Takei, S. Akita, T. Arie, 2D Mater. 4, 025019 (2017).

Corresponding Author: T. Arie
Tel/Fax: +81-72-254-9265
E-mail: arie@pe.osakafu-u.ac.jp

Fabrication of graphene sheets intercalated by carbon spheres for high-performance supercapacitor electrodes

○Zhipeng Wang[1], Hironori Ogata[2,3], Wei Gong[1], Yanqing Wang[1], Adavan Kiliyankil Vipin[1], Gan Jet Hong Melvin[4], Josue Ortiz-Medina[5], Rodolfo Cruz-Silva[5], Shingo Morimoto[5], Yoshio Hashimoto[5,6], Bunshi Fugetsu[7], Ichiro Sakata[1,7] Mauricio Terrones[5,8], Morinobu Endo[5]

[1]Department of Technology Management for Innovation, School of Engineering, The University of Tokyo, Bunkyo-ku, Tokyo 113-0032, Japan
[2]Department of Chemical Science and Technology, Faculty of Bioscience and Applied Chemical and Graduate School of Engineering, Hosei University, 3-7-2, Kajino-cho, Koganei, Tokyo 184-8584, Japan
[3]Research Center for Micro-Nano Technology, Hosei University, 3-11-15, Midori-cho, Koganei, Tokyo 184-0003, Japan
[4]Faculty of Engineering, Universiti Malaysia Sabah, Jalan UMS, 88400 Kota Kinabalu, Sabah, Malaysia
[5]Institute of Carbon Science and Technology, Shinshu University, 4-17-1 Wakasato, Nagano 380-8553, Japan
[6]Department of Electrical and Computer Engineering, Shinshu University, 4-17-1 Wakasato, Nagano 380-8553, Japan
[7]Policy Alternative Research Institute, The University of Tokyo, Bunkyo-ku, Tokyo 113-0032, Japan
[8]Department of Physics, Department of Materials Science and Engineering & Materials Research Institute, The Pennsylvania State University, University Park, Pennsylvania 16802, United States

Due to their excellent physicochemical properties, nanocarbons including activated carbon, carbon nanotubes, graphene, and their derivatives have stimulated many researchers to explore the applications of energy conversion and storage systems [1]. Among them, graphene, a two-dimensional atomic layer of hexagonal carbon atoms, is a dazzling star in the exploration journey of supercapacitor applications. Until now, graphene has been synthesized by three main routes: chemical vapor deposition of carbonaceous gases, annealing of silicon carbide, and chemical exfoliation of graphite. Compared to the other two counterparts, the chemical exfoliation technique has some advantages such as easy mass production and low cost for graphene synthesis with a reduction process of graphite/graphene oxide to graphene [2, 3]. However, this technique could achieve only partial reduction of graphite/graphene oxide and encounter the problems of an agglomeration of graphene sheets during the drying of the solution, further affect their performances in the practical applications. Thus, it is highly desirable to develop a new synthetic approach to solve the issues and enhance the performances. In particular, intercalation of other materials including conductive polymers, metal oxides, and other carbon structures between two graphene sheets to form the composites is popular in the application of supercapacitors [4-6].

In this work, we employed a hydrothermal technique to fabricate a composite consisting of graphene sheets and carbon spheres, and heated our samples at high temperatures. Heat treatment here could further remove the oxygen species of graphene sheets and carbon spheres, increase the conductivity of the composites, and adjust the microstructures of carbon spheres. The detailed results and discussion will be presented in the coming conference.

[1] W. Gu, *et al.* WIREs Energy Environ. 3, 424 (2014). [2] Q. Ke, *et al.* J. Materiomics 2, 35 (2016). [3] S. Zheng, *et al.* ACS Nano 11, 4009 (2017). [4] Q. Wu, *et al.* ACS Nano 4, 1963 (2010). [5] Z-S. Wu, *et al.* Adv. Funct. Mater. 20, 3595 (2010). [6] J. Li, *et al.* Chem. Phys. Lett. 693, 60 (2018).

Corresponding Author: Zhipeng Wang.Tel/Fax: +81-3-5841-7461,E-mail: z.wang@ipr-ctr.t.u-tokyo.ac.jp

Spin-orbit interaction in Pt and Bi_2Te_3-nanoparticle decorated graphene

H. Kudo[1], M. Hatsuda[1], T. Nanba[1], R. Tamura[1], T. Nakamura[2], S. Katsumoto[2], J. Haruyama[1,2]

[1]*Faculty of Sciences and Engineering, Aoyama Gakuin University, 5-10-1 Fuchinobe, Sagamihara, Kanagawa252-5258, Japan*

[2]*Institute for Solid State Physics, The University of Tokyo, 5-1-5 Kashiwanoha, Kashiwa, Chiba 277-8581, Japan*

The introduction of spin-orbit interactions (SOIs) and the subsequent appearance of a two-dimensional (2D) quantum phenomena with resolving degenerate degrees of freedom are crucial for voltage-controlled spintronic devices. In contrast, graphene basically lacks SOIs due to the small mass of the carbon atom. Recently, SOIs have been experimentally introduced into graphene [e.g., surface decoration by (1) small-mass adatoms (hydrogen [1] or fluorine) and (2) by heavy nanoparticles (gold, silver), and (3) using heavy substrates (copper, Bi_2Se_3, WS_2)]. When graphene is sufficiently isolated from the influence of the substrate, long spin relaxation times (τ_s) and large mean free paths of electrons are provided. If SOIs can be introduced without reducing them, graphene possessing SOIs can yield various quantum phenomena [e.g., 2D or 1D topological insulating (TI) states (quantum spin Hall effect (SHE)), quantum anomalous SHE, and quantum valley HE] and those practical applications. Indeed, many theories have predicted SOI and TI states in adatom-decorated graphene [2,3].

Here, we introduce large SOIs into mono-layer graphene by controlling decoration of heavy-nanoparticles [platinum (Pt) or bismuth telluride (Bi_2Te_3)], using an innovative nanoneedle technique [4]. The precise and clean(damageless) decoration leads to the emergence of particle density-dependent non-local resistance (R_{NL}) peaks at room temperature (Fig.1) and those oscillatory behaviors under in-plane magnetic fields. They suggest presence of the SOI energies as large as 30 ~ 50 meV and (inverse) SHE. Only Bi_2Te_3-particle decorated samples within a low density regime demonstrate quarter integer fractions of resistance quantum in R_{NL} peaks (Fig.1(b)). The present observation opens doors to novel physics for topological and quantum phases of graphene, introducible by precise heavy-nanoparticle decoration. More details are presented in poster.

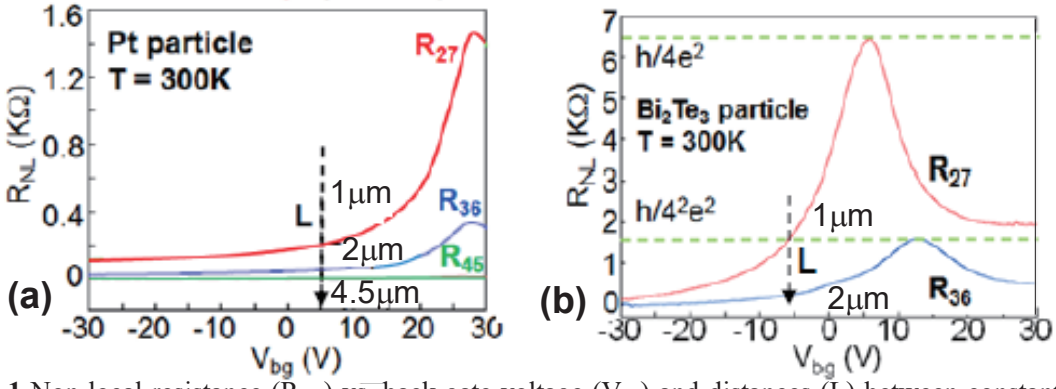

Fig. 1 Non-local resistance (R_{NL}) vs. back gate voltage (V_{bg}) and distances (L) between constant-current and R_{NL} probes, measured for **(a)** Pt- or **(b)** Bi_2Te_3-nanoparticle decorated graphene.

[1] T. Kato, S. Katsumoto, S. Roche, J. Haruyama *et al.*,, *Royal Soc. Chem. Adv.* **6**, 67586 (2016).

[2] M.T. Deng *et al.*, *Science* **354**, 1557 (2016). [3] L. Brey, *Phys. Rev. B* **92**, 235444 (2015).

[4] T.Nanba, J. Haruyama *et al., Phys. Rev. Lett.* submitted

Corresponding Author: J. Haruyama
Tel: +81-42-759-6256, E-mail: J-haru@ee.aoyama.ac.jp

Energetics and electronic structure of graphene adsorbing CO_x under an external electric field

Manaho Matsubara and Susumu Okada

Graduate School of Pure & Applied Sciences, University of Tsukuba, Tsukuba 305-8571 Japan

Graphene has been attracting much attention in the fields of fundamental and applied sciences for these decades, because of its unique physical properties. The energetics and electronic properties of graphene are found to be sensitive to the external environments such as molecular adsorbates and an external electric field. Owing to these characteristics, graphene is regarded as the key material for the sensing devices. It is expected that tuning of carrier density on graphene can further improve the sensing and adsorption ability, because the electronic properties of graphene is sensitive to the carrier density near the Fermi level. Thus, in the present work, we aim to give theoretical insight into the energetics and electronic properties of graphene adsorbing CO_x molecules in the field effect transistor in terms of the molecular arrangements and carrier concentration, using the density functional theory with generalized gradient approximation combined with the van der Waals correction and the effective screening medium method.

Our calculations show that the optimum spacing between CO_x and graphene strongly depend on the carrier concentrations (Fig. 1). Both electron and hole injection decrease the optimum spacing than that under the neutral condition, indicating that the molecules are tightly bound to graphene. The enhancement of the binding energy is ascribed to the Coulomb interaction between polarized CO_x molecules and graphene under the carrier injection. These results indicate that the external electric field plays crucial role to determine the energetics and electronic properties of graphene for the molecular adsorption.

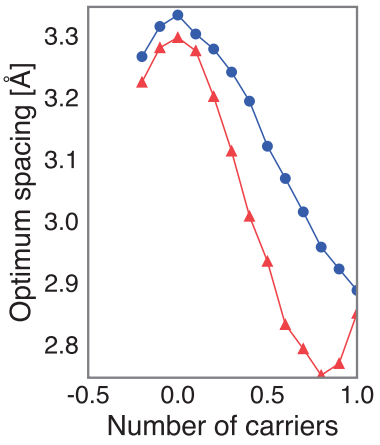

Fig.1 Optimum spacing between graphene and COx as a function of carrier concentration with various molecular orientations. Circles and squares denote horizontal and vertical COx to graphene, respectively.

Corresponding author: M. Matsubara
Email: mmatsubara@comas.frsc.tsukuba.ac.jp

Topology tuning of graphene lattice structure by chemical modification

○Kentaro Tajima[1], Kazuyuki Takai[1,2]

[1] *Graduate School of Science and Engineering, Hosei University, Tokyo 184-8584, Japan*
[2] *Department of Chemical Science and Technology, Hosei University, Tokyo 184-8584 Japan*

Honeycomb lattice of graphene consists of two A, B sublattices. Braking symmetry of A, B sublattices by chemical modifications causes change in electronic structure of graphene. In the case of graphene oxide (GO) having oxygen containing functional groups, the difference in type of functional groups gives difference in the symmetry of the A, B sublattices and causes the localized electronic states. Indeed, hydroxyl groups bonded to a carbon atom on graphene plane cause the larger spin magnetism, compared with the epoxy group bonded to two adjacent carbon atoms [1]. Functionalization of graphene by addition of benzene has been investigated in recent years, which affects the surface charge of graphene depending on the type of substituent [2]. The difference in bonding manner between benzene and graphene gives difference in the topological modification, same as oxygen containing functional groups in GO. Therefore, it is supposed that the radical addition reaction by bonding benzene to a carbon atom at graphene plane strongly affects the electronic states of graphene compared with the cycloaddition reaction by bonding benzene to two adjacent carbon atoms. In this study, we evaluated functionalized graphite synthesized by radical addition and cycloaddition reaction, in terms of chemical structure and electronic properties.

Graphite powder were functionalized by the reactions shown in **Scheme 1** and labeled as R-graphite (**1**) and C-graphite (**2**). Raman spectroscopy was measured by LabRAM HR Evolution at 532 nm.

The Raman spectra of graphite and functionalized graphite (**1**, **2**) were shown in **Fig. 1**. After functionalization the D band increased, because sp^3 carbon binding to benzene exists as defect in graphene lattice. In Raman spectrum for **1**, the G-band position shifts toward the higher energy side compared with graphite and **2**, suggesting hole doping caused by nitro substituent which behaves as electron withdrawing group from benzene. The intensity ratio of D' to G band ($I_{D'}$ / I_G) of **1** becomes larger as compared with that of **2**. The difference in topology tuning in functionalized graphites **1** and **2** might affect carrier scattering in graphene lattice.

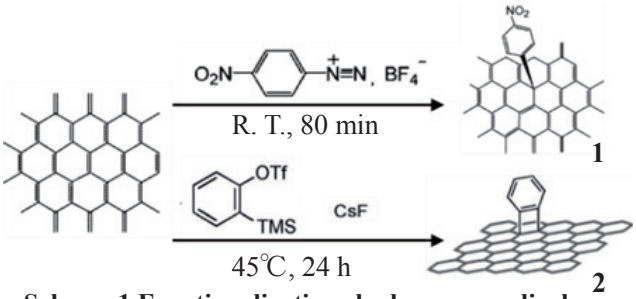

Scheme 1 Functionalizations by benzene radical addition (1) and arene cycloaddition (2)

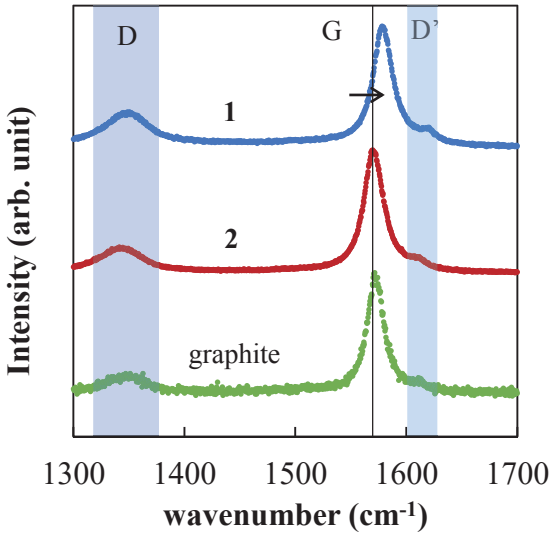

Fig. 1 Raman spectrum of graphite, 1 and 2

[1] K.Tajima et al, Polyhedron, **136**, (2017)
[2] F. M. Koehler et al, small, **6**, 10, (2010)
Corresponding Author: K. Takai (takai@hosei.ac.jp)

Magnetism arising from edge spins of few-layer MoS_2 nanomeshes

A. Mine[1], H. Kudo[1], Y. Hashimoto[2], G. Kondo[1], C. Ohata[1],
S. Katsumoto[2], J. Haruyama[1,2]

[1]*Depts. Electrical Eng. and Electro. Aoyama Gakuin University, 5-10-1 Fuchinobe, Sagamihara, Kanagawa252-5258, Japan*
[2]*Institute for Solid State Physics, The University of Tokyo, 5-1-5 Kashiwanoha, Kashiwa, Chiba 277-8581, Japan*

Magnetism arising from edge spins is highly interesting, particularly in 2D atomically thin materials in which the influence of edges becomes more significant. Among such materials, molybdenum disulfide (MoS_2; one of the transition metal dichalcogenide (TMD) family) is attracting significant attention. The causes for magnetism observed in the TMD family, including in MoS_2, have been discussed by considering various aspects, such as pure zigzag atomic-structure edges, grain boundaries, and vacancies. In order to reveal such edge-spin based magnetisms of 2D atom-thin layers, we formed nanomeshes (NMs; honeycomb-like array of hexagonal nanopores with low-contamination and low-defect pore edges) using a specific non-lithographic method (nanoporous alumina template mask) on various atom-thin layers (e.g., graphene, black phosphorus, and hexagonal boron-nitride (hBN)[1-3]) previously and reported observation of ferromagnetism (FM) derived from the pore-edge spins, which is highly sensitive to foreign atoms terminating the pore edges.

Here, we adopt this NM structure to few-layer MoS2 and observe FM [4]. We confirm robust FM arising from pore edges in oxygen(O)-terminated MoS_2-NMs at room temperature, while it disappears in hydrogen(H)-terminated samples. The observed high-sensitivity of FM to NM structures and critical annealing temperatures suggests a possibility that the Mo-atom dangling bond in pore edge is a dominant factor for the FM. The result is analogous to those observed in hBN-NMs. This finding of edge-spin-derived room-temperature FM must enable the use of atomically thin (or few-layer) MoS_2 in unique magnetic and spintronic applications in addition to well-established electronic and photonic applications.

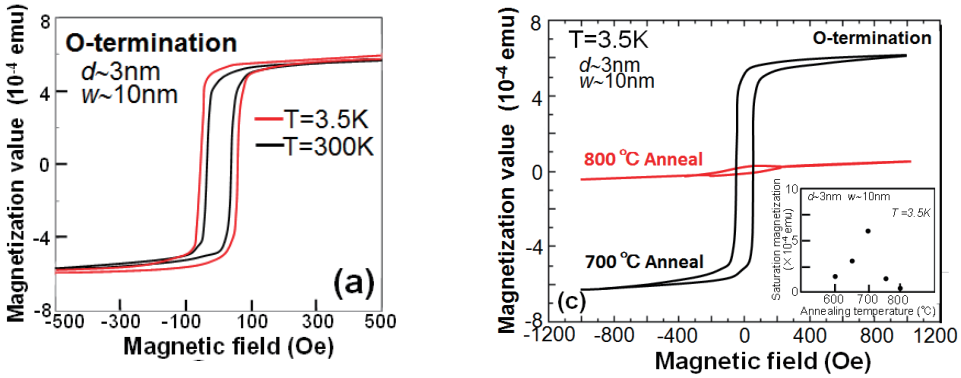

Fig.1: (a) Typical magnetization curves of the oxygen(O)-terminated few-layer MoS2-NM. **(b)** Magnetization curves of the O-terminated few-layer MoS_2-NMs annealed at two different temperatures, including that shown in (a). **Inset:** M_s values as a function of annealing temperature.

[1] J. Haruyama, *Electronics*, ***2*(4)**, 368 (2013).
[2] Y. Nakanishi, J. Haruyama et a., *Nano Research* **10,** 718 (2017).
[3] C. Ohata, J. Haruyama et al., *Appl. Phys. Lett.* **109**, 133110 (2016).
[4] G. Kondo, J. Haruyama et al., *AIP Advances* **7**, 125019 (2017).

Corresponding Author: J. Haruyama
Tel: +81-42-759-6256, E-mail: J-haru@ee.aoyama.ac.jp

Effect of the water presence in optical phenomena of hydrazine-adsorbed MoS_2

○Naoko Kodama[1], Y. Ishiguro[2], K. Takai[1,2]

[1]*Graduate School of Science and Engineering, Hosei University, Tokyo 184-8584, Japan*
[2]*Department of Chemical Science and Technology, Hosei University, Tokyo 184-8584, Japan*

The optical properties of 2D materials such as MoS_2 strongly depend on the chemical environments [1]. Indeed, an electron doping by hydrazine monohydrate adsorption makes Raman A_{1g} mode of MoS_2 soften and broaden. However, PL for MoS_2 adsorbed with hydrazine monohydrate measured at 77 K apparently shows irreversible hole-doping behavior [2]. Since half of hydrazine monohydrate is water, the effect of water might be involved. In this study, MoS_2 single layer adsorbed with water is investigated in order to clarify the effect of molecular doping on the optical properties of MoS_2 in terms of its kinetics.

MoS_2 single layer on 90 nm SiO_2/Si substrate was prepared by mechanical exfoliation. Hydrazine monohydrate or water were dropped on MoS_2 on the substrate and dried with air blow, followed by immediate Raman and PL measurement with an excitation wavelength of 532 nm. The same operation was repeated while varying the adsorption time.

As shown in Fig.1, the trion peak contribution A^- decreases and exciton peak A increases in PL as time passes after water adsorption, indicating hole-doping via water adsorption. On the other hand, Raman spectra is not sensitive to hole-doping unlike electron-doping. From these results, the apparent irreversible hole-doping observed at 77 K for hydrazine adsorbed MoS_2 is explained by the competition between n-doping by hydrazine and long-term hole doping by atmospheric oxygen assisted by water, similar to that in graphene[3].

This project was supported by JSPS and RFBR under the Japan - Russia Research Cooperative Program.

[1] S. Mouri *et al., Nano Lett*., 13, 5944 (2013) [2] N. Kodama *et al.,* FNTG symposium (2017) [3] T. Umehara *et al.,* JPS meeting (2015)

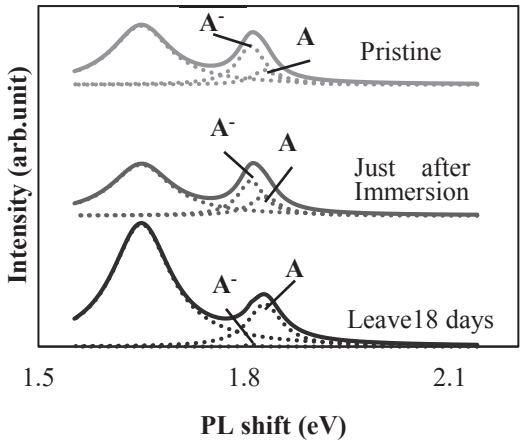

Fig.1 Time evolution of PL at 77 K for water adsorbed MoS_2

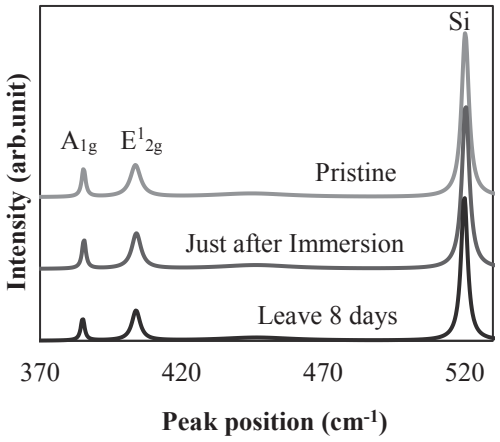

Fig.2 Time evolution of Raman for water adsorbed MoS_2

Corresponding Author: Kazuyuki Takai
Tel: +81-42-387-6138, Fax: +81-42-387-7002,
E-mail: takai@hosei.ac.jp

Continuous heteroepitaxy of two-dimensional multi-heterostructures based on layered chalcogenides

○Yu Kobayashi[1], Shoji Yoshida[2], Mina Maruyama[2], Kota Murase[2], Susumu Okada[2], Yutaka Maniwa[1], Hidemi Shigekawa[2], Yasumitsu Miyata[1]

[1]*Department of Physics, Tokyo Metropolitan University, Hachioji 192-0397, Japan*
[2]*Faculty of Pure and Applied Sciences, University of Tsukuba, Tsukuba 305-8573, Japan*

Atomic layers of transition metal dichalcogenides (TMDCs) have attracted significant attention because of their unique physical and chemical properties. To utilize their full potential, it is highly desired to develop a versatile growth process of TMDC-based functional heterostructures. However, conventional growth processes are usually required multiple complicated step including interface degradation and/or alloying, and are also difficult to control growth rate precisely [1,2].

Here, we report versatile heteroepitaxial growth of two-dimensional multi-heterostructures based on TMDCs (Fig. 1a). The use of liquid precursors enables the growth of highly-crystalline MoS_2, WS_2, $MoSe_2$, WSe_2 monolayers and their in-plane heterostructures (Fig. 1b). The present process can also realize atomically sharp and zigzag-edge straight junctions without defect and alloy formations around interface (Fig. 1c). The high-quality interface allows us to probe intrinsic band diagram, and is found to have larger band offset along conduction band minimum at MoS_2-WS_2 heterojunction, which is almost consistent with the results of first-principles calculations. Furthermore, the present heteroepitaxy also demonstrate the controlled growth of ribbon-shaped monolayer TMDC with less than 20 nm width from the straight edges of firstly-grown monolayers. These results open up a novel way to realize diverse atomically-thin quantum wires and superlattices, and further advanced applications in electronic and opto-electronics.

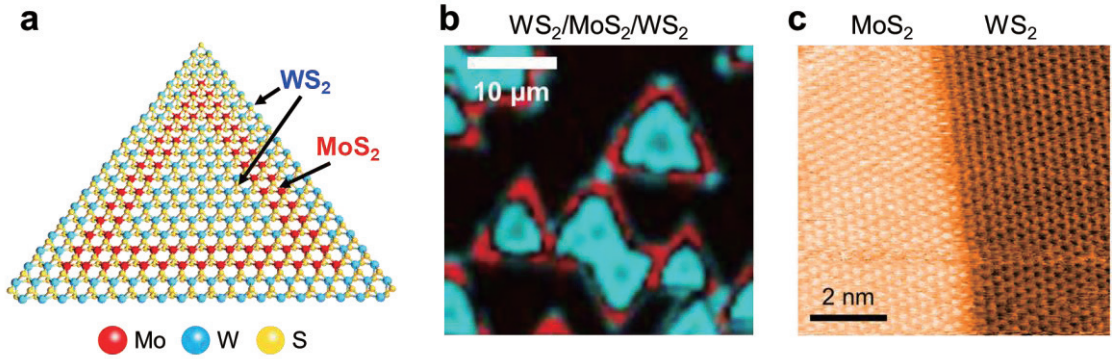

Figure 1. (a) Schematic illustration and (b) PL intensity map of in-plane $WS_2/MoS_2/WS_2$ multi-heterostructure. Red and cyan correspond to the intensities of the MoS_2 and WS_2 PL peaks, respectively. (c) STM image of MoS_2/WS_2 heterointerface.

[1] Z. Zhang *et al.*, Science, **357**, 788 (2017)., [2] M.-Y. Li, *et al.*, Science, **349**, 6247 (2015).
Corresponding Author: Y. Miyata, Tel: +81-42-677-2508, E-mail: ymiyata@tmu.ac.jp

Electric-field-induced Metal-Insulator Transition and Quantum Transport in Large-Area Polycrystalline MoS_2 Monolayers

○Tomoyuki Yamada[1], Jiang Pu[1], Lain-Jong Li[2], Taishi Takenobu[1]

[1]*Department of Applied Physics, Nagoya Univ., Nagoya 464-8603, Japan*
[2]*Physical Sciences and Engineering Division, KAUST, Thuwal 23955-6900, Saudi Arabia*

Molybdenum disulfide (MoS_2) is attracting increasing interests for future nanoelectronics [1]. The exfoliated single crystalline flakes have realized high mobility, metal-insulator transition, and superconductivity [2]. In addition, quantum transports arising from strong spin-orbit interaction have also been observed; thus, these superior transport properties offer potentials of MoS_2 for exploring quantum device applications [3]. Although it is necessary to apply large-area films for scalable device integration, the chemically synthesized polycrystalline films commonly showed poor transports, such as low mobility, due to the effects of grain boundaries and/or impurities. To overcome this issue, we recently combined electric double layer transistors (EDLTs) with polycrystalline MoS_2 films, and achieved high mobility of 30 cm^2/Vs [4]. This result suggests that high carrier density accumulations can reduce the adverse effects of grain boundaries. Here, we apply EDLTs to investigate the temperature- and carrier-density-dependence of resistance and magnetoresistance, resulting in the observation of metallic conduction and quantum transport in large-area polycrystalline MoS_2 monolayers.

Large-area polycrystalline MoS_2 monolayers were grown by chemical vapor deposition on sapphire substrate, and then, we deposited electrodes on it. Finally, ion gel films, mixture of ionic liquids and polymers, were spin-coated on MoS_2 and electrode surfaces to perform four terminal and Hall measurements (Fig. 1). Figure 2 shows the temperature dependence of the sheet resistance (R_S) with different gate voltage (V_g). At low V_g, the R_S increases as decreasing temperature (T), meaning insulating behavior. In contrast, at high V_g, the R_S shows metallic conduction down to T of 1.9 K, which clrealy indicates metal-insulator transition. Hall measurement also revealed the carrier density and mobility up to 2.1×10^{14} /cm^2 and 27 cm^2/Vs, respectively. Moreover, we observed unique magnetoresistance characteristics of the crossover from weak localization to weak antilocalization, as shown in Fig. 3. These results indicate that high carrier density eliminates the effects of grain boundaries, consequently realizing quantum transports in polycrystalline MoS_2 monolayers. We will quantitatively evaluate these magnetoresistance behaviors, and discuss the possibility for superconductivity.

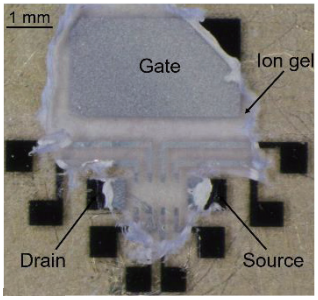

Fig. 1

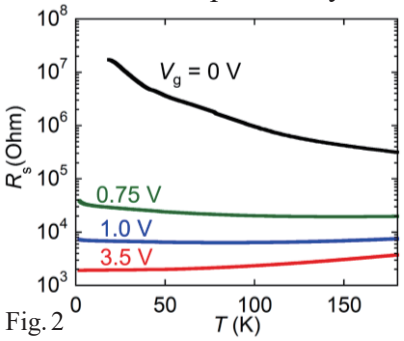

Fig. 2

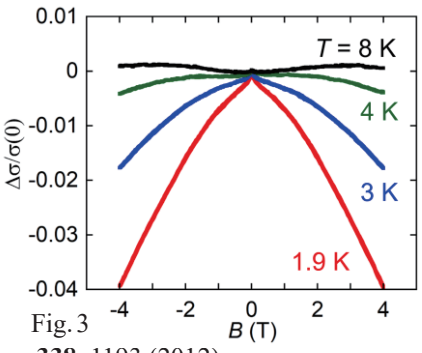

Fig. 3

[1] G. Fiori, *et al*. *Nat.Nanotechnol.* **9**, 768 (2014), [2] J. T. Ye, *et al*. *Science* **338**, 1193 (2012)
[3] H. Schmidt, *et al*. *Phys. Rev. Lett.* **116**, 046803 (2016), [4] J. Pu, *et al*. *Adv. Mater.* **28**, 4111 (2016)

Corresponding Author: T. Takenobu, Tel/Fax: +81-52-789-5165, E-mail: takenobu@nagoya-u.jp

Second quantization of surface plasmon in graphene and the applications

M. Shoufie Ukhtary, Riichiro Saito
Department of Physics, Tohoku University, Sendai 980-8578, Japan

Surface plasmon (SP) is electromagnetic wave propagating on the surface of a material. SP is associated with the collective oscillation of charge on the surface of material. The strength of electromagnetic field decreases in the perpendicular direction to the surface, making the SP confined. It is well-known that the excitation of SP by external electromagnetic wave requires the matching between energy-momentum of external wave and SP. It is also assumed that the energy-momentum matching will cause an enhancement of electromagnetic wave absorption by the material which is shown by the dip of reflection spectra. However, the explicit physical explanation of the SP excitation is not understood clearly.

Due to the confinement nature of SP, the quantum treatment of SP is possible, where the SP is considered as a quasiparticle travelling on the surface. In this work, we study how the SP can be quantized as an oscillator harmonic, similar to the quantization of phonon [1, 2]. In this study, we use the quantization scheme given by Archambault et al [1], where they quantized the energy of electromagnetic wave on the surface by introducing creation-annihilation operator. By quantizing the SP, we can explain why the excitation of SP requires the energy-momentum matching from which we can obtain the matrix element of photon-plasmon interaction (optical absorption probability). Quantization of SP also enables us to determine the partition function of SP, which can be used to determine the thermodynamic quantities such as internal energy and energy spectral the SP.

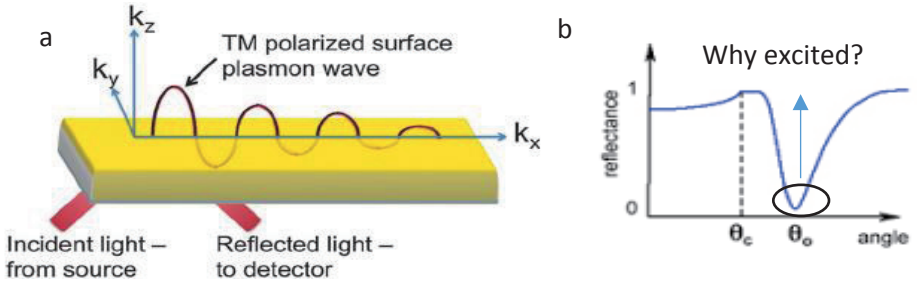

(a) Excitation of SP by light. (b) The reflection spectra. The dip on the spectra is the excitation of SP.

References:

[1] Archambault et al. PRB 82 035411 (2010)

[2] Finazzi et al. PRB 86 035428 (2012)

Effect of thermal stress on resonance properties of atomically thin electromechanical resonators

○Taichi Inoue, Yuta Mochizuki, Yuki Imakita, Kuniharu Takei, Takayuki Arie, Seiji Akita

Department of Physics and Electronics, Osaka Prefecture University, Sakai 599-8531, Japan

Atomically thin mechanical resonators [1] including stacked MoS_2/graphene are expected to be a highly sensitive optical or thermal sensor because of novel opto-mechanical functionalities. However, the thermal effect on resonance properties is still open subject. Here, we investigate thermal stress on resonance property of the stacked resonator.

Graphene synthesized by chemical vapor deposition was transferred onto a pair of electrodes on a Si/SiO_2 substrate and trimmed by O_2 plasma. For the stacked resonator, the mechanically exfoliated MoS_2 was transferred onto the graphene by the gel transfer method. Lastly, the 300 nm-thick SiO_2 layer underneath of the graphene was etched by buffered HF to obtain the suspended structure. Fig. 1(a) shows Scanning electron microscope image of drum type stacked MoS_2/graphene mechanical resonator with a diameter of ~ 6 μm. The resonance properties were measured by using the electrical method [2], where the resonator was driven by electrostatically by applying the AC source drain voltage V_{sd}. The gate voltage V_g can modulate tension of the resonator. The temperature dependence of the resonance properties were measured in vacuum at 10^{-3} Pa.

Fig. 1(b) and 1(c) show temperature dependences of resonance frequency shifts of graphene-only or stacked MoS_2/graphene mechanical resonators under linear oscillation regime, respectively. In the case of the graphene-only resonator, the frequency shift changed linearly for all V_g with the temperature. This indicates that the temperature dependence of the thermal stress can be modified by V_g. Note that the slope of frequency shift is changed from positive to negative as increasing V_g. In the case of stacked MoS_2/graphene mechanical resonator, the frequency shift was suppressed to ~ 2.5% compared with graphene-only resonator for all V_g. The cause of this shift is most likely due to the combination of the positive and negative thermal expansion coefficients of MoS_2 and graphene.

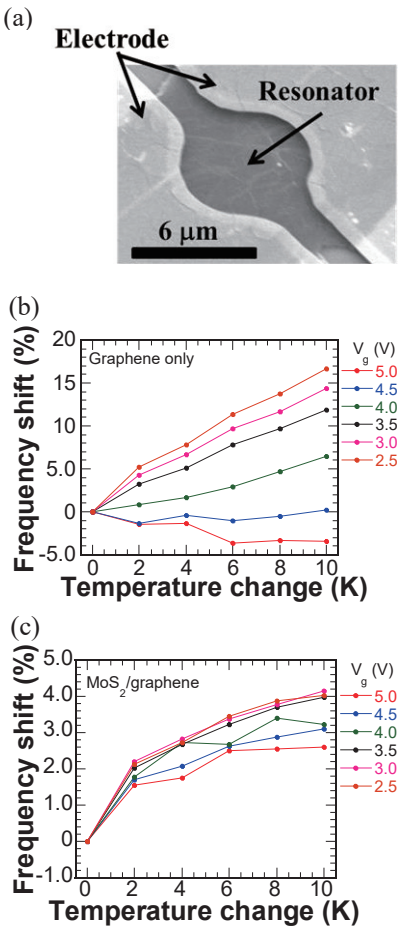

Fig. 1(a) SEM image of resonator. (b) and (c) are temperature dependence of resonance frequency shift of graphene only or stacked MoS_2/graphene mechanical resonator, respectively.

Acknowledgements This work was partially supported by KAKENHI Grant Number JP15H05869, JP16K14259, JP16H00920, and JP17H01040. **Reference** [1] T. inoue *et al*. ACS Omega, 2017, 2(9), pp 5792-5797 [2] Vera Sazanova *et al*. Nature 431, 284-287 (2004).

Corresponding Author: T. Inoue, Tel: +81-72-254- 9261, E-mail: t_inoue-4@pe.osakafu-u.ac.jp

Fabrication and characterization of field-effect transistors based on CVD-grown monolayer MoS_2

○Hiroshi Shimizu, Shun Ogawa, Yu Kobayashi, Takahiko Endo,
Yutaka Maniwa, Yasumitsu Miyata*

Department of Physics, Tokyo Metropolitan University, Hachioji 192-0397, Japan

Atomic layers of transition metal dichalcogenide (TMDC) have been intensively studied because of their unique properties and potential applications in electronics. In early studies, atomic layers are mainly prepared by mechanical exfoliation of bulk crystals. However, obtained crystals were usually small flakes of around 10 μm in size. In contrast, recently, large single crystals of TMDC with more than 100 μm can be grown by chemical vapor deposition (CVD). It is, therefore, an important subject to evaluate fundamental crystal quality and electric transport properties of such samples. For this purpose, we have investigated the transport properties of large-area monolayer MoS_2 single crystals grown by CVD [1]. In this presentation, we report recent progress of fabrication process and electrical performance of CVD-grown monolayer MoS_2 FETs.

Monolayer MoS_2 was grown at 760 °C on a silicon substrate using halide-assisted CVD [2]. In this work, molybdenum oxide (MoO_2) powder and sulfur flakes were used as precursors. To fabricate MoS_2 FETs, Ni/Au (or Cr/Au) electrodes were deposited on the triangle-shaped monolayer grains using maskless photolithography (Fig.1a). Typical n-type behaviors can be observed for MoS_2-FETs with Si back gate at room temperature in air (Fig.1b,c). Carrier mobilities and on/off ratios were evaluated to be 10~40 cm^2/Vs and 10^4~10^5, respectively, for the present devices. These results are comparable to the highest values reported for previous exfoliated and CVD samples [3], and suggest the potential of CVD-grown MoS_2 monolayers for electronics applications.

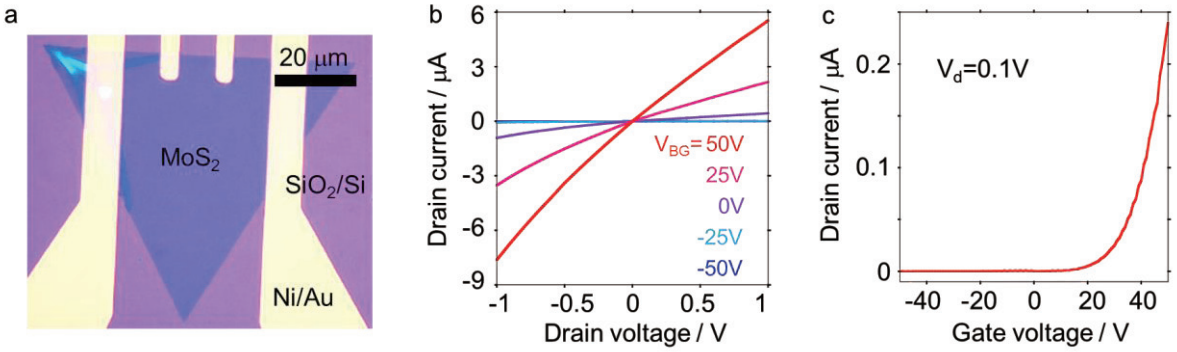

Fig. 1 (a) Optical image, (b) I_d-V_{ds}, and (c) I_d-V_{gs} curves of a monolayer MoS_2 FET.

[1] T. Uchida *et al*., The 53rd FNTG symposium (2017).
[2] S. Li *et al*., Appl. Mater. Today, **1**, 60 (2015).
[3] Z. Yu *et al*., Adv. Fanct. Mater., **27**, 1 (2017).
Corresponding Author: Yasumitsu Miyata
Tel: 042-677-2508, E-mail: ymiyata@tmu.ac.jp

Observation of graphene quantum dot using ion trap ion mobility measurement system

○Yudai Hoshino, Hiroki Morita, Ryota Jinnouchi, and Toshiki Sugai

Department of Chemistry, Toho University, Miyama 2-2-1 Funabashi, 274-8510, Japan

Graphene quantum dots (GQD) are nanometer-size graphene fragments, which have high potential to be applied in a wide range of fields with their unique photoluminescence (PL) properties and low toxicity, etc. However, their structure has not been fully understood let alone the PL mechanism. Here, we present structural evaluation of single GQD particles by our ion trap ion mobility measurement system with high voltage assisted laser desorption ionization (HALDI).

Figure 1 shows a schematic view of our system with an ionization YAG (266 nm) laser, an observation semiconductor (405 nm) laser, N_2 gas inlets, a metal sample rod, multiply stacked ring ion guide copper electrodes as an ion trap, and power supplies. The sample GQD produced in our laboratory[1] were placed on the top of the sample rod where the HALDI voltage and the YAG laser were introduced to ionize them. The ionized GQD were held and observed in the trap under N_2 at atmospheric pressure.

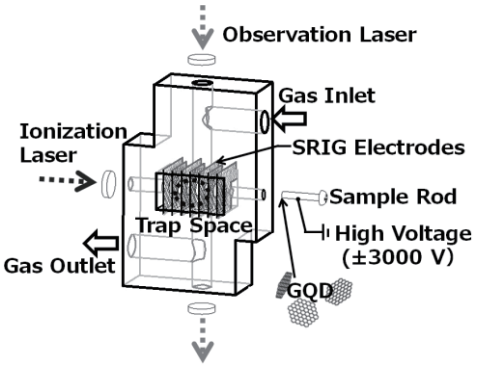

Fig.1. Schematic view of ion trap ion mobility measurement system

Figure2 shows the velocity distribution of GQD under the electric field of 3.3 kV/m with the HALDI of ± 3 kV. Several peaks appears in every 3.5 mm/sec and the velocity distributions shift to larger with the larger HALDI voltage. When we applied the lowest HALDI voltage of 300 V, the distribution converged to a single peak. Those results show that quantized charges were observed with high structural uniformity of the GQD and the single charge state were realized with the voltage control. The evaluated structure from the velocity of the singly charged GQD [2] is the single layer graphene disk with the diameter of 20 nm, which are consistent with those obtained with TEM[1]. The polarity and the amount of charge can be control by HALDI voltage. Further measurements on optical spectroscopy are in progress.

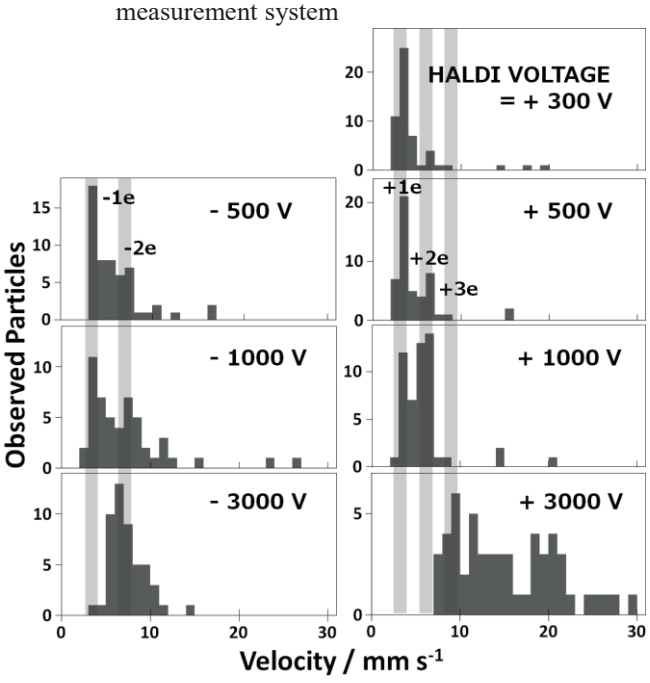

Fig.2. Distribution of drift velocity in each HALDI voltage

[1] H.Morita and T.Sugai, The 53th symposium 2P-23 (2017).

[2] T. Sugai, J. Mass. Spectrom. Soc. Jpn., 58, 2, (2010).

Corresponding Author: T. Sugai, Tel: +81-47-472-4406, E-mail: sugai@chem.sci.toho-u.ac.jp

Control of photoluminescence and solubility of graphene quantum dots

○H. Morita, K. Somei, Y. Hoshino, R. Jinnouchi, T. Sugai

Department of Chemistry, Toho University, Miyama 2-2-1, Funabashi 274-8510, Japan

Graphene quantum dots (GQD) are nanometer-size graphene fragments with unique properties such as photoluminescence (PL), low toxicity, and photostability. GQD are derived from various carbonaceous bulk materials by top-down approaches with highly oxidized processes in which hydrophilic carboxylic groups are combined [1]. Thus obtained high water solubility together with the PL properties is useful for bio-sensors [2]. The high water solubility, however, results in low solubility in organic solvent, which restricts numbers of chemical modification techniques [3] In addition, the hydrophilic carboxylic groups have been known to be combined to the PL active site closely [4,5,6]. To control PL property such as modulation of wavelengths and enhancement of quantum yield, the chemical modification is inevitable. Here we present chemical modification of GQD soluble in organic solvents and modification of PL properties.

GQD were prepared from CoMoCAT-SWNTs (Sigma-Aldrich) by oxidation in a mixture of concentrated H_2SO_4 and HNO_3. The produced water soluble GQD were converted to organo-soluble GQD-Hex and GQD-Me by esterification together with 1-hexanol and methanol as brown oily substances. They were characterized by optical and TEM observation.

GQD-Hex and -Me are both soluble in hexane, toluene and acetone. Fig.1 shows PL emission-excitation 3D mapping of pristine water-soluble GQD, GQD-Hex and GQD-Me. water-soluble GQD shows molecular-like excitation-independent sharp emission peaks around 420nm and 520nm (Fig.1a). GQD-Hex and –Me, in contrast, show the broad excitation-dependent peaks at 425nm and 320nm (Fig.1b and c). Those results show that the chemical modification has strong effect not only to the solubility but also to the PL properties. These methods should contribute to clarify the unknown PL mechanisms of GQD.

[1] Bacon, M., *et.al. Part. Part. Syst. Charact.* **31,** 415 (2014) [2] Ananthanarayanan, A., *et.al.* Adv. Funct. Mater. **24**, 3021(2014) [3] Sekiya, R. *et.al*. *Chem. -A Eur. J.* **22**, 1–10(2016). [4] Santiago, S. R. M., *et.al. Physical Chemistry Chemical Physics*, **18,** 2259 (2016). [5] Zhu, S., *et.al. Nano Research*, **8,** 355 (2015). [6] Dong, Y. *et.al.*;. *Mater. Chem. Phys.*, 203, 125–132, (2018)

Corresponding Author: T. Sugai. Tel: 047-472-4406, E-mail: sugai@chem.sci.toho-u.ac.jp

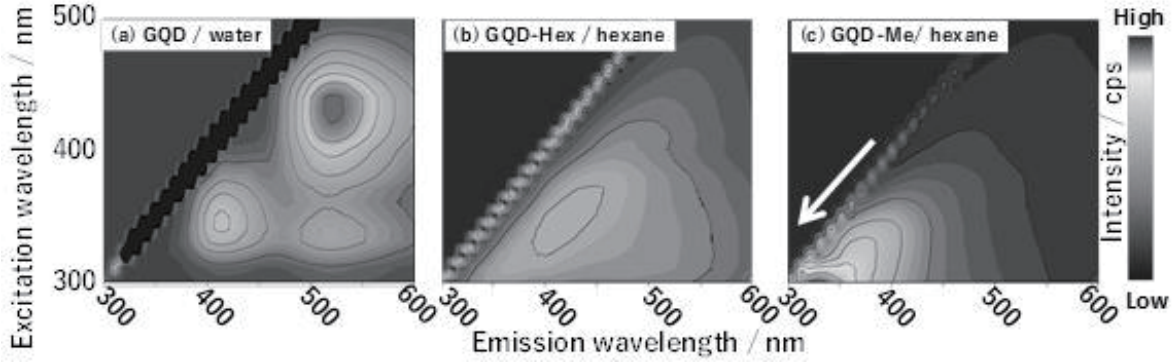

Fig.1 PL mapping of (a) GQD-Me (b) GQD-Hex.

Energetics and electronic structure of all-benzene nanostructures

Masaki Mieda and Susumu Okada

Graduate School of Pure and Applied Sciences, University of Tsukuba, Tsukuba 305-8571, Japan

Electronic structure of hydrocarbon molecules is sensitive to the topology of π electron distributed throughout their covalent network attributed to σ electron. The electronic structures are ranging from closed-shell to open-shell, depending on the molecular shapes and sizes. It has been well known that the hydrocarbon molecules sorely consist of hexagonal rings basically possess symmetric electronic structure with respect to their π and $\pi*$ states. In contrast, in the molecules with curvature, such as fullerenes, $\pi-\pi*$ symmetric electronic structure is absent near the Fermi level, making them unique materials for observing unusual physical and chemical phenomena. In the present work, we theoretically design the all-benzene cage and cyclic structures by oligomerrization of phenyl group, using the density functional theory with the generalized gradient approximation.

Figure 1 shows the geometric structures and total energy of [n]cyclometaphenylene ([n]CMP) designed here. The total energy of [n]CMP has the energy minimum at n=7 with the staggered structure to reduce the Coulomb repulsive interaction between H atoms. By assembling [n]CMP, where n=3, 4, and 5, we also designed all-benzene cage nanostructures which possesses moderate energetic stability and HOMO-LUMO gap ranging from 1.25 to 2.25 eV.

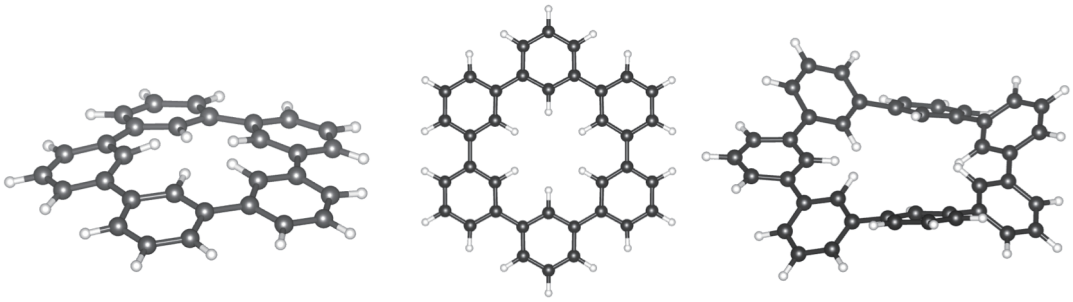

Fig. 1 Optimized geometries of [5]CMP, [6]CMP, and [7]CMP.

Correspond authors, M. Mieda and S. Okada

E-mail: sokad@comas.frsc.tsukuba.ac.jp

Plasticity of carbon nanotubes under combined axial and torsional stress

○Masafumi Yamanashi[1], Masayuki Toyoda[1], Susumu Saito[1, 2]

[1] *Department of Physics, Tokyo Institute of Technology, 2-12-1 Oh-okayama, Meguro-ku, Tokyo 152-8551, Japan*
[2] *Materials Research Center for Element Strategy, Tokyo Institute of Technology, 4259 Nagatsuta-cho, Midori-ku, Yokohama, Kanagawa 226-8503, Japan*

It is known that electronic properties of carbon nanotubes (CNTs) depend on their chiral indices, (n,m). Therefore, it is desirable to selectively obtain CNTs with desired chirality for various device applications. As for manipulation of chirality of CNTs, dislocation theory applied to CNTs under axial tension has shown that plastic elongation of CNTs can accompany with the change of their chirality from (n,m) to $(n,m-1)$ through sequential Stone-Wales transformations [1]. Here, we study plasticity of CNTs under combined axial and torsional stress by extending the previous study [1]. It is now revealed that any of six dislocation directions that change chiral indices from (n,m) to $(n+1,m)$, $(n-1,m)$, $(n,m+1)$, $(n,m-1)$, $(n+1,m-1)$ or $(n-1,m+1)$ can become the most energetically favorable direction depending on applied combined stress (Fig.1). We also show our extended model can explain molecular dynamics (MD) studies reported so far.

Also, to study energetics of the Stone-Wales transformations in CNT under the combined stress, we have carried out tight-binding MD simulations that well reproduce the energetics of local density approximation. We confirm that the energetics obtained by MD simulations show good agreement with our extended model.

From our results, one can optimize the combined stress for any of six transformations to occur. The present finding therefore opens the way to manipulate the chirality of a CNT and consequently their electronic properties. Since CNTs have been studied as super-strong wire materials, this work is also beneficial for comparing yield strength of CNTs having different chirality against the combined stresses.

[1] B. I. Yakobson, Appl. Phys. Lett. **72**, 918 (1998).

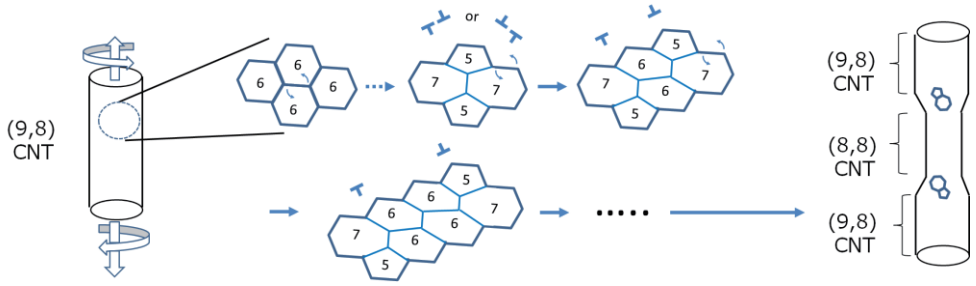

Fig.1. Plastic transformation of a (9, 8) CNT to a (8, 8) CNT under combined axial and torsional stress through sequential Stone-Wales transformations shown as an example.

Corresponding Author: M. Yamanashi
Tel: +81-3-5734-2721
E-mail: yamanashi@stat.phys.titech.ac.jp

Dependence of optical band gap on aggregational state of iron oxide nanotube prepared by sol-gel method

Shiori Takakura, ○Shunji Bandow

Department of Applied Chemistry, Meijo University, Nagoya 468-8502, Japan

Iron oxide nanotubes (Fe-ox-NTs) were synthesized by co-plymerization of iron-nitrate hydrate on the surface of non-ionic surfactant of a Pluronic F-127 in 1-propanol [1]. As-prepared nanotubes form bundle-like lump in which the individual nanotubes are agglutinated each other as shown in Fig. 1. In order to segregate these agglutinated nanotubes into individual ones, we carried out a method based on the collision of highly pressureized oncoming fluids so called Jet Mill (JM) for the nanotubes dispersed in ethanol (EtOH). Briefly ~10 mg of Fe-ox-NTs were dispersed in 15 ml of EtOH and crushed by JM at the pressure of 180 MPa for 100 times. Then the colloidal solution was centrifuged several steps by increasing centrifugal acceleration in order to isolate nanotubes. Figue 2 is the NTs observed in the supernatant at 1000 G. Upon progressing the centrifugal stage, size of the lump decreased.

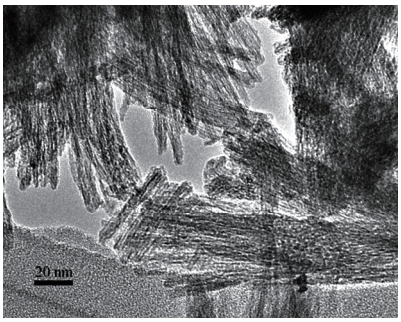

Fig. 1. Bundle-like agglutinated Fe-ox-NTs (TEM of as-prepared sample).

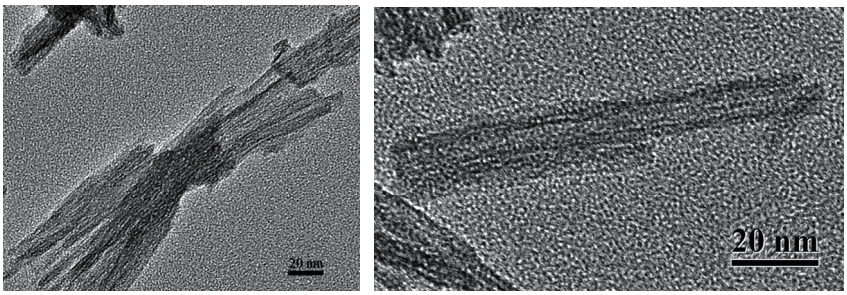

Fig. 2. TEM of isolated Fe-ox-NTs by centrifuge after JM. Left panel shows the bunble formed by several tens of Fe-ox-NTs. Right panel is single Fe-ox-NT. Supernatant solution includes both type of NTs, but the mixing rate of single NT increases as increasing the isolation stage.

X-ray diffraction patterns of the samples indicated that Fe-ox-NTs have Fe_3O_4 (magnetite) structure. Optical band gap was evaluated by the Tauc plot method, which clearly showed the increase of band gap as increasing the centrifugal isolation stage. Highly aggregated Fe-ox-NTs have the optical band gap between ~2.1 and ~2.3 eV (like the sample indicated in Fig. 1), while the isolated ones have much wider band gap of ~2.7 eV (dominated by the small size of NT-bundle lumps like the left of Fig. 2) and of ~ 2.9 eV (dominated by isolated NTs like the right of Fig. 2). These values did not depend on the environment of NTs whether dispersed in EtOH or dry powder.

[1] Y. Kosugi, S. Bandow, J. Inorg. Organomet. Polym. **24**, 933 (2014).
Corresponding Author: S. Bandow, E-mail: bandow@meijo-u.ac.jp, Tel: +81-52-838-2404

発表索引
Author Index

Author Index

< Z >

2018 年 3 月 10 日発行

第 54 回フラーレン・ナノチューブ・グラフェン総合シンポジウム
講演要旨集

≪フラーレン・ナノチューブ・グラフェン学会≫

〒113-8656 東京都文京区本郷 7-3-1

東京大学大学院工学系研究科　機械工学専攻

丸山研究室内

Phone/Fax：03-3830-4848

E-mail：fntg@photon.t.u-tokyo.ac.jp

URL：http://fullerene-jp.org

印刷　/　製本　（株）創志企画

HORIBA
Scientific

- ELEMENTAL ANALYSIS
- MOLECULAR SPECTROSCOPY
- OPTICAL SPECTROSCOPY
- PARTICLE CHARACTERIZATION
- SURFACE CHARACTERIZATION
- WATER QUALITY ANALYSIS / pH

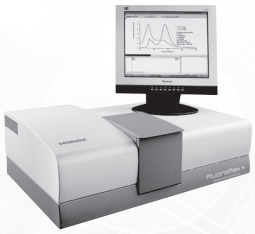

Bench-Top Spectrofluorometer

Particle Size Distribution Analyzer

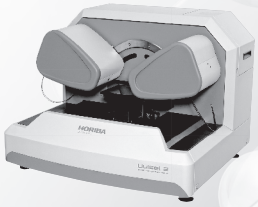

Ellipsometer

GD-OES

Spectrometers

Oxygen/Nitrogen/ Hydrogen Analyzer

Raman Microscope

Carbon/Sulfur Analyzer

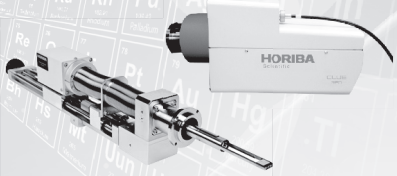

Cathodoluminescence

XploRA Nano
AFM with Raman Microscope

Tip-Enhanced Raman (TERS): chemical imaging at the nanoscale

TERS brings you the best of both worlds: the chemical specificity of Raman spectroscopy with imaging at spatial resolution typically down to 10nm.

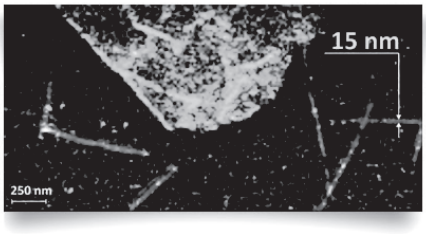

High-speed TERS imaging!

HORIBA Scientific is the first equipment manufacturer to guarantee TERS imaging capability and nano-resolution thanks to our STM-TERS tips, AFM-TERS tips and test samples.

info-sci.fr@horiba.com | horiba.com/scientifc

Explore the future

Automotive Test Systems | Process & Environmental | Medical | Semiconductor | Scientific

HORIBA

書籍のご案内

◈定価は本体価格＋税です。

カーボンナノチューブ・グラフェンハンドブック

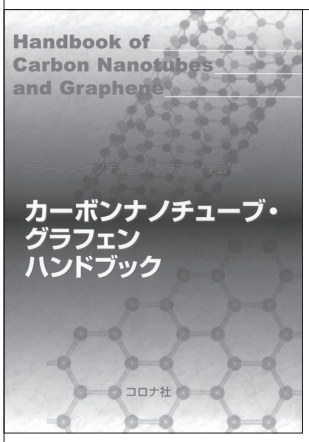

フラーレン・ナノチューブ・グラフェン学会 編
B5判／368頁
本体10,000円

本ハンドブックでは，カーボンナノチューブの基本的事項を解説しながら，エレクトロニクスへの応用，近赤外発光と吸収によるナノチューブの評価と光通信への応用の可能性を概観。最近嘱目のグラフェンやナノリスクについても触れた。

カーボンナノチューブの材料科学入門

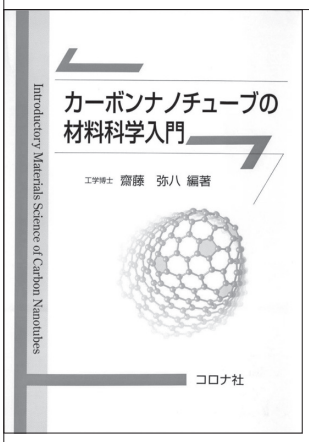

齋藤弥八 編著
坂東俊治・中山喜萬・春山純志・久保佳実 共著
A5判／250頁
本体3,400円

材料科学に新分野を創出し，エレクトロニクスからエネルギー分野まで広範囲な応用が期待されるナノテクノロジー材料の典型物質「カーボンナノチューブ」について，その製法から物性，実用の可能性までを解説した。

ドライプロセスによる表面処理・薄膜形成の応用

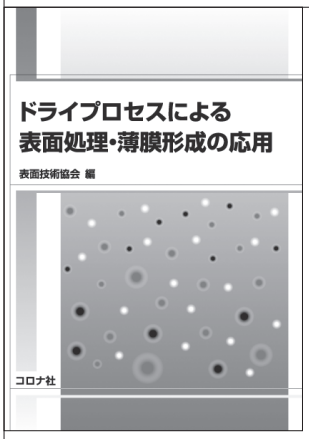

表面技術協会 編
A5判／318頁
本体4,600円

「ドライプロセスによる表面処理・薄膜形成の基礎」の応用編。第Ⅰ編「ドライプロセスの基礎技術」および第Ⅱ編「ドライプロセスの応用」から構成され、研究現場や製造現場で的確にドライプロセスが実施できるよう工夫し解説した。

関連書籍のご案内

カーボンナノチューブの基礎

齋藤弥八・坂東俊治 共著／A5判／220頁／本体2,800円

ドライプロセスによる表面処理・薄膜形成の基礎

表面技術協会 編／A5判／208頁／本体2,800円

ゼロからの最速理解量子化学

佐々木健夫 著／A5判／262頁／本体3,300円

機械屋のための分析装置ガイドブック

日本塑性加工学会 編／A5判／236頁／本体3,400円

真空科学ハンドブック

日本真空学会 編／B5判／2018年3月末刊行

科学技術と共に歩む

株式会社 コロナ社

〒112-0011 東京都文京区千石4-46-10 振替00140-8-14844
TEL (03)3941-3131（代），-3132，-3133（営業部直通）
http://www.coronasha.co.jp FAX (03)3941-3137
E-mail eigyo@coronasha.co.jp

モデルチェンジ　～スマートなデザインに簡単操作～

BRANSON 超音波ホモジナイザー

長くご愛顧いただいておりますBRANSON超音波ホモジナイザーで新たなモデルが誕生しました。

主な特長

1.電気エネルギーから超音波振動への変換効率が95%以上
　→ 無駄なエネルギーロスが小さく、安定した振幅が得られる。

2.通常では、液体の種類によって振幅が安定し難い。
　→ 条件を変えても一定の振幅を保つ機能がついている。

3.ジュール（watt/sec）による発振制御が可能
　→ Total何ジュールでこの処理が完了するという情報が論文に掲載できる。

20kHz超音波ホモジナイザー
BRANSON SONIFIER SFX250,550

40kHz超音波ホモジナイザー
BRANSON SONIFIER SFX150HH

主なアプリケーション

分散

カーボンナノチューブ　有機顔料　無機顔料　セラミック　セメント　感光体　記録材料
磁性粉　粉末冶金　酸化鉄　金属酸化物　シリカ　アルミナ　カーボンブラック
ポリマー　ラテックス　製紙　ファンデーション
研磨剤　電池　フィラー　光触媒　触媒　ワクチン　体外診断薬　歯磨き粉　シャンプー
半導体　電子基盤　液晶　貴金属　金属　宝石　タイヤ　発酵菌類　その他

乳化

エマルジョン製剤　農薬　トナー　ラテックス　界面活性剤　クリーム　乳液　その他

日本国内販売総代理店　株式会社 セントラル科学貿易

東京本社:　〒136-0071 東京都江東区亀戸1-28-6　タニビル3F　TEL 03-5627-8150 FAX 03-5627-8151
技術物流センター:〒272-0146 千葉県市川市広尾2-1-9　TEL 047-701-6100 FAX 047-701-6116
大阪支店:　〒533-0031 大阪府大阪市東淀川区西淡路1-1-36 新大阪ビル　TEL 06-6325-3171 FAX 03-6325-5180
福岡営業所:〒812-0016 福岡県福岡市博多区博多駅南1-2-15 事務機ビル　TEL 092-482-4000 FAX 092-482-3797
札幌出張所:〒001-0911 北海道札幌市北区新琴似11条13-7-13-2　TEL 011-764-3611 FAX 011-764-3612
http://www.cscjp.co.jp

当日出荷対象製品が大幅に増加しました。

ソーラボジャパンでは国内在庫を大幅に増やし、
ますます多くの製品がご注文当日あるいは翌営業日に
出荷可能になりました*。

お急ぎの製品は、是非一度当社ウェブサイトで
納期をご確認ください。
お客様の急なニーズにも迅速に対応いたします。

当日出荷が可能な製品の一例です。

出荷予定日はウェブサイトでご確認いただけます。

■ パワー＆エネルギーメータ

PM400
タッチパネル式パワー＆
エネルギーメーターコンソール
(マルチタッチ対応)

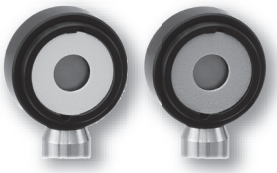

S120シリーズ
フォトダイオードパワーセンサ

ES220C　S470C

サーマルセンサ、焦電エネルギーセンサなども
当日出荷対象製品を取り揃えています。

「Today」の表示は
当日出荷の対象製品

+1	数量	資料	型番 - Universal		定価(税抜)		出荷予定日
+1			PM400	タッチパネル式パワー＆エネルギーメーターコンソール、マルチタッチ対応	¥175,032	√	Today

+1	数量	資料	型番 - Universal		定価(税抜)		出荷予定日
+1			S120VC	標準フォトダイオードパワーセンサ、Si 、200～1100 nm、50 mW	¥55,162	√	Today
+1			S120C	標準フォトダイオードパワーセンサ、Si、400～1100 nm、50 mW	¥39,780	√	Today
+1			S121C	標準フォトダイオードパワーセンサ、Si、400～1100 nm、500 mW	¥43,228	√	Today
+1			S122C	標準フォトダイオードパワーセンサ、Ge、700～1800 nm、40 mW	¥79,427	√	Today

■ レーザ保護メガネ

LG11

LG11A

+1	数量	資料	型番 - Universal		定価(税抜)		出荷予定日
+1			LG11	レーザ保護メガネ、クリアレンズ、可視光透過率：75%	¥45,760	√	Today
+1			LG11A	レーザ保護メガネ、クリアレンズ、可視光透過率：75%、コンフォートタイプ	¥45,760	√	Today

＊弊社に直接ご注文いただいた場合の出荷予定日です。また、出荷予定日は在庫状況に応じて変わる可能性がありますので
ご了承ください(上記の出荷予定日、価格などは2018年1月現在のウェブサイト上の製品情報です)。

www.thorlabs.co.jp　E-mail: sales@thorlabs.jp

THORLABS
ソーラボジャパン株式会社
〒170-0013 東京都豊島区東池袋2-23-2 TEL：03-5979-8889 FAX：03-5979-7285

研究から量産まで

グラフェン、カーボンナノチューブ & 2Dマテリアル用 先端成長技術

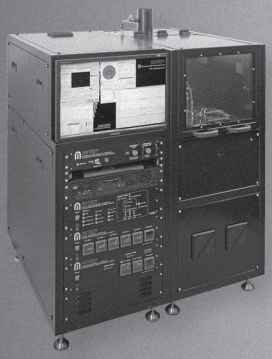

BM Pro

Your deposition workhorse
for wafer scale

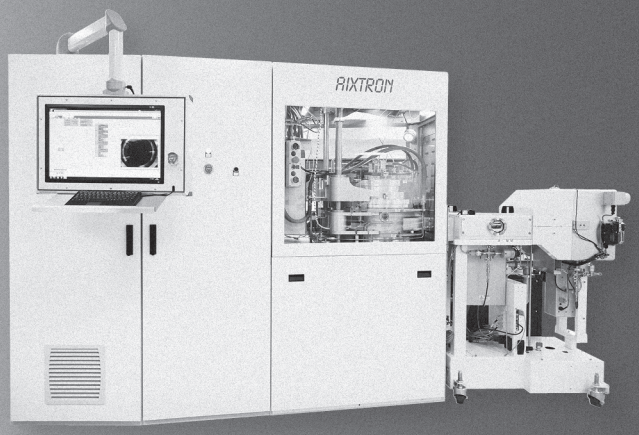

BM 300T

For your production needs
at wafer scale

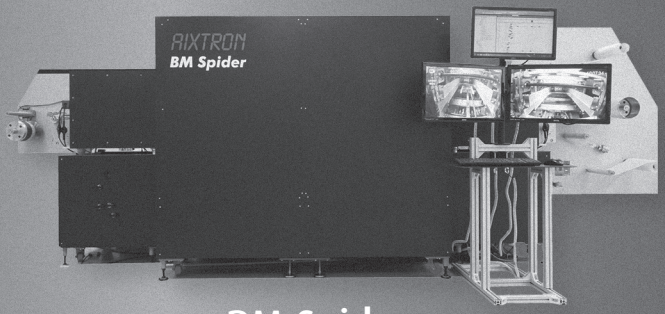

BM Spider

Your roll-to-roll solution

	BM Pro	BM 300T	BM spider
プロセス	CVD/PECVD Batch	CVD/PECVD Batch	CVD / Roll-to-roll
材料	CNTs, graphene & other 2D	CNTs & graphene	CNTs & graphene
基板サイズ	Up to 8″	8″ & 12″	300 mm web width
基板タイプ	wafer & foil	wafer	foil
最高温度	1,050° C (*up to 1,700° C)	1,050° C	1,050° C
シャワーヘッド方式 ガス供給	Yes	Yes	Yes
プラズマ	Yes	Yes	No
ハンドラー/インライン インテグレーション	No	Yes	Yes
両面コーティング	No	No	Yes

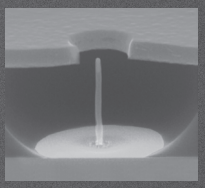
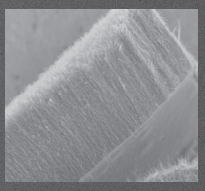
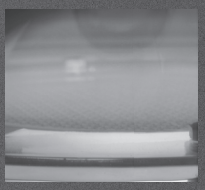
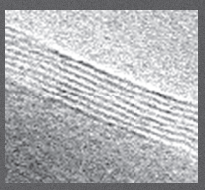
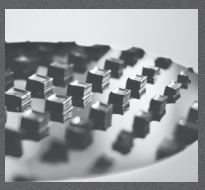
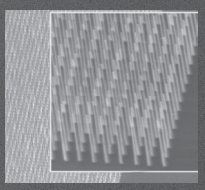
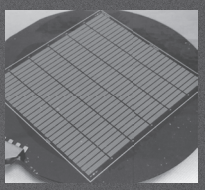
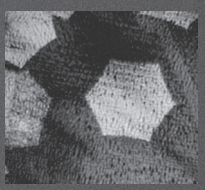

アイクストロン株式会社 · www.aixtron.com
〒140-0001 東京都品川区北品川1-8-11 Daiwa品川Northビル 9F
E-mail: japaninfo@aixtron.com · Phone: 03-5781-0931 · Fax: 03-5781-0940

AIXTRON
Our technology. Your future.

極微を観る

私たちJEOLグループは1949年に電子顕微鏡の開発・製造会社として設立されました。これからも電子顕微鏡のリーディングカンパニーとして、ナノテクノロジー、バイオテクノロジー、ライフサイエンスなどさまざまな分野に最適なソリューションを提供していきます。

原子分解能分析電子顕微鏡

NEOARM JEM-ARM200F

“NEOARM”は、当社独自の技術で開発された
冷陰極電界放出形電子銃(Cold-FEG)と
高次の収差まで補正可能な
新型球面収差補正装置(ASCOR)を標準搭載し、
200 kVの高加速電圧だけでなく
30 kVの低加速電圧においても
原子分解能での観察を実現しました。

ショットキー電界放出形走査電子顕微鏡

JSM-7900F

新開発の次世代型電子光学制御システム
Neo Engineを搭載。
超高分解能観察と操作性の両方を実現し、
オペレーターのスキルに依存することなく、
常に高いパフォーマンスを発揮する
JEOLの新しいフラッグシップFE-SEMです。

JEOL 日本電子株式会社

本社・昭島製作所　〒196-8558　東京都昭島市武蔵野3-1-2　TEL:(042)543-1111(大代表)　FAX:(042)546-3353
www.jeol.co.jp　ISO 9001・ISO 14001 認証取得

JEOLグループは、「理科学・計測機器」「産業機器」「医用機器」の3つの事業ドメインにより事業を行っております。
「理科学・計測機器事業」電子光学機器・分析機器・計測検査機器　**「産業機器事業」**半導体関連機器・産業機器　**「医用機器事業」**医用機器